INDUCED POLARIZATION AND SEISMIC 3D IMAGING OF LANDSLIDES

Publication No. FHWA-CFL/TD-11-006 **September 2011**

U.S. Department of Transportation
Federal Highway Administration

CTIP

Federal Lands Highway
Commitment to Excellence

Central Federal Lands Highway Division
12300 W. Dakota Ave.
Lakewood, CO 80228

FOREWORD

The Federal Lands Highway (FLH) promotes development and deployment of applied research and technology applicable to solving transportation related issues on Federal Lands. The FLH provides technology delivery, innovative solutions, recommended best practices, and related information and knowledge sharing to Federal agencies, Tribal governments, and other offices within the Federal Highway Administration (FHWA).

The objective of this study was to develop an understanding of new, state-of-the-art, applications of two geophysical methods – induced polarization (IP) and three-dimensional (3D) seismic refraction – for imaging landslides.

This report includes an overview of the geophysical methods used during the investigation followed by text elaborating selected views if the geophysical data. The primary observations and conclusions of the study are summarized at the end of the report.

F. David Zanetell, P.E., Director of Project Delivery
Federal Highway Administration
Central Federal Lands Highway Division

Quality Assurance Statement

The FHWA provides high-quality information to serve Government, industry, and the public in a manner that promotes public understanding. Standards and policies are used to ensure and maximize the quality, objectivity, utility, and integrity of its information. FHWA periodically reviews quality issues and adjusts its programs and processes to ensure continuous quality improvement.

Technical Report Documentation Page

1. Report No.	2. Government Accession No.	3. Recipient's Catalog No.
FHWA-CFL/TD-11-006		

4. Title and Subtitle	5. Report Date
Induced Polarization and Seismic 3D Imaging of Landslides	September 2011
	6. Performing Organization Code

7. Author(s)	8. Performing Organization Report No.
Phil Sirles, James Schofield, and David Butler	

9. Performing Organization Name and Address	10. Work Unit No. (TRAIS)
Zonge International, Inc. 7711 W. 6th Ave., Suite G Lakewood, CO 80214	11. Contract or Grant No. DTFH68-07-D-00001

12. Sponsoring Agency Name and Address	13. Type of Report and Period Covered
Federal Highway Administration Central Federal Lands Highway Division 12300 W. Dakota Avenue, Suite 210 Lakewood, CO 80228	Final Report August 2009 – August 2010
	14. Sponsoring Agency Code HFTS-16.4

15. Supplementary Notes

COTR: Roger Surdahl, FHWA-CFLHD. Advisory Panel Members: Khamis Haramy and Matthew Demarco, FHWA-CFLHD; Rick Andrew and Howard Hume, Yeh and Associates. This project was funded under the FHWA Federal Lands Highway Coordinated Technology Implementation Program (CTIP).

16. Abstract

The project was to develop an understanding of new applications using induced polarization (IP) and seismic refraction for three-dimensional (3D) imaging of landslides. Three 3D geophysical surveys were performed over the East Fork and Jackson Mountain Landslides near Wolf Creek Pass, Colorado during October 2009 a few months after the most recent movement on both landslides. Their geometries differ with the East Fork Landslide being primarily translational whereas the Jackson Mountain Landslide is a rotational slide.

The surveys at both locations identified many small IP anomalies in the near-surface (upper 50 ft) with no discernible pattern. The random distribution of IP features is interpreted to be the signature of formerly layered material now jumbled by mass movement down slope. Volumes of higher IP response are present at bedrock depths under the Jackson Mountain Landslide, as well as outside the most recent slidemass at the East Fork Landslide.

Anomalies with low resistivity correlated with a higher water content at the East Fork Landslide. Anomalies with higher resistivity correlated with near surface topographic highs or with areas adjacent to steep topography each of which might aid in drainage of the higher resistivity areas. Thus, a correlation with water content and resistivity is present.

At both landslide sites the 3D seismic models show a generally increasing velocity with depth, and based on borehole data there is only a marginal correlation to the observed slip surface. Within the slidemass some localized, near-surface high-velocity zones were imaged. These likely represent undisturbed soil and/or rock blocks which can be observed on the surface at both sites, but were not confirmed in the subsurface. 2D refraction modeling, used to check the 3D imaging, correlates with the 3D velocities obtained to about 50 or 60 feet. 3D volume images at depths greater than about 60 feet do not match 2D velocity cross-sections because the 3D results were limited in depth of investigation by the numerical modeling algorithm used.

17. Key Words	18. Distribution Statement
LANDSLIDE, 3D, IP, INDUCED POLARIZATION, REFRACTION SEISMIC, RESISTIVITY, GEOPHYSICS, WOLF CREEK PASS	No restriction. This document is available to the public from the sponsoring agency at the website http://www.cflhd.gov.

19. Security Classif. (of this report)	20. Security Classif. (of this page)	21. No. of Pages	22. Price
Unclassified	Unclassified	542 (142 printed) (400 on CD ROM)	

Form DOT F 1700.7 (8-72) **Reproduction of completed page authorized**

SI* (MODERN METRIC) CONVERSION FACTORS

APPROXIMATE CONVERSIONS TO SI UNITS

Symbol	When You Know	Multiply By	To Find	Symbol
		LENGTH		
in	Inches	25.4	millimeters	mm
ft	feet	0.305	meters	m
yd	yards	0.914	meters	m
mi	miles	1.61	kilometers	km
		AREA		
in^2	square inches	645.2	square millimeters	mm^2
ft^2	square feet	0.093	square meters	m^2
yd^2	square yard	0.836	square meters	m^2
ac	acres	0.405	hectares	ha
mi^2	square miles	2.59	square kilometers	km^2
		VOLUME		
fl oz	fluid ounces	29.57	milliliters	mL
gal	gallons	3.785	liters	L
ft^3	cubic feet	0.028	cubic meters	m^3
yd^3	cubic yards	0.765	cubic meters	m^3
		NOTE: volumes greater than 1000 L shall be shown in m^3		
		MASS		
oz	ounces	28.35	grams	g
lb	pounds	0.454	kilograms	kg
T	short tons (2000 lb)	0.907	megagrams (or "metric ton")	Mg (or "t")
		TEMPERATURE (exact degrees)		
°F	Fahrenheit	5 (F-32)/9 or (F-32)/1.8	Celsius	°C
		ILLUMINATION		
fc	foot-candles	10.76	lux	lx
fl	foot-Lamberts	3.426	$candela/m^2$	cd/m^2
		FORCE and PRESSURE or STRESS		
lbf	poundforce	4.45	newtons	N
lbf/in^2	poundforce per square inch	6.89	kilopascals	kPa

APPROXIMATE CONVERSIONS FROM SI UNITS

Symbol	When You Know	Multiply By	To Find	Symbol
		LENGTH		
mm	millimeters	0.039	inches	in
m	meters	3.28	feet	ft
m	meters	1.09	yards	yd
km	kilometers	0.621	miles	mi
		AREA		
mm^2	square millimeters	0.0016	square inches	in^2
m^2	square meters	10.764	square feet	ft^2
m^2	square meters	1.195	square yards	yd^2
ha	hectares	2.47	acres	ac
km^2	square kilometers	0.386	square miles	mi^2
		VOLUME		
mL	milliliters	0.034	fluid ounces	fl oz
L	liters	0.264	gallons	gal
m^3	cubic meters	35.314	cubic feet	ft^3
m^3	cubic meters	1.307	cubic yards	yd^3
		MASS		
g	grams	0.035	ounces	oz
kg	kilograms	2.202	pounds	lb
Mg (or "t")	megagrams (or "metric ton")	1.103	short tons (2000 lb)	T
		TEMPERATURE (exact degrees)		
°C	Celsius	1.8C+32	Fahrenheit	°F
		ILLUMINATION		
lx	lux	0.0929	foot-candles	fc
cd/m^2	$candela/m^2$	0.2919	foot-Lamberts	fl
		FORCE and PRESSURE or STRESS		
N	newtons	0.225	poundforce	lbf
kPa	kilopascals	0.145	poundforce per square inch	lbf/in^2

*SI is the symbol for the International System of Units. Appropriate rounding should be made to comply with Section 4 of ASTM E380. (Revised March 2003)

TABLE OF CONTENTS

LIST OF FIGURES

LIST OF ABBREVIATIONS AND SYMBOLS

2D	Two-dimensional
3D	Three-dimensional
bgs	below ground surface
CD ROM	Compact Disk Read Only Memory
CFLHD	Central Federal Lands Highway Division
COTR	Contracting Officer's Technical Representative
CTIP	Coordinated Technology Implementation Program
DGPS	Differential Global Positioning System
DOT	Department of Transportation
ERT	Electrical Resistivity Tomography
FLH	Federal Lands Highway
FHWA	Federal Highway Administration
ft/sec	feet per second
GAP	Geostructural Analysis Package
GPR	Ground Penetrating Radar
GPS	Global Positioning System
GRM	Generalized Reciprocal Method
Hz	Hertz
IP	Induced Polarization
mrad	milliradians
ms	millisecond
NFS	National Forest Service
ohm-m	ohm-meters
PDF	Portable Document Format
Ra	apparent Resistivity
RTK	Real Time Kinematics
TDEM	Time-domain Electromagnetic
TDIP	Time Domain Induced Polarization

US	United States
US DOT	United States Department of Transportation
UTM	Universal Transverse Mercator
Vo	observed voltage
Vs	secondary voltage
Yeh	Yeh and Associates, Inc.
ZETA	Zonge Electrical Resistivity Tomography Acquisition
Zonge	Zonge International, Inc.

ACKNOWLEDGMENTS

The authors would like to thank the many people who have contributed to the success of this project. The work has involved many steps from the design of the original concept, field data acquisition, data processing and analysis and reporting.

The field work was directed by J. B. Shawver from Zonge's Minnesota office. Mark Olson of Advanced Geosciences, Inc. was the seismic observer for the refraction surveys on both landslides. Samuel Harworth from Zonge's headquarters in Tucson, AZ, directed the electrical surveys. The field crews came from both Colorado and Arizona. The laying out and picking of cable and receivers was done by Tyson Jesser, Ethan Frost, Paul Rodriguez, and Ann Ryan.

A number of people contributed to the processing or modeling of the electrical or seismic refraction data. From Zonge J.B. Shaver, Justin Rittgers, Jacob Sheehan, and Greg Jones all assisted with the processing and analysis of the data. Alan Rock of Summit Peak Technologies is responsible for the Geostructural Analysis Package (GAP) code and the 3D refraction numerical modeling (inversions) on both landslides.

A special thanks is extended to Khamis Haramy and Roger Surdahl of the FHWA CFLHD, and Rick Andrew and Howard Hume of Yeh and Associates for their continuing support during this study project from the initialization of the project through the completion of the final report.

Finally "cover art" credit goes to Yeh and Associates as the landslide photo on the cover of this report comes from their Geotechnical Investigation Report on the Jackson Mountain Landslide.

(blank page)

CHAPTER 1 – INTRODUCTION

The purpose of this project was to develop a fundamental understanding of new applications of induced polarization (IP) and seismic refraction – for three-dimensional (3D) imaging the limits of landslides and groundwater in the subsurface.

A series of geophysical investigations were performed over two known landslides in the area near Pagosa Springs, Colorado. The two slide sites were selected by the FHWA Central Federal Lands Highway Division (CFLHD), in cooperation with contractors based on three items: 1) the slides are known to be active with recent movement; 2) each slide is under extensive geologic and geotechnical investigation for remediation design; and, 3) the slides have unique and different geologic conditions. The designated landslides are the East Fork Landslide on a US Forest Service Road 667, three miles east of Highway 160 and 12 miles northeast of Pagosa Springs; and, Jackson Mountain Landslide, seven miles northeast of Pagosa Springs, where US Highway 160 crosses the active slide. The study areas are shown on Figure 1.

The purpose of the investigation was to determine if a 3D geophysical approach using seismic refraction and induced polarization methods could characterize the subsurface and assess bulk material properties over large and potentially dangerous site. These conditions are normally investigated with standard geotechnical tests, boreholes and sampling. This new 3D approach could be used on landslides to optimize or enhance the drilling, sampling and other field analysis for landslides impacting roadways. The two slides investigated had existing information which was used in the geophysical analyses. These data were incorporated into the analysis to aid in determining the effectiveness, benefits, and limitations of performing geophysics on ‘active’ landslides. While the geophysical data (acquisition methods, interpretation, and presentation of geophysical results) may be useful for future engineering design and remediation efforts, the primary purpose was to evaluate the value of using wide-area geophysical surveys (i.e., three-dimensional) to help better characterize translation and variable soil slides for the purpose of technology transfer. The specific objectives are outlined below, with the emphasis on use of 3D data acquisition, processing, interpretation and visualization of seismic refraction, IP, and electrical resistivity volumes.

SETTING

East Fork Landslide – the principle geologic formation associated with this translational slide is a lahar deposit. The lahar deposits are common along the flank of the San Juan Volcanic field. Lahar deposits are, in fact, mudflow deposits developed off the volcanic mountains, and as such are quite prone to continued and renewed movement during wet seasons. Several recent mud flows have occurred along Wolf Creek pass in past decades, often blocking Highway 160. The East Fork Landslide is a large slide, which had renewed movement over a small piece of the entire slide area in the spring of 2009. The recent landslide movement closed the National Forest Service (NFS) road, as well as displaced an Excel gas pipeline, which was carrying methane from the San Juan gas field. The new displacement occurred in May of 2008, over a narrow (side-to-side) but long (uphill-downhill) area, and was quickly investigated in order to excavate the debris field near the NFS road, re-open the road, clear the blocked flow of East Fork creek, as well as repair of the Excel gas pipeline. The total slide, including the previously active area is

about 1500 feet wide by 2500 feet upslope, with the 'renewed' or 'active' slide portion being approximately 500 feet wide at the base, and about 1500 feet up the slope.

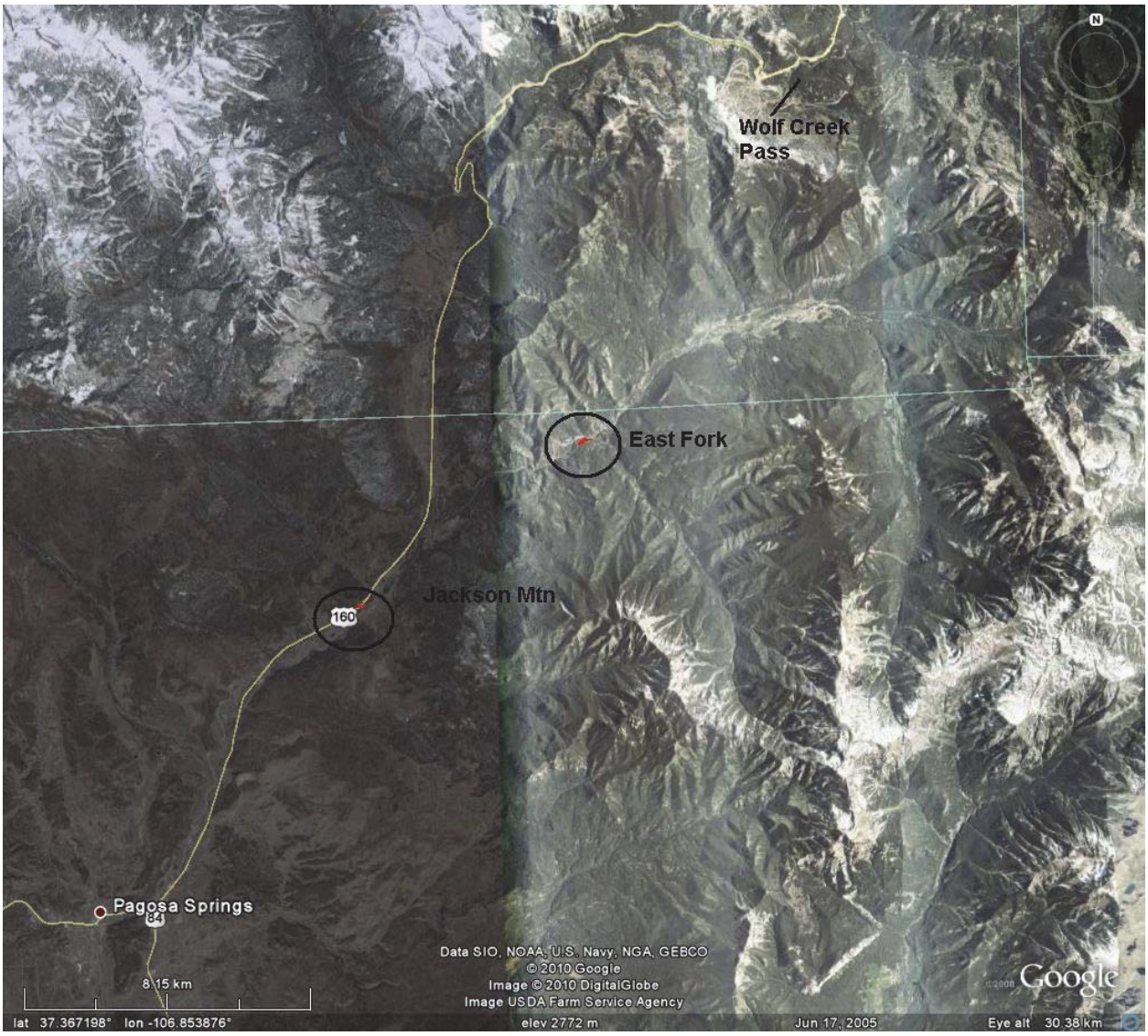

Figure 1. Satellite Image. Landslide locations along U.S 160, Wolf Creek Pass, Colorado.

Jackson Mountain Landslide – the Jackson Mountain Landslide is believed to be a rotational landslide with a more typical circular-shaped slip surface. This slide has been active in recent decades. In the spring of 2009 a portion was re-activated which closed a short portion of Highway 160 and caused damage to another Excel gas pipeline (although not as severe as at the East Fork Landslide). The geology is steeply dipping Cretaceous-age shales and sandstones of the Mesa Verde Formation. The active slide is in the Lewis Shale unit. The Lewis shale is a thin-bedded shale compared to the Mancos Formation. The shale has slipped along the steep hogback in this area repeatedly. The most recent movement, which occurred on May, 2008, dammed up the San Juan River. The Jackson Mountain Landslide is more symmetric than the East Fork Landslide, and has the classic arcuate structure of a circular failure landslide. The

slide is approximately 2000 feet wide at its base (near the San Juan River), and extends about 2500 feet up the slope. US Highway 160 is approximately one-third up the slope from the slide's base. The active or renewed portion of the slide is generally centered in the larger inactive slide. The active slide is roughly 800 feet wide at its base, and almost 1000 feet in length up the slope to the current / fresh headscarp. The depth to the slide plane is thought to be about 50 to 60 feet in the middle of the active portion of the slide. The slide does extend down to the San Juan River to the southeast, and is bounded by Turkey Creek on the northeast.

SURVEY METHODS

To determine if geophysical imaging can help with geologic engineering assessment of the two slides, two 3D geophysical methods were applied during the investigation: 1) Seismic refraction, using compressional-wave (P-wave) velocity mapping; and, 2) Induced Polarization (IP), along with resistivity mapping. The aim of the two methods was to examine the mechanical properties of the slide materials via seismic refraction imaging, and the geo-electrical and lithologic properties via the IP. Each method was acquired using 3D field acquisition parameters, 3D data processing, and 3D visualization of the results. Additionally, for quality control, each method was tested in the more conventional two-dimensional (2D) mode as well. The purpose of this study was to evaluate a 3D geologic problem with difficult subsurface conditions (i.e., odd geometry with mixed soils and rock) using 3D geophysics. There are no commercial analytical tools or software available to evaluate seismic refraction and electrical data using a joint-inversion approach for this project. Therefore each geophysical method was acquired, processed and interpreted independently. The joining of the methods took place at the interpretation stage.

From the overall geophysical investigation point-of-view, each slide had the same 3D field methods applied. In this fashion, the results can be 'viewed' in a similar fashion for two slides with different geometries, movements, and geology. Seismic refraction tests were performed over an area of approximately 180,000 sq. ft. using an approximate 600 x 300 foot area of investigation for the 3D. A single (long) 2D line, transverse to the slide movement, was acquired for the purpose of obtaining 2D data on both the active and inactive areas. The 3D survey areas were laid out in such a fashion as to evaluate only a selected area within the 'active' portion of the slides, and set over an area that is conducive to acquiring quality data. Each slide has unique surface characteristics and cultural features (e.g., roadways, pipelines, fences, etc.), and as such the final location of the 3D "grid" was established in the field.

(blank page)

CHAPTER 2 – BACKGROUND

LANDSLIDE GEOPHYSICS

Various geophysical tools have been applied to the investigation of landslides over the years. The methods include gravity, GPR, resistivity, TDEM, and both refraction and reflection seismic techniques. The present project was conceived as way of expanding the list of available tools to include the electrical method of induced polarization and the 3D version of seismic refraction.

The reference section has several papers on landslide geophysics. For other perspectives on the use of geophysics for landslide analysis besides this report see Lapenna and others (2005), Calvert and Hyde (2002), Suzuki and Higashi (2001), Rainone and Torrese (2007), Nawawi, Saad, and Ghazali (2006) and lastly, Bogoslovsky and Ogilvy (1977).

GEOPHYSICAL METHODS

This landslide study was focused on applying two conventional geophysical methods in novel ways. The sections below describe the basis of the methods to provide the reader with an overview of the geophysical tools. Consult the references included for more details about the methods.

Both the electrical and seismic geophysical methods require accurate positioning of sources and sensors for proper analysis of the data. The field arrangement of sensors – geophones and electrodes – used the same measured positions at each slide, and thus the sampling for both methods was equal. Similarly, the line spacing used for both study areas was roughly the same. Differences in sensor separation or line spacing were predicated on site conditions. The target line spacing was 30 feet with a nominal station spacing of 20 feet. Line and station spacing was dictated by access, topography, and cultural obstacles. The line locations mandated that the signal sources and receiving equipment be carried in on foot.

Positioning of the geophysical field receivers was done with the satellite-based global positioning system (GPS). Differential GPS (DGPS) was used to achieve the desired degree positioning accuracy. Positioning uncertainty is affected by the degree of tree cover in the survey areas and the GPS satellite coverage at the time of surveying. Station positioning is done in three dimensions as the vertical location is critical for the data processing of 3D surveys. Surveying of station locations was done prior to data acquisition. Location data were acquired in latitude and longitude then converted into the Colorado State Plane coordinate system (Colorado CS83, South Zone).

Induced Polarization

The Induced Polarization (IP) method is an extension of the commonly-used, surface-based resistivity survey used to provide information about the subsurface electrical properties. The field acquisition for IP is very similar to that of a resistivity survey with the primary difference being an additional set of measurements are made once the equipment has been positioned on the ground, thus the two electrical data sets are usually acquired simultaneously during the same

survey using the same equipment and array. Resistivity surveys have been used extensively by the mineral, geothermal, hydrocarbon, and groundwater exploration industries, and IP is commonly used in mineral exploration, as well as environmental studies.

Induced Polarization and resistivity data are acquired by introducing an electrical current into the ground between two current electrodes (electrodes A and B of Figure 2) and making measurements of the induced voltages between two potential electrodes (electrodes M and N of Figure 2). The geometry between the transmitter and receiver electrodes can be varied and several standard types of electrode arrays are used. Some typical arrays are dipole-dipole, pole-dipole, pole-pole, gradient, Schlumberger, and Wenner. For IP surveys the most often used configuration is the dipole-dipole array as shown in Figure 3. For the dipole-dipole array, current is introduced into the ground at two adjacent (current) electrodes and the resulting electric field is measured at two adjacent (potential) electrodes.

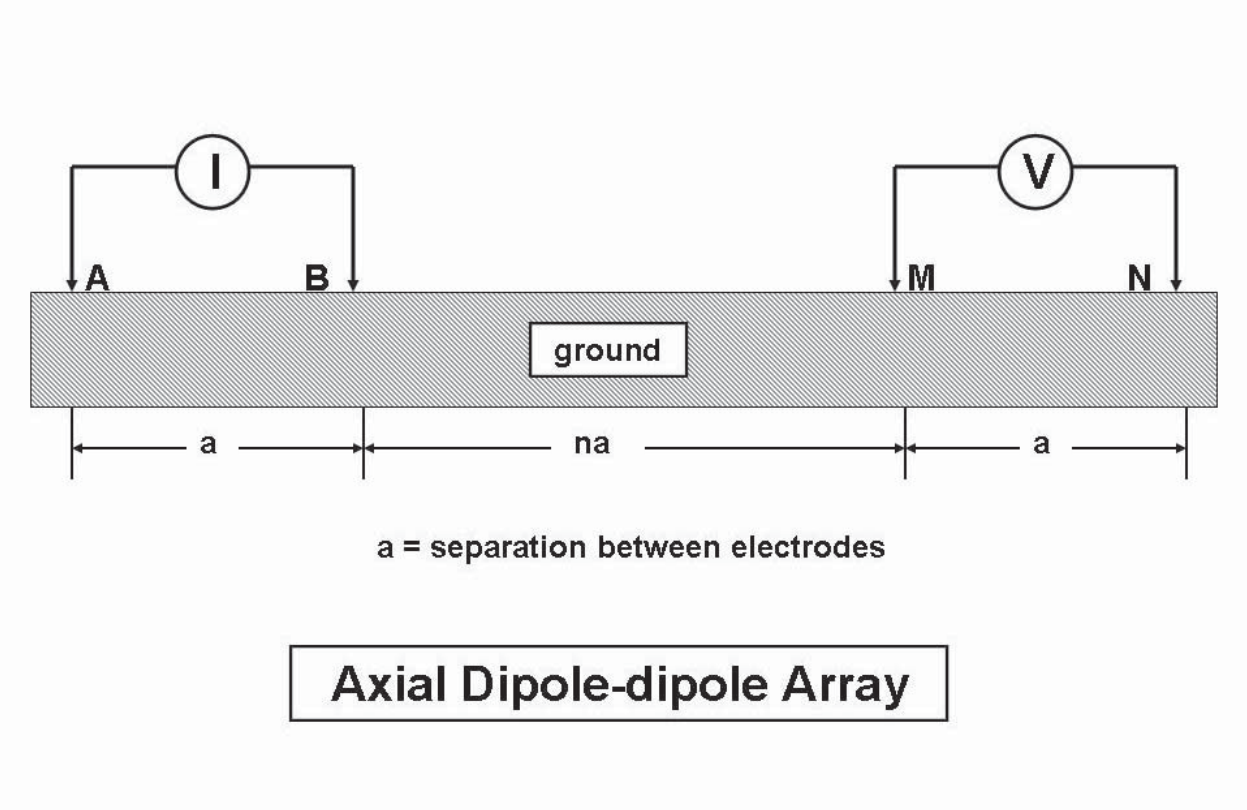

Figure 2. Diagram. Basic axial array for dipole-dipole surveys.

By comparing the transmitted signal to the received signal, electrical properties of the ground can be calculated. As the survey crew traverses the planned profile, changes in ground resistivity (the ability of the ground to conduct electrical current) affects the strength of the received signal. The parameter of interest for a resistivity survey is referred to as the apparent resistivity (Ra) which has units of ohm-meters (ohm-m). Apparent resistivity is a function of distance between the electrodes of the current dipole and the potential dipole as well as the separation between the dipoles. In order to simplify the calculations the distance between both sets of electrodes is fixed

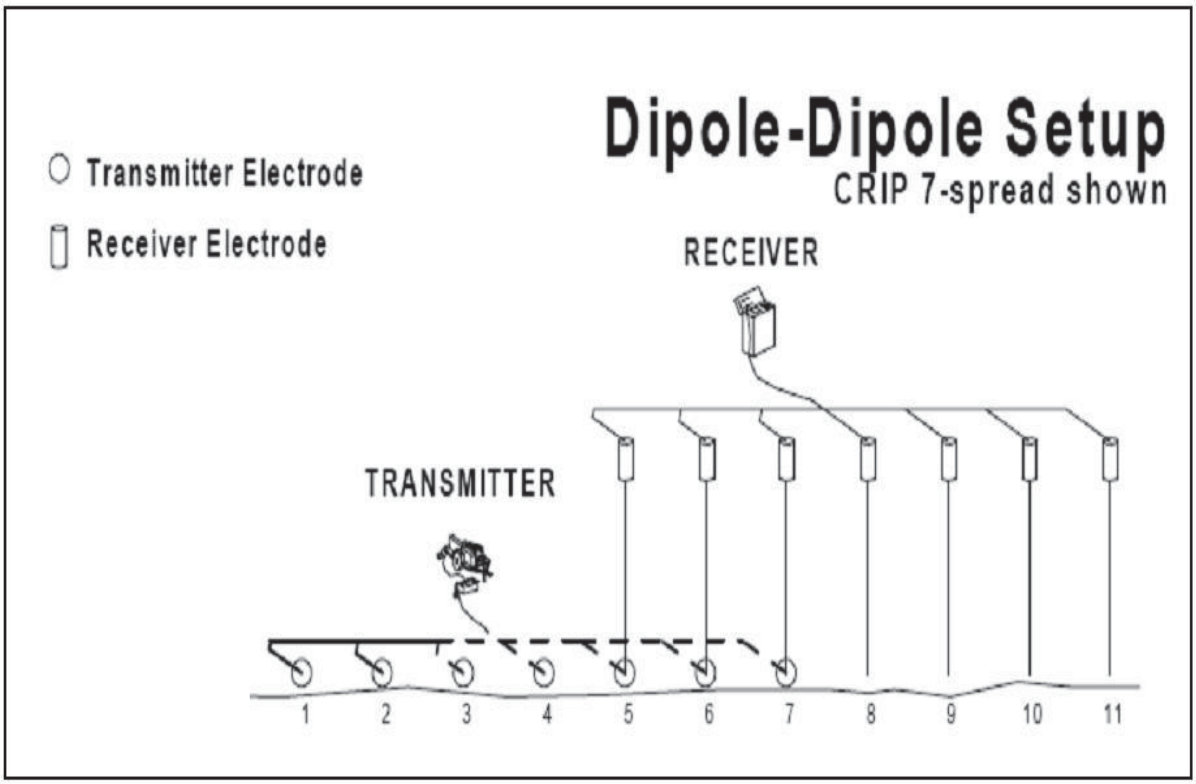

Figure 3. Diagram. Dipole-dipole transmitter-receiver IP setup.

at "a" as shown on Figure 2 and the distance between dipoles is "na" where n is an integer (n = 0, 1, 2, 3, 4, etc.). The size of "n" is determined by the depth-of-penetration desired, the power of the transmitter used, and other factors.

The induced polarization method measures the ability of material in the ground to polarize at interfaces; this polarization affects the shape and timing of the received waveform. The measurements can be made in two ways, in the frequency domain or in the time domain. When the data is collected in the frequency domain the strength of the IP response is indicated by the amount, and direction, of the phase shift between the source signal and the recorded earth signal. The phase shift is reported in units of milliradians (mrad). The work on the landslide was done in the time domain where the units of measure are milliseconds (ms).

The physical parameter of interest with time-domain IP is chargeability. A simplified model of induced polarization can be visualized by considering a current crossing an interface between an ionic solution and a metallic mineral. At the interface, a voltage drop, called the over-voltage effect, is present. An ion that approaches the surface from the fluid during current flow but which does not have enough energy to overcome this overvoltage cannot donate or accept an electron to the electron conduction process in the metal. The charged ion remains at the interface and its electrical charge decreases the current flow through the interface. If the current flow is terminated, these ions will return to their side of the interface and regain an electrical balance within the ionic solution. This transient flow of charged ions will be measured as a voltage that

exists just after current flow is terminated. This voltage will decay rapidly with time. This voltage, measured just after the driving current is terminated, is the chargeability or induced polarization effect. Clay minerals also exhibit an induced polarization effect but the physics of the effect is described as a membrane potential. IP due to clay minerals is a complex function of clay types, clay percentages, and particle size.

The observed voltage, Vo, is due to the signal from the electrode array. Chargeability is expressed as a percentage or as a pure ratio of Vs/Vo in millivolts per volt where Vs is the secondary voltage at the interface. What is measured in the field is somewhat different and is referred to as apparent chargeability. Apparent chargeability is the area under the voltage-time decay curve at a defined time interval after the transmitter current stops. Apparent chargeability is normalized so chargeability has units of millivolt-seconds per volt or just milliseconds.

To determine the area under the decay curve the analog signal is sampled rapidly. A number of windows (up to 15 for the landslide surveys) are selected and a value for each window is derived by integrating the voltages and normalizing. Chargeability is frequency dependent. Typical a frequency of 0.125 Hz (an 8 second period) is used as a reference and data for other frequencies are normalized to this standard.

In the field the 3 to 5 people on the field crew set up a series of transmitter electrodes and receiver electrodes with each dipole being “a” in length as shown on Figure 2. The example setup shown in Figure 3 has seven transmitter electrodes (six dipoles) and seven receiver electrodes (six dipoles). Typically a linear array of electrodes is set up and connected by wires to the transmitter equipment at a central location. The transmitter equipment is usually in a small truck with a generator mounted in the back or on a trailer behind the truck. The transmitter used for these two landslide investigations is the Zonge GGT-30, a 30-kilowatt generator designed specifically for electrical geophysical investigations. The GGT-30 is shown in Figure 4. This equipment transmits a very carefully controlled signal at specific frequencies into the ground. A predetermined schedule is entered into the control software which then directs the collection of all desired combinations of transmitter and receiver dipoles. After all combinations are recorded the array is shifted along the acquisition line and the measurement sequence is repeated. When all the measurements for a line have been stored in the field instrument the data is ready to be processed. Data processing can be done in a field office but is usually handled in the home office after the data and field conditions are transmitted from the field.

Figure 4. Photo. Zonge IP Transmitter.

The transmitter dipole consists of thin insulated wire stretched out across the ground. The wire is coupled to the ground with a metal stake about ½ inch in diameter, pounded into the ground about six to 18 inches. The stakes are doused with saltwater to provide good electrical contact with the ground. The separation of a pair of electrode stakes defines the "a" spacing of the survey. Figure 5 illustrates the dipole-dipole set-up used for the IP and resistivity measurements acquired at both East Fork and Jackson Mountain landslides. Depth is plotted as a function of "n", the integer multiple of separation of the electrodes. Once the field measurements (Rxy) are plotted, the inversion routine converts the depth from "n" to elevation in feet (or meters). This plot of the field data is often referred to as a *pseudo-section*, due to the axis being in terms of "n" not an actual depth section.

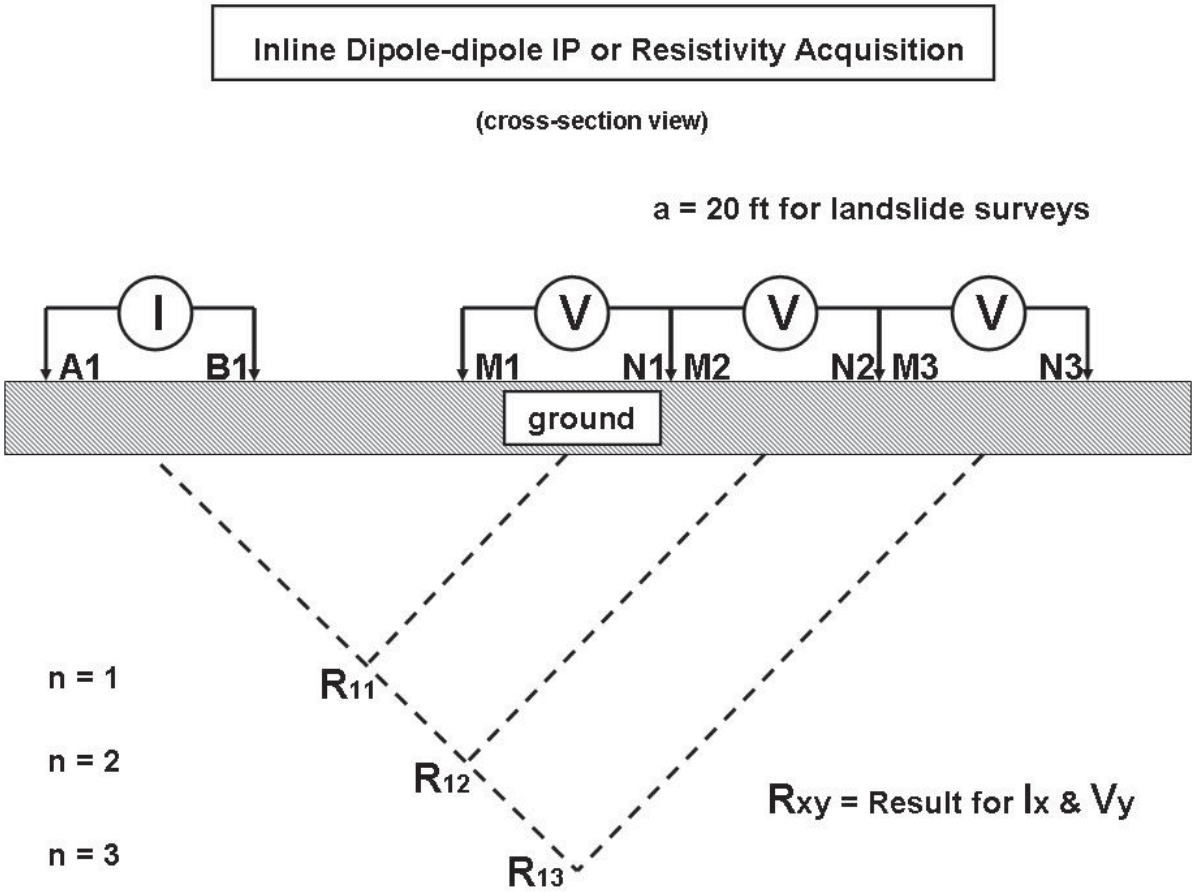

Figure 5. Diagram. Transmitter electrode array.

The measurements were made with a Zonge GDP-32II, backpack-portable receiver and recording system connected to the different dipoles (Figure 6). The dipoles for the receiver are also simply wires laying on the ground, but in this case they are grounded using small porous ceramic "pots" about 6 inches tall and two inches in diameter, buried about one inch in the soil. Usually, the receiver equipment is carried along the survey line to the approximate center of a given setup for the recording of the measurement. By making measurements at numerous stations along a line, a cross-section of the earth's electrical resistivity properties can be produced.

For the axial dipole-dipole array used for landslide surveys, current is introduced into the ground at two adjacent (current) electrodes and the resulting electric field is measured at two adjacent (potential) electrodes. No trenching, drilling, or road-making, was involved for receiver or transmitter installation. The survey was done on foot using backpack-able equipment as shown in Figure 6. The majority of commercial IP surveys are done in remote areas.

Figure 6. Photo. Zonge GDP-32 receiver configured for IP on backpack.

Resistivity variations in rocks and soils are caused by the conductivity of the saturating fluids, degree of saturation, porosity, resistivity of rock or soil framework, consecutiveness of pore spaces, permeability, mineral and grain size and temperature, in approximately that order. Cultural features (man-made objects such as fences, power lines, pipelines, etc.) can also affect ground resistivity measurements. Compared to changes in resistivity, there are relatively few subsurface conditions that create an IP response. Metallic mineralization, particularly disseminated sulphides, causes increased IP values. Certain dissolved solids in groundwater have been shown to increase IP response, and in some environments, some types of clay can also increase IP response if the abundance of the clay is within specific ranges (dependent on the type

of clay). Clay minerals in the subsurface often contribute to background or normal IP effect. The normal IP effect is contrasted with interface effects which are due to the presence of disseminated metallic minerals and are generally larger. Like resistivity data, IP data can also be influenced by cultural features.

Data Processing for IP Surveys

After the data was recorded, the raw files were processed by the using Zonge commercially available programs to convert the measurements into apparent resistivity and apparent phase shift values along the survey profile. The processing software uses the electrode locations and survey configuration in addition to the measurements of transmitter currents and dipole voltages to make the calculations. The output at this stage of the processing is a series of apparent resistivities and phase shifts with a "depth" parameter in the form of "n" value of the acquisition schedule. For a first approximation, the results are plotted half way between the current and potential dipoles and "n" tiers below the surface.

Modeling software is required to translate the IP and resistivity data into a cross-section for 2D data or an earth volume for the 3D data. The modeling package used for this translation step was the Solver module of ERTLab created by Multi-Phase Technologies and Geostudi Astier. Results were checked in the Viewer module before transferring the output to analysis databases for the project. The ERTLab is software capable of handling large volumes of Electrical Resistivity Tomography (ERT) data created during the acquisition of a 3D grid of dipoles. The core of ERT is an inversion algorithm that permits three-dimensional topography to be included with the resistivity and IP data. The geometric factors for each quadrapole (pair of current and potential dipoles) are calculated based on the actual location of each electrode. The output is a data volume of resistivity and IP values. The inversion calculates a smooth, constrained, least-squared fit to the observed data to determine the most likely subsurface configurations of IP and resistivity values.

2D sections of resistivity or IP versus depth can be created from the 3D data volume as shown in Figure 7. Similarly, a constant depth slice through the data volume can be presented as a contour map as with the horizontal IP slice of Figure 8.

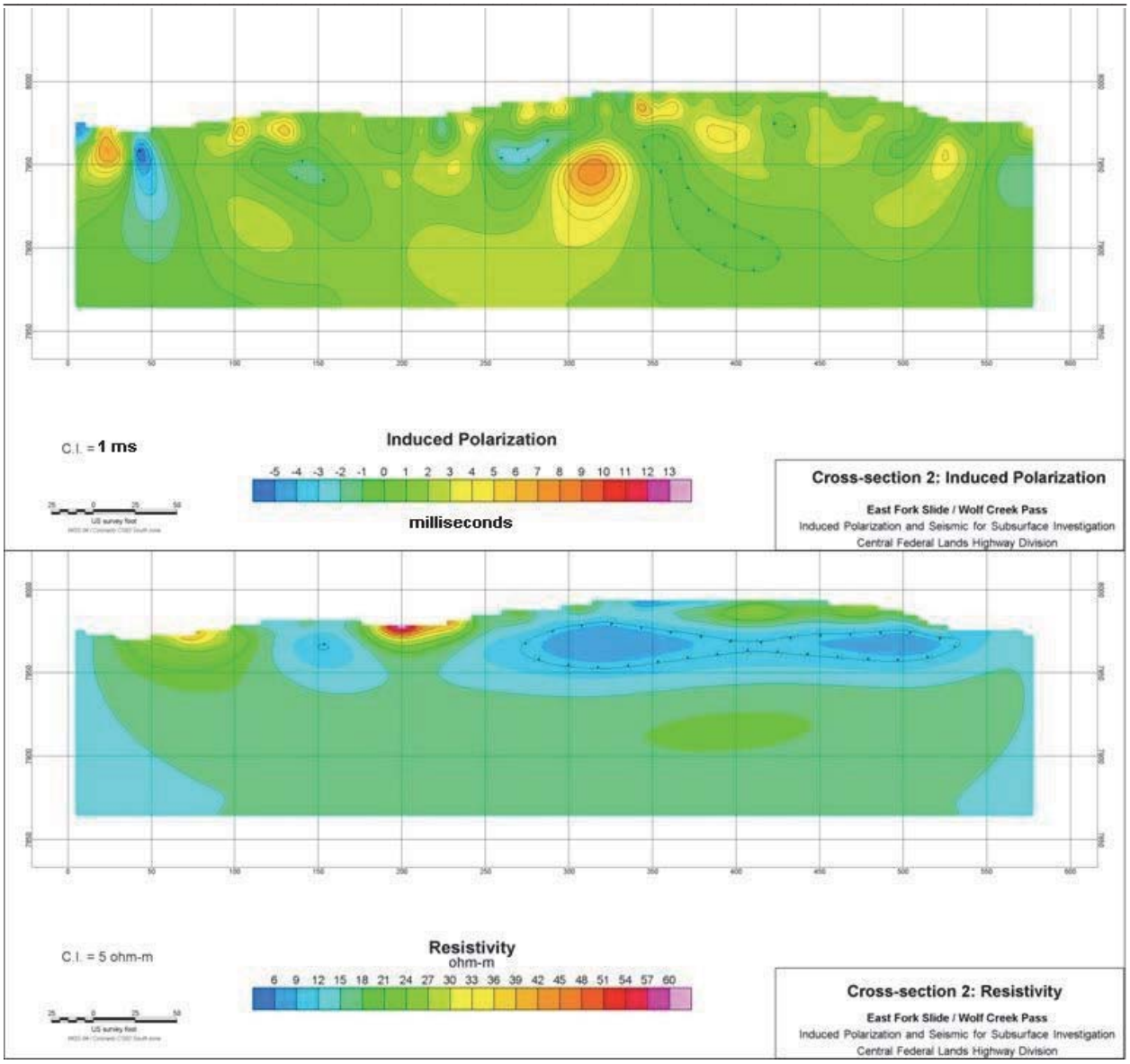

Figure 7. Model. Example of IP and resistivity inversion models.

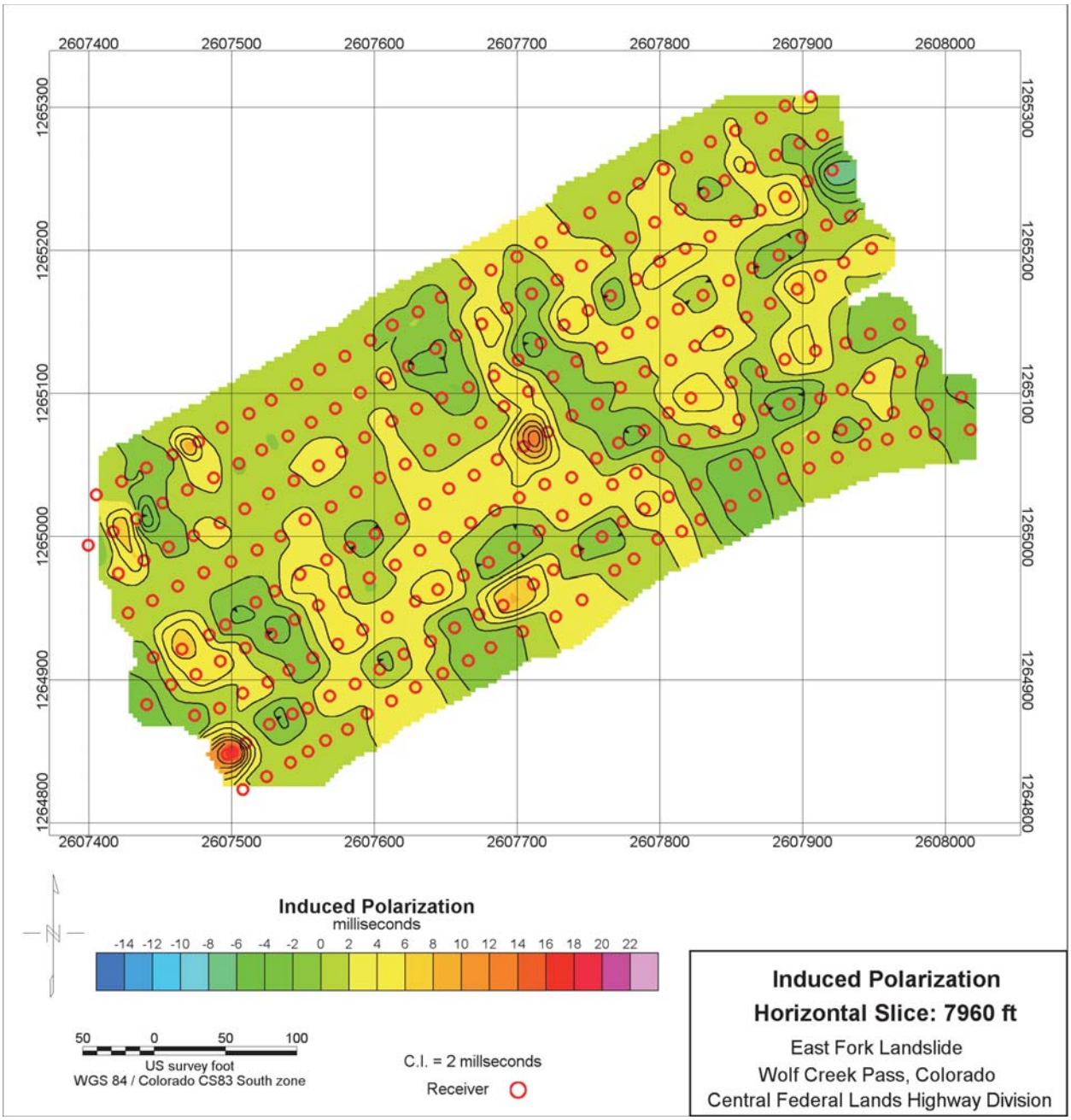

Figure 8. Map. Example of IP model results displayed as colored contour map.

When stations are collected along several lines in the same area, data can be displayed in plan view plots at a constant elevation or depth bgs. Plan views can help highlight trends between lines

For further details about IP and resistivity surveys see Coggon, 1973; Roy and Apparao, 1971; Sumner, 1976; Tripp, Hohmann, and Swift, 1984; and Zonge, Wynn, and Urquhart, 2005 in the references for this report.

Seismic Refraction

The seismic refraction method is based on the fact waves bend (refract) when the waves moves from one medium into another which has different physical properties. For seismic (acoustic) waves the critical properties are velocity, and to a lesser degree, density. A familiar case of refraction is the bending of light as the waves travel from the medium of air into the medium of water. Seismic refraction defines the near-subsurface in both velocity and structure.

Seismic refraction involves placing an array of sensors (geophones) on the surface and measuring the relative arrival time of a seismic wave at the sensors. The seismic source can be any well-timed disturbance such as hammer blows or explosive charges as shown in Figure 9.

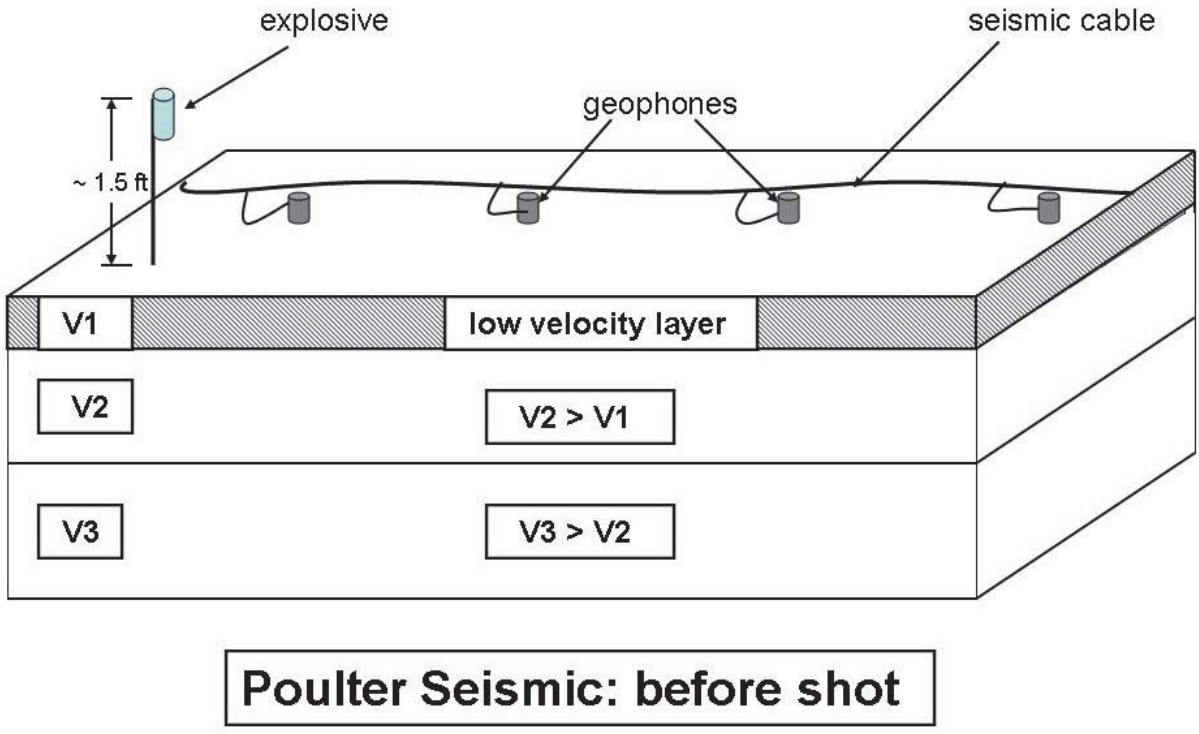

Figure 9. Diagram. Prepared Poulter shot over layered Earth.

The drawing in Figure 10 illustrates how refracted waves travel through a layered subsurface. Waves are created by an energy source and travel through the ground at some particular velocity until an interface with acoustic properties is encountered. Some of the energy passes through the interface and some is transmitted along the interface. After traveling along the interface for some distance a portion of the seismic energy is redirected upward to the surface where the geophones detect it. The simplest case for the seismic refraction method is when each deeper layer has a faster transmission velocity than the overlying layer as seen in the diagram of Figure 10. As the geology of survey sites does not always consist of layers with successive higher velocities, sophisticated mathematical tools have been developed to aid in analyzing refraction data. One such modeling method is refraction tomography.

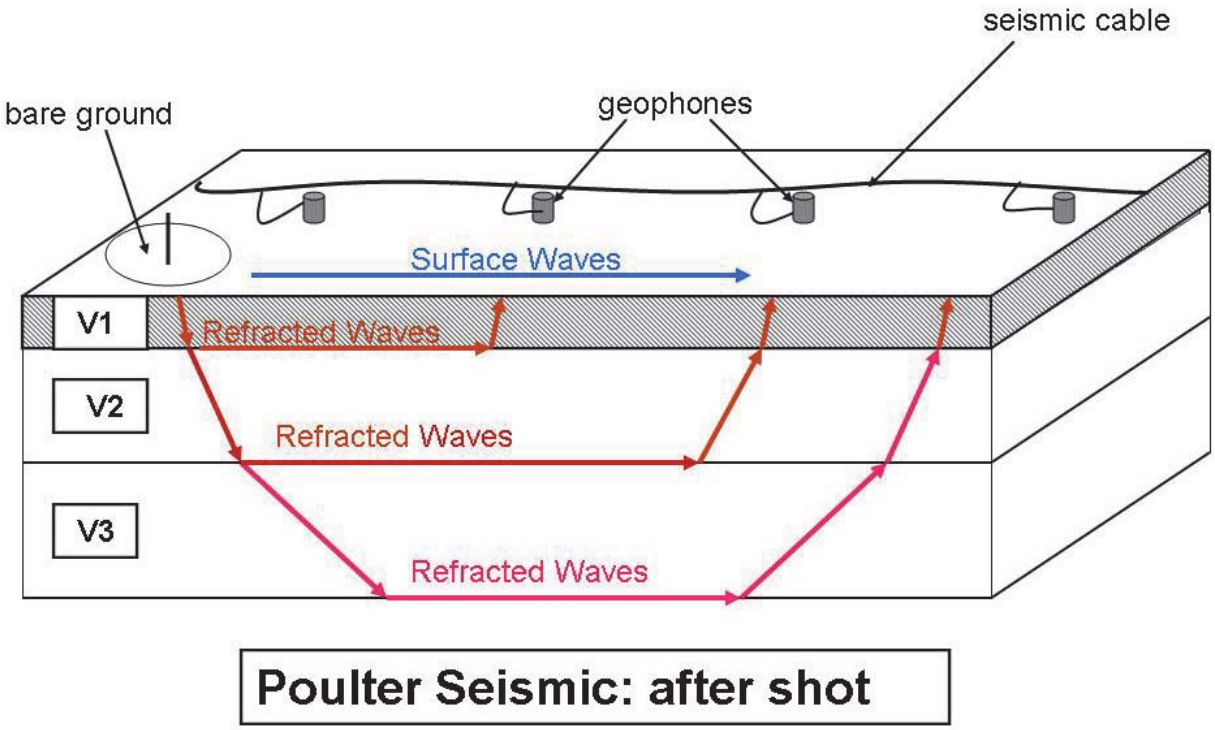

Figure 10. Diagram. Refracted and surface waves generated by explosive shot.

The depths and velocities of the subsurface material are determined by calculation. The first step in the analysis is to plot the arrival data for the compression waves in a travel-time curve. Compression waves are also known as p-waves. The seismograms shown as squiggly lines in Figure 11 are examined or "picked" to obtain source-receiver travel times. First arrivals of p-wave energy for a seismic survey are usually manually picked. The seismic data from the landslide surveys was picked using FirstPix, a commercially available routine from Interpex, LLC of Golden, Colorado. The picks for each shot record were stored with the respective geometry of source and receiver positions in GRM files, standard output from FirstPix.

These travel times along with source-receiver distances were used to construct a time-distance plot for each shotpoint. The relative arrivals were used to define the subsurface. The critical ingredients for refraction surveying include accurate placing of sensors and timing of relative arrivals to a precision of a millisecond or so. The velocities inferred from the travel time curves are apparent velocities, and not necessarily true velocities. True velocities are determined from arrival times for many shotpoints during the modeling procedure.

Successful modeling depends on accurate traveltime picks. Recording instrumentation used presently allows accurate timing of first arrivals to better than tenths of milliseconds. Even when the first break analysis is highly accurate ambiguity remains. The two factors of velocity and structure are intrinsically related in refraction theory, thus the independent determination from refraction surveying alone is impossible. The ambiguity is that structure can be traded for velocity differences over a broad range of velocity-structure pairs. One justification for 3D refraction is to constrain the uncertainty. Additionally, modeling ambiguity can be introduced

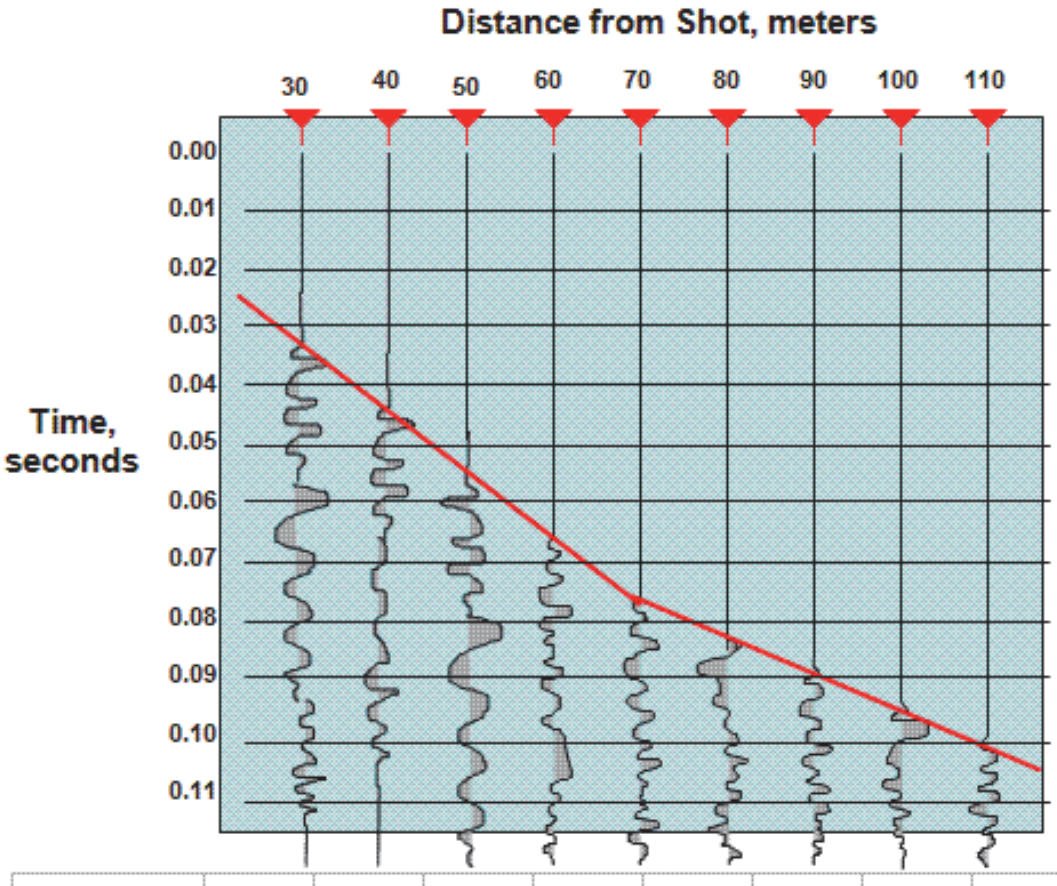

Distance (meters)	30	40	50	60	70	80	90	100	110
1°' Arrival Time, sec	0.0353	0.0471	0.0589	0.0706	0.0806	0.0872	0.0938	0.1000	0.1069

Figure 11. Diagram. Red line connects travel time picks of the first breaks.

due to the existence of low-velocity material. As there is no refracted information from a buried interface with a velocity less than that of the overlying material, a low-velocity zone will be hidden in the arrival time data. When this situation occurs, calculated depths to deeper refractors can be offset and in error. Geologic information is used to limit the range of the uncertainties.

All the first arrival times and associated geometry data for the landslide surveys were read directly from the GRM files into modeling programs. For the 2D analysis, Rayfract (Version 3.11) from Intelligent Resources of Vancouver, British Columbia, Canada, was used. For the 3D seismic data the proprietary Geostructural Analysis Package (GAP) was used by Summit Peak Technologies of Parker, Colorado, to create the 3D refraction tomograms. The discrete element inversion used all available shot-receiver pairs for a given landslide to generate the velocity volumes used in the interpretation in Chapter 5.

A seismic source introduces energy into the ground. For the landslide investigations both sledge hammer impacts on a metal plate and explosive charges were used as seismic sources of compression waves. Hammer impacts were primarily used in the interior of receiver grids where the "shot" to geophone distances were small. The particular form for the explosive charges was the Poulter seismic source (Poulter, 1950). The Poulter method involves generating seismic energy by detonating explosive charges above the ground surface as shown in Figures 9 and 10. For the landslide study the small charges were detonated about 1.5 feet above the ground, usually on wooden poles. The method is illustrated by Figures 12-15. The seismic signal was created when the airborne shockwave strikes the ground. Modern usage of the air-charge method is described by Davis and Lawton (1985).

Figure 12. Photo. Preparing Poulter charge.

Figure 13. Photo. Poulter charge on short pole.

Figure 14. Photo. Poulter charge on tree stump.

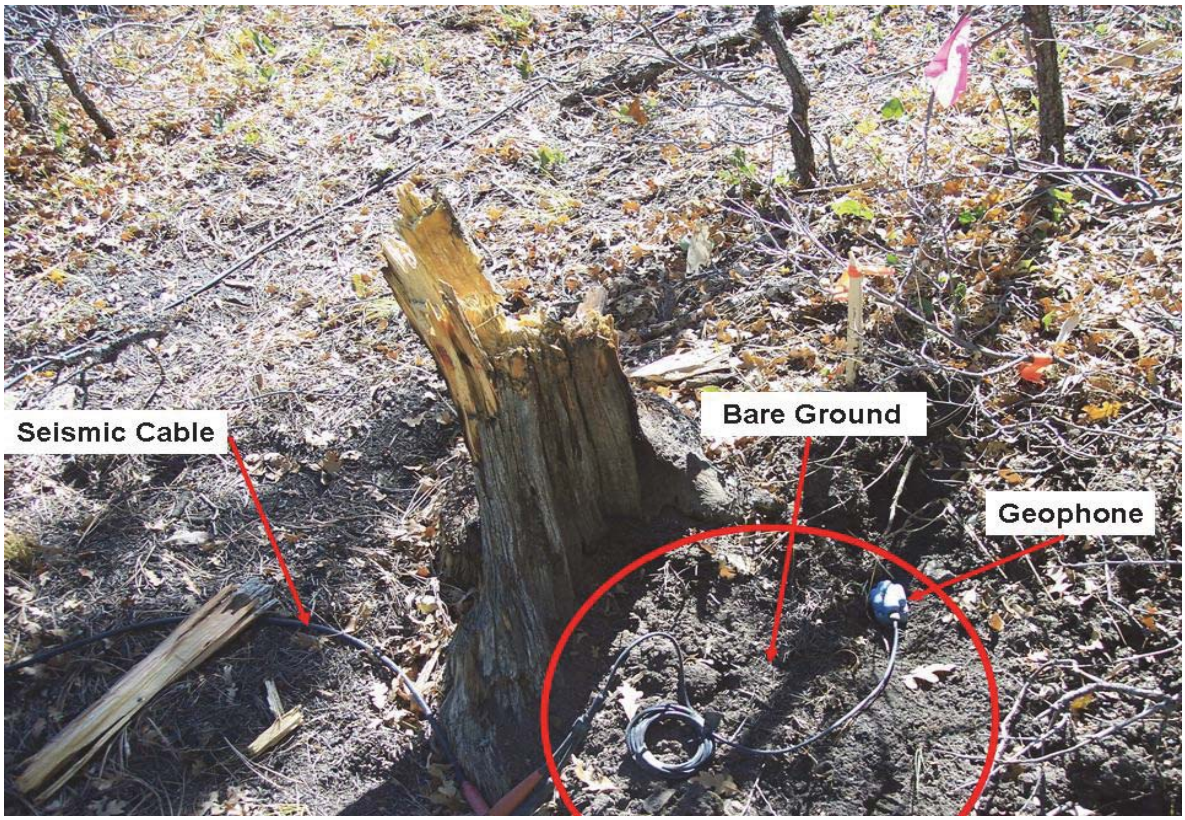

Figure 15. Photo. Tree stump and bare ground after Poulter shot.

The small explosive charge has sheared off the dead tree stump in Figure 15 and has cleared the surface debris for a couple feet around the blast exposing the seismic cable and geophone. However, no permanent damage has been done to any live vegetation and the ground disturbance is minimal.

The recording instruments were packed into a self-contained unit and transported on a trailer as shown in Figure 16 from the East Fork Landslide site. The unit is often referred to as the "doghouse" and is the work space for the "observer" who operated the recording equipment and was responsible for field-checking the data quality.

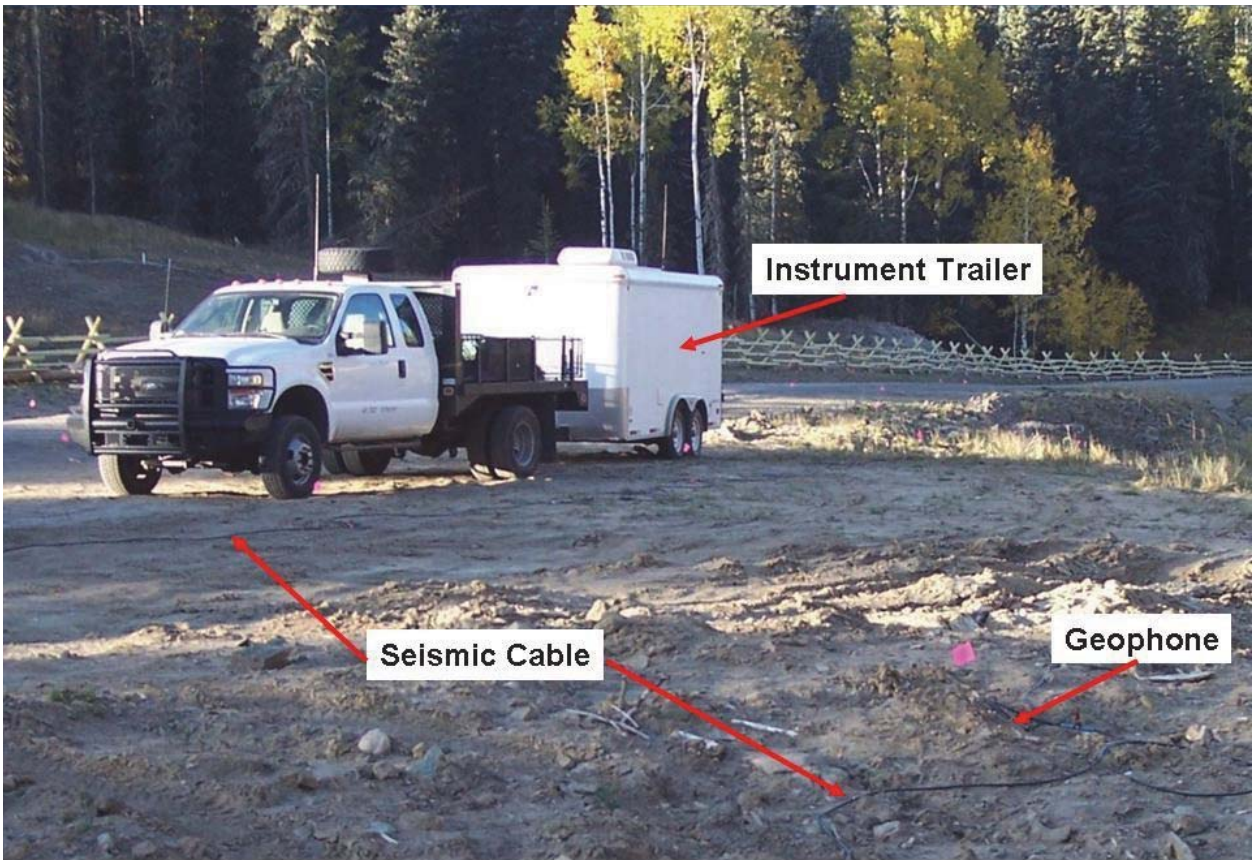

Figure 16. Photo. Seismic Recording Trailer.

(blank page)

CHAPTER 3 – SURVEY SITES

EAST FORK LANDSLIDE

The field acquisition started on the East Fork Landslide. This area of reoccurring ground movement is near longitude 106° 51’ 00” W and latitude 37° 23’ 15’’ N and is shown in Figure 17. An extensive report on the slide was published by Haramy (2007) and is the source of much of the geologic information included in this geophysical report. The details of specific locations of the geophysical sensors in the main grid are shown on Figure 18.

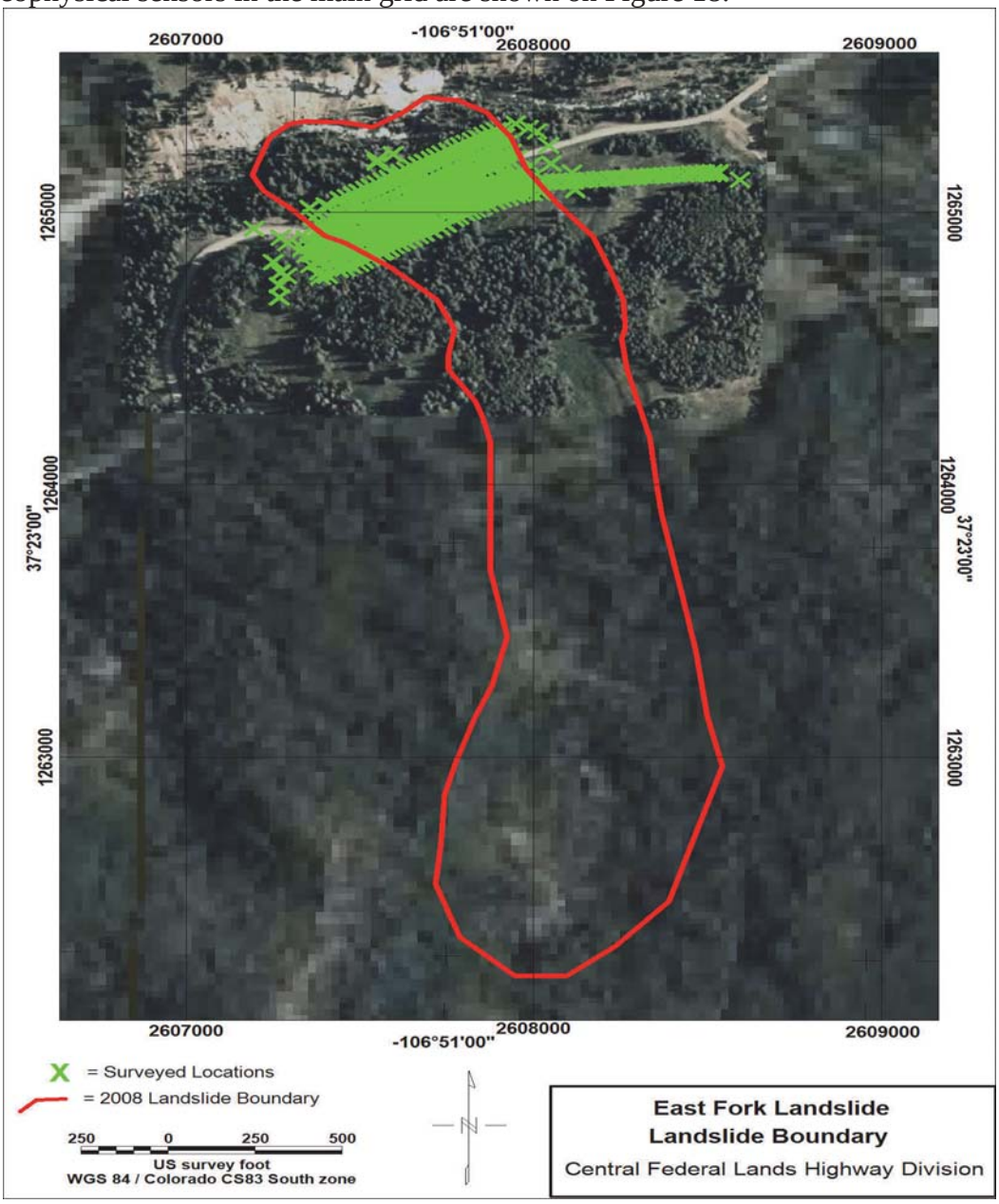

Figure 17. Photo. Outline of the full extent of East Fork Landslide with project GPS locations marked.

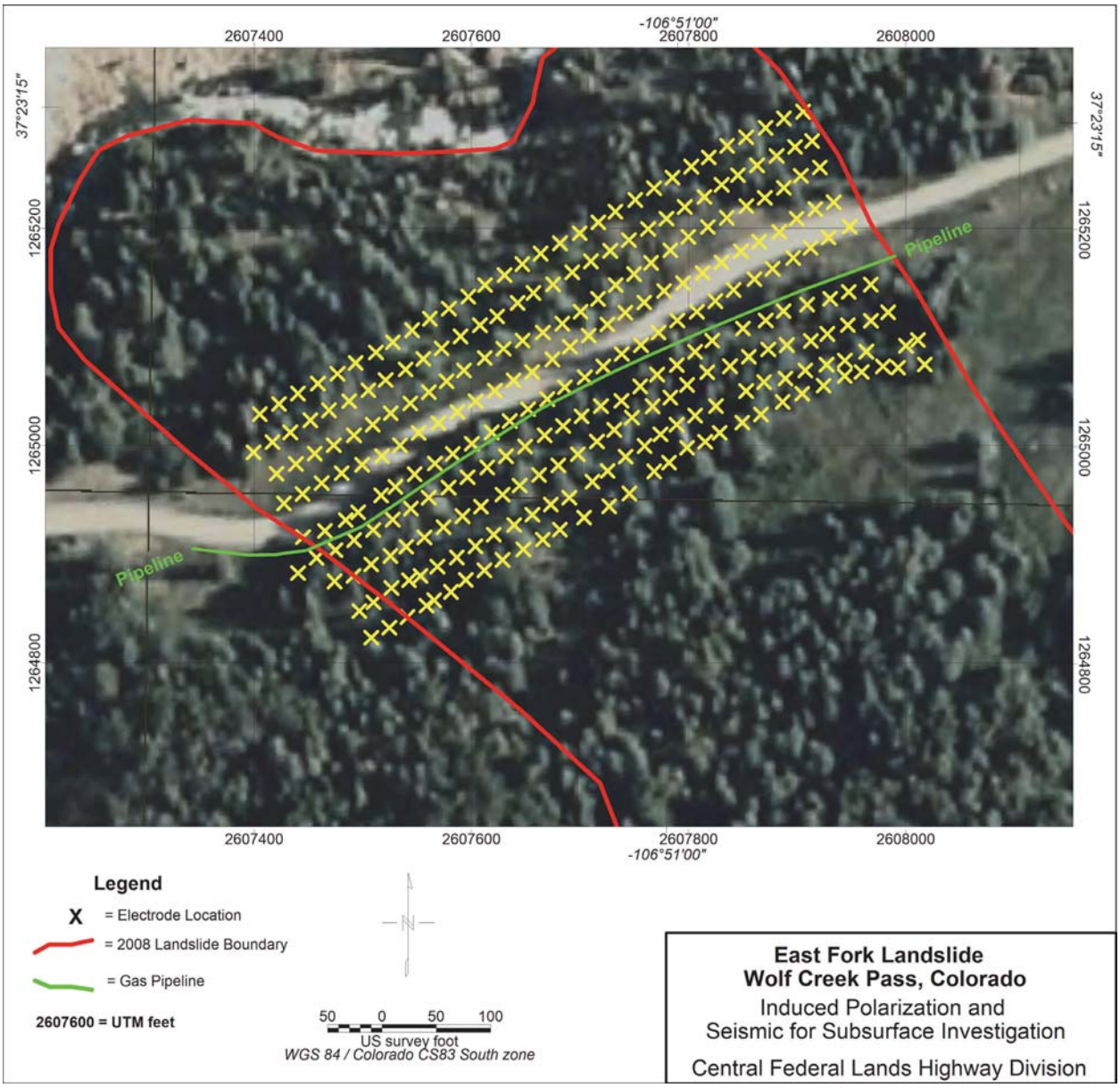

Figure 18. Photo. Location of geophysical sensors on the East Fork Landslide with electrode positions denoted with yellow X's.

Background

This investigation was to evaluate a massive landslide known as the East Fork Landslide as shown in detail on Figure 18. The landslide is located approximately 2 miles east of US Highway 160 along East Fork Road and approximately 12 miles northeast of Pagosa Springs in San Juan National Forest, Archuleta County, Colorado. This recurrent landslide-earth flow reactivated the evening of May 2nd, 2008, and crossed Forest Road 667. Following reactivation, the slide continued to move at a rate of several feet per day across a 600-ft-wide section of roadway embankment. A total downslope displacement of 150 feet was measured below the roadway, tapering to several feet of slope movement above the roadway. The slide displaced the roadway downslope, forcing road closure. Surface measurements indicated that the slide continued to move with a decreasing rate until the end of June, 2008. Currently, the slide is stable and is not showing movements of any significance. Most of the measured movement occurred below the roadway and up to 500 feet above the roadway; however, indications of movement were observed over 2,000 feet above the roadway.

Regional Geology

The general geologic conditions at the site consist of Tertiary and Upper Cretaceous sedimentary rocks overlain by more recent volcanic rocks. The sedimentary rocks consist of shales and sandstones. The volcanics consist of basalt flows, ash beds and breccia, and are related to several phases of volcanic activity.

The terrain is characterized by hummocky ground and shallow depressions which are indicative of ancient landslides that have been oversteepened due to glaciation. The top of these landslides exhibit graben features, where unstable ground has moved away from stable ground causing the head of the unstable slope to sink into the gap. Slope movement is accelerated by undercutting of the toe by the East Fork of the San Juan River. Extensive slope failures have occurred from high groundwater levels as a result of ice retreat during periods of glaciation.

The landslide debris is a heterogeneous mixture of clay soils from the sedimentary rocks and volcanic rock clasts from the upper volcanics. Upon weathering and exposure to prolonged wet and dry cycles, these soils exhibit very low shear strength and are prone to slope instability. It is also very likely that there may be water bearing pockets of broken rock surrounded and isolated by impermeable soils that can be recharged from the surface and feed water continuously into the landslide mass.

Landslides of various magnitudes have occurred in many areas within this region for years. The East Fork Landslide, in the East Fork Valley, is part of a larger complex of prehistoric landslides, evidenced by an extensive and prominent 300-ft high headscarp of volcanic bedrock covering over 300 acres several thousand feet upslope from the roadway. The ancient slide purportedly extends eastwards approximately one mile along the current roadway. The current slide shows some signs of lateral growth toward the east within the first 1,000 feet upslope from the roadway, confirming more ancient slide debris adjacent to this event. The landslide toe daylights into the East Fork of the San Juan River. Large volcaniclastic conglomerate boulders have been

deposited into the river partially constricting the channel flow and increasing the local stream velocity.

The East Fork Landside was discovered when a break was detected in a buried Xcel Energy natural-gas pipeline along the East Fork Road via the remote gas-load control center in Golden, Colorado. The pipeline was sheared as a result of the landslide activation. The slide impacted the roadway for a lateral distance of approximately 600 ft. The roadway was displaced about 150 ft downslope. A lateral shear existing along eastern and western flanks of the slide extends approximately 3,500 ft to the south (upslope from the roadway). The landslide extent is depicted on Figure 17. Associated with this shear are a series of pressure ridges that parallel the slide direction. Lateral scarps trend north-south, with at least two east-west sets of headscarps identified above the roadway. No evidence of mudflow or deep water ponding was detected on tree trunks. Extensional land features (such as sag ponds) were also observed at various locations, some of which contained water. Large conifer and aspen trees were dramatically downed and some were leaning precariously due to differential earth movements as shown on the cover photo. The slide had deposited materials 200 ft below the roadway in the East Fork of the San Juan River evidenced by freshly downed trees in the river.

The East Fork Landslide is perhaps best characterized as a translational slide with signs of minor rotational sliding below the roadway. These types of landslides exhibit sudden, rapid failure, are relatively shallow-seated, and are typically composed of loose, highly disturbed, saturated soils. Movements of these masses commonly occur along depositional boundaries that dip parallel to the slide surface, as observed on both sides of the slide, but may also occur along the upper portions of larger, deeper-seated, ancient landslide regions. Translational slides consist of downslope displacements of material parallel to the ground surface; they commonly occur along planes with increased pore pressure, faults, or contacts between bedrock and overlying soil and intermediate deposits. Rotational slides (or “slumps”) occur along a well-defined curved surface, and are likely to occur in incompetent, clayey sand material under saturated soil conditions (regions with reduced overburden effective stress). Most transitional and rotational slides feature a nearly vertical scarp near the head or sides. The presence of sag ponds or wet-site vegetation may indicate the impaired drainage that is characteristic of slide deposits. A landslide hazard is directly proportional to the depth of the saturated zone relative to the depth of the soil layer. In the case of this slide, the portion of the slide extending above the roadway is believed to have moved as a saturated soil mass along a defined shear plane, while the portion below the roadway rotated from the increased loading of the upper slide mass. The initiation trigger for the slide is yet unknown, though the accumulation of groundwater over the previous 3-5 years, during which high winter snow packs and substantial summer monsoons have recharged the subsurface soil mass faster than it can drain is a contributing factor.

Additionally, the stability of the slope is decreased by a poorly drained sag-pond headscarp area that contributes to concentrating groundwater recharge along the landslide. Although active creek erosion at the toe of the slide or soil slip failure at the toe of the slide are also possible causes for initiating the landslide, USFS personnel observations suggest the slide started above the roadway (the creek only barely runs in early May, and the creek channel has been stable for many years). A small slip (rotational slide) located between the creek and the roadway may have started the movement by removing the resisting forces on surcharged slope followed by

progressive failure up the slope. In any event, the slide moved over 150 ft downslope at the roadway, nearly 30-40 ft downslope at the main scarp which is approximately 2,500 ft up slope, and 10-20 ft at the current slope strain locations (3,500 ft upslope).

Boreholes

Three exploratory borings, labeled SI-1, SI-2, and P-1, were advanced at the landslide site with one boring located above the roadway and the other two borings downslope of the roadway. Locations of these boreholes and their detailed logs are shown with the geophysical sections later in this report.

In general, the surficial and subsurface materials at the site are mostly sandy clays interbedded with some rock fragments (gravel) with medium to low elasticity (Plasticity Index between 15 and 30). The natural moisture content of the materials encountered during drilling was generally above optimum.

Site Characterization

The landslide was evaluated by reviewing the slide conditions, groundwater conditions, subsurface materials, surface topography, and aerial photographs to produce a generalized cross section. The limited site investigation program suggested that for conservative evaluations and design, the subsurface can be subdivided into 3 types of materials: (1) 0 to 58 feet includes soft, low density, medium plasticity clays that are brecciate with low shear strengths (i.e. the material easily crumbles under finger pressure); (2) 58 to 82 feet includes hard, dense claystone with low plasticity; and (3) hard bedrock below 82 feet. The site model assumed saturated groundwater conditions of the clay/claystone unit in the vicinity of the roadway. This assumption was based on the observation of multiple groundwater seeps present below the existing roadway at the time of the investigation. It is also assumed the claystone exhibits enough hydraulic conductivity to allow propagation of groundwater either by permeability or fracture flow pathways. Low shear strengths of normally consolidated clays cause frequent problems with the stability of slopes. Accurate determination of undrained shear strength of the clay layer, a critical factor in evaluating stability, is difficult due to problems obtaining an undisturbed sample.

JACKSON MOUNTAIN LANDSLIDE

The second field site was the Jackson Mountain Landslide, a large-scale landslide complex, which extends on both side of Highway 160 at longitude 106° 55’ 23” W and latitude 37° 20’ 47’’ N. Figure 19 illustrates the location of the slide and the sensor array used for the investigation. Yeh and Associates produced a report in 2007 which is the source for much of the geologic background for this landslide.

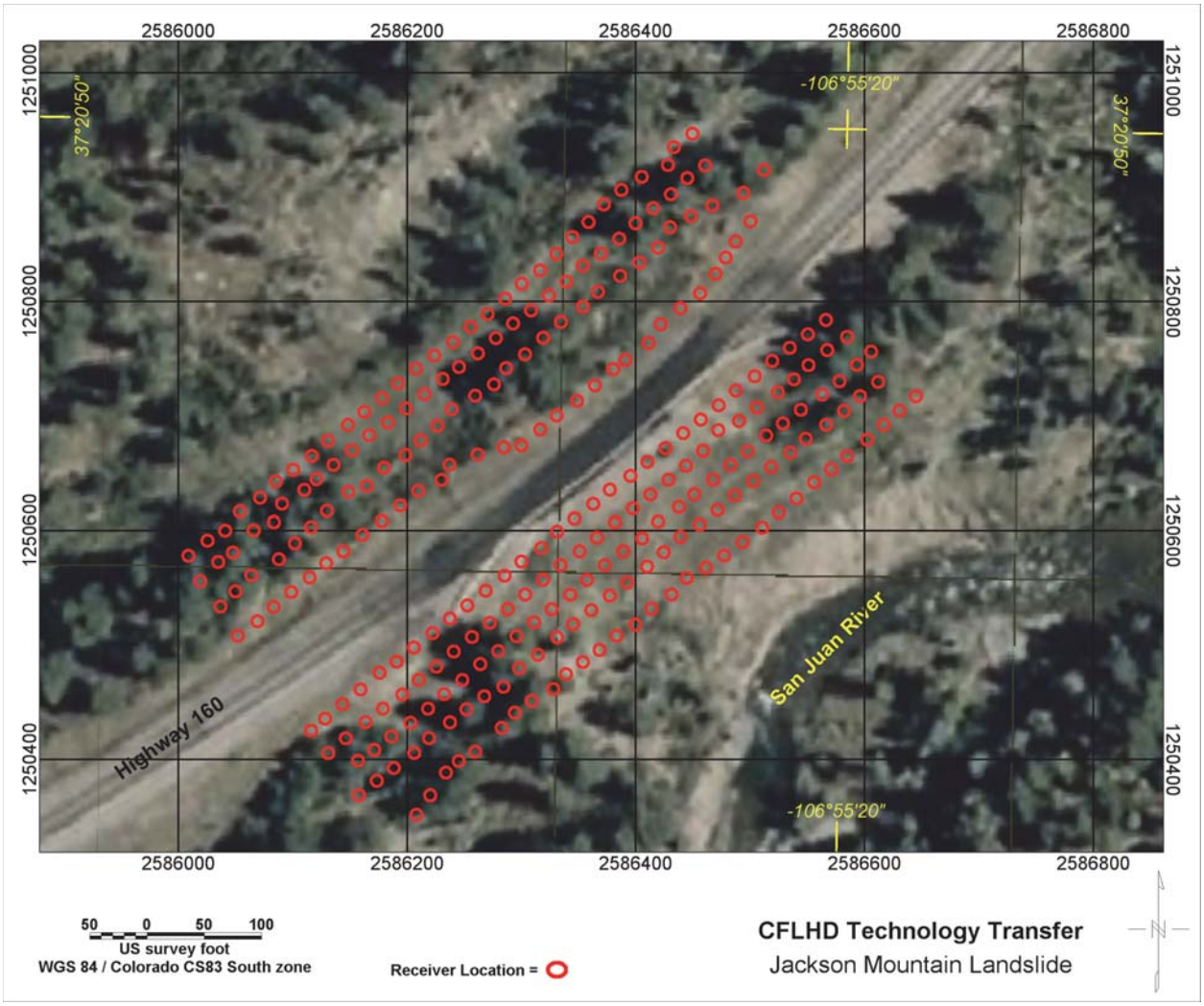

Figure 19. Photo. Location of geophysical surveys on the Jackson Mountain Landslide with receiver positions denoted with red circles.

The landslide is located approximately between Mile Markers 151.2 and 151.5 along US Highway 160. Slope movement has occurred for more than 40 years and has significantly impacted the existing roadway for approximately 900 feet. The current roadway is aligned through an active section of the landslide complex that is likely more than 2,400 feet across. Recently, an active section of approximately 300 feet of the roadway exhibited severe pavement cracking and distress that resulted from movement of the landslide. Asphalt patching and re-patching occurred every two to three months in 2009. Overall, it appears the San Juan River is actively eroding the toe of the landslide complex causing slope failures that propagate to, and above, the roadway. Additionally, the stability of the slope is decreased by a poorly drained headscarp area that contributes to already high groundwater levels.

Geologic Conditions

The project area is located on Upper Cretaceous aged sedimentary rock that was likely uplifted and displaced by a localized Tertiary aged intrusive body known as Jackson Mountain. The location of the landslide complex is on the southern flank of Jackson Mountain. To the north of the project area, the bedrock consists of glaciated Tertiary aged volcanic rock that comprises much of the Eastern San Juan Mountains. The geologic material at the project site consists of clays, weathered claystone, and relatively unweathered claystone bedrock. The more competent geologic material underlying the site was mapped as bedrock. Upon weathering and exposure to prolonged wetting and drying the strength of the claystone is reduced to that of a clay soil that typically will exhibit very low shear strength and is prone to slope instability. The landslide deposits that overlie the bedrock appear to consist of clay materials and clasts of claystone. Small intrusive igneous sills and dikes also were present in the claystone bedrock likely related to the Tertiary intrusion of Jackson Mountain.

Bedrock

The bedrock was mapped by the USGS as the Upper Cretaceous Lewis Shale. Published mapping describes this material as dark-gray clay shale that contains thin sandstone beds near its top and rusty-weathering concretions in its lower part. The sedimentary unit reportedly has a maximum thickness of 2,700 feet. Jackson Mountain is mapped as an intrusive volcanic rock that intruded the sedimentary rock units during Tertiary time. The rock unit is described as a heterogeneous intermediate to silicic hyper abyssal intrusive rock with a wide range in textures and compositions.

Surficial Deposits

Although not mapped on readily available published geologic maps, the surficial materials at the site consist of old landslide deposits with multiple episodes of movement. It appears that the most active sliding occurred within an area that is located within a larger dormant landslide complex. The material in these deposits consists primarily of clay with clasts of claystone and appears to be primarily derived from the Lewis Shale. Thin intrusive volcanic layers that are typically a few feet thick were also observed in the core. These volcanic layers were encountered within the slide material generally near the bedrock surface as documented in the driller logs from a 1988 report. Well-rounded cobbles and boulders of volcanic rock were scattered about the ground surface and were also encountered in the exploratory borings.

(blank page)

CHAPTER 4 – GEOPHYSICAL SURVEYS

The following section summarizes the geophysical field acquisition for the landslide project by site and then by technique. The field work took place from the 1st through the 11th of October 2009. There were no significant equipment problems during acquisition. The most important field issue was the positioning of the lines relative to road access and cultural features such as gas pipelines and power lines. The weather during the field operations began warm and sunny and ended with light snow.

EAST FORK LANDSLIDE

The majority of the data acquired at the East Fork Landslide site was within the 3D grid as shown on Figure 20 which in turn was mostly within the borders of the landslide. As seen in the figure below, a single line extends out from the body of the survey. The single line, which is considered to be an extension of line 8, was designed to provide comparison data outside the recently disturbed ground. The extension also provides a 2D comparison to the nearby 3D data. Figure 20 displays the locations surveyed during the acquisition with the cultural features such as gas pipeline marked with red triangles.

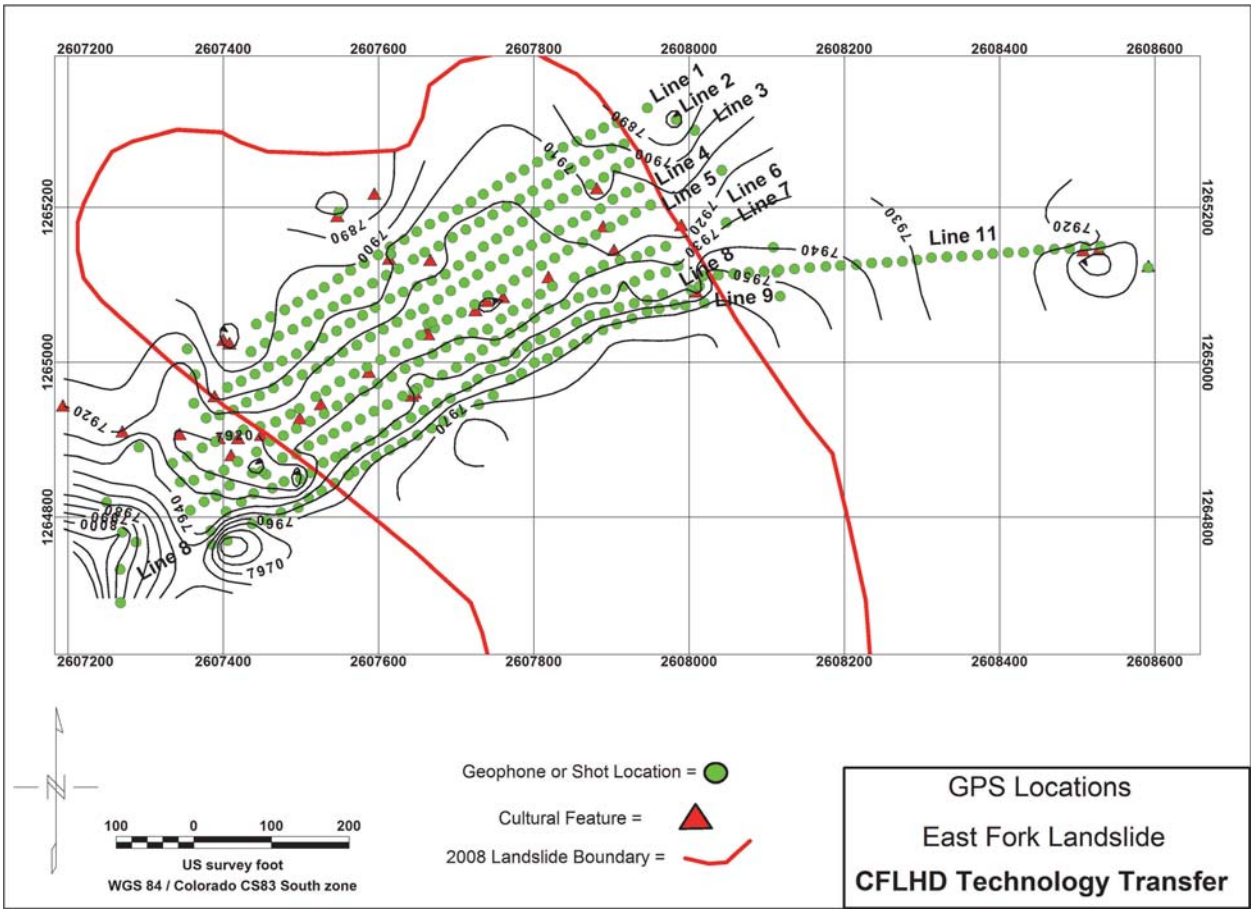

Figure 20. Map. GPS positions (culture, geophones and electrodes) and elevations for East Fork Landslide.

Induced Polarization

Electrical data acquisition consisting of induced polarization and resistivity surveys for the East Fork Landslide was done October 8-10, 2009. Figure 20 shows the field survey design for the electrical survey. The two electrical surveys were carried out together by a Zonge Electrical Resistivity Tomography Acquisition (ZETA) system. The ZETA is a 31 channel system which allows for 30 pairs of electrodes. Electrodes were placed at the same positions as the geophones had previously occupied. The electrode stations were laid out in the form of 9 lines roughly perpendicular to the flow direction of the landslide. The lines of electrodes were used as individual 2D lines, and then the receivers were used again as part of a 3D grid. A three-spread extension of Line 8 as shown on Figure 20 was acquired to provide data both within and outside of the currently recognized landslide area. The extended Line 8 was a 2D induced polarization and resistivity section for comparison with the 3D grid of electrical data.

In addition to the standard inline acquisition schedule described in the geophysical methods section of Chapter 2, an innovative broadside schedule was developed. The broadside array pattern consisted of two parallel lines of electrodes as seen in Figure 21. One line was used as for the transmitter (current) electrodes and another was the receiver (potential) electrodes. The current dipole was thus alongside the line of receiver rather than inline as conventionally done. With the "broadside" configuration the volume of rock between the two lines is affected by the changes in the electric field caused by the transmitter.

For the landslide field work the electrode lines were divided into groups of three with first and third lines being active. To get the desired lateral separation the middle line of each triple was inactive. For the East Fork Landslide the pairings were L1-L3, L4-L6, and L7-L9.

A number of cultural (man-made) features were identified within the survey boundary or nearby, the most important of which was an Xcel gas line which runs through the center in the survey area. Effect of the cultural features on the electrical data was not a significant problem at the East Fork Landslide site.

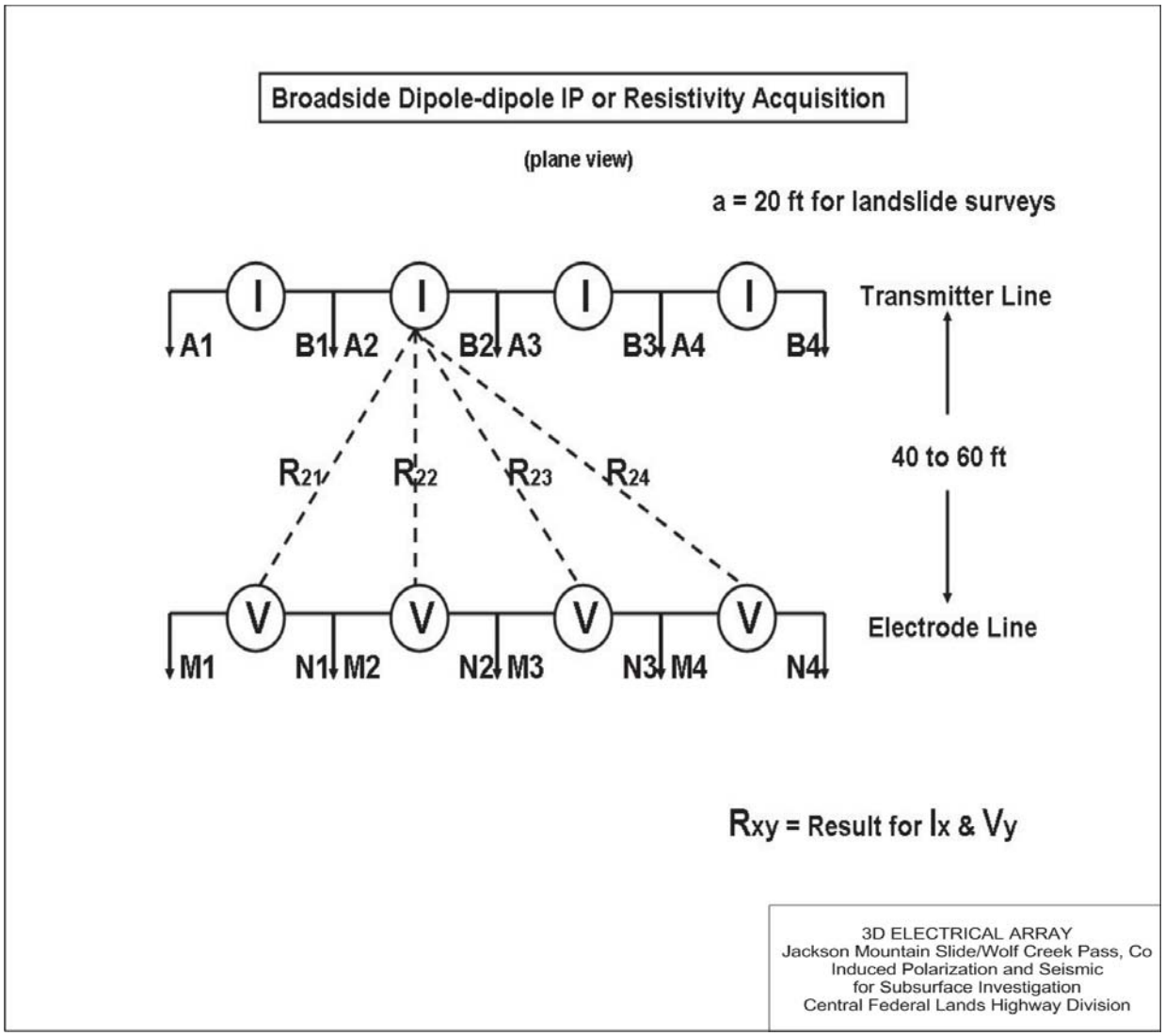

Figure 21. Diagram. Electrical acquisition with a broadside array for 3D data.

Seismic Refraction

The 3D seismic refraction acquisition took place October 1-3, 2009. Figure 22 shows the seismic field survey design. The geophone spreads were setup in 2D patterns along Lines 1-9 as shown in Figure 20. Geophone spacing along each grid line was nominally 20 ft (surveyed by DGPS). The cross line spacing for the grid was approximately 30 feet. Shot points were placed along lines and at off end in-line locations (also surveyed by DGPS). The recording equipment for this survey was a Seistronix EX-6 seismograph recording a total of 306 channels. This system is a 24-bit digital system and record length was 500 ms sampled at a rate of 0.25 ms. The data was recorded using the SEG2 format. The receivers consisted of one or two 30-Hertz geophones at each station. Mechanical P-wave seismic energy was created with the 20-pound sledgehammer striking an aluminum plate at locations shown on Figure 22. Four hammer blows were used per station and the impacts were stacked to create the seismic trace for the station. Explosive charges for the Poulter shots consisted of 90 grain Trojan cast booster detonated 1.5 feet above ground surface were detonated at locations shown on Figure 22.

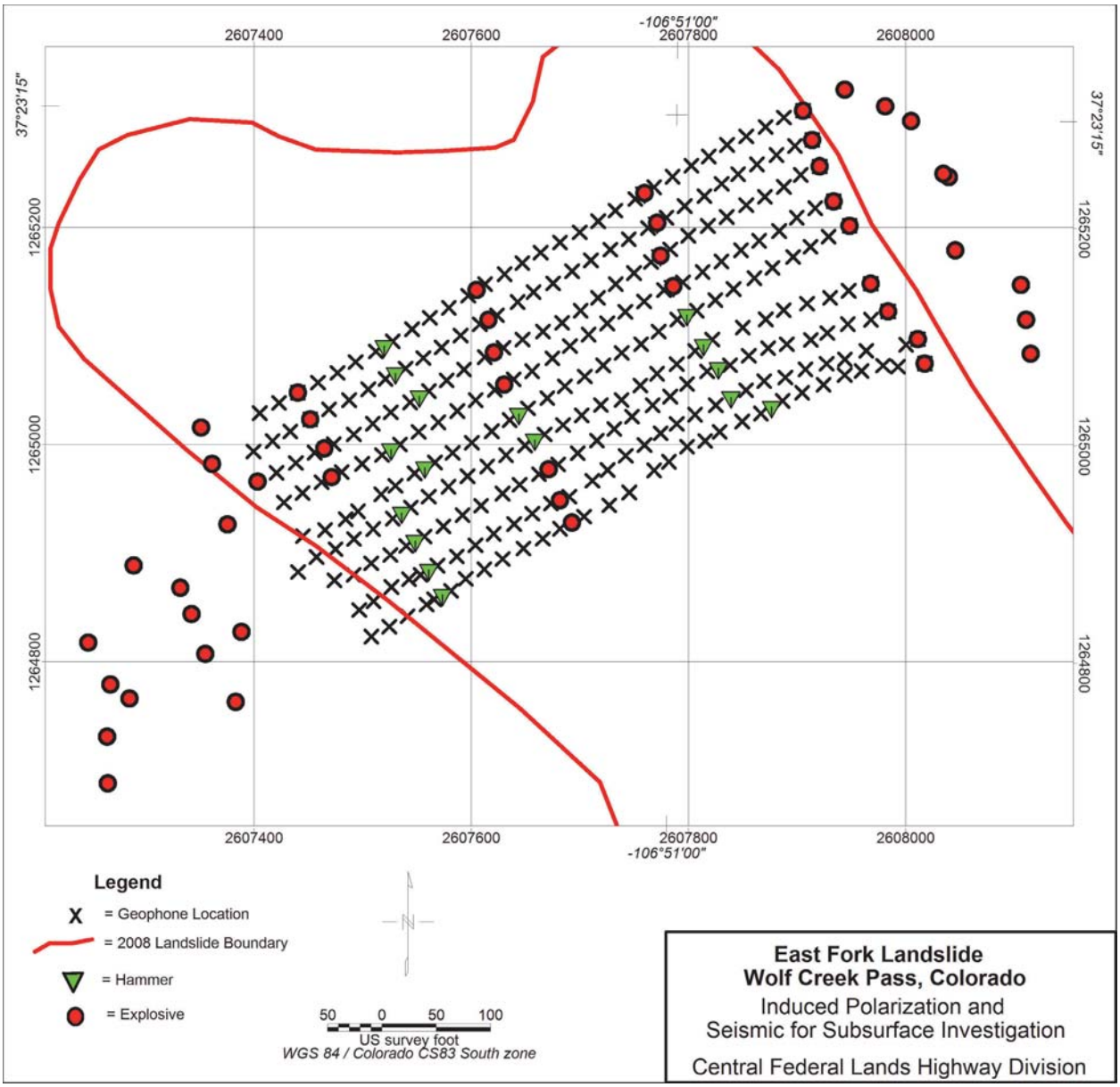

Figure 22. Map. GPS positions for shotpoints and geophones for the 3D grid at East Fork Landslide.

2D seismic refraction data was also collected at the East Fork Landslide site on October 3, 2009. The 2D line consisted of re-shooting the grid Line #8 with a fixed 64-channel geophone spread setup. Line 8 was then extended 540 ft east to provide off-landslide data for comparison to the data from the 3D grid. The recording parameters were the same as those used for the 3D grid. The seismic energy source for all shots along this 2D line was a 20-pound sledge hammer impacting metal plate. For the 2D survey the number of hammer impacts was increased from 8 to 12, which were then stacked for the final seismic record.

JACKSON MOUNTAIN LANDSLIDE

The data acquired at the Jackson Mountain Landslide site was divided into two small 3D grids due to the fact US Highway 160 runs through the center of the survey area. As shown on Figures 23 and 24, the highway (marked with black lines) split the survey area into a four-line block on the uphill (northwest) side and a five-line block on the downhill (southeast) side. Data collection was confined to within the borders of the landslide.

Induced Polarization

Electrical data was acquired at the Jackson Mountain Landslide site on October 10-11, 2009. Figure 23 shows the field layout of electrodes. In addition to the IP data, resistivity values were also collected with the Zonge Electrical Resistivity Tomography Acquisition (ZETA) system. A total of nine receiver lines were surveyed. For the electrical observations sequential acquisition of IP and resistivity data was performed using the same receiver locations on nine lines, eight of which were used for the geophone positions for the 3D seismic refraction survey (Figure 24). The electrode stations were laid out on the lines roughly perpendicular to the flow direction of the landslide and parallel to the highway which runs through the survey area. A line of electrodes was used as an individual 2D line of receiver and again as part of a 3D grid consisting of three parallel lines of receivers. The data for the three line grids (two active lines) were acquired using the transmitters in a broadside configuration described in the previous East Fork Landslide section as shown on Figure 21. The broadside triples were bounded by lines 1-3, 3-5, and 7-9.

Figure 23 identifies positions of the electrical and seismic sensors used at this site. Note the survey area includes Highway 160. Also a gas pipeline line, a power line, and a fence line are present on the north side of the highway. These cultural features did not have any significant effect on the electrical (or seismic) data. The highway traffic could have had a major impact on the seismic survey, but traffic was halted for each shot record acquired. Therefore, the highway did not impact the geophysical data quality but rather its presence distorted the ideal layout geometry and caused a gap in the desired 3D array pattern.

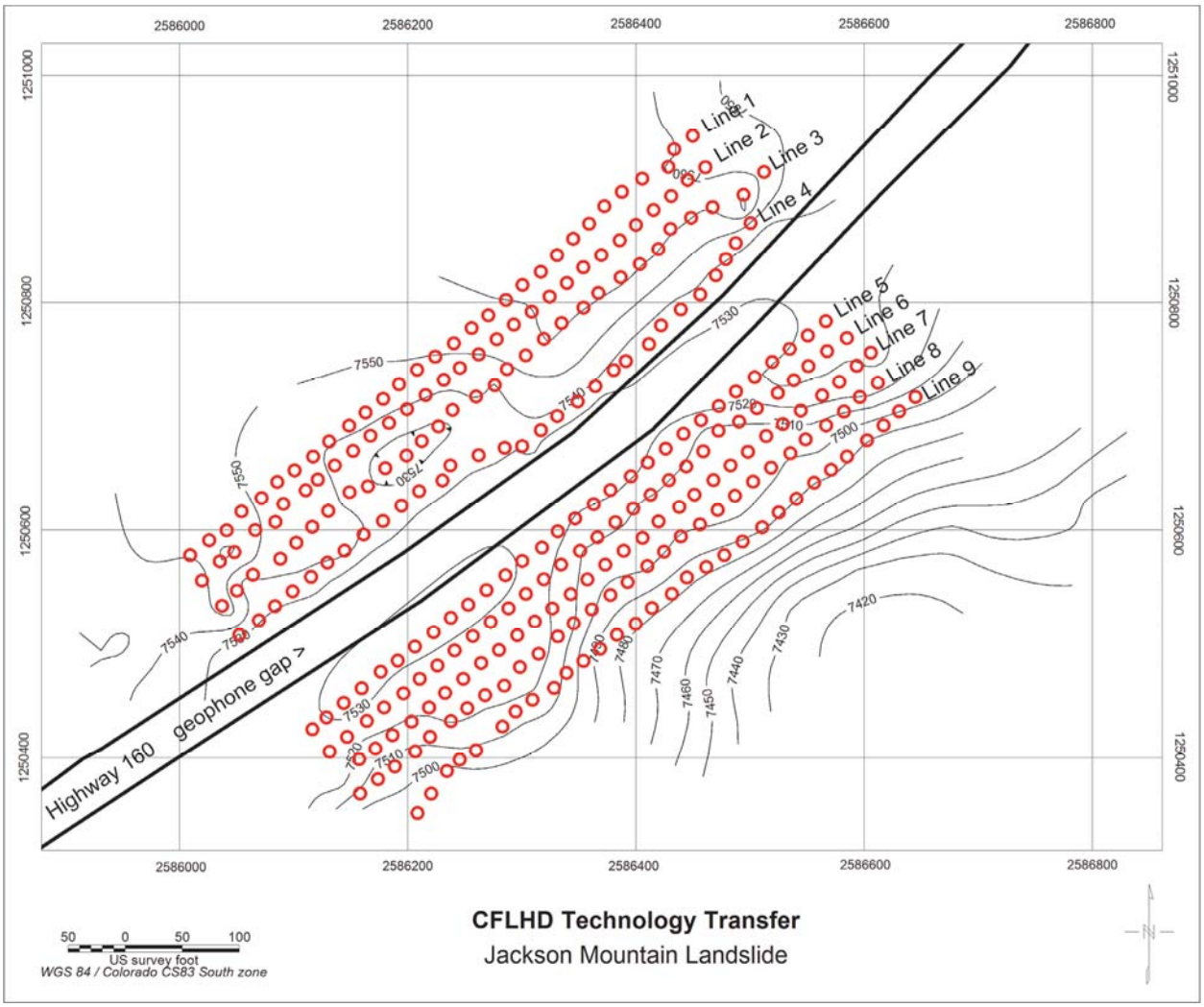

Figure 23. Map. GPS positions of receivers (geophones and electrodes) with elevation contours for the Jackson Mountain Landslide.

Seismic Refraction

The seismic refraction acquisition for the Jackson Mountain Landslide took place October 6, 2009. Figure 24 show the seismic field survey design for the 3D grids. Because of the busy roadway geophones were setup in two separate 3D grid patterns, one each side of Highway 160. The fixed 3D array on the downhill side of the highway, that is, on the southeast side consisted of 124 geophones as shown on Figure 24. The uphill (northwest) side had a 3D array of 123 geophones. Each 3D array of geophones was positioned in the form of four lines. Geophone spacing along each grid line was approximately 20 ft (surveyed by DGPS). The cross line spacing for the grid was nominally 25 to 30 feet with a larger gap for the highway. Shot points were placed along lines and at off end in-line locations (also surveyed by DGPS). The recording equipment: for this survey was a Seistronix EX-6 seismograph. Record length was 500 ms sampled at a rate of 0.25 ms. The data was recorded using the SEG2 format. The receivers were one or two 30-Hz geophones at each station. Mechanical P-wave seismic energy was created with the 20-pound sledgehammer striking an aluminum plate at positions shown on Figure 24.

Four hammer blows were used per station and the impacts were stacked to create the seismic trace for the station. Explosive charges for the Poulter shots consisted of 90 grain Trojan cast booster detonated 1.5 feet above ground surface detonated at positions shown on Figure 24.

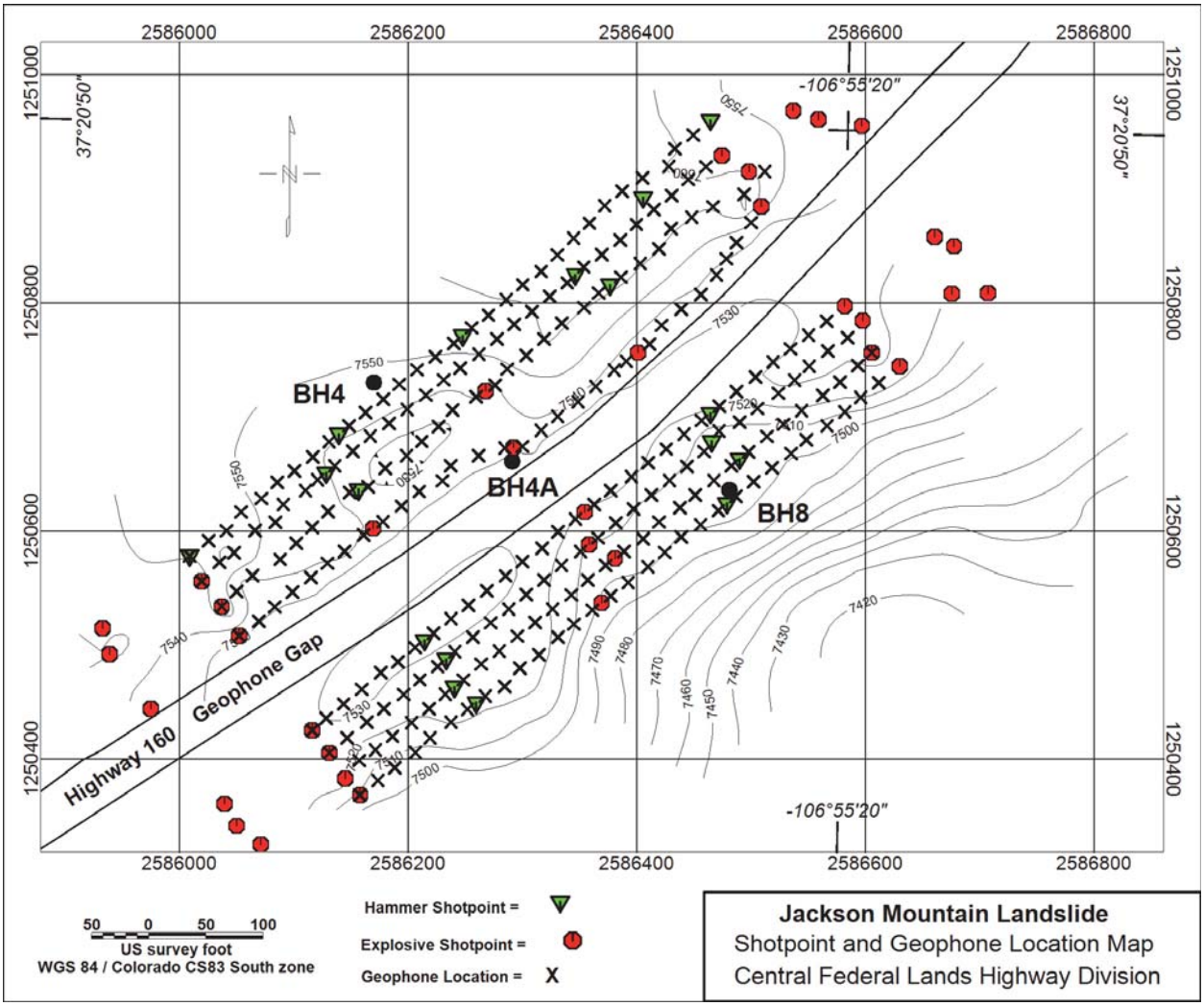

Figure 24. Map. GPS positions for shotpoints and geophones for the 3D grid at Jackson Mountain Landslide; also shown are boring locations used for geologic correlation.

(blank page)

CHAPTER 5 – GEOPHYSICAL ANALYSIS AND RESULTS

EAST FORK LANDSLIDE

The receiver locations on the East Fork Landslide are shown in Figure 25. A convention for numbering slices that are extracted from the 3D volume images, which will be shown in the following results sections, is also defined on Figure 25. Generally, the slice numbers increase southward, which is progressively up the slope.

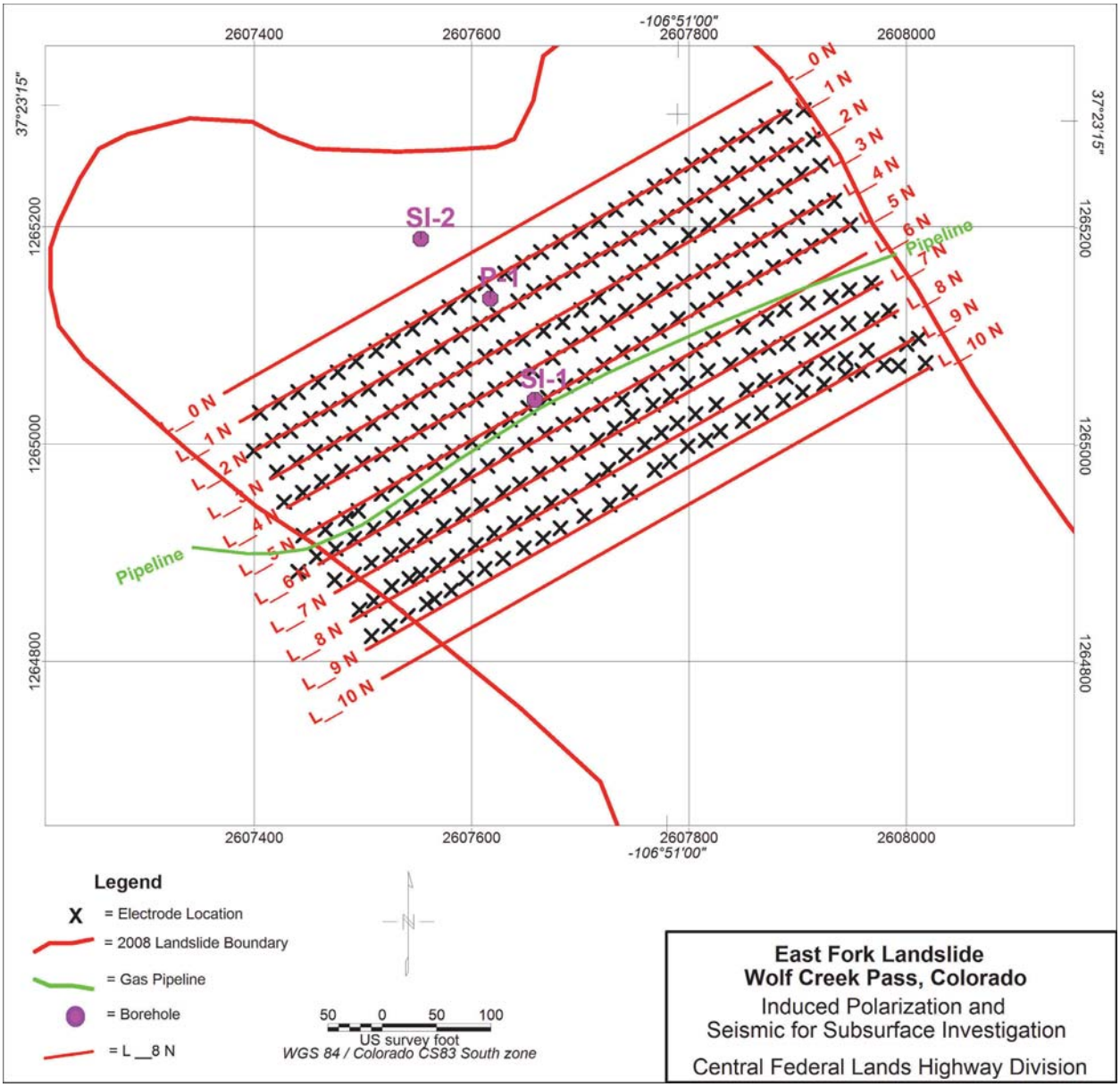

Figure 25. Location and numbering of slices through the 3D volume based on receiver locations within the 3D grid. Representative IP, resistivity, and velocity slices are presented in report figures in the following sections.

Induced Polarization

The following series of 2D plan maps, presented in Figures 26 through 30, are horizontal slices through the 3D IP data volume starting at the highest elevation and working downward at 30-foot depth increments. The IP slices show values that are a chaotic mix of low amplitude anomalies that apparently have no pattern which would relate to geology or features of the slidemass. The haphazard pattern may reflect the response of clay minerals that have been jumbled during travel down the slope. Appendix A contains horizontal and vertical slices through the IP data volume; a CD is included with this report that has a 3D PDF file of the IP volume image results which can then be viewed in 3D using the Adobe 3D viewer.

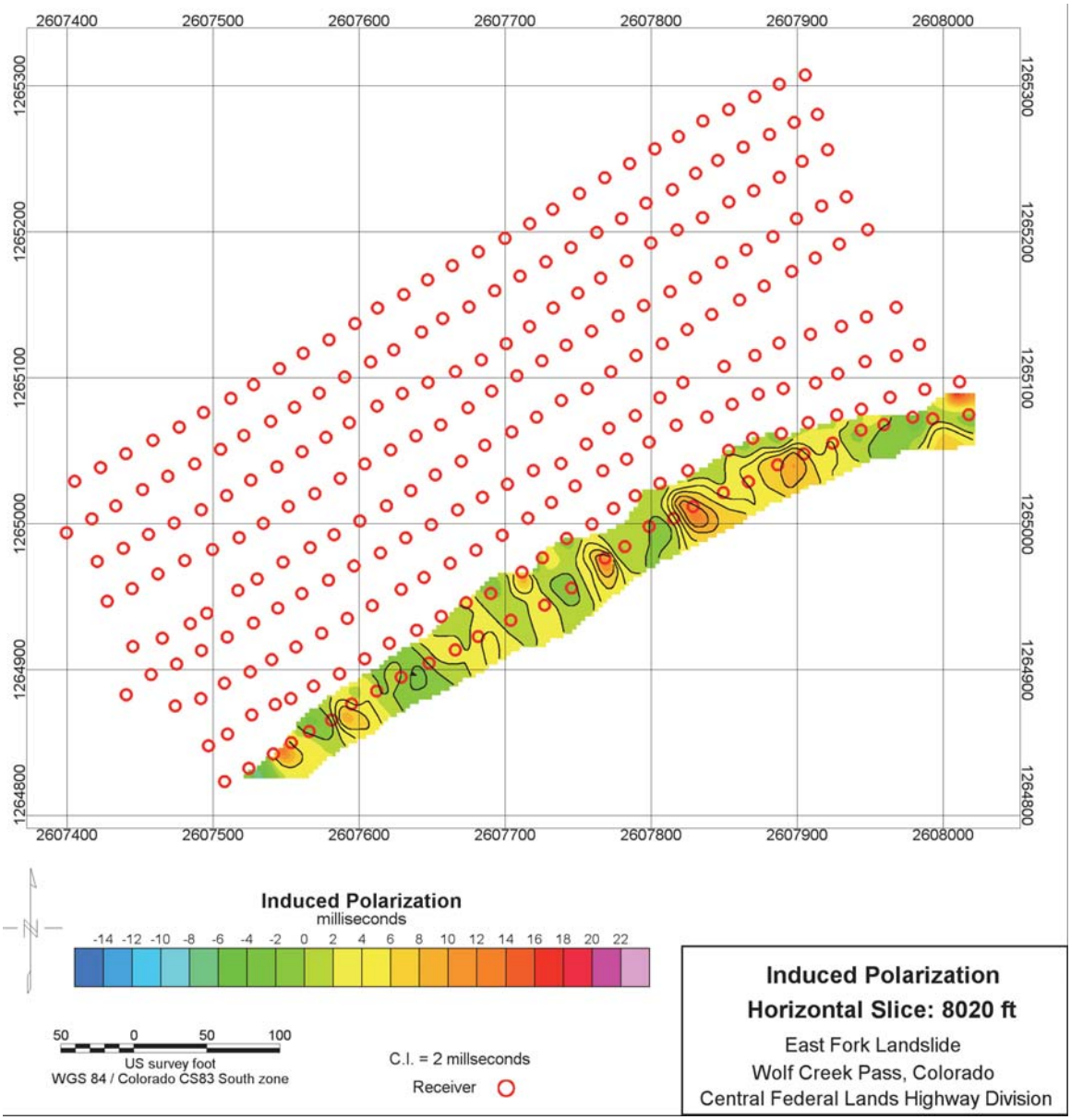

Figure 26. Map. Horizontal slice through East Fork Landslide IP volume at elevation 8020 feet.

The horizontal slice at an elevation of 8020 feet, shown in Figure 26, just clips the highest elevations found within the survey area. The strip of IP data reflects the shallow response to the transmitted signal. The features in the data vary rapidly (spatially) but are small amplitude.

The IP data at 7990 feet as shown on Figure 27 represent a slice ranging from the surface at the northwest edge of the contours to roughly 40 feet deep at the southeast edge. The shallow response at the northwest edge has fewer small anomalies and is distinctly "quieter" than the areas farther beneath.

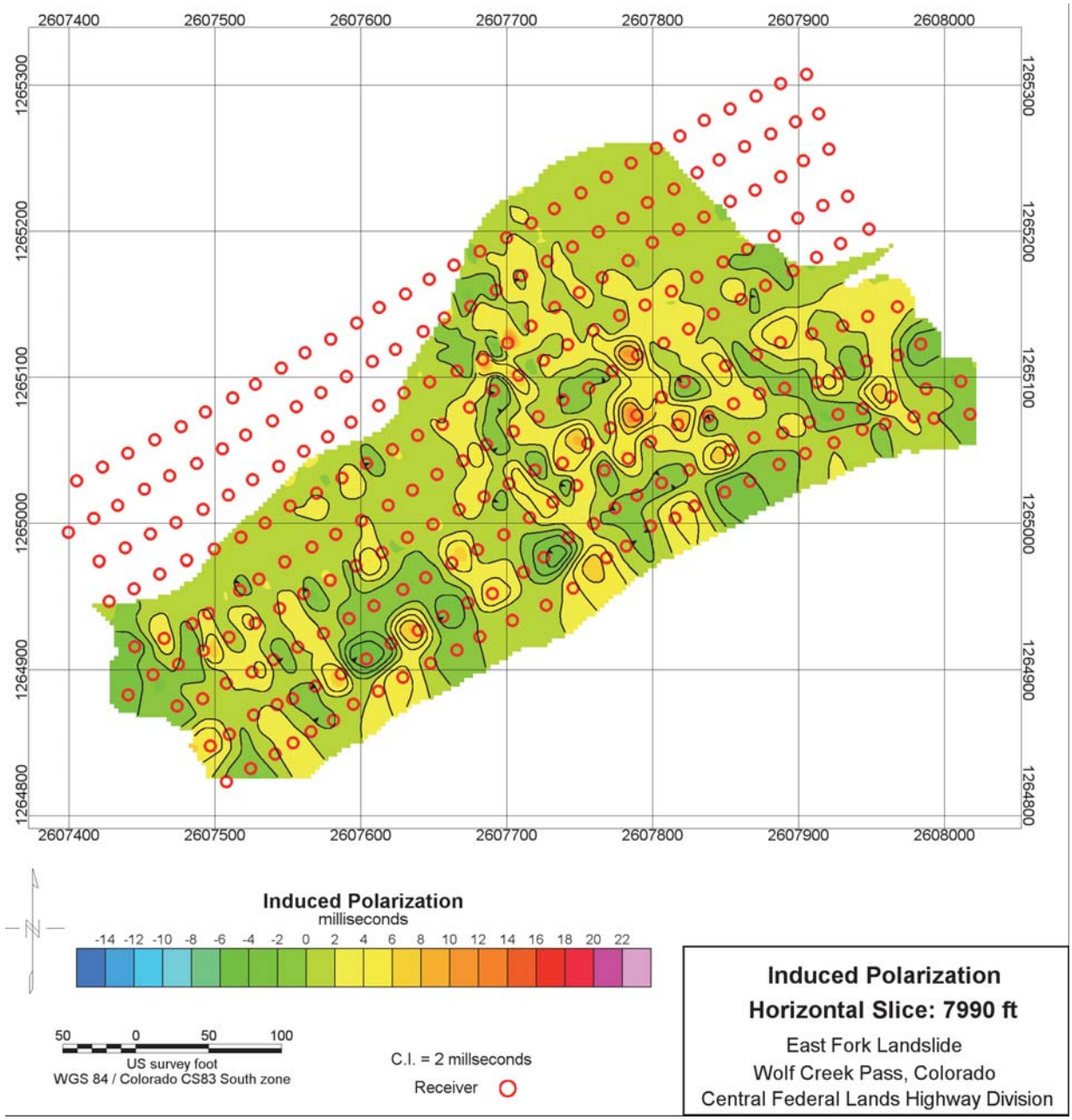

Figure 27. Map. Horizontal slice through East Fork Landslide IP volume at elevation 7990 feet.

The slice at 7960 feet as shown on Figure 28 has a few, very local, anomalies over 15 milliseconds. These responses are still well within the expected response for clays but they do represent an increase relative to the shallower IP slices. Additional IP depth slices at decreasing elevations are shown on Figures 29 and 30.

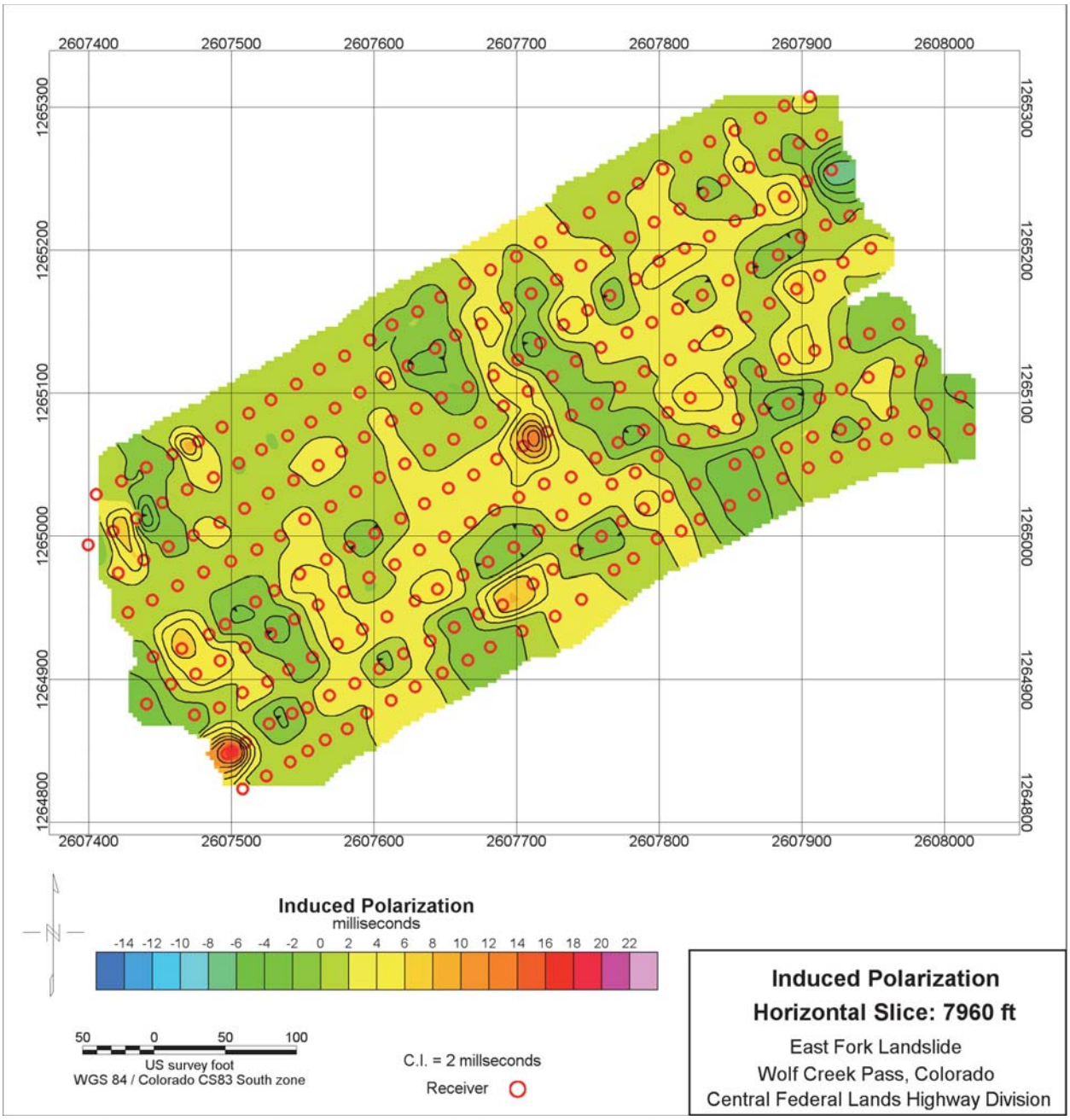

Figure 28. Map. Horizontal slice through East Fork Landslide IP volume at elevation 7960 feet.

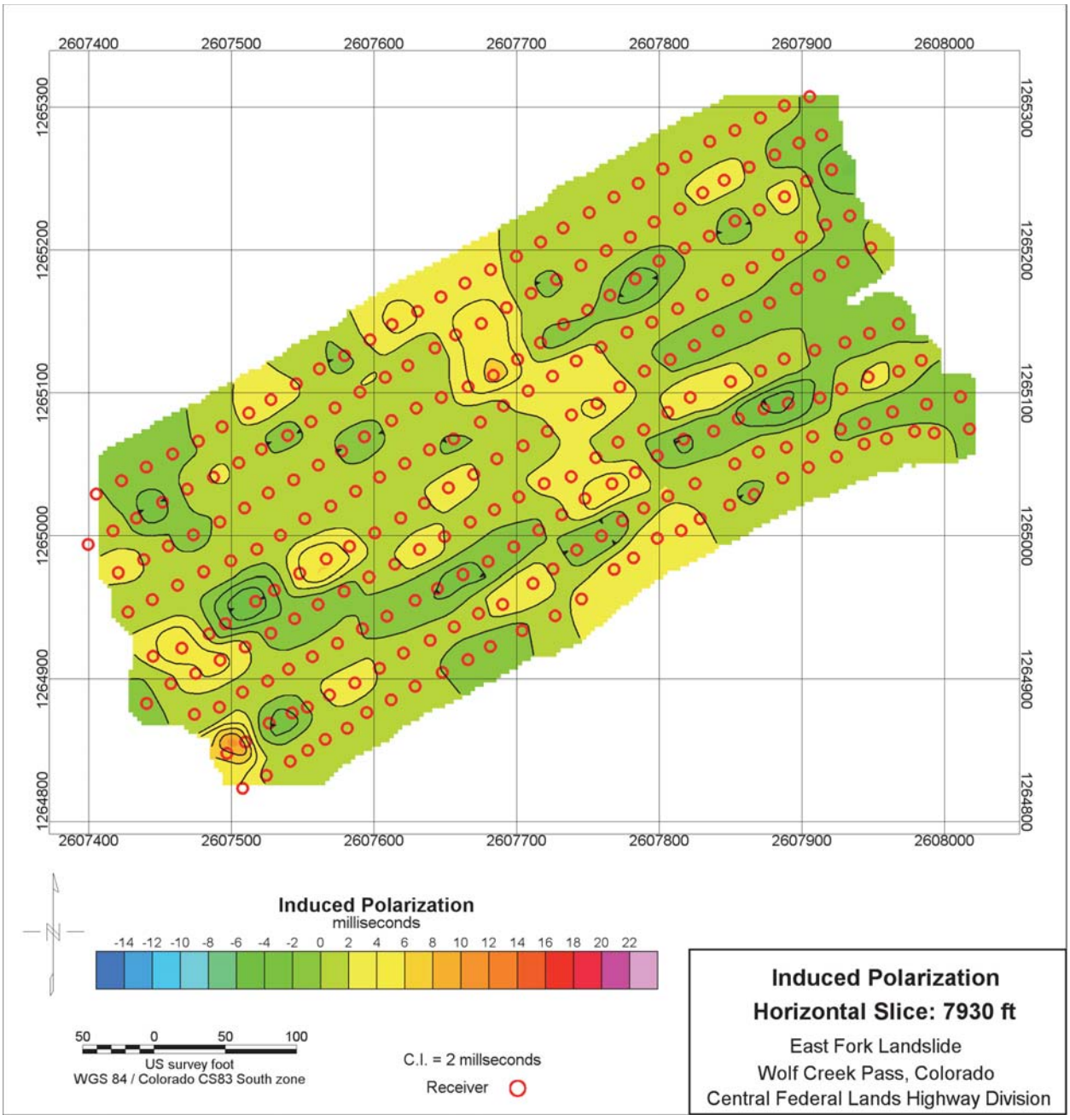

Figure 29. Map. Horizontal slice through East Fork Landslide IP volume at elevation 7930 feet.

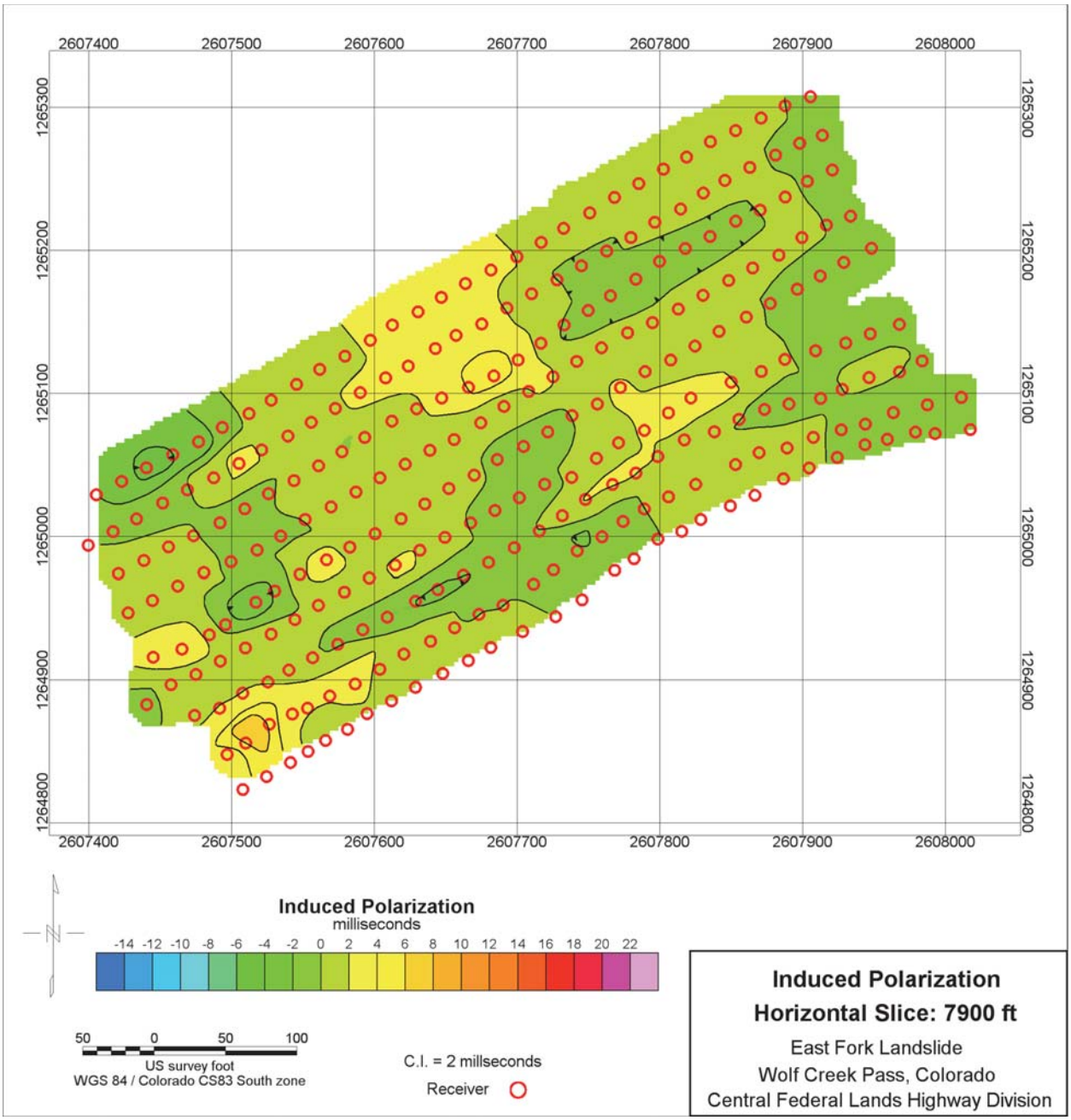

Figure 30. Map. Horizontal slice through East Fork Landslide IP volume at elevation 7900 feet.

The IP effect can be seen to decrease deeper beneath the slope. The chaotic nature of the low-amplitude anomalies in the near-surface are not present at the deepest elevation presented (7900 feet). It is likely that at this depth the majority of the horizontal slice is below the slide plan, and the more smooth nature IP map reflects materials which were not translated, as opposed to the near-surface slidemass materials.

A series of 2D slices, or vertical cross-sections, extracted from the 3D IP volume are presented below; see Figure 25 for location of the slices. Figures 31 through 35 are slices through the 3D IP volume. Note the color scale (i.e., range of IP values) for the 2D vertical slices has changed compared with the 2D horizontal depth slices. The change is because the range of IP values in the vertical slices is half as great as the range for the larger plan maps. The IP contour interval is 1 ms for the 2D cross-sections (2 ms was used for the horizontal depth slices).

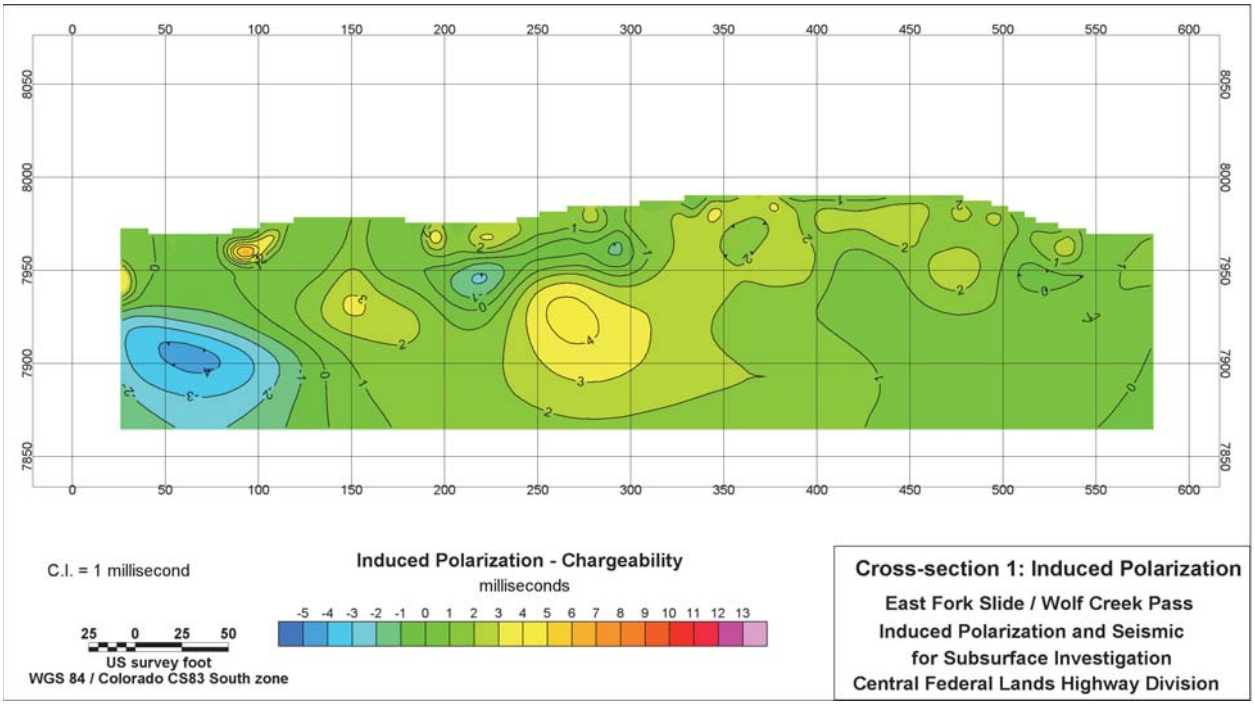

Figure 31. Plot. East Fork Landslide IP receiver slice #1N.

It can be seen in this series of cross-sections that the upper 50 feet (approximately) has many more localized anomalies, with a wider variability. Deeper in each section, the IP values are smooth, larger, less variable and less jumbled, which is interpreted to represent materials that are more geologic-like than slide-mass materials which are anticipated to have extreme variability.

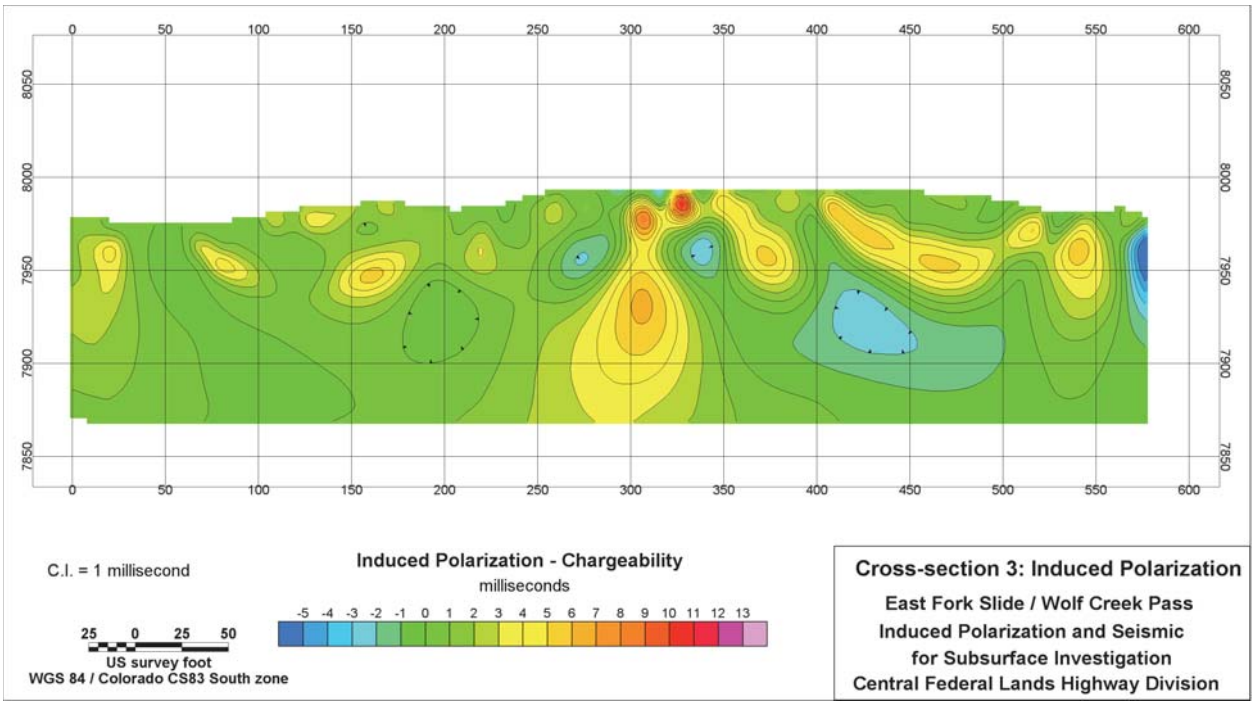

Figure 32. Plot. East Fork Landslide IP receiver cross-section #3N.

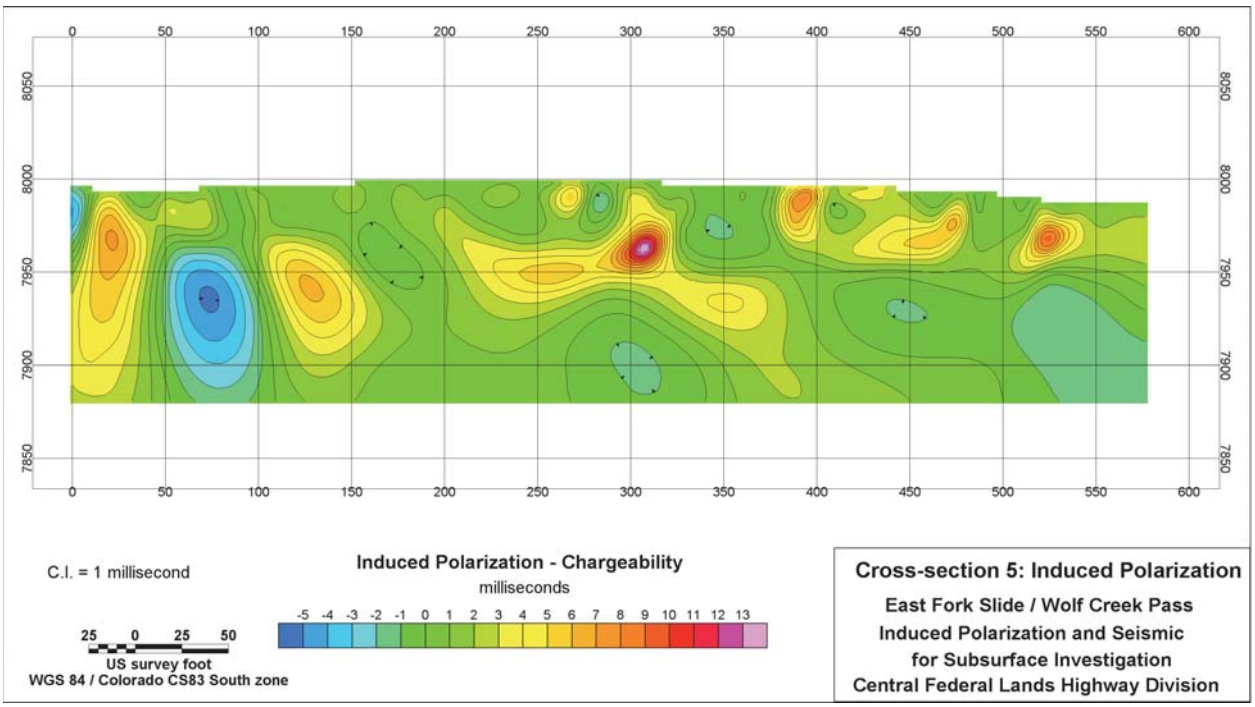

Figure 33. Plot. East Fork Landslide IP receiver cross-section #5N.

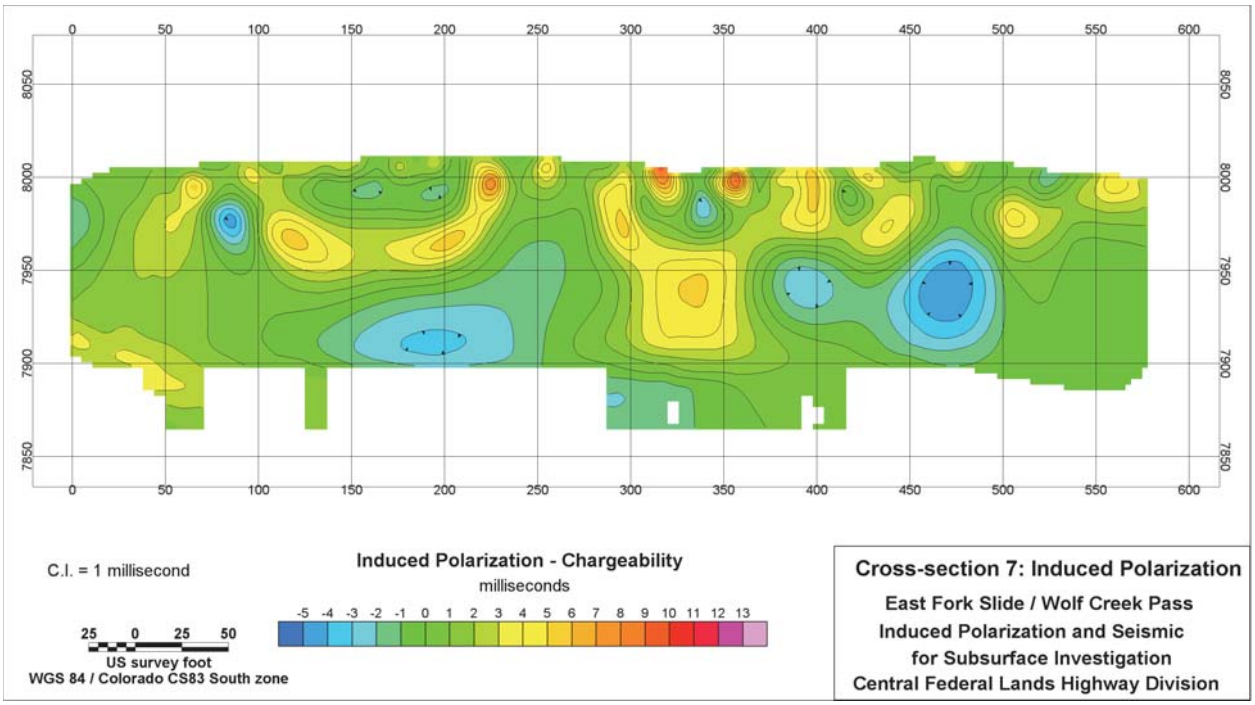

Figure 34. Plot. East Fork Landslide IP receiver cross-section #7N.

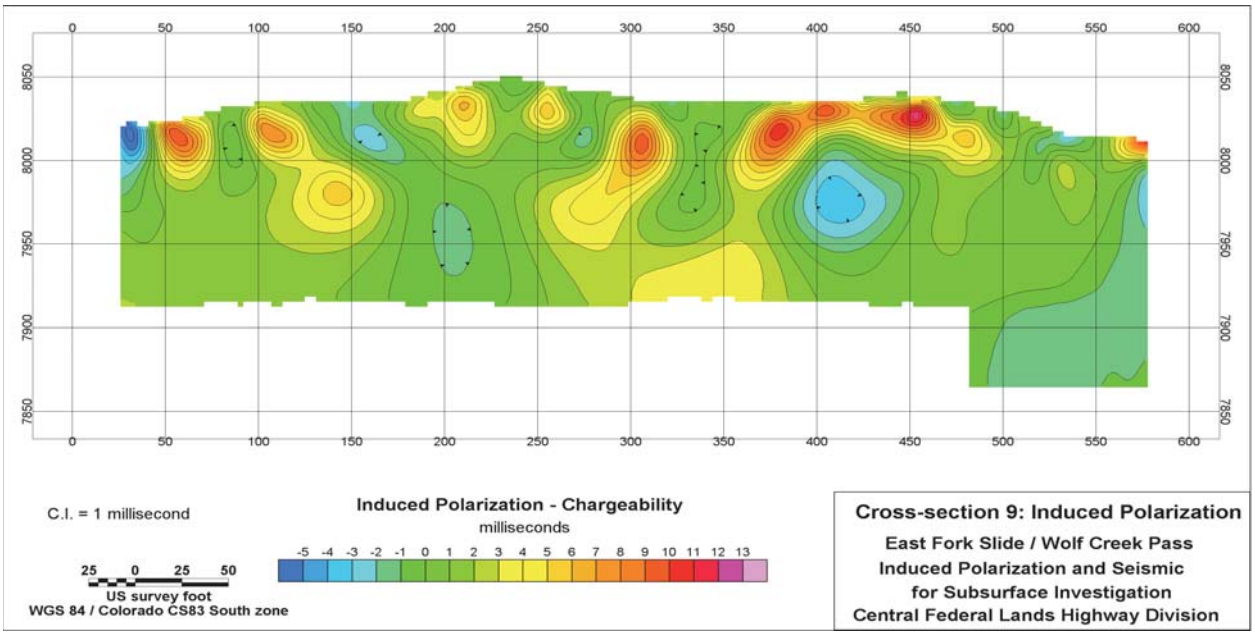

Figure 35. Plot. East Fork Landslide IP receiver cross-section #9N.

IP data were to be collected off the slide for comparison. The long 2D line which extends beyond the edges of the most recent movement of East Fork landslide has similar mapped IP response inside and outside the known (2008) landslide. This long line is identified as "Line 11"; it is the in-slide portion of Line 8 plus a northeast extension. Figure 36 shows the full extent of Line 11 and its relationship to the rest of the 3D IP grid. Figures 37 and 38 present the 2D IP cross-sectional results from this long line.

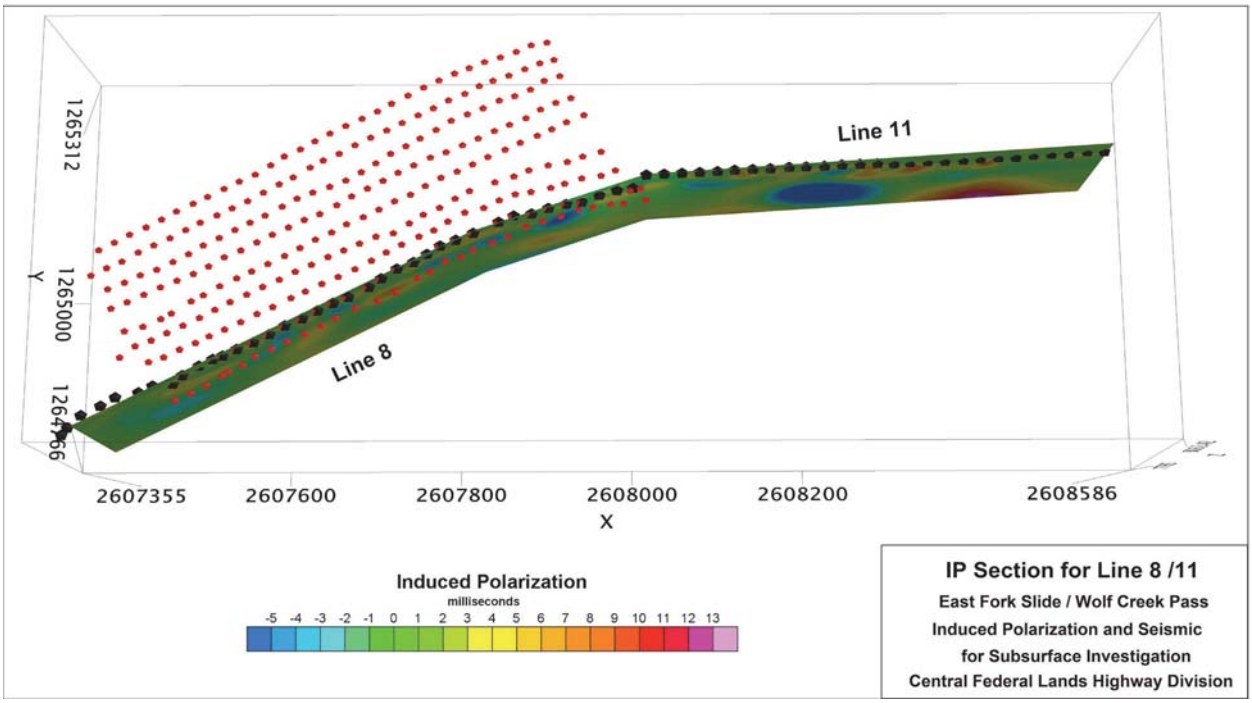

Figure 36. Plot. Location of long 2D IP, combination of Line 8 and 11 (Line 8/11), line relative to the East Fork Landslide 3D grid.

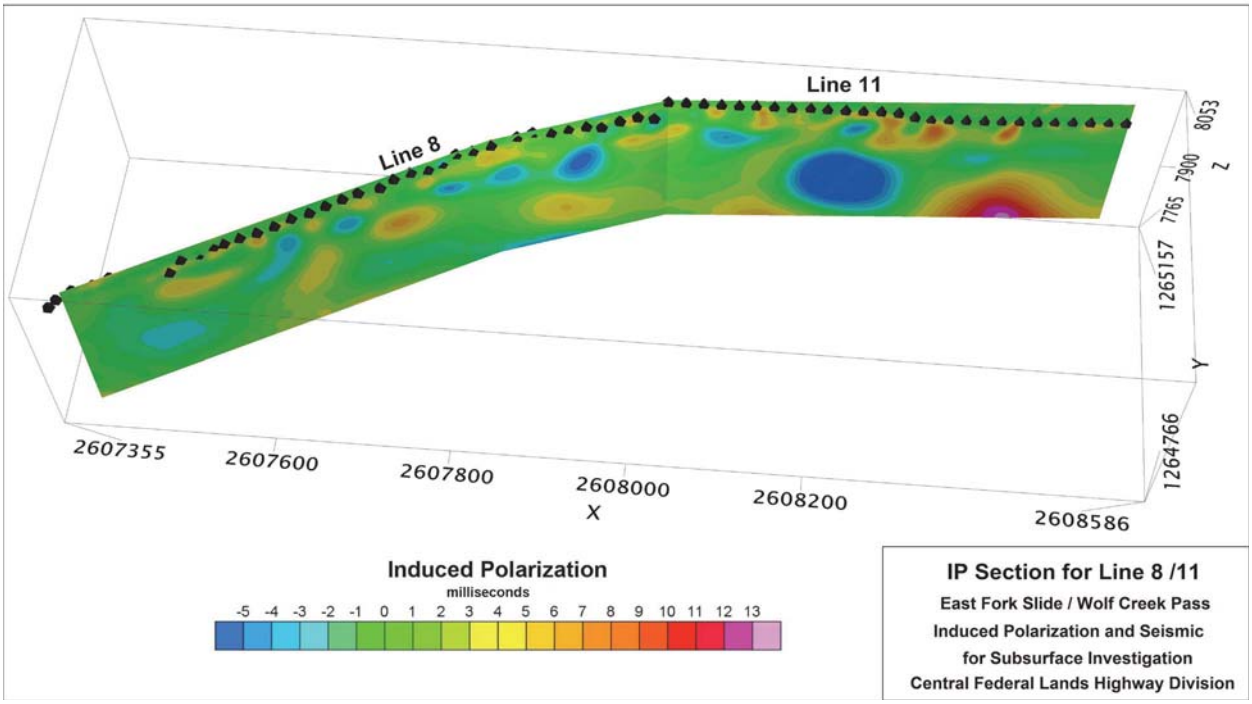

Figure 37. Plot. 2D IP section along Line 8/11 with electrodes marked with black triangles

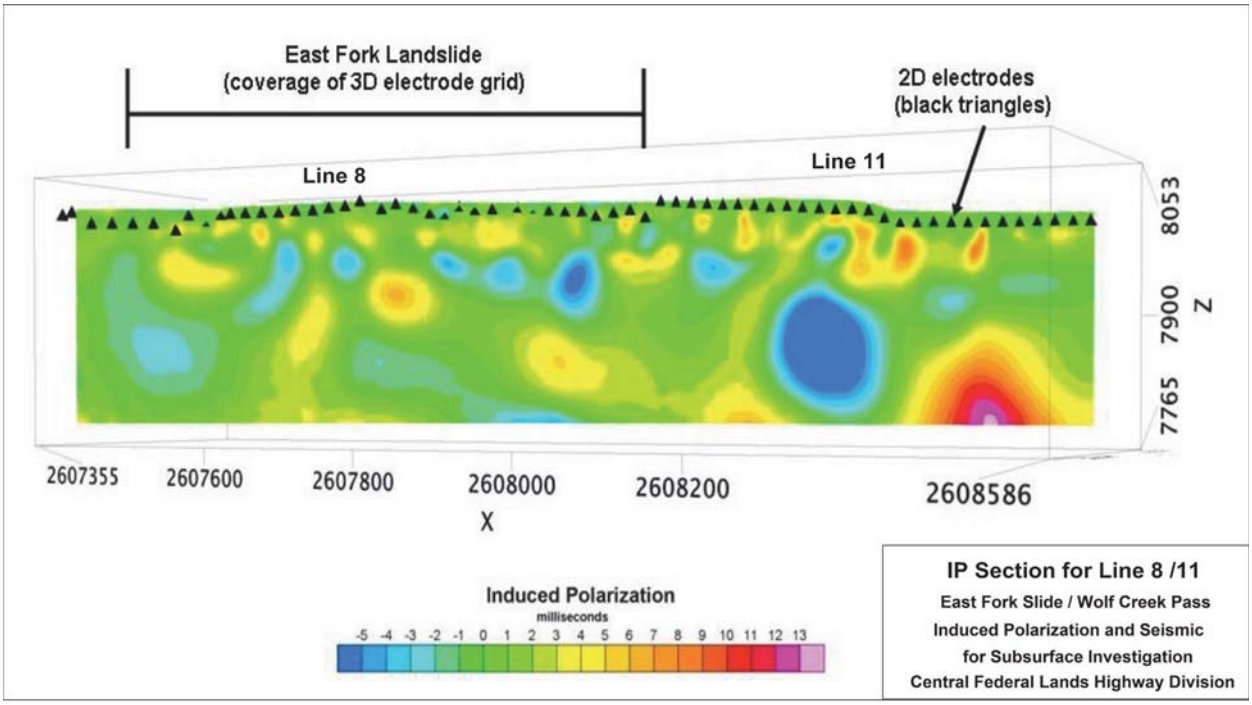

Figure 38. Plot. Line 8/11 IP section with same color range as applied to IP slices extracted from the 3D IP volume.

Very similar trends in the IP data are seen within the landslide mass (imaged with the 3D array) and within materials that were *anticipated* to be outside the landslide. Further inspection of the Google Earth areal imagery indicates that the northeast extension did not, in fact, get on native

geologic materials. That is, the extension appears to be on a historic portion of East Fork landslide that did not reactivate in 2009. This was not observed in the field; the line was extended beyond the most obvious and recent edge of the slidemass. The IP data reflect that with the same chaotic upper 50 feet of low-amplitude IP anomalies and broader IP responses at depth. The high and low IP values (red and blue, respectively) obtained at depth beneath the extension off the grid are unlike other IP values beneath this site. They may represent in situ volcanic bedrock, which often causes IP effect because of the mafic minerals and the quick breakdown or weathering to clay that occurs in the Tertiary basalt flows in the San Juan Volcanic field.

Resistivity

Similar to the IP data presentation the following 2D plan maps, shown in Figures 39 through 43, are horizontal depth slices through the resistivity data volume starting at the highest elevation and working downward through the volume at 30-foot intervals. Figure 39 is a horizontal slice at an elevation of 8020 feet. The strip of resistivity data reflects the shallow (fifteen feet or less) response of the earth. The color range for all of the following resistivity contour maps is designed to reveal small changes in subsurface resistivity. The overall range of resistivity values obtained is small compared to geologic settings which may contain a variety of soil and rock types. The southwestern portion of the strip in the yellow and orange colors, high resistivity, is near the western edge of the mapped landslide or perhaps outside the slidemass.

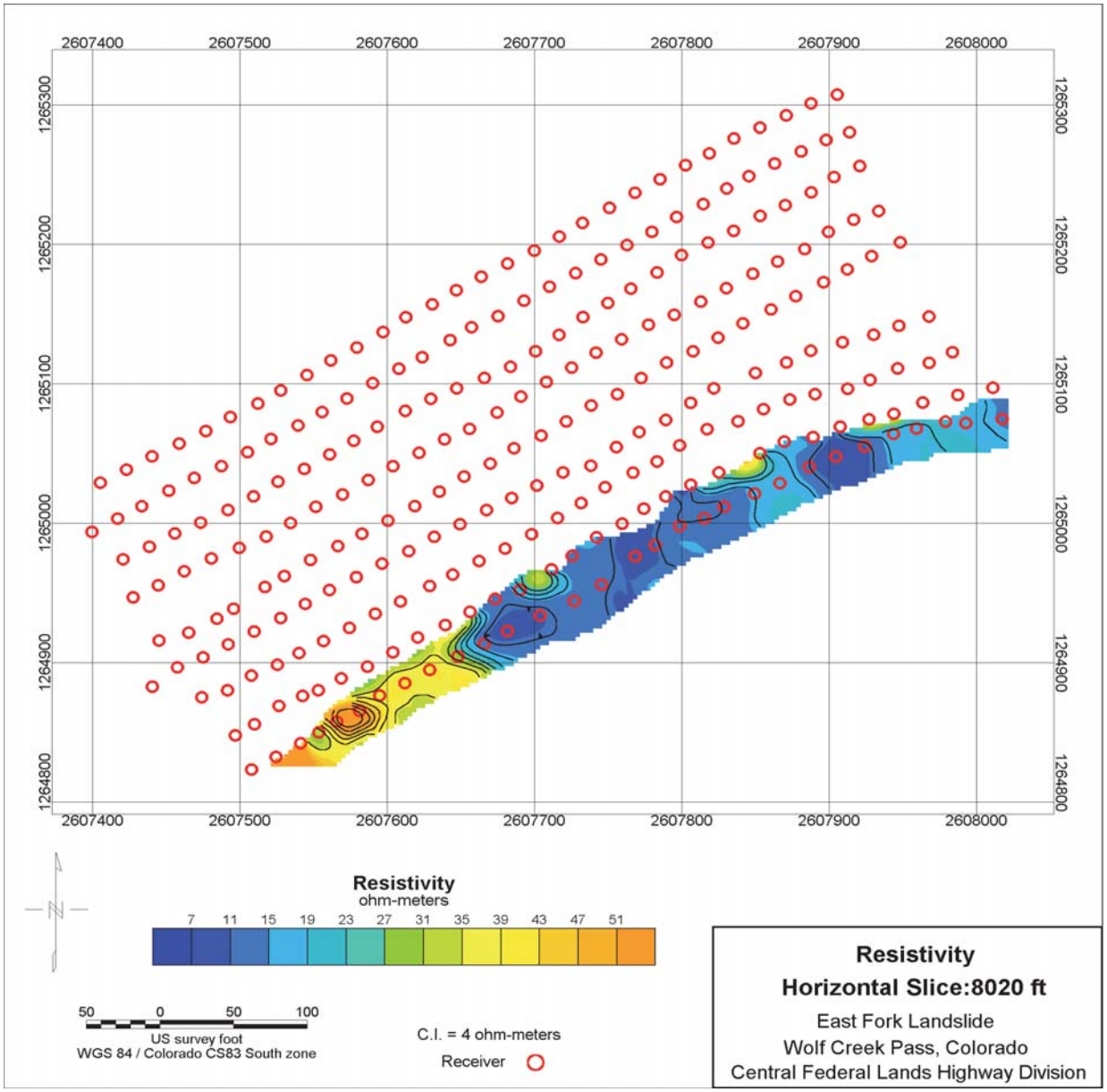

Figure 39. Map. Horizontal slice through East Fork Landslide resistivity volume.

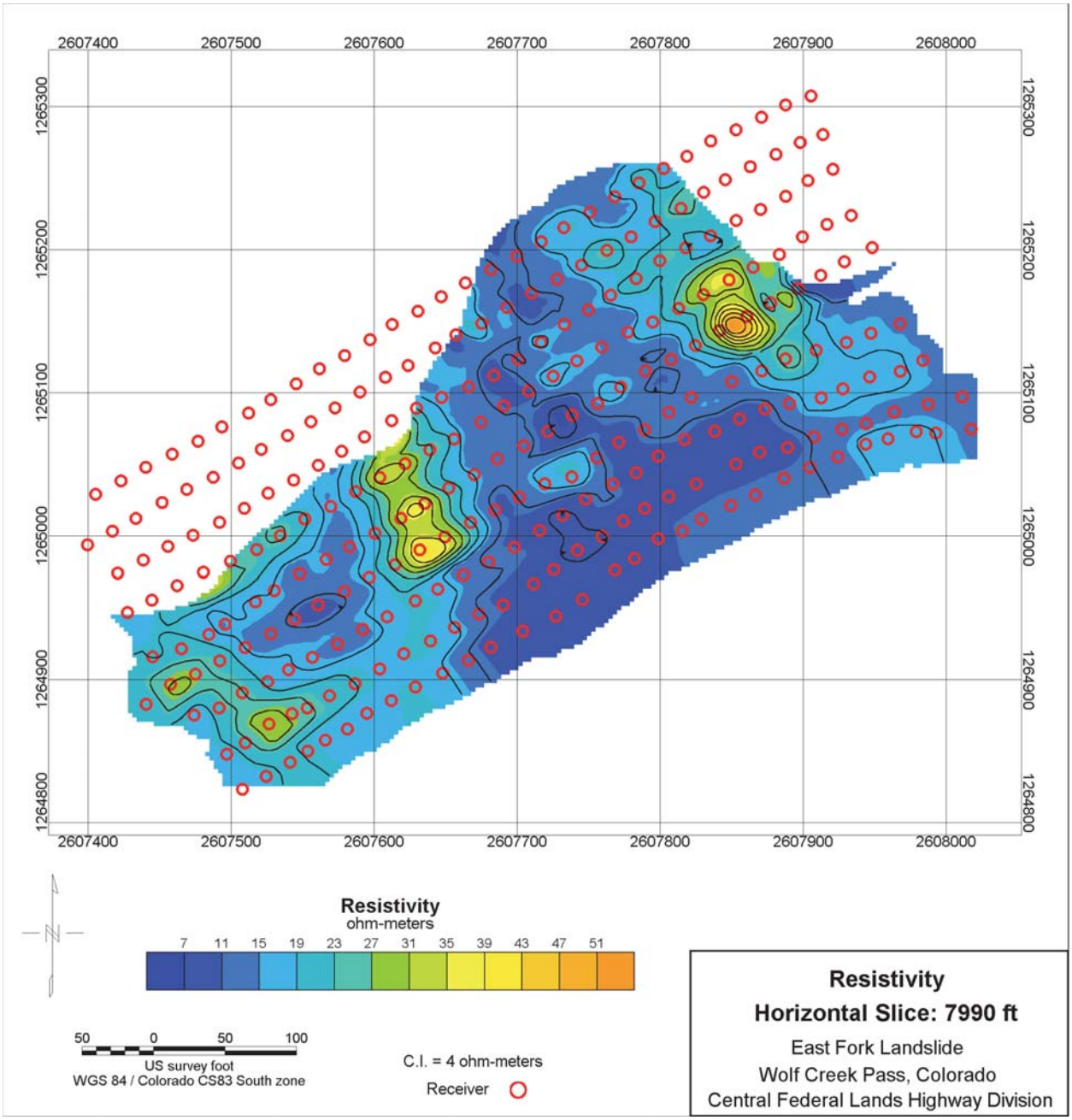

Figure 40. Map. Horizontal slice through East Fork Landslide resistivity volume.

Also similar to the IP results, the resistivity data shown in the elevation 7990 feet depth slice (Figure 40) shows broader characteristics and less variability. The resistivity values are low, less than 10 ohm-meters, in the core of the recent landslide. When the soils or rock type are not changing dramatically, low resistivity values are associated with increased moisture content. It appears that the central portion of the slidemass, at this depth, had not yet drained. Both of the other high resistivity areas (orange) are coincident with large blocks of intact materials that appear to have been translated down the slope but not disturbed from their original character.

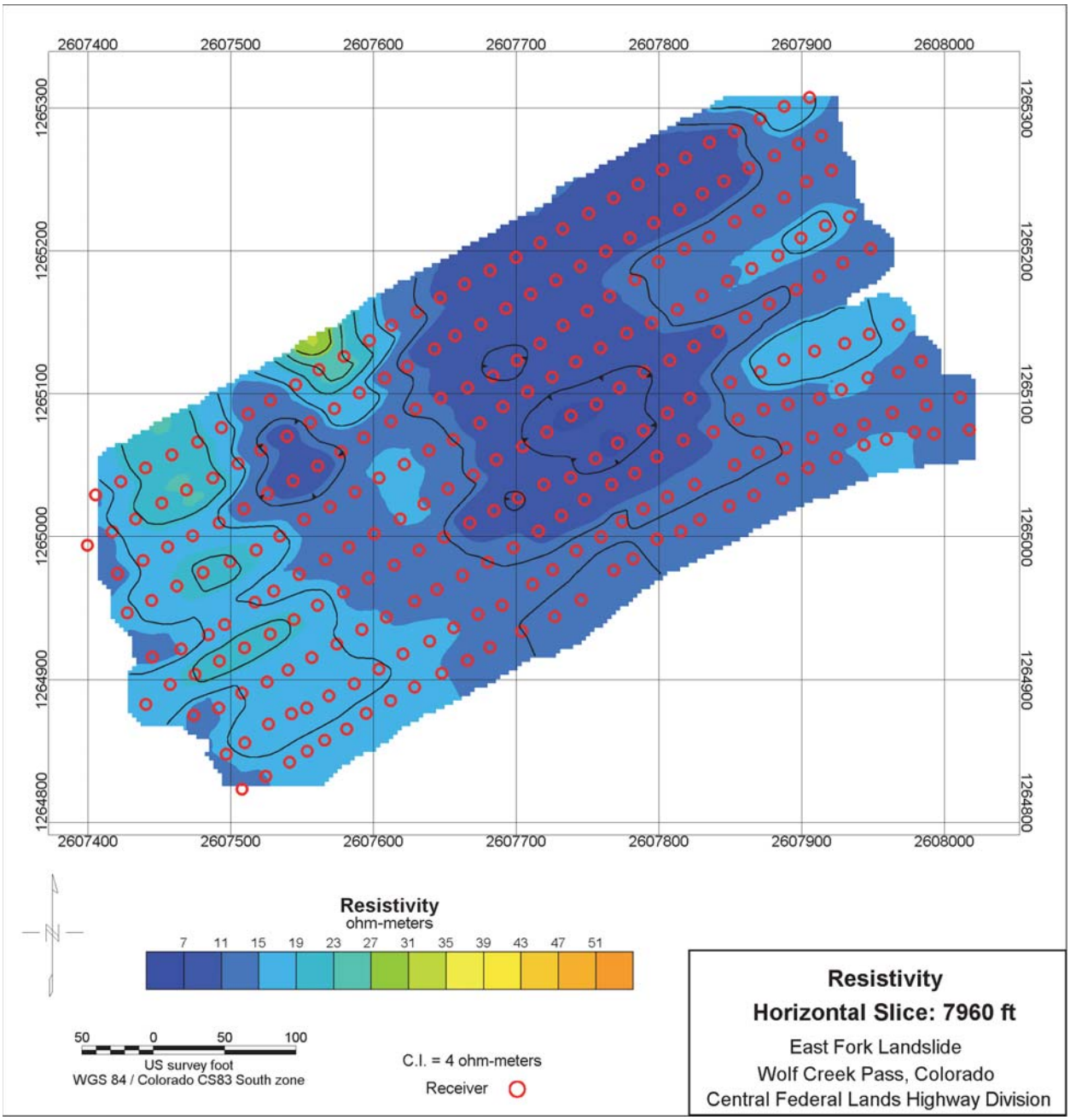

Figure 41. Map. Horizontal slice through East Fork Landslide resistivity volume.

The resistivity depth slices at elevations 7960, 7930 and 7900 feet (Figures 41-43) indicate even lower resistivity values in the core of the recent landslide. The range of resistivities is almost uniform, ranging between 7 and 20 ohm-meters, reflecting that the moisture content at these depths is likely very consistent; that is, they are likely saturated materials. Very little data about depth to ground water are available to corroborate these results but the uniformity and lack of any high resistivity areas would indicate groundwater has been encountered at these depths.

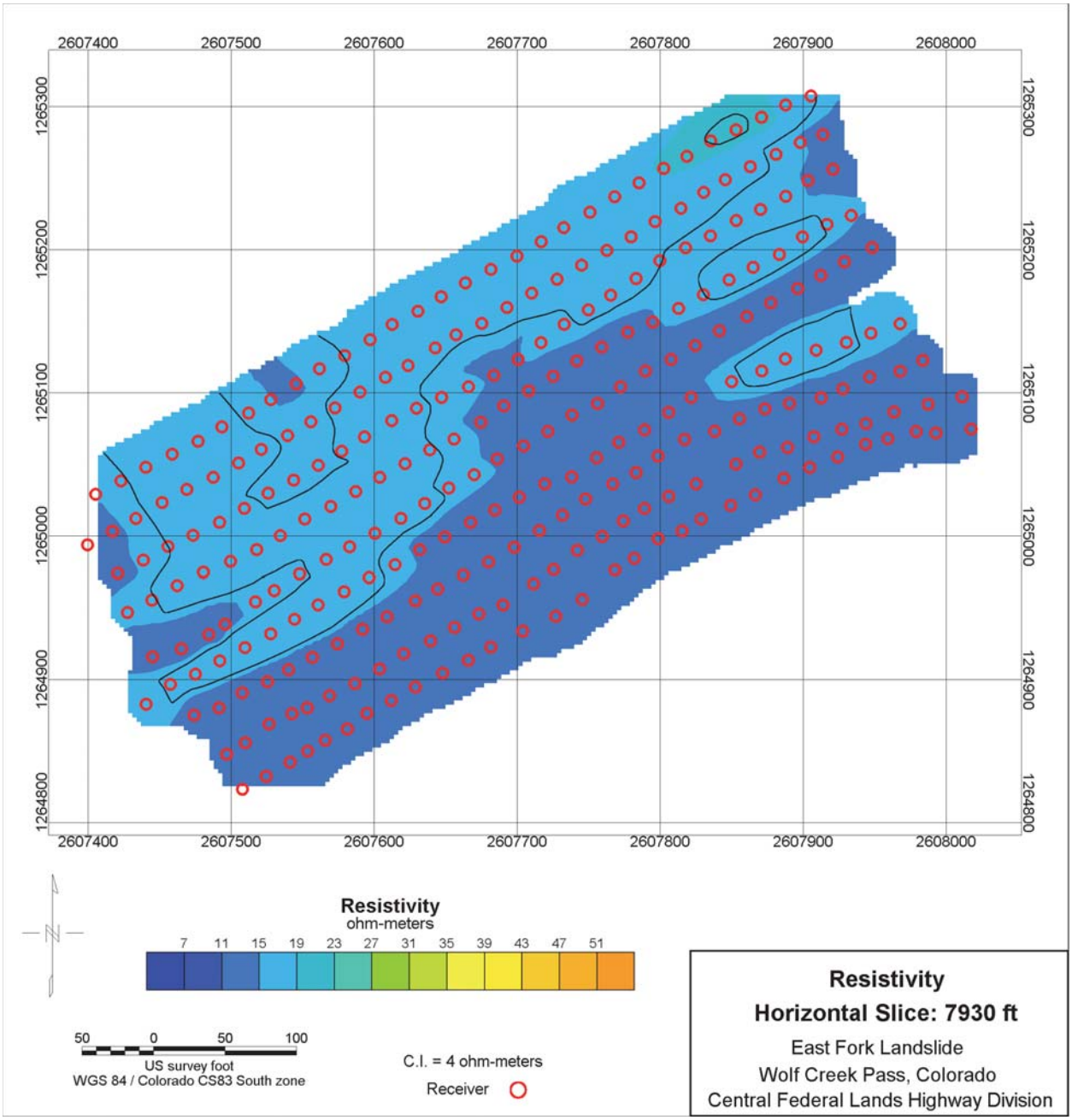

Figure 42. Map. Horizontal slice through East Fork Landslide resistivity volume.

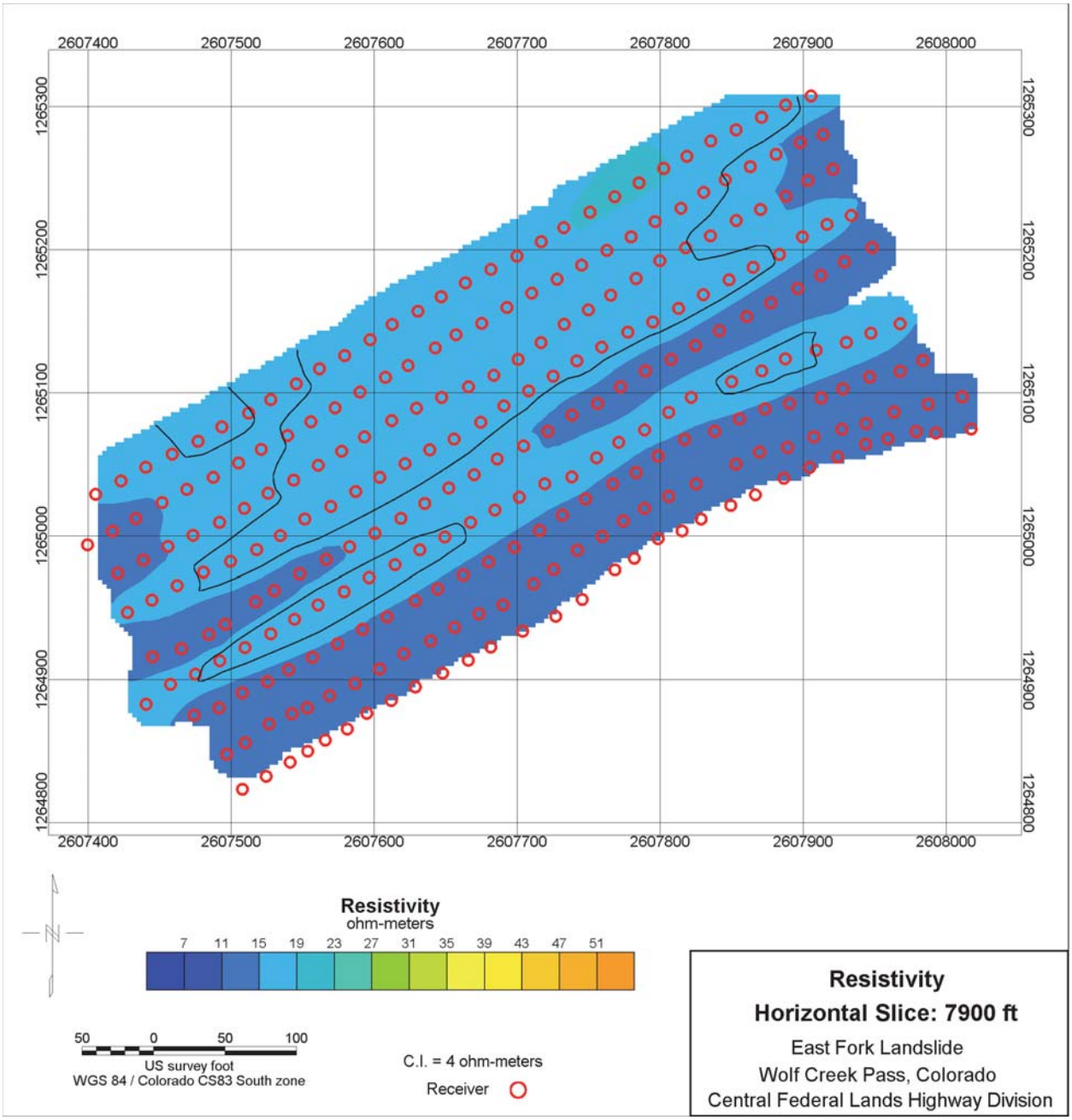

Figure 43. Map. Horizontal slice through East Fork Landslide resistivity volume.

Figures 44 through 48 present 2D cross-sections through the calculated resistivity volume. The cross-section locations are shown on Figure 25. Note the resistivity color scale has changed compared with the horizontal depth slices.

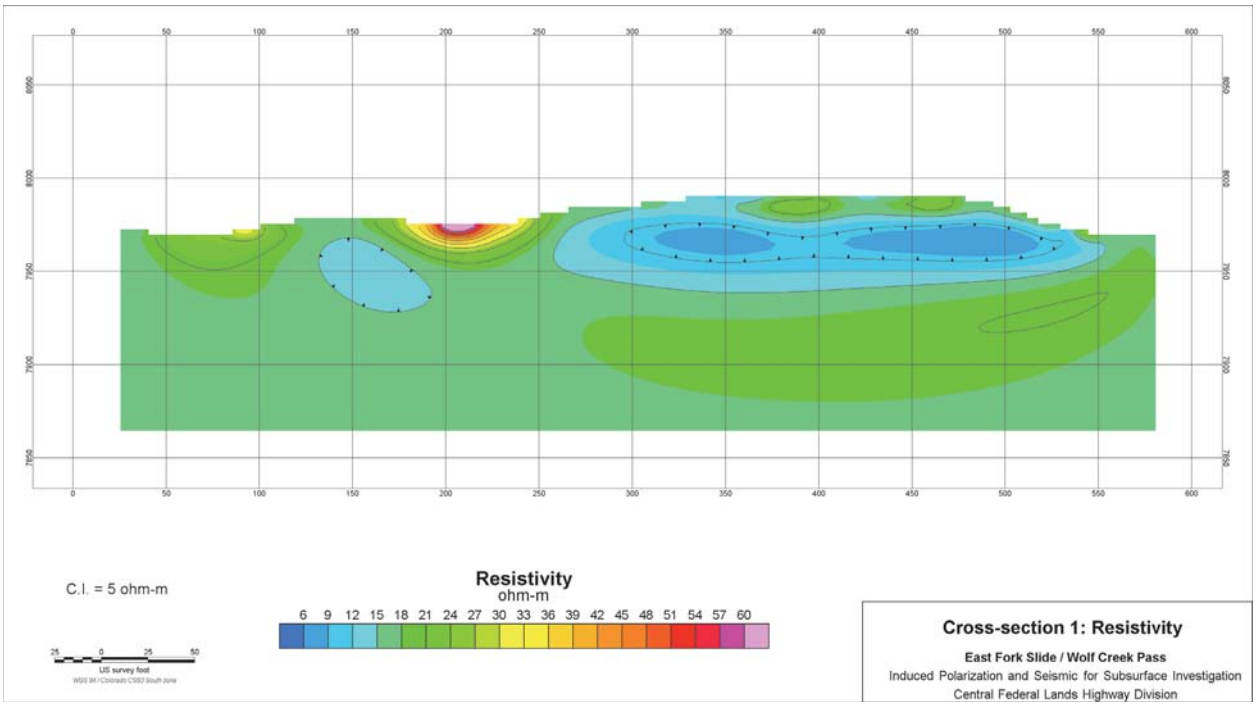

Figure 44. Plot. East Fork Landslide resistivity slice #1N.

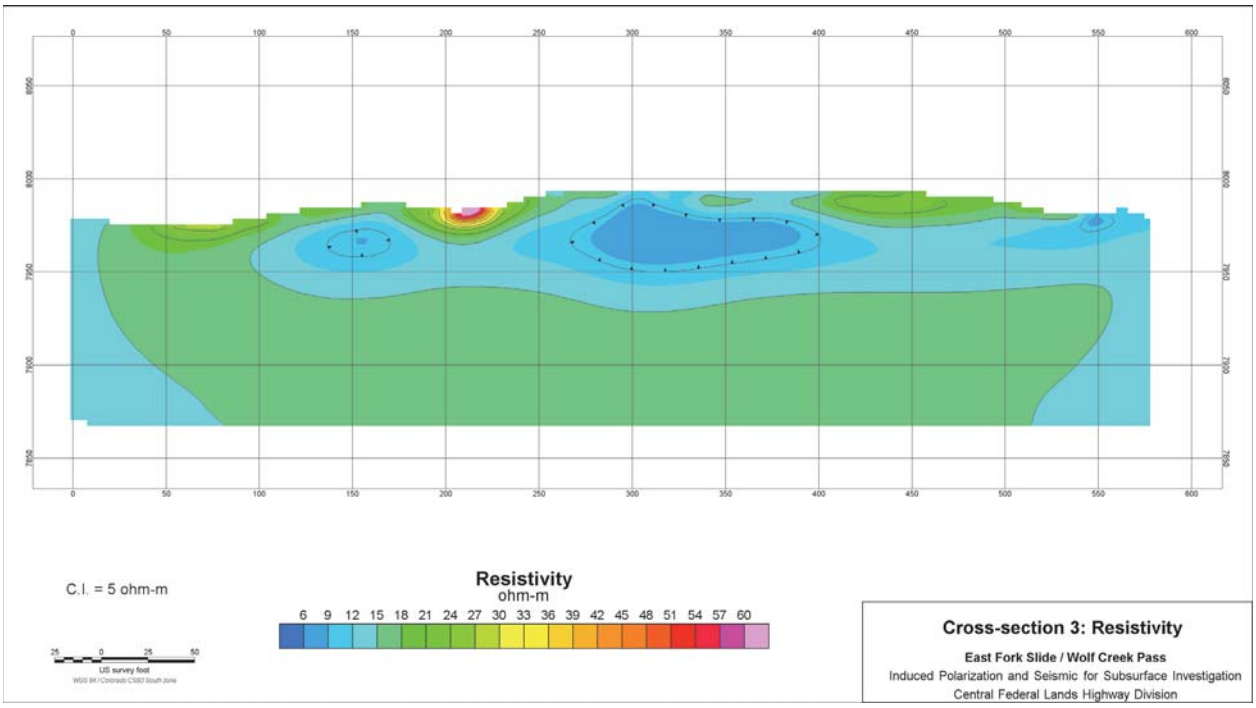

Figure 45. Plot. East Fork Landslide resistivity slice #3N.

All the resistivity cross-sections show considerable near-surface variation and narrow or small anomalies. But there is a decreasing variation with depth, much more so than on the IP sections, which is certainly the effect of a water table and saturated materials in the slidemass itself or in the in situ, undisturbed soil and bedrock materials.

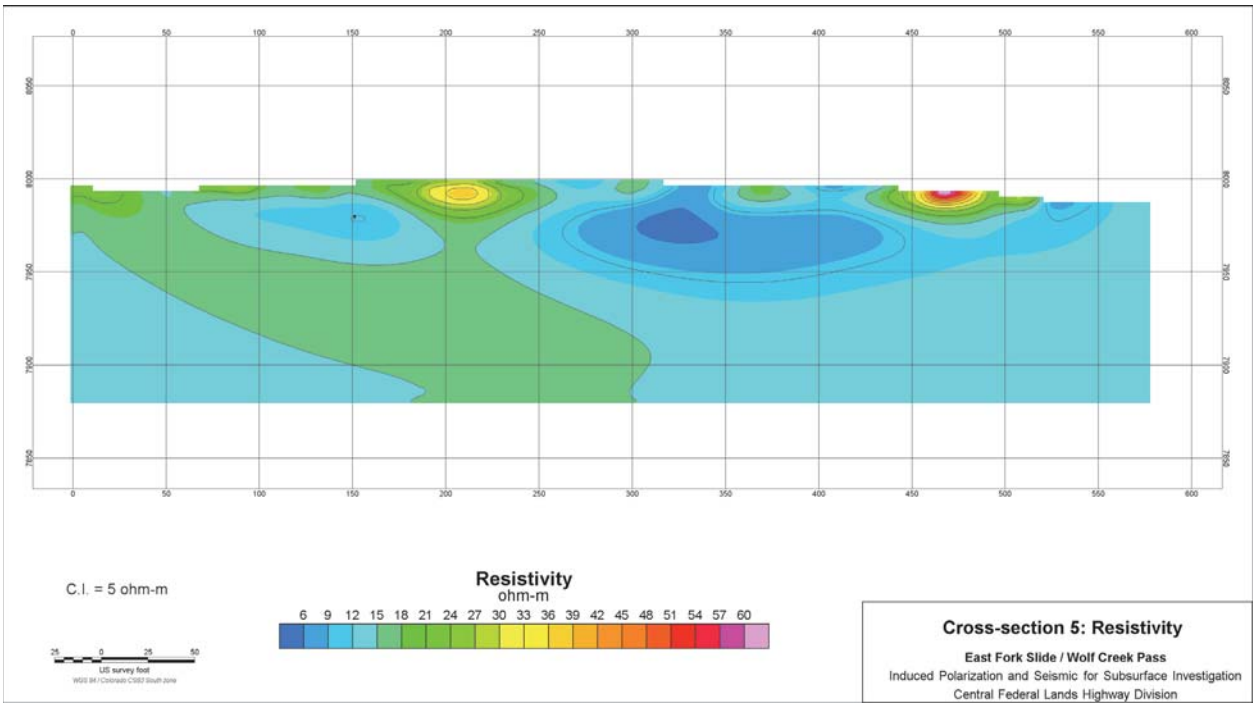

Figure 46. Plot. East Fork Landslide resistivity slice #5N.

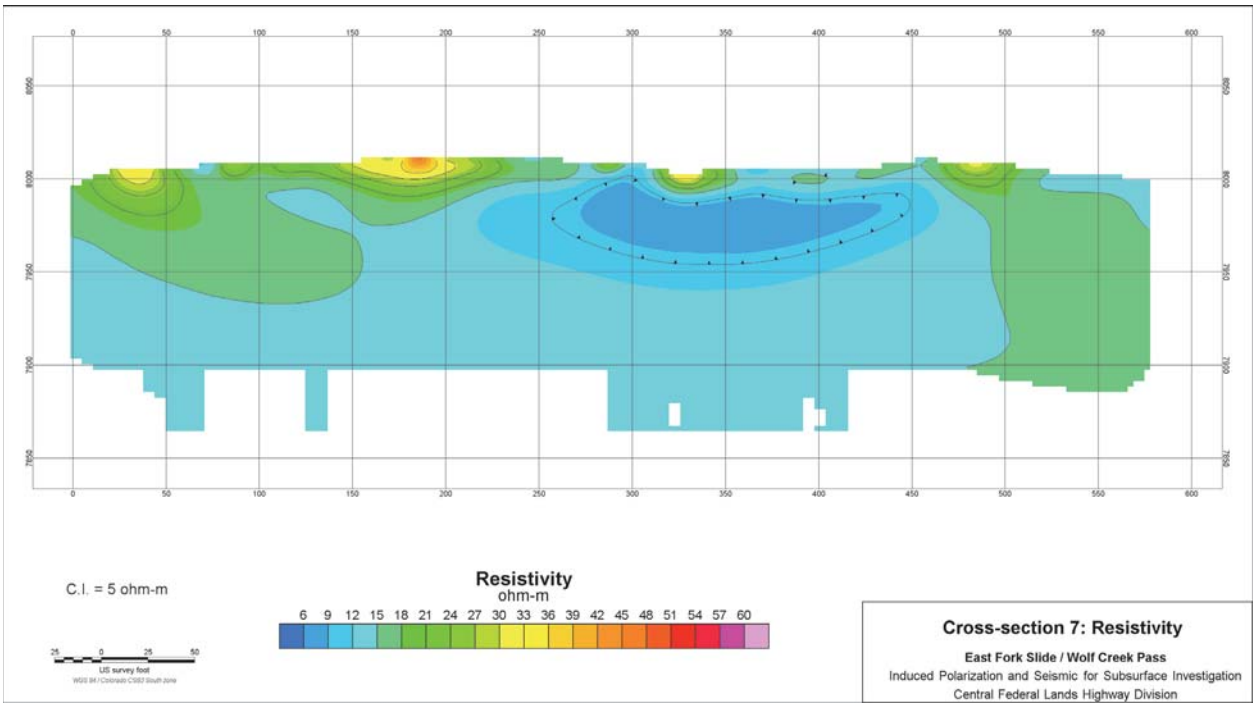

Figure 47. Plot. East Fork Landslide resistivity slice #7N.

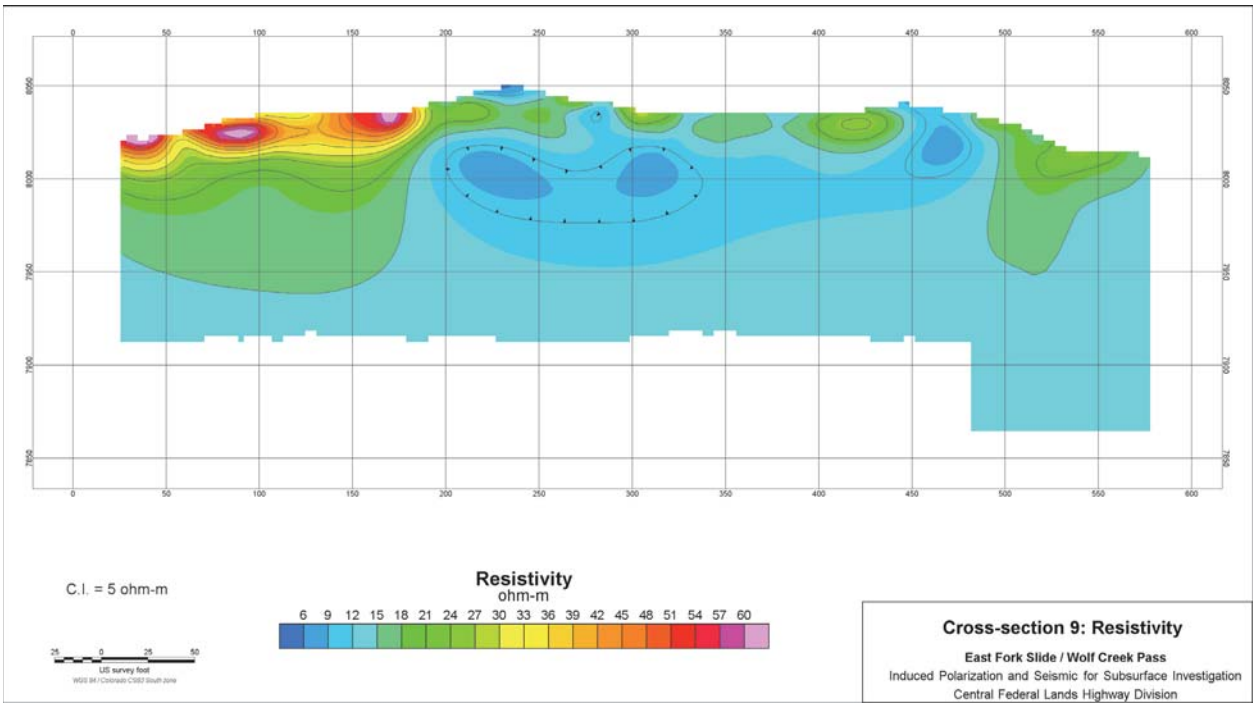

Figure 48. Plot. East Fork Landslide resistivity slice #9N.

Figures 49, 50, and 51 show resistivity data obtained along the combination of Line 8 (slice at edge of the 3D grid) and Line 11 which is the extension off the landslide. Location of this combination 3D and 2D line is shown in Figure 20. Figure 49 is a downward perspective view of the 3D grid and Line 8/11. Figures 50 and 51 are better cross-sectional style views of the Line 8/11 results showing the distribution of resistivities beneath the southern edge of the 3D grid and the area northeast off the landslide. Based on surface expression of the 2008 landslide movement, it was anticipated that Line 11 extended well off the East Fork slidemass. At depths of up to forty feet below the ground surface, generally in the central portion of Line 8/11 is a low-resistivity zone (blue and green). It is about two-thirds of the width of the grid, and thicker to the west. The low-resistivity zone corresponds to the central part of the slidemass and is interpreted to be saturated soils at the time of this survey; it is bound by resistive materials. That is, to the east and west of the low-resistivity zone, there are high-resistivity zones (red and pink). The limits of this higher resistivity section are not contained within the edges of the 2008 landslide. The resistive measurements extend east and west from the edge into the slidemass. The resistive zones are shifted slightly away from the higher terrain to the west and southwest of the survey grid and likely represent materials which drained since the slide movement to the time of the geophysical surveys. As discussed in the IP results section, it is believed this area is also part of a larger complex of the East Fork landslide. However, the resistivity results indicate that this northeast area is drained, or unsaturated, when compared to the slidemass known to have moved in 2008.

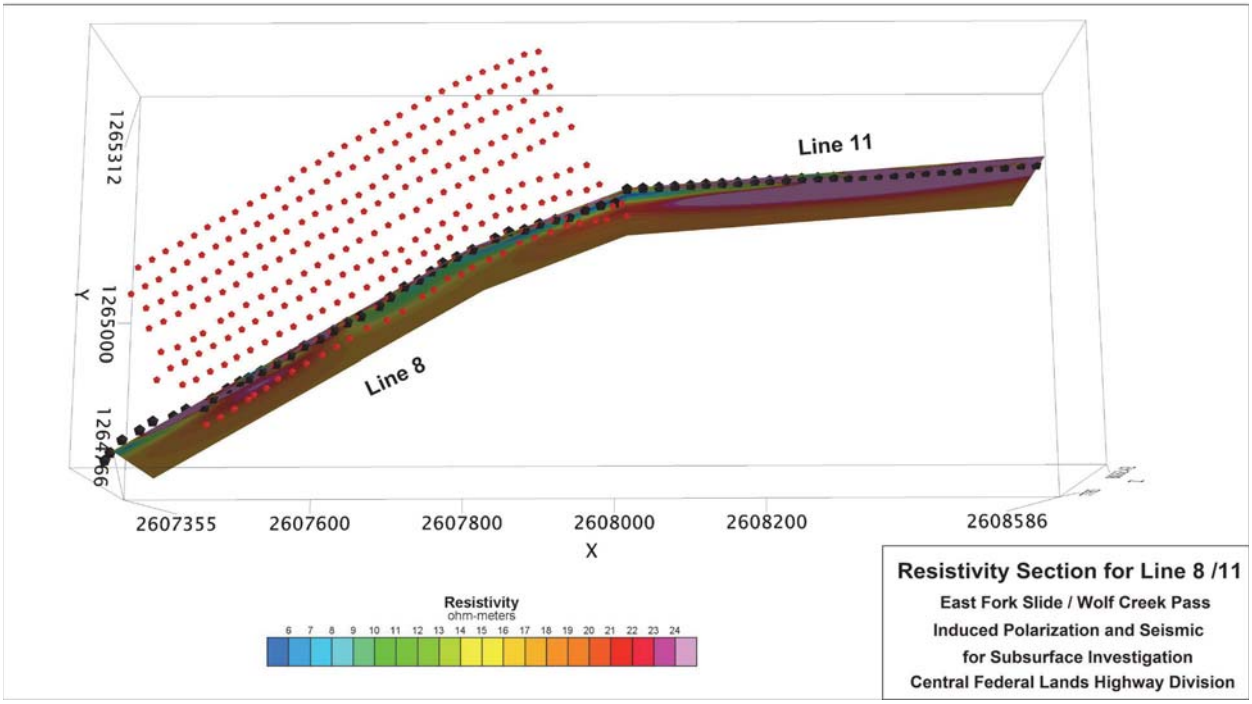

Figure 49. Plot. Interpreted resistivity results along the 3D slice (#8N) and the 2D extension line (Line 11), relative to the resistivity grid.

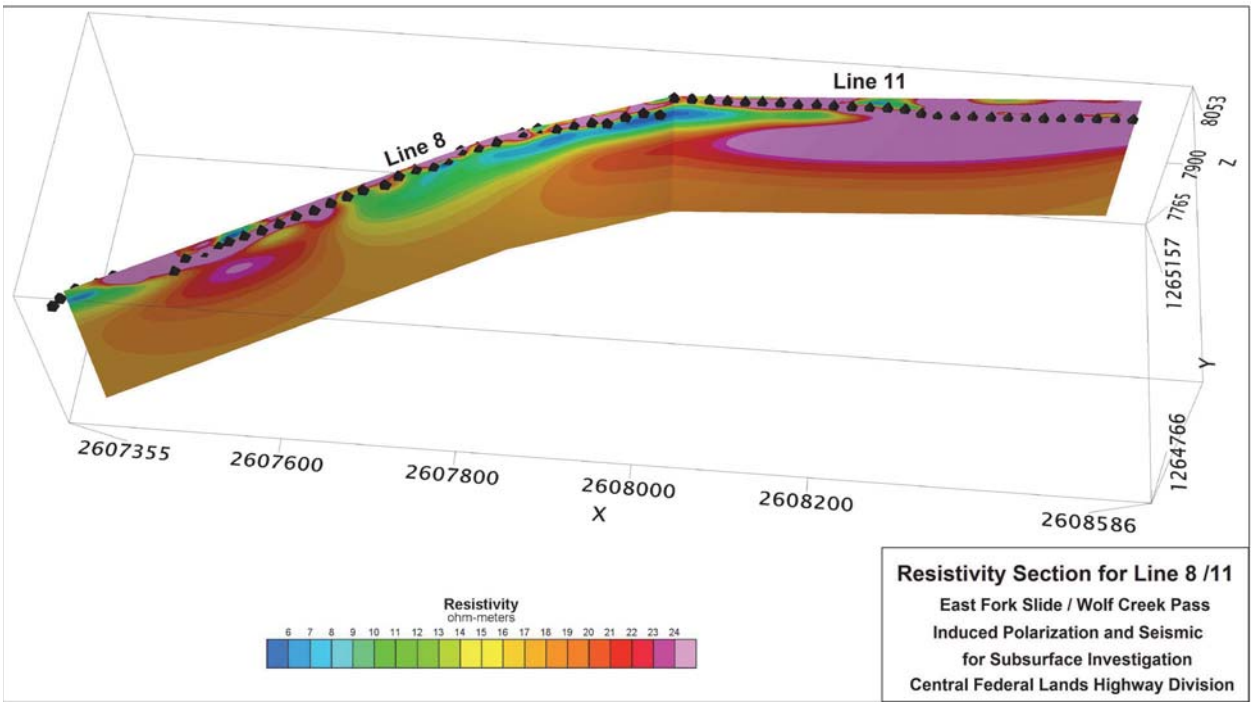

Figure 50. Plot. 2D resistivity cross-section interpreted for Line 8/11, with electrodes marked by black triangles and line in relation to 3D grid.

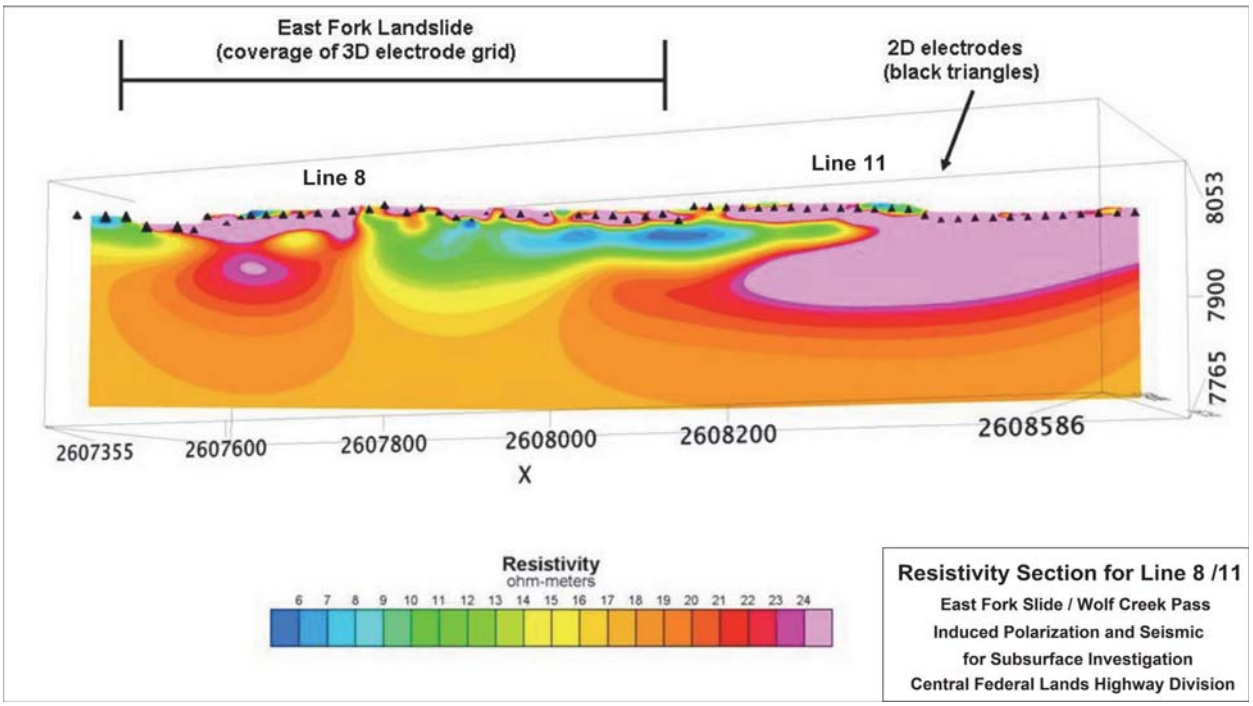

Figure 51. Plot. 2D resistivity cross-section along Line 8/11 with color range selected to highlight difference between center of- and the eastern flank of- the landslide.
Note change of color scale from other resistivity horizontal slices and 2D slices.

Seismic Refraction

Figure 52 presents a slice extracted from the 3D velocity volume. The locations and numbers of each 2D slice through the 3D volume are shown on Figure 25. Velocity slice #1N is located close to borehole P-1. For geologic information from P-1 see the borehole section after this seismic refraction results discussion.

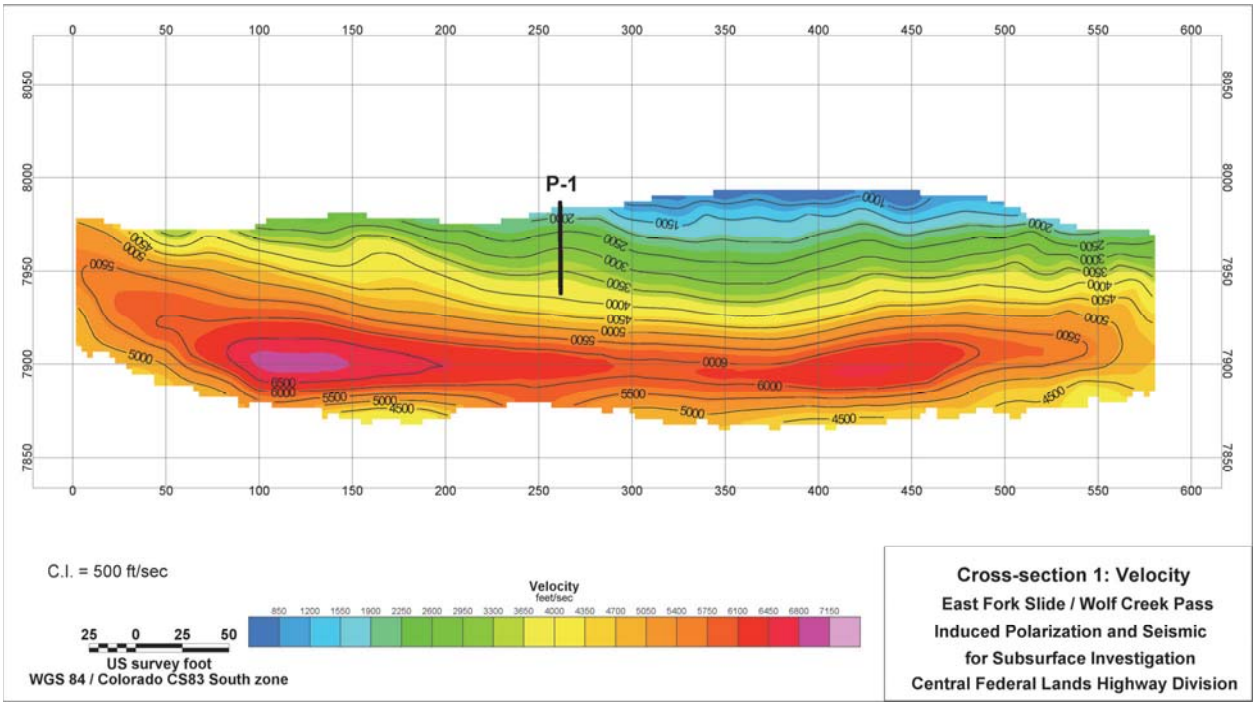

Figure 52. Plot. East Fork Landslide velocity slice #1N located near borehole P-1.

The 2D velocity slice in Figure 52, displaying the distribution of P-wave velocities, is representative of most of the slices extracted from the 3D volume image, either parallel to- or perpendicular to- the slidemass. That is, there is a trend of gradually increasing velocity with depth, with velocities ranging from less than 1000 feet/second (ft/sec) to greater than 6000 ft/sec. This is a range of velocities anticipated for the loose, unconsolidated landslide materials and soft / weathered bedrock materials at this site. It must be noted, however, that the lower P-wave velocities at depth (i.e., decreasing values with depth beneath the highest velocities obtained) are an artifact of the Geostructural Analysis Package imaging algorithm. The GAP algorithm used for the numerical modeling, similar to tomographic modeling, utilizes a uniform background velocity prior to initiation of the model. P-wave data displayed in the slices are not realistic beneath the depth of the highest velocities. The decreasing velocities at depth are simply the remaining portion of the 3D volume not influenced by rays traveling through that portion of the volume. These deeper and lower P-wave velocities should not be used. Based on experience and the data acquired along the longer 2D seismic line (i.e., Line 8/11discussed later in this section), rather than decreasing velocities at depth the bedrock velocities are either predicted to be either constant or to gradually increase with depth. Additional velocity slices, extracted from representative locations within in the 3D velocity volume, are shown on Figures 53 through 55.

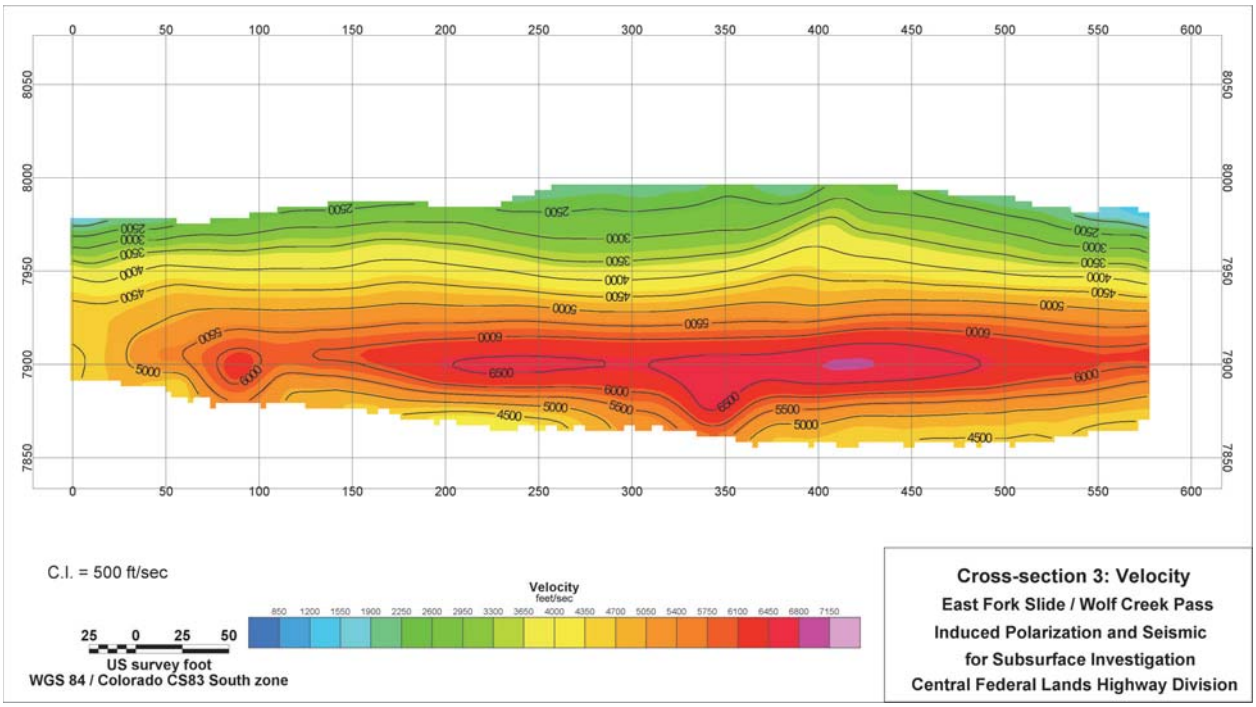

Figure 53. Plot. East Fork Landslide velocity slice #3N.

Velocity slice #5N, shown on Figure 54, is located close to borehole Sl-1. Information about the borehole is in the borehole section after the seismic refraction figures. A thick layer of low velocity materials, obtained down near the toe of the slidemass (Figure 52), are not present further up the slope at slice 5N. Higher velocities (e.g., 2000-2500 ft/sec) are present at or near the ground surface.

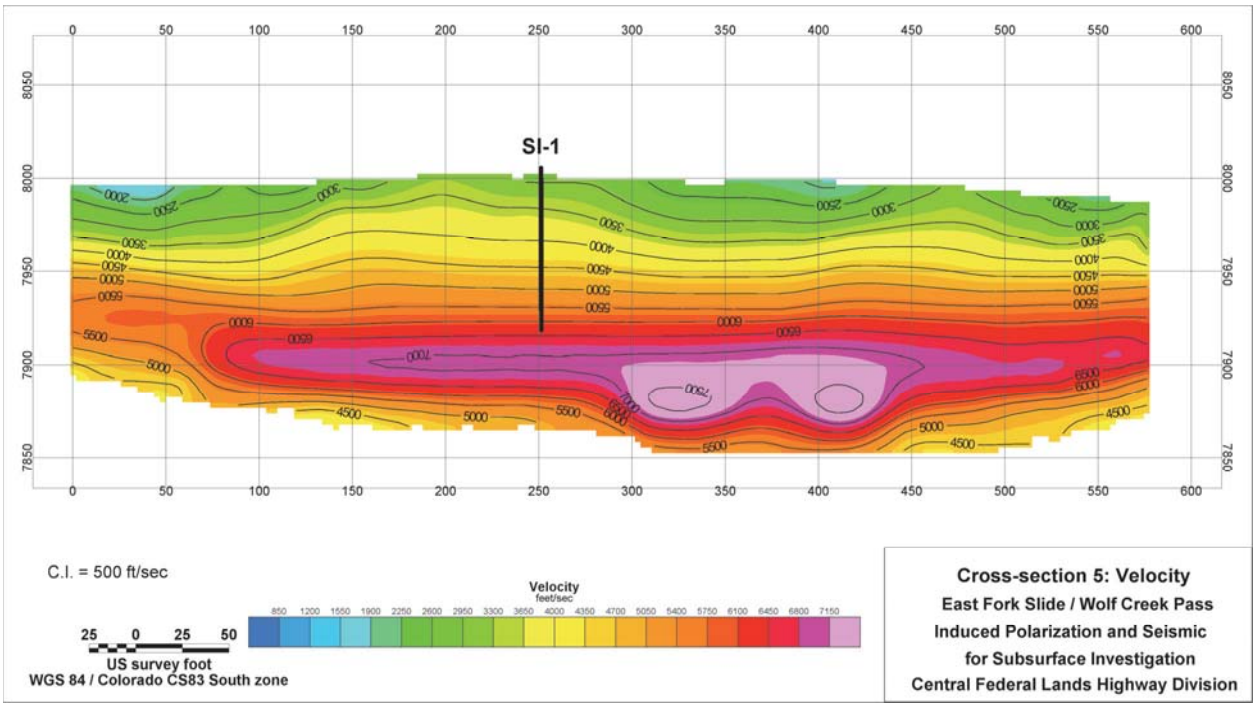

Figure 54. Plot. East Fork Landslide velocity slice #5N located near borehole Sl-1.

Velocity slice #8N, shown on Figure 55, is located near the south edge of the 3D seismic grid. Again, there is little- to no- layer of low velocity material this high on the slidemass. Generally, there is about 25-40 feet of materials with velocities below about 2500-4000 ft/sec. Although the velocities gradually increase with depth, the contours are not flat across the velocity slice showing both undulations up and down.

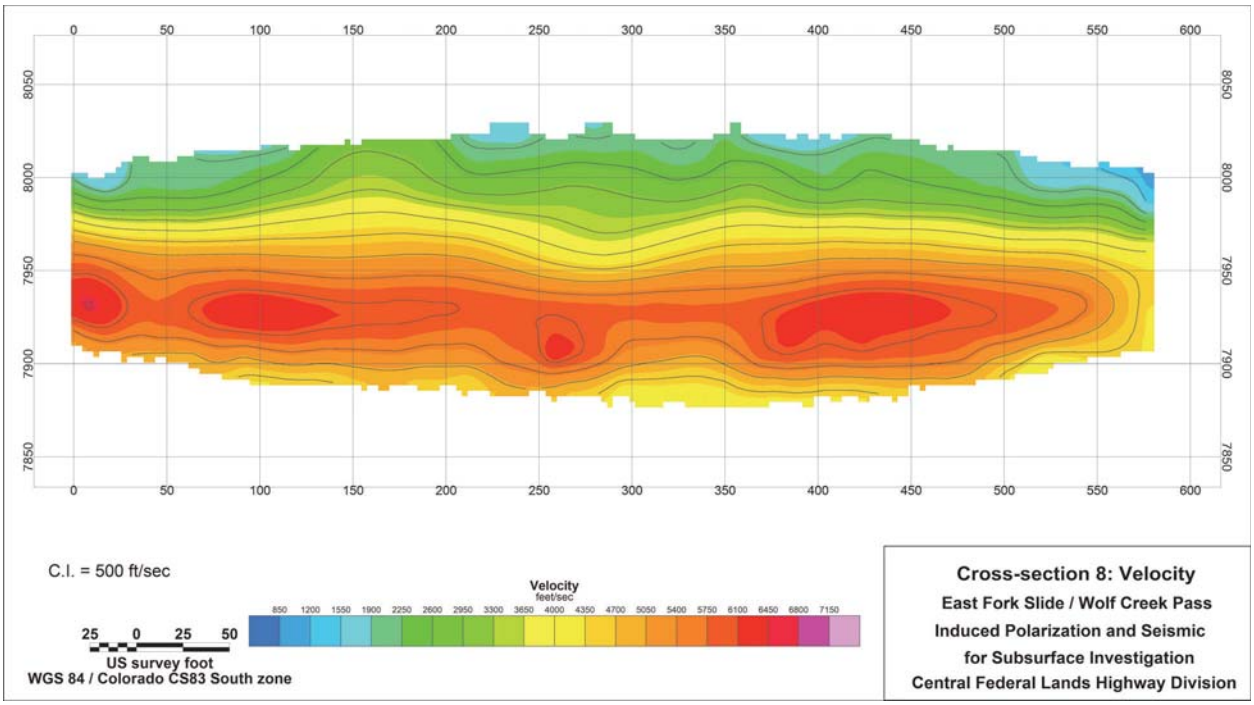

Figure 55. Plot. East Fork Landslide velocity slice #8N.

Figures 56 and 57 present the comparative results from the seismic analysis using advanced 3D refraction volume imaging and conventional 2D refraction analysis. 2D seismic results were obtained using Rayfract (version 3.11). Figure 55 is the velocity slice (along line #8N) extracted from the 3D volume. Figure 56 presents the long cross-section resulting from a 2D analysis of all the data along Line 8/11 independently. The trend of increasing velocity with depth and undulations in the contours of high (3,500-4000 ft/sec) velocities, are very similar. The results shown in Figure 56 confirm that velocities at depths greater than about 65-75 feet do, indeed, increase with depth. This is the expected condition for this geologic setting and supports earlier claims that the results from the 3D volume imaging should not be used below the zone of the highest velocity measured. Data shown in cross-sectional format obtained from the 2D analysis show the difference of having a low-velocity model as the initial starting model used in the 3D analysis (as seen in Figure 55).

Figure 57 shows the 3D velocity slice #8N (same as Figure 55) overlain on the entire results from analysis of the 2D Line 8/11. Note the velocity range and color scales used in Figures 55, 56 and 57 are the same. There is very good comparison between the velocities obtained in the upper about 60-70 feet with both 2D and 3D analysis techniques. The thickness and character of the velocities obtained independently with two computational methods is correlative. This will lead to confidence to using the 3D seismic technique as an approach to characterize much larger and more complex subsurface areas; as long as limits to the depth of investigation are considered.

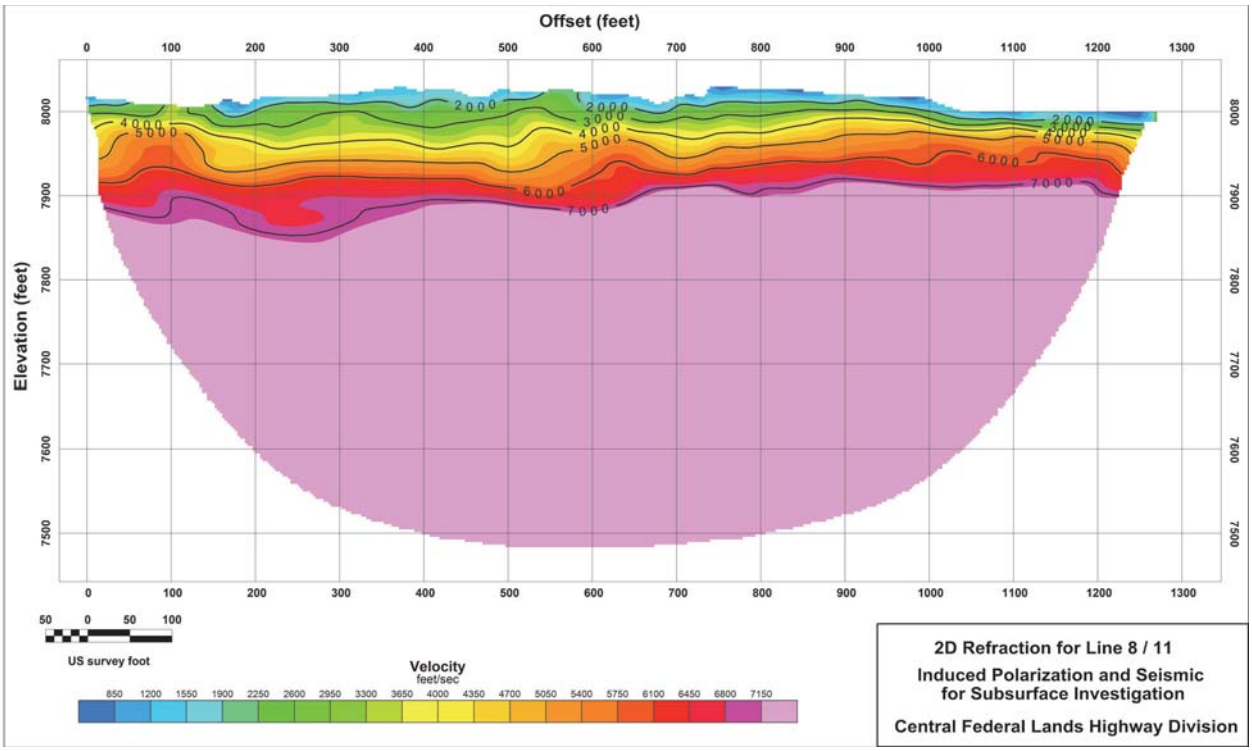

Figure 56. Plot. East Fork Landslide independent 2D velocity cross-section along Line 8/11.

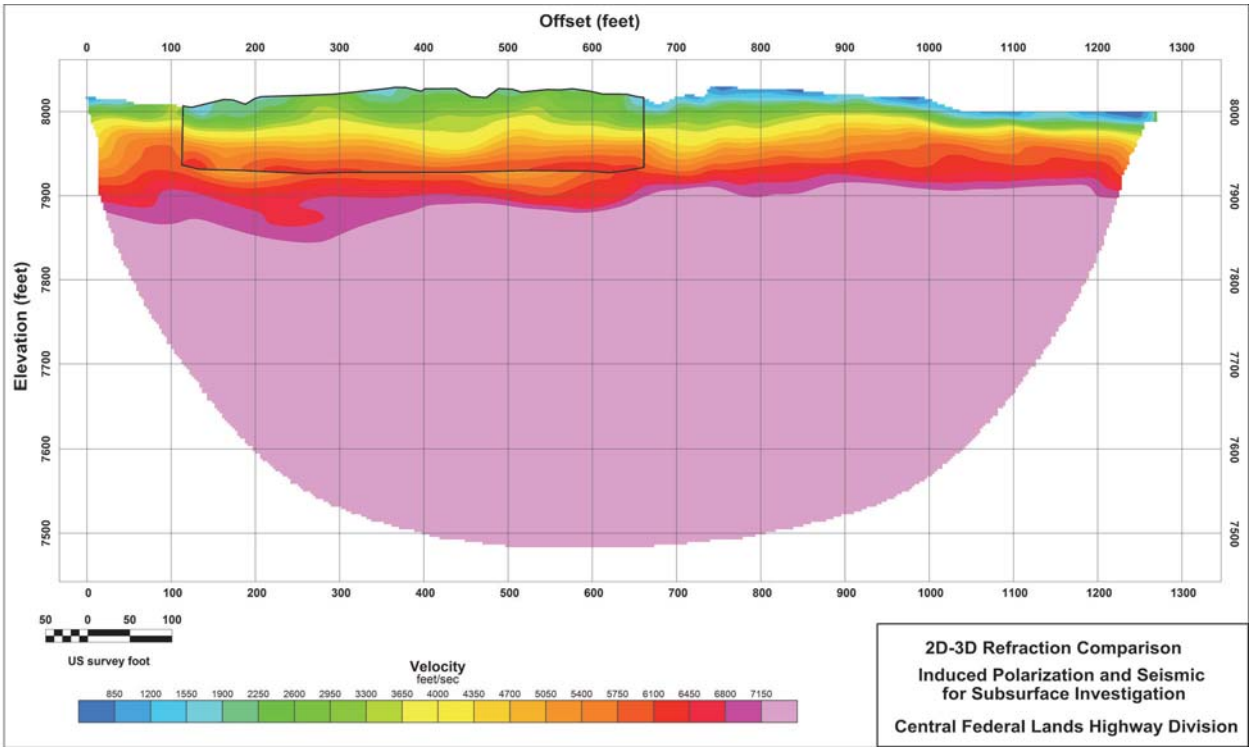

Figure 57. Plot. East Fork Landslide 2D velocity cross-section along Line 8/11 and overlain Line #8N slice extracted from the 3D volume.

Figures 58 and 59 are used to show comparisons and potential correlations between P-wave seismic velocities and electrical resistivities obtained in the respective 3D volumes. Two slices #6N (Figure 58) and #9N (Figure 59) are briefly described and used as examples of the correlations that can be observed within 3D data sets. See Figure 25 for location of the slices.

Comparing the seismic velocity data (colors) and resistivity data (contours) distribution beneath slice #6N there is a good correlation between the two data sets. Figure 58 shows that in the near-surface there is a high velocity area, at about distance 200 feet, which correlates very well with the most resistive portion of the cross-section. This area is likely an isolated block of material that is well-drained, and stiff. This cross-section and the two data sets appear to support existence of a coherent block of material that was not disturbed during sliding, and that as a tight block of material it has less water in it. Whether the entire block of material was transported, but not disturbed, during mass movement is unknown, however several large coherent blocks can be observed within the slidemass; this set of data likely represents that type of phenomenon. Additionally, beneath this slice #6N there is moderate variability in both data sets within the upper 50 feet, and then both the seismic velocities and resistivities become more laterally uniform and consistent with depth, indicative of the geologic formations below the slidemass.

Figure 59 presents the seismic data (colors) and resistivity data (contours) overlain in 2D cross-section for slice #9N; the respective data were extracted from the 3D volumes. This line is located at the top of the area investigated, the southern-most slice from the volume image(s). Slice #9N data show more variability than the previously discussed #6N (Figure 58) for both the velocities and resistivities obtained. In the upper 50 feet, the correlation is evident that lower resistivity areas are associated with areas of lower P-wave velocity. This is interpreted to represent less stiff/less dense soils which are part of the slidemass which remain saturated (or high moisture content at a minimum). Similar to slice beneath #6N, the areas with highly resistive materials occur where the seismic refraction results indicate stiffer (i.e., more competent) materials. These are either undisturbed blocks that moved, or in situ materials which did not slide as part of the earth movement. Both the velocities and resistivities become more consistent and uniform below about 50 feet.

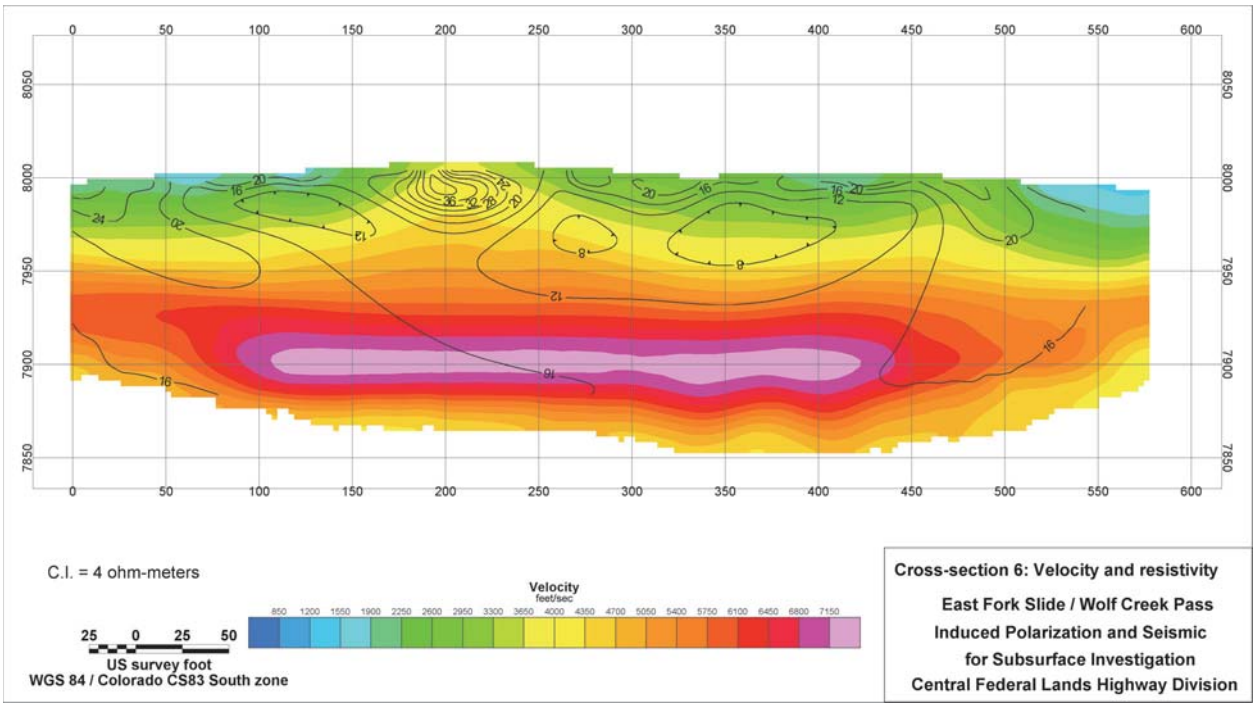

Figure 58. Plot. East Fork Landslide velocity slice #6N with resistivity contours overlain on the section. Both seismic and resistivity data are extracted from the respective 3D volumes along slice #6N.

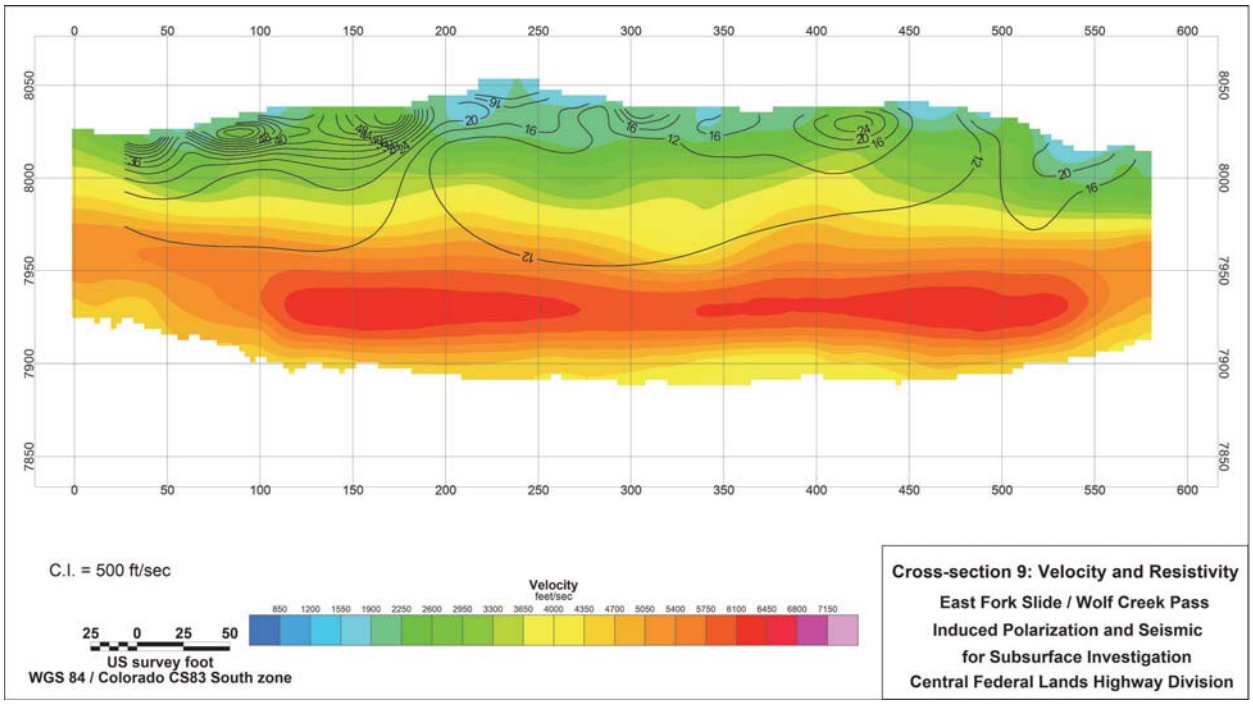

Figure 59. Plot. East Fork Landslide velocity slice #9N with resistivity contours overlain on the section. Both seismic and resistivity data are extracted from the respective 3D volumes along slice #9N.

Borehole Correlation

Subsurface information for the East Fork Landslide is available in the form of three borings drilled after the most recent (2008) movement of the slidemass. The identifier and locations of these boreholes are shown on Figure 60. Using data from these three geotechnical borings, two slope-indicator (SI) and one piezometer (P), a series of geophysical cross-sections can be created for data correlation. Location of the cross-section (*labeled "Borehole X-S"*) is shown on Figure 60. Figure 61 displays the lithologic data from the borings with the left boring being upslope and the right boring being downslope, but they are not plotted relative to elevation. Figures 62 through 64 represent the integration of borehole data onto the respective geophysical data for a slice through the 3D volume extracted along the '*Borehole X-S*' position.

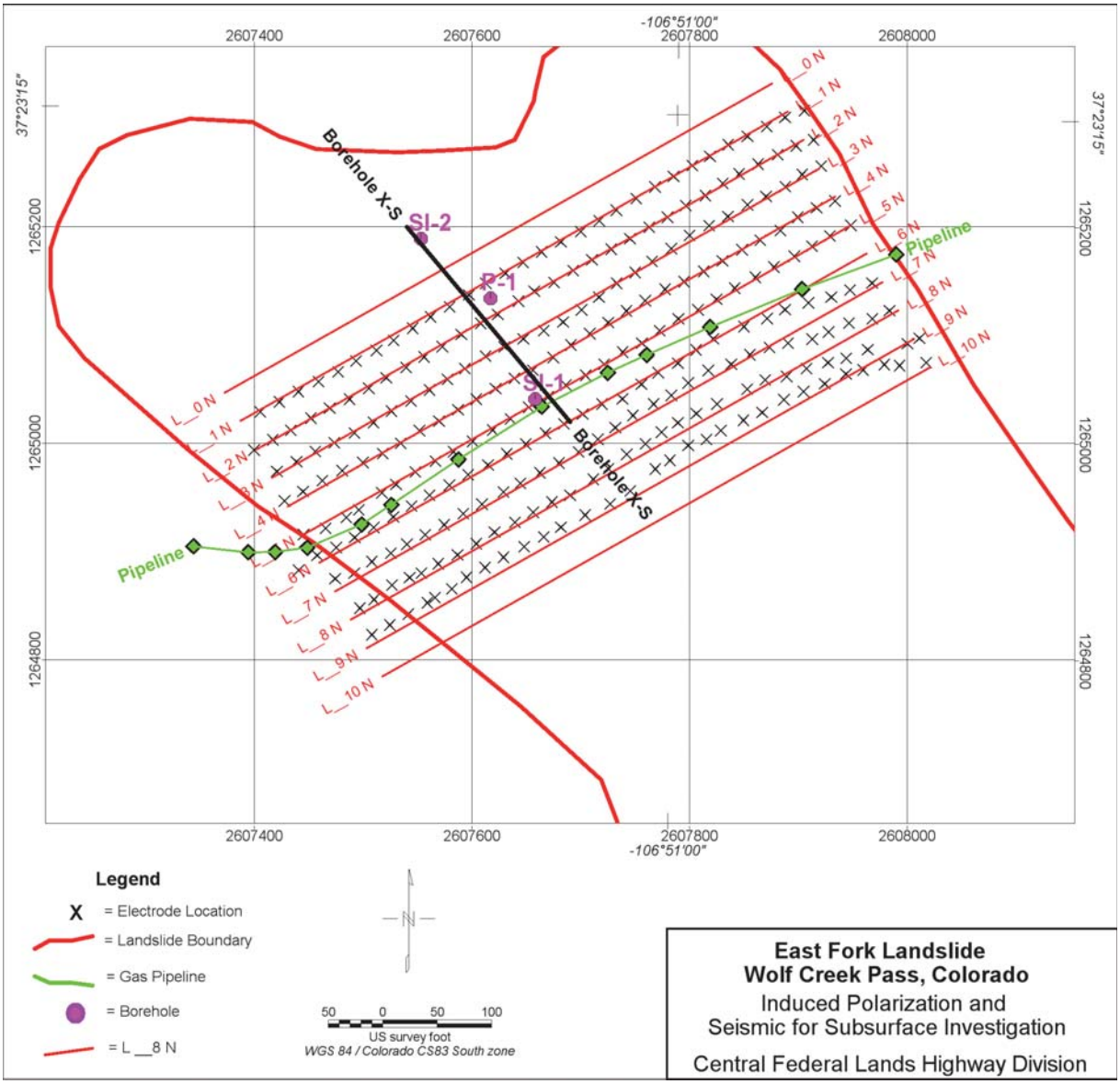

Figure 60. Map. Location map of boreholes at the East Fork Landslide and the borehole cross-section (X-S) location.

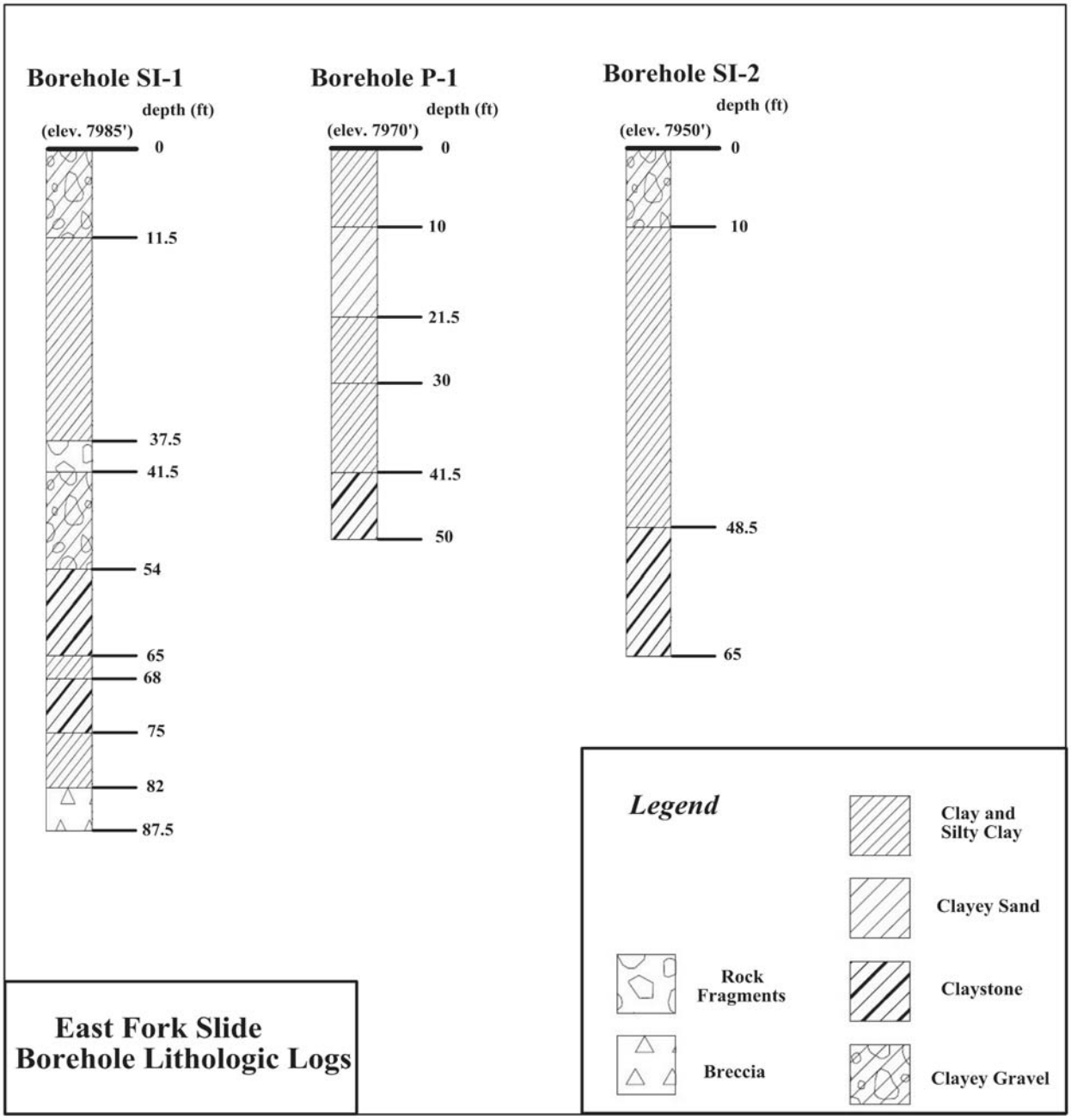

Figure 61. Diagram. Lithologic logs for East Fork Landslide boreholes. Elevation of the borings is not taken into account; all data are depths below ground surface.

Standard Penetration Tests (SPT) were performed with samples obtained at 5 or 10 foot intervals using a standard 2-inch split spoon sampler and an automatic hammer system with a hammer efficiency of 85%. The number of blows to drive the split spoon sampler for three consecutive 6-inch intervals, or a total of 18 inches was recorded on the test-hole logs. Representative soil samples were retrieved with the split spoon and unified soil classification system lithology of the soils or rock were obtained. Groundwater levels in each boring were measured and recorded as depth below the top of the borehole casing at the time of drilling. Due to high percentage of gravel and rock fragments encountered during drilling, obtaining undisturbed Shelby tube

samples was not successful. Slope-indicator (SI) inclinometers were installed in borings SI-1 and SI-2 and a piezometer (P) installed in boring P-1.

In general, the surficial and subsurface materials at the East Fork Landslide can be described as mostly sandy clays, interbedded with some rock fragments (gravel) with medium to low plasticity (Plasticity Index between 15 and 30). Natural moisture contents of materials encountered above the water table during drilling were generally above optimum.

Relative soil density ranged from loose to very dense (refusal - >50 blows/foot) in the course-grained deposits, and soft to very hard in the fine-grained soils based on the SPT N-values obtained. It should, however, be noted that SPT tests in gravels and cobbles typically result in high blow counts, and as such are not generally good indicators of the actual in-situ soil densities.

Groundwater was encountered during drilling at depths of 20 feet, 8 feet, and 8 feet (below ground surface) in Borings SI-1, P-1, and SI-2, respectively. A groundwater depth of 28 feet was recorded for Boring P-1 on October 29, 2008; approximately one month after drilling was completed. It is anticipated that groundwater depths will have significant fluctuations during the spring and summer months. Drilling was relatively easy with the exception of drilling in layers with cobbles and/or boulders. Competent rock (breccia) was only encountered in SI-1 at a depth below 82 feet or, at approximately elevation of 7,903.0 feet.

Lithologies determined from the SPT samples are shown in the '*lith-log*' format on Figure 61. The following is a brief description of the subsurface materials encountered at each boring: The report containing data from these boreholes, as well as other East Fork Landslide site-specific information, can be found in Appendix E (Federal Highways Geotechnical Report CO-FE-0667-09-01).

Boring SI-1 is located just above the existing roadway, below the natural gas pipeline, and along a profile near the center axis of the 2008 slidemass. The boring was augured to a depth of 87.5 feet, beginning from a ground surface elevation of 7,985.2 feet. Drilling encountered 11.5 feet of moist, brown-gray clay with some rock fragments overlying moist brown-gray clay from 11.5 ft. to 37.5 feet. A harder clay layer, with more rock fragments, was encountered between 37.5 and 41.5 feet overlaying interbedded clay/claystone layer from 41.5 feet to 82 feet and gray breccia bedrock from 82 feet to 87.5 feet. A claystone layer exhibiting high strength was encountered at a depth of 58 feet below the top of the boring. Groundwater was encountered at a depth of 20 feet measured on the second day of drilling. The boring was instrumented with a 2.75 inch diameter inclinometer casing grouted in place with a lean cement/bentonite mixture.

The middle boring, piezometer P-1, is located along the embankment just below the existing roadway. The boring was augured to a depth of 50 feet, beginning from a ground surface elevation of 7,969.6 feet. Brown clay and rock fragments were encountered to a depth of 10 feet. Brown-gray sandy clay was encountered below the brown clay to a depth of 30 feet. Gray clay was encountered below the sandy clay to a depth of 41.5 feet, overlaying hard gray claystone to a depth of 50 feet. A 2-inch-diameter stand-pipe piezometer was installed prior to completion of this boring. Groundwater was encountered at a depth of 8 feet, measured at the time of drilling.

Groundwater was measured at a depth of 28 feet a month after completion of drilling, in late-October 2008. Slope inclinometer and piezometer data were only acquired twice prior to winter closure of the site. Insufficient movement occurred in either inclinometer to definitively locate a slide plane. Information from the boring logs suggests that translational sliding is likely occurring at or near the clay/claystone interface. This interpreted slide plane is approximately 58 feet below the roadway surface at P-1, or at approximately 7,925 feet elevation.

Boring SI-2 is located along the embankment below the existing roadway near the toe of the slide along a profile near the center axis of the 2008 slidemass. The boring was augured to a depth of 65 feet, beginning from a ground surface elevation of 7,949.8 feet. Drilling encountered 10 feet of brown sandy gray clay and rock fragments overlying brown-gray gravelly clay from 10 feet to 48.5 feet, and hard gray claystone from 48.5 feet to 65 feet. Groundwater was encountered at a depth of 8 feet, measured at the time of drilling. This boring was also instrumented with a 2.75-inch-diameter inclinometer casing grouted in place with a lean cement/bentonite mixture.

Soil samples obtained in all three boreholes are dominated by clay and clay-rich soils. Each borehole encountered a claystone '*bedrock'* surface. Weathering of the claystone made identification of the contact difficult at the time of drilling. Competent breccia was encountered at a depth of 82 feet in borehole SI-1. Seismic velocities obtained in the area of boring Sl-1 are representative of materials to depths of at least 100 feet below ground surface; therefore the velocities can be correlated with bedrock.

Figure 62 presents IP results, extracted from the 3D volume, along the 'borehole cross-section'. As previously discussed in the IP section, this short up-slope-to-downslope IP slice through these borings shows the chaotic nature of the small and low-magnitude IP anomalies obtained in the near-surface, and also the more uniform nature of the IP values obtained at depth. For example, a positive IP anomaly is observed at about 50 feet below the surface in borehole SI-1. The lith-log identifies a clayey gravel at that depth. However, near borehole P-1 there is not a similar IP anomaly, and the lith-log does not indicate a clayey gravel layer. The overall very-low and uniform IP response below each of the three borings is interpreted to indicate either uniform bedrock or materials which did not slide during the mass movement. The jumbled or chaotic nature of the IP results in the upper 50 feet are interpreted to indicate the variation in moisture and clay content as the slidemass disturbed the natural / in-situ geologic fabric of these materials.

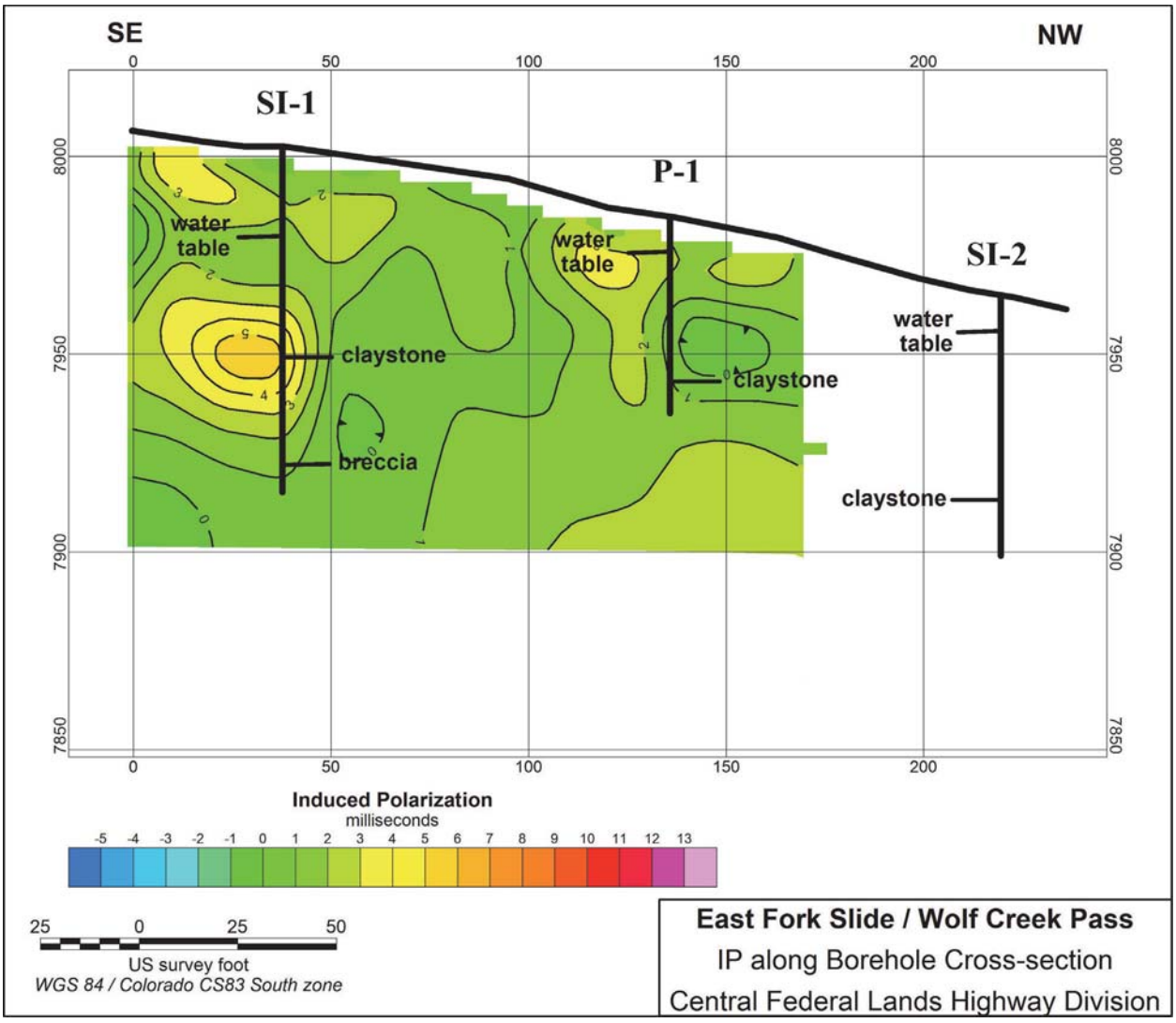

Figure 62. Plot. IP slice extracted from 3D volume through the boreholes.

Figure 63 presents resistivity results extracted from the 3D volume along the borehole cross-section. The resistivity slice shows low resistivities (i.e., <15 ohm-meter) above the claystone interface and below the water table. This is the same low-resistivity zone that is observed in the central portion of Line 8/11 (Figure 51). This is interpreted to be a zone of slide materials which are saturated (at the time of this geophysical survey) and extend to a depth of about 50-60 feet. The shallow and small area of higher resistivity materials (>25 ohm-meter) downslope from P-1 are representative of the remediated National Forest roadway, which was well drained and very dry at the time of this survey. Below about 50 feet, the resistivities become very uniform in the claystone.

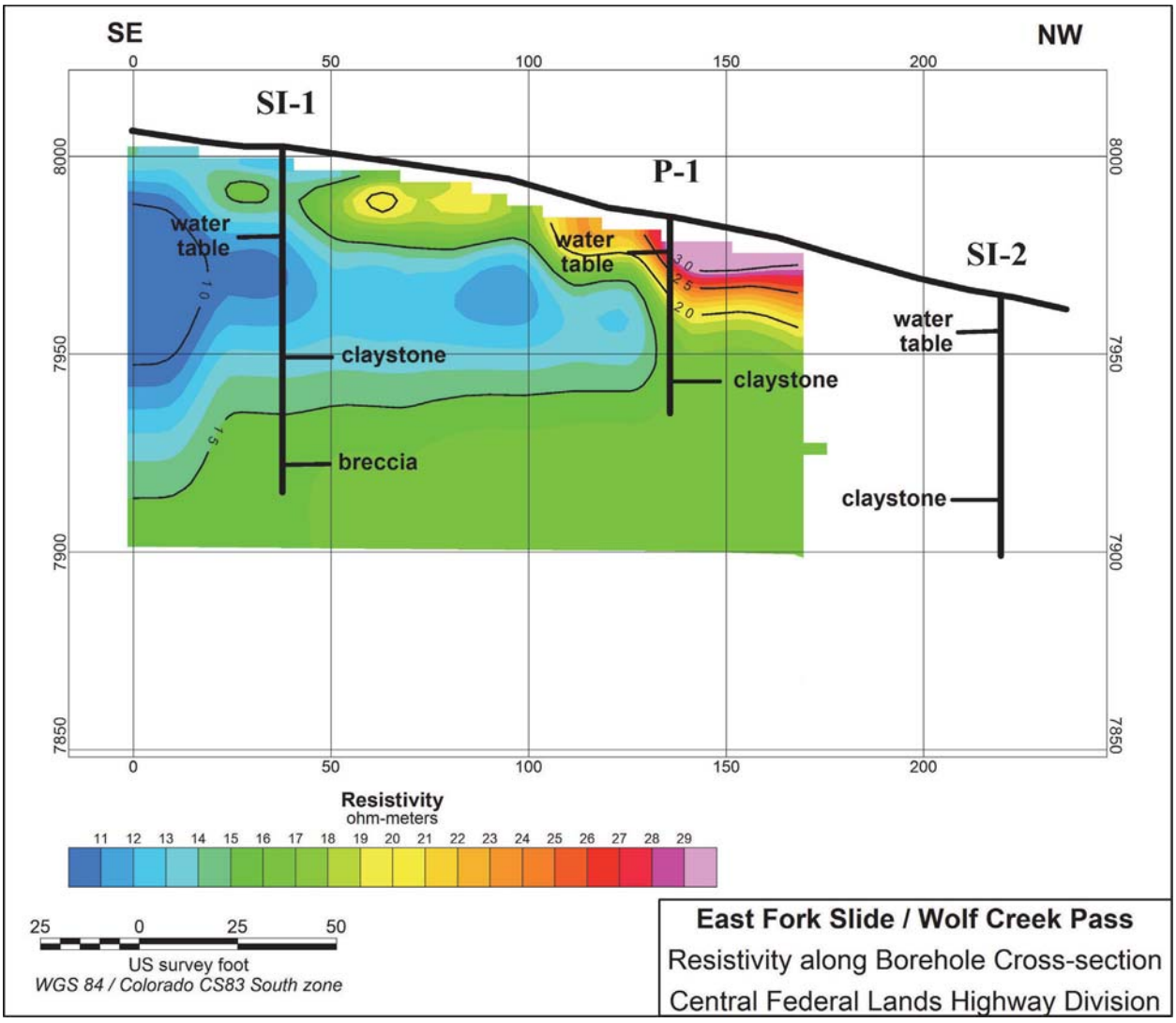

Figure 63. Plot. Resistivity slice extracted from 3D volume through the boreholes.

Figure 64 presents seismic velocity results extracted from the 3D volume along the borehole cross-section. The velocity slice through these boreholes has been truncated at about elevation 7,900 feet, which generally corresponded to the maximum velocities obtained along this slice. This was done to remove the '*apparent*' decrease in velocity beneath the high-velocity layer, as shown on other velocity slices (e.g., Figures 55-59). This decrease in velocity is known to be an artifact of the numerical modeling. Based on water table measurements in the borings, the P-wave velocities obtained within the volume sampled below the water table are not greater than 5,000 ft/sec; this implies that the materials within the slidemass at the time of the seismic survey were not 100% saturated. Allen and others (1980) have shown that even a 0.2% reduction in the percent saturation will yield compressional-wave velocities that are representative of the soil skeleton, not the bulk compressibility of the pore-fluid (i.e., groundwater). Therefore, the water table did not have an effect on the P-wave velocities imaged within the 3D grid. The claystone (bedrock) mapped in borings SI-1 and P-1 correlate with a P-wave velocity of 4000-4500 ft/sec. If this velocity can be used as the calibration for the interpreted slide plane, then the relief on the slide plane can be observed on other velocity slices (Figures 55-59). The lithologic log of SI-1 indicates breccia at 82 feet which correlates with the 6000 ft/sec velocity contour. At the southern-most end of the slice, a maximum velocity of 7500 ft/sec was obtained; this represents velocities at about 100 feet below the surface. This slice, like the others from the 3D seismic volume, shows the variability and general trend of increasing velocity with depth above the interpreted depth to the slide plane at the soil/claystone interface, which may be the result of obtaining the seismic data 1 ¼ years after movement and the slidemass has consolidated.

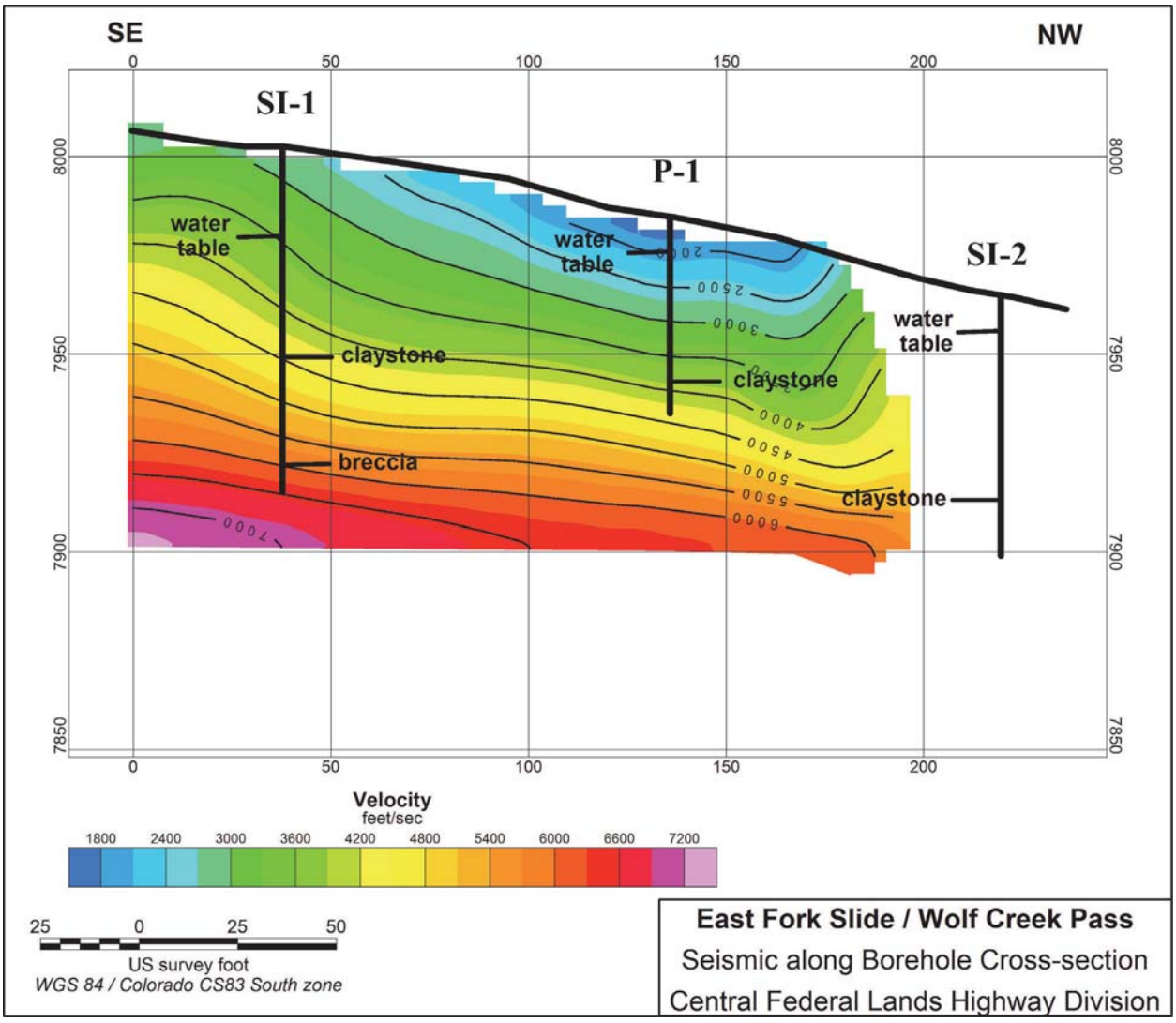

Figure 64. Plot. Velocity slice extracted from the 3D volume through the boreholes.

JACKSON MOUNTAIN LANDSLIDE

Although the field investigation at the Jackson Mountain Landslide wanted to utilize the same field set-up and approach as used at the East Fork Landslide, it was not possible because Highway 160 cuts through the middle of the area to be investigated – the 3D grid. Therefore, the survey area at the Jackson Mountain Landslide was subdivided into two smaller 3D survey grids, one on either side of Highway 160. The field set-up splitting the area to be surveyed into two separate / independent 3D grids is illustrated in Figure 65. The existence of the highway in the middle of the survey site greatly increased the complexity of the data acquisition, processing, analysis and presentation.

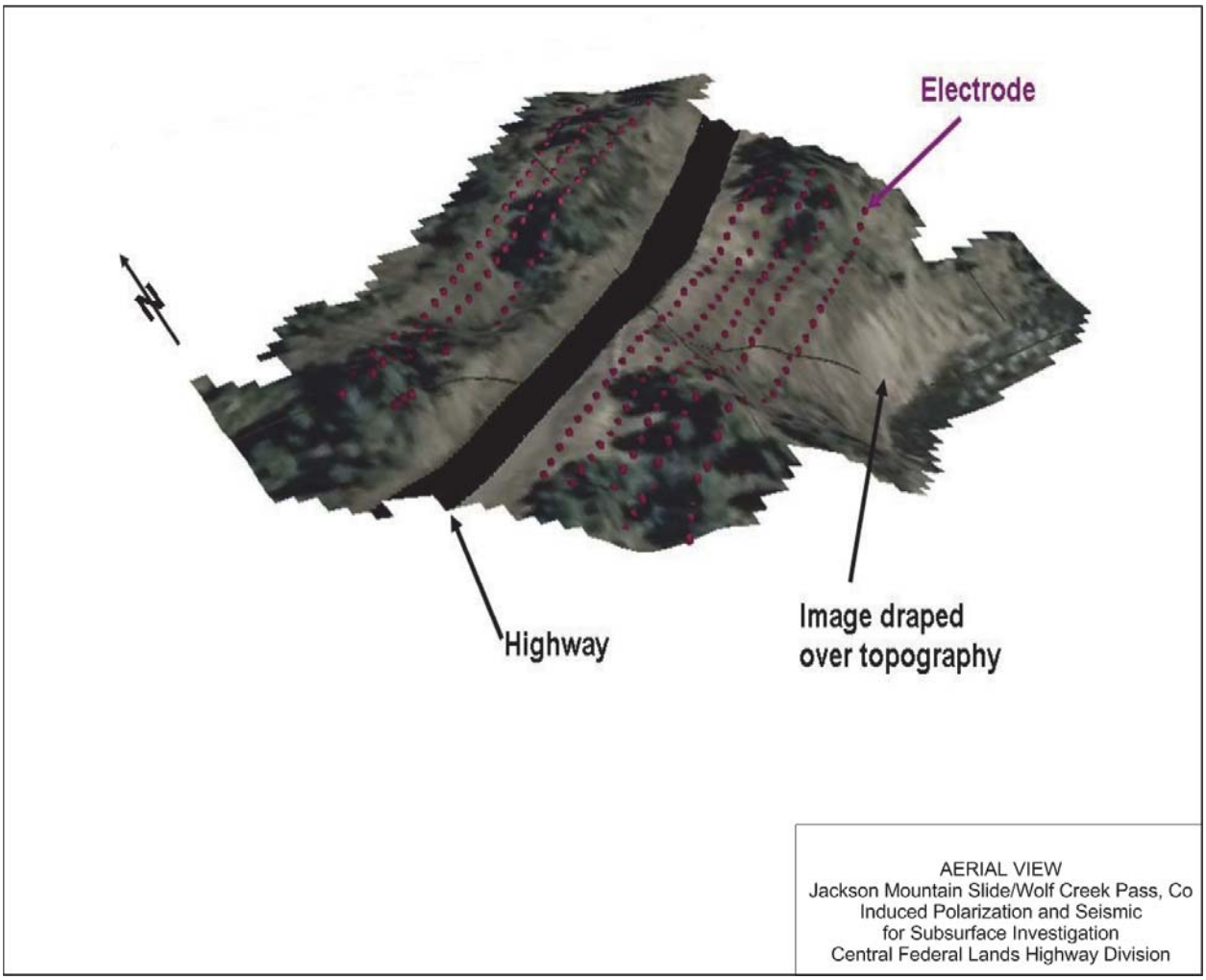

Figure 65. Photo. Digital elevation model for the Jackson Mountain Landslide showing the position of the two 3D grids with respect to Highway 160.

Induced Polarization

Electrical (IP and resistivity) data were collected in three sets of three lines each, similar to that described for the East Fork survey. Also, the ERT inversions were run using the same line sequencing as at East Fork. The data volumes were constructed by loading all the inversion

values into Geosoft databases and applying minimum curvature gridding to the entire volume. The IP and resistivity values computed in the area beneath the highway (i.e., between the two 3D grids) are interpolated, and as such are of lower quality and less confidence should be placed in the results.

Figures 66 through 71 are horizontal slices through the IP volume at various elevations cutting downward at 30-foot intervals. The color scale for the horizontal IP slices beneath Jackson Mountain Landslide matches the scale used at the East Fork Landslide. The horizontal slice at an elevation of 7530 feet shown in Figure 66 cuts into the highest elevations found within the survey area and Figure 71 cuts through the deepest portion of the survey area investigated at elevation 7380 feet.

The IP anomalies observed at the Jackson Mountain Landslide are broader, smoother, larger amplitude and much more dramatic than those obtained at the East Fork Landslide. Additionally, the amplitude and areal extent of the large IP anomalies, both positive and negative, increased with increasing depth of investigation. The reason for this difference is unclear, but since the two slides are completely different failure types (i.e., translational at the East Fork Landslide and rotational at the Jackson Mountain Landslide) and have very different geologic settings, maybe horizontal slicing is not an appropriate way to view the variation of 3D geophysical data at the Jackson Mountain Landslide.

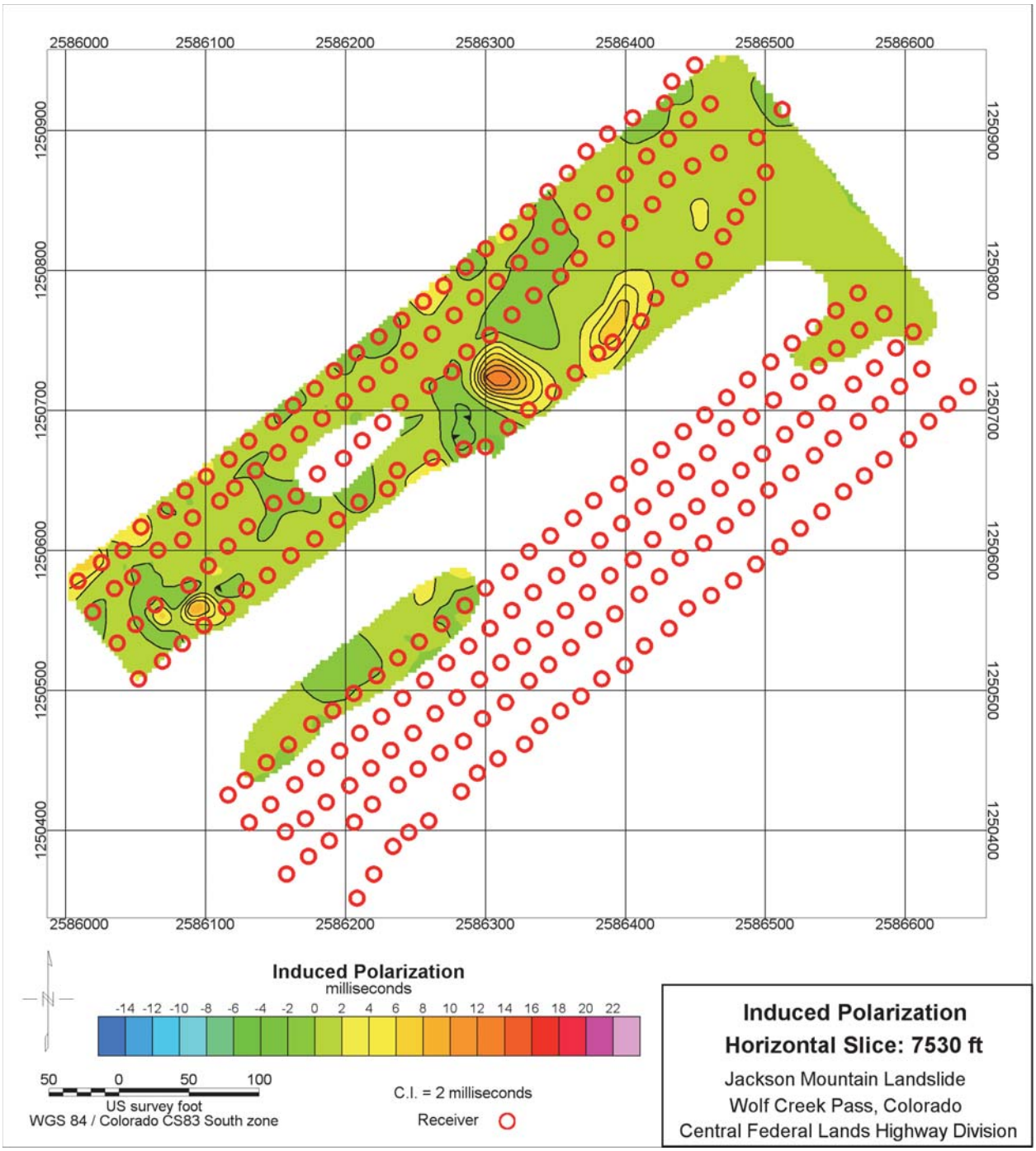

Figure 66. Map. Horizontal slice through the Jackson Mountain Landslide 3D IP volume.

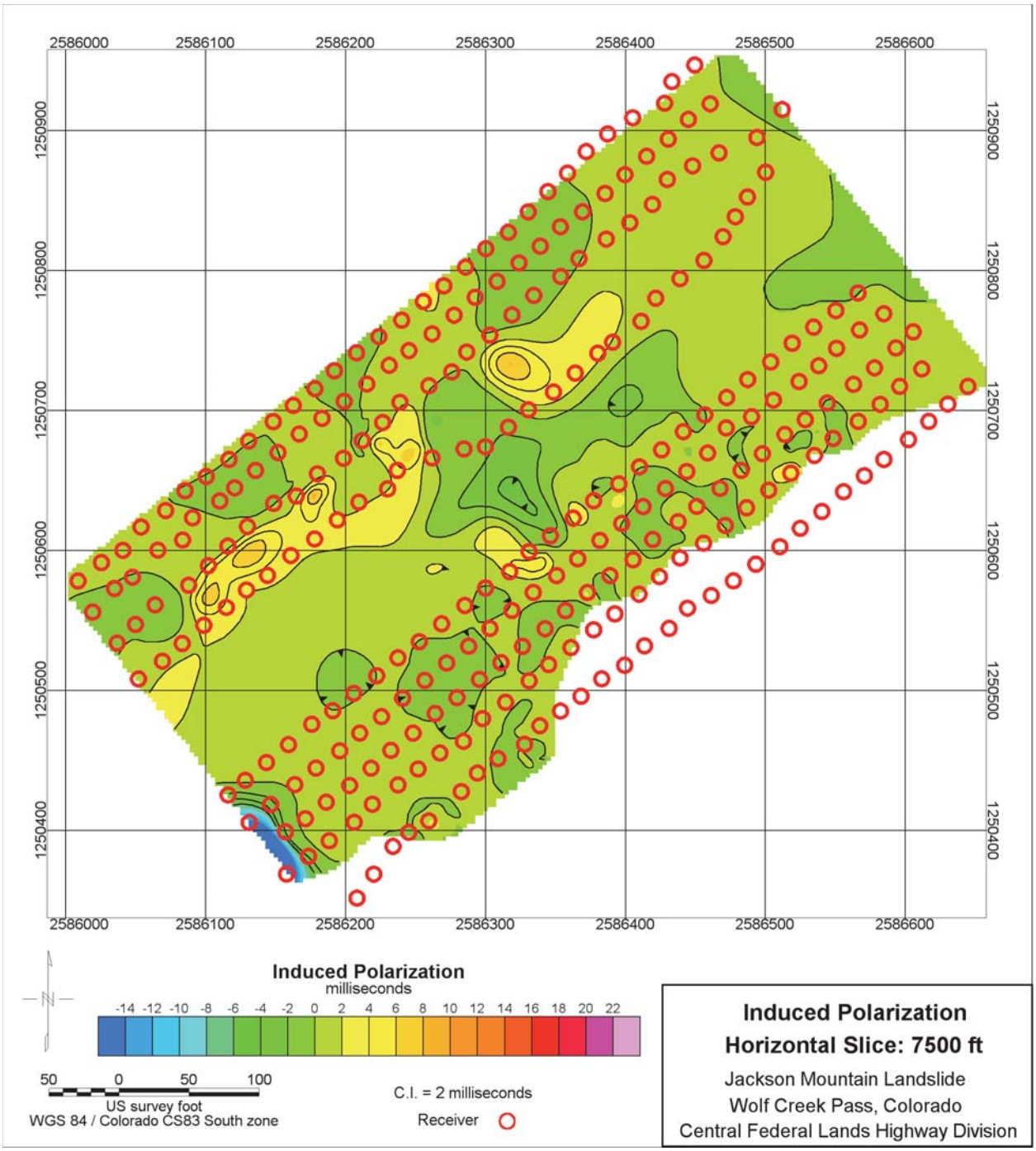

Figure 67. Map. Horizontal slice through the Jackson Mountain Landslide 3D IP volume.

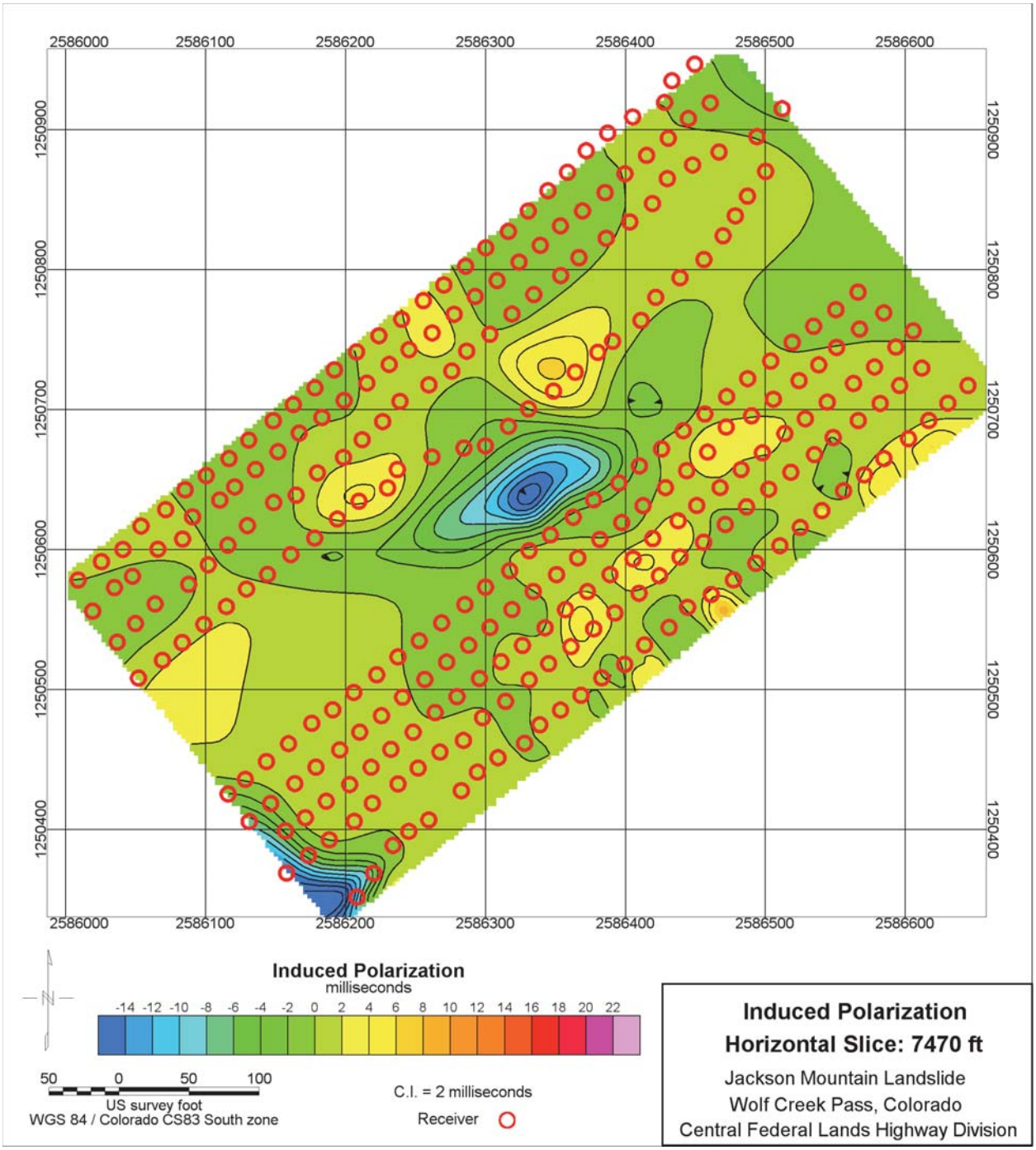

Figure 68. Map. Horizontal slice through the Jackson Mountain Landslide 3D IP volume.

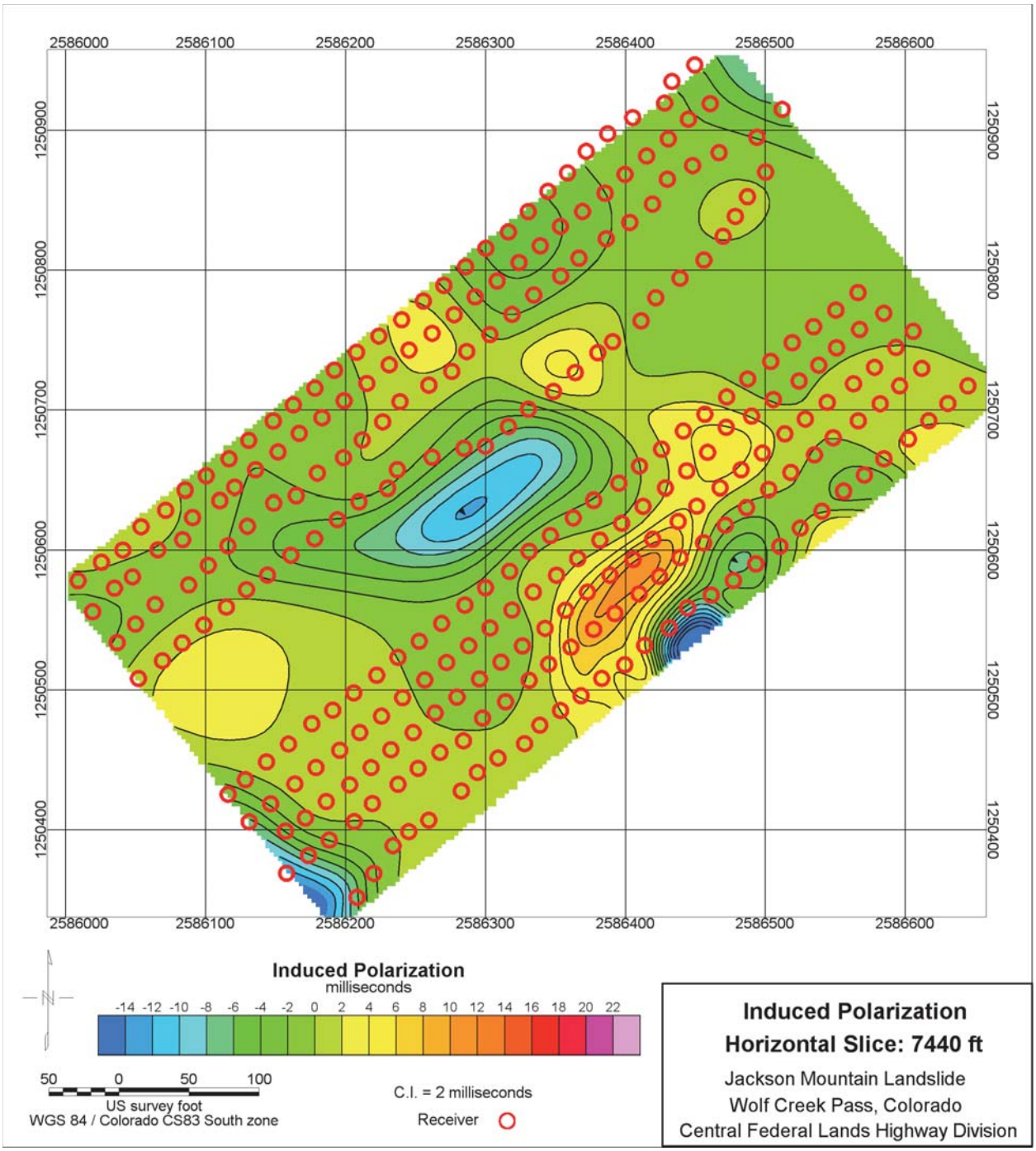

Figure 69. Map. Horizontal slice through the Jackson Mountain Landslide 3D IP volume.

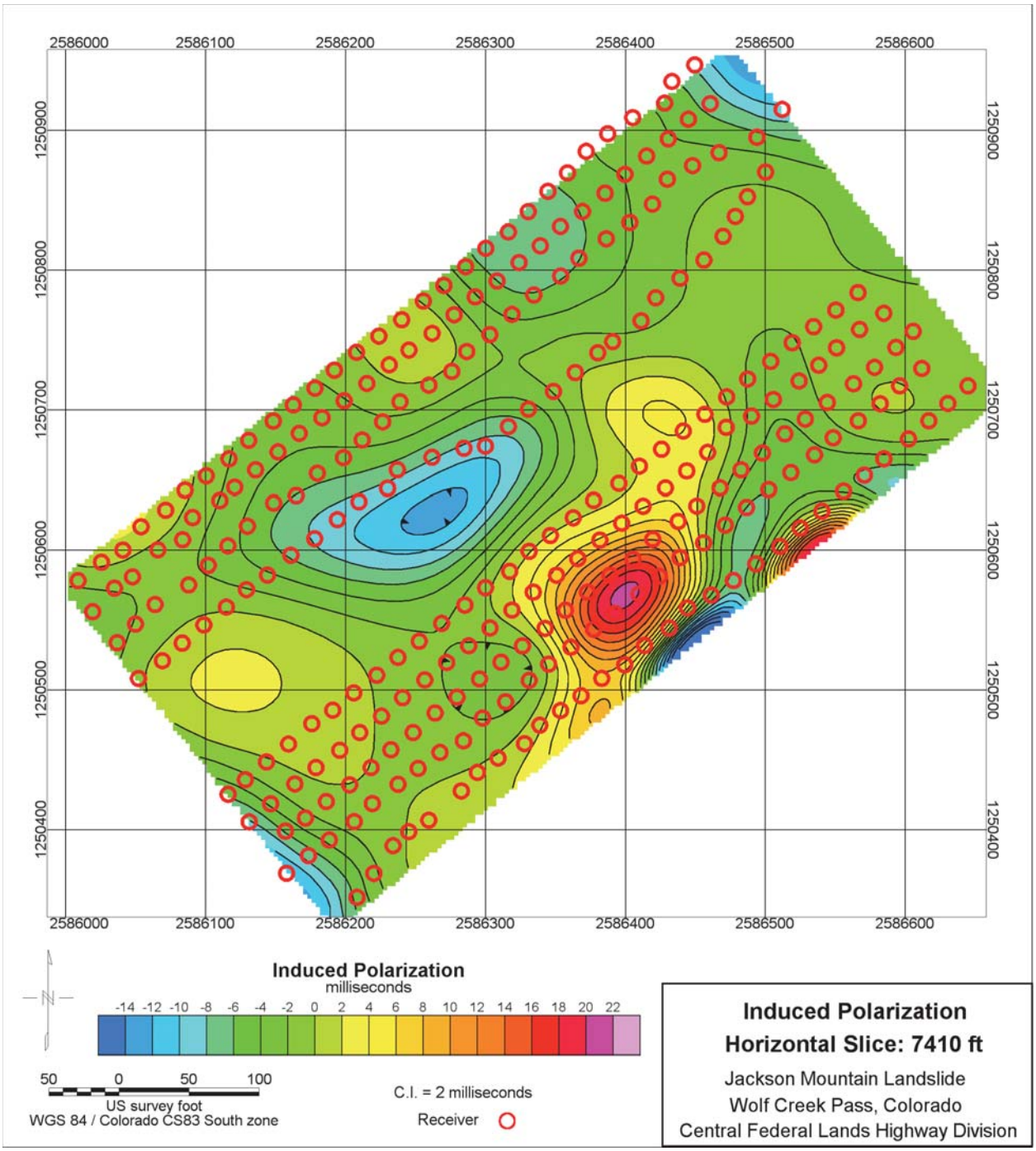

Figure 70. Map. Horizontal slice through the Jackson Mountain Landslide 3D IP volume.

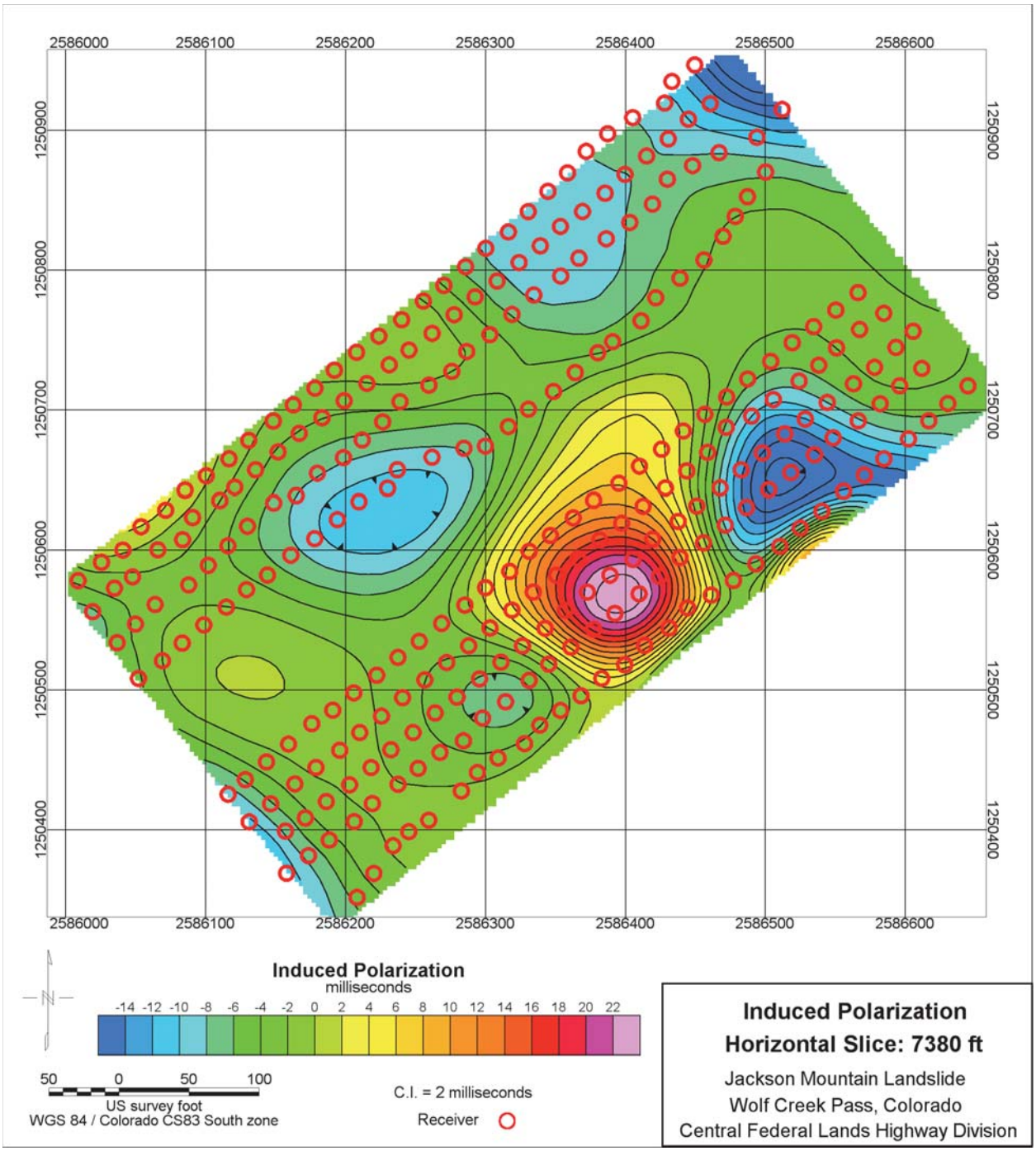

Figure 71. Map. Horizontal slice through the Jackson Mountain Landslide 3D IP volume.

Figure 72 shows a thin surface-following slab of the IP data volume viewed from directly above. Figure 73 is a view of this same slab from the side. Highway 160 is marked with black lines running across the IP data. Receiver locations are noted with black cubes. Color range for all IP slabs runs from -5 ms in dark blue to 15 ms in pink.

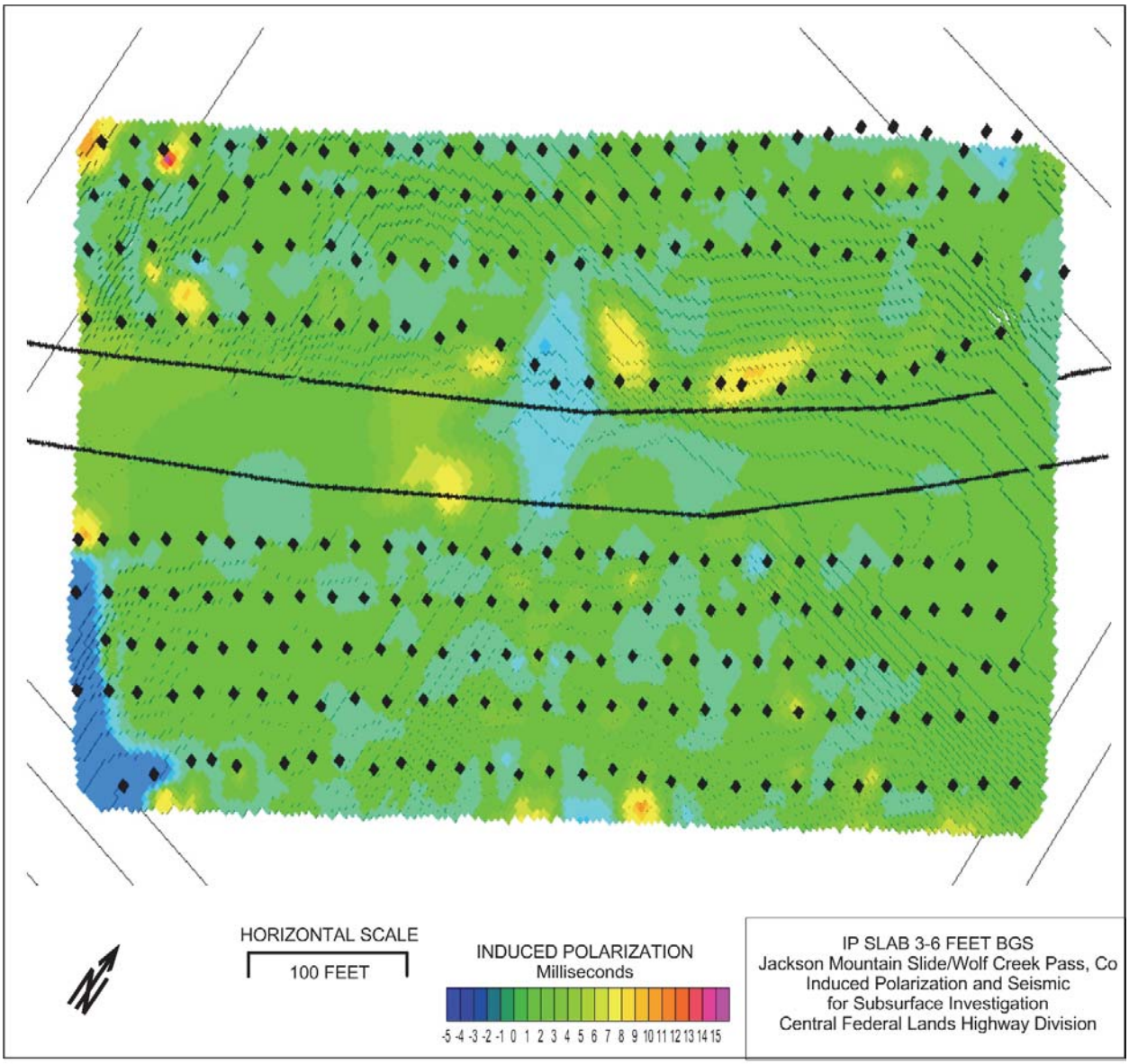

Figure 72. Map. Surface-following IP slab: 3-6 ft below ground surface with highway edge marked with black lines.

Note that the amplitude of the IP anomalies increases with depth below the ground surface on Figures 72 and Figures 74 through 77.

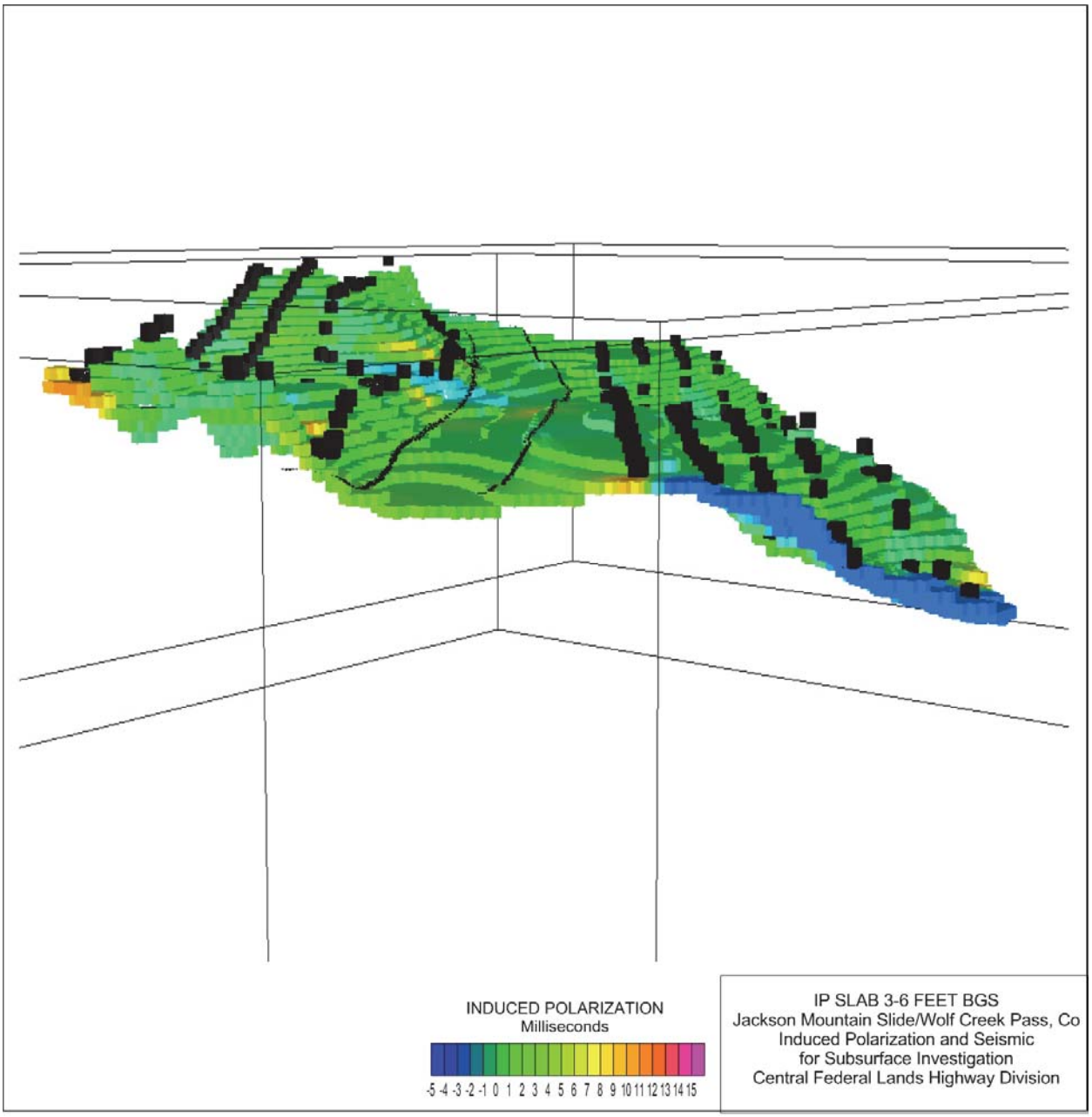

Figure 73. Map. Surface-following IP slab: 3-6 ft below ground surface viewed edge-on, looking along highway to northeast.

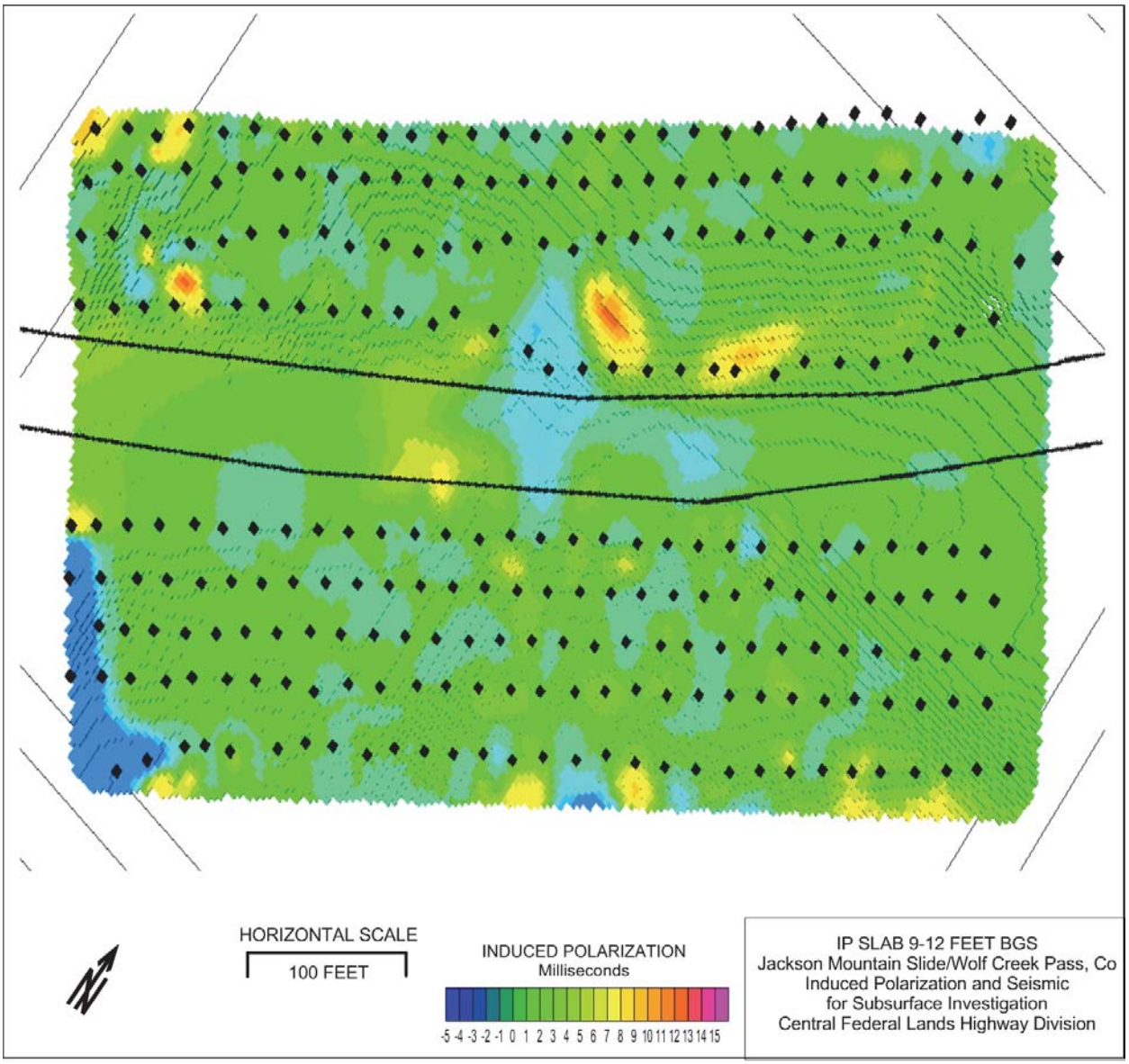

Figure 74. Map. Surface-following IP slab: 9-12 ft below ground surface.

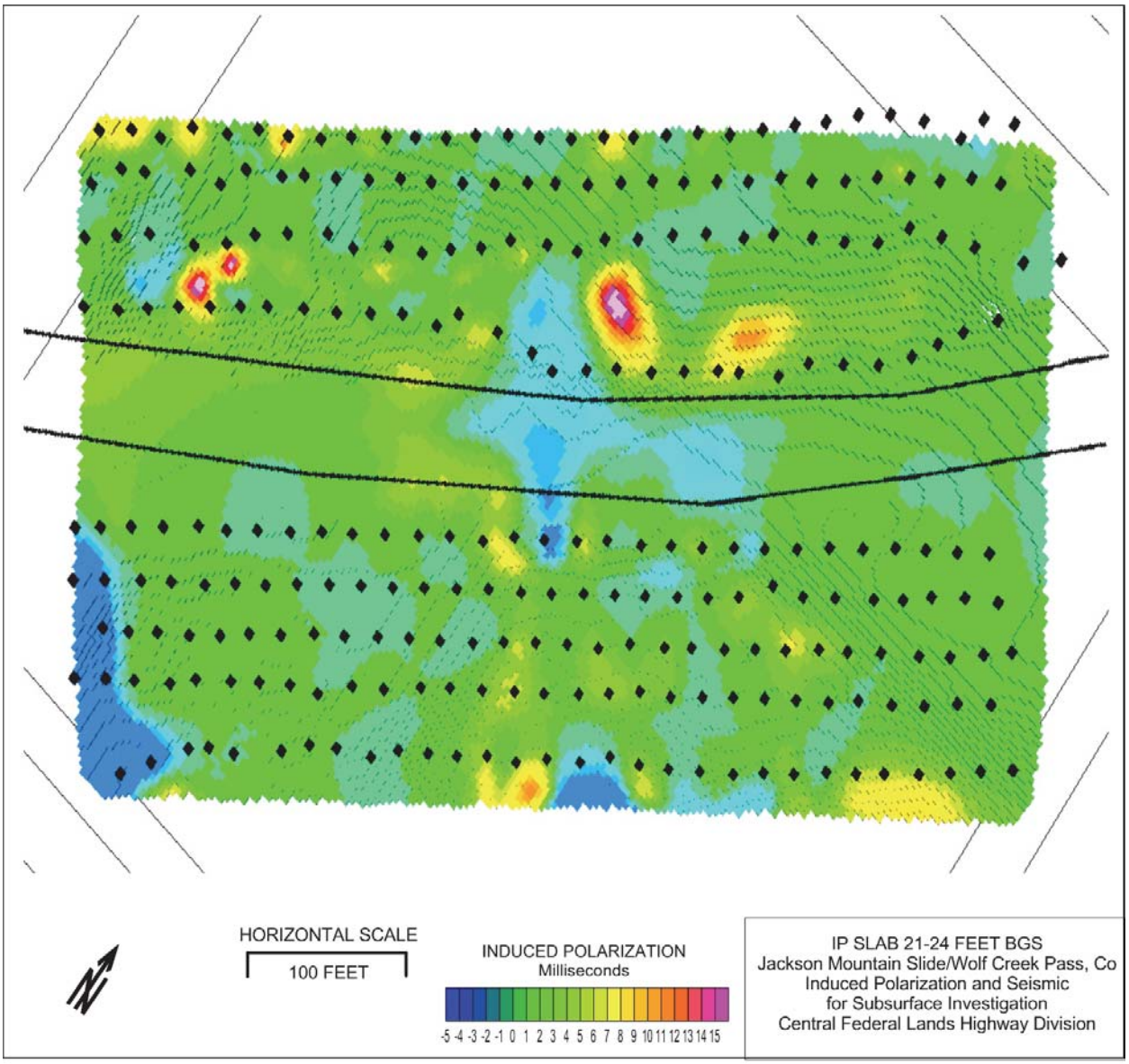

Figure 75. Map. Surface-following IP slab: 21-24 ft below ground surface.

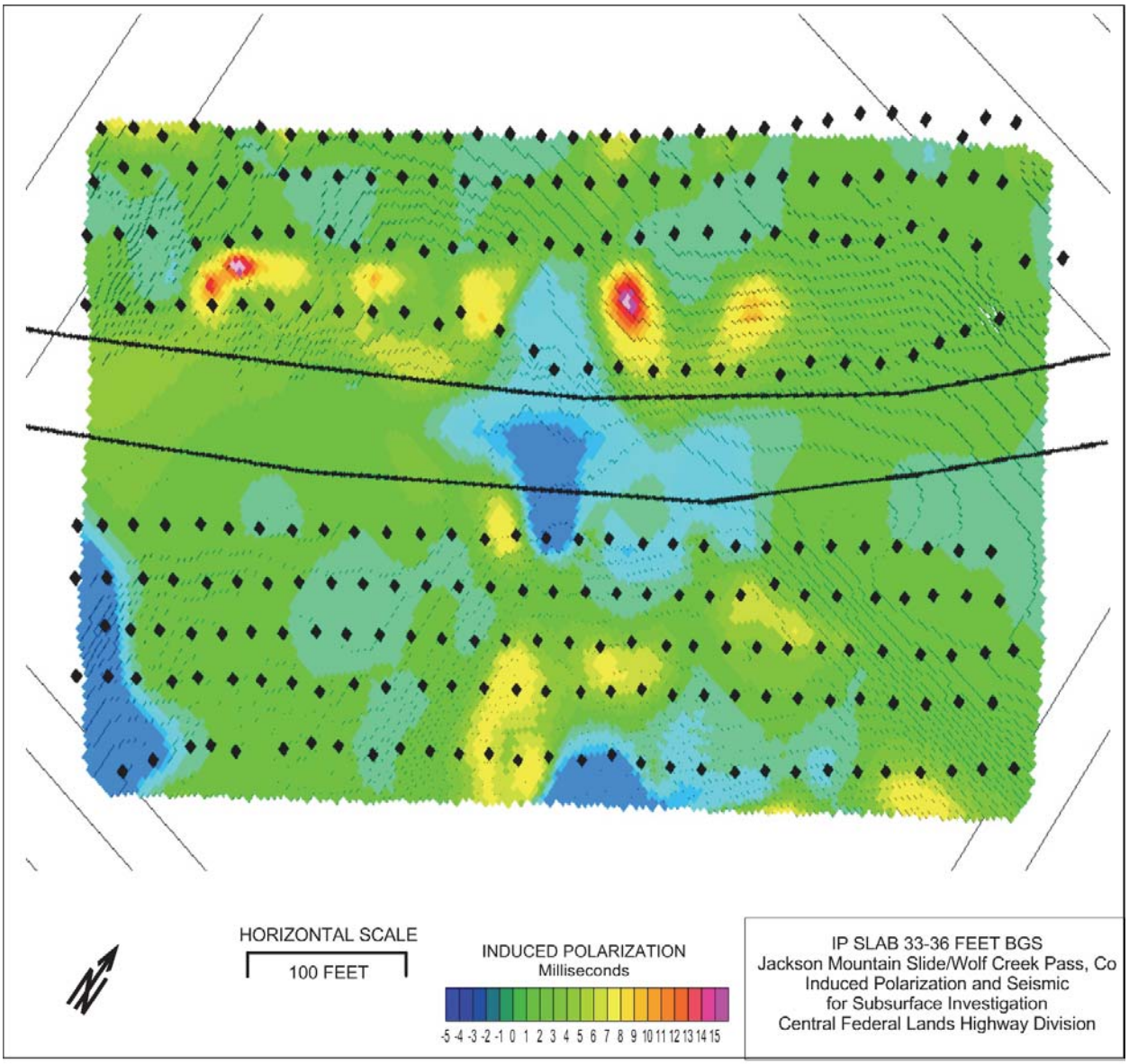

Figure 76. Map. Surface-following IP slab: 33-36 ft below ground surface.

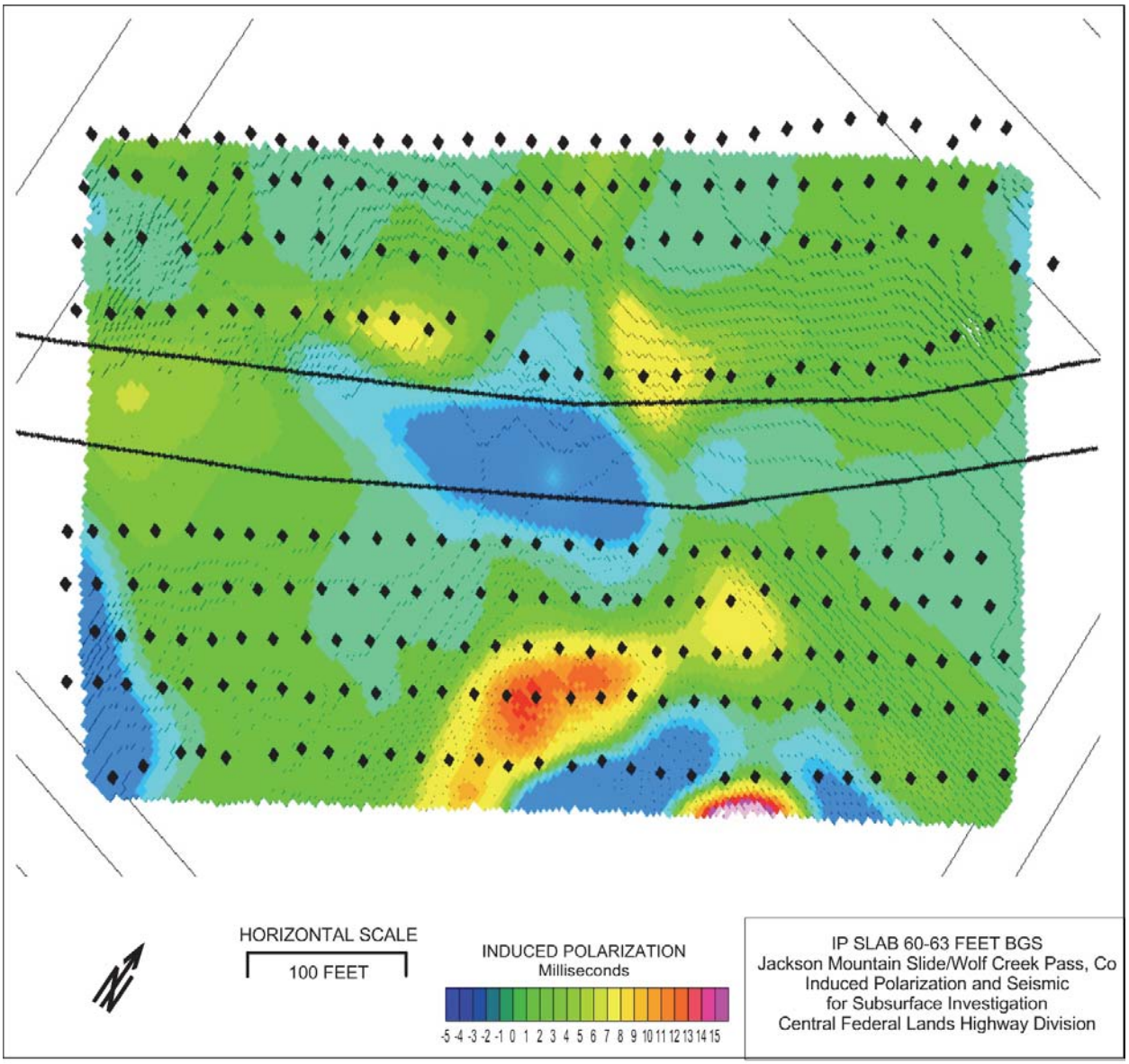

Figure 77. Map. Surface-following IP slab: 60-63 ft below ground surface.

Resistivity

The horizontal slice at an elevation of 7530 feet shown on Figure 78 cuts into the highest elevations found within the survey area. The slice has results from both the 3D subgrids and a gap where the highway is cut into the hillside. For resistivity, the color scales are the same. Figures 78-83 are slices at decreasing elevations through the resistivity volume.

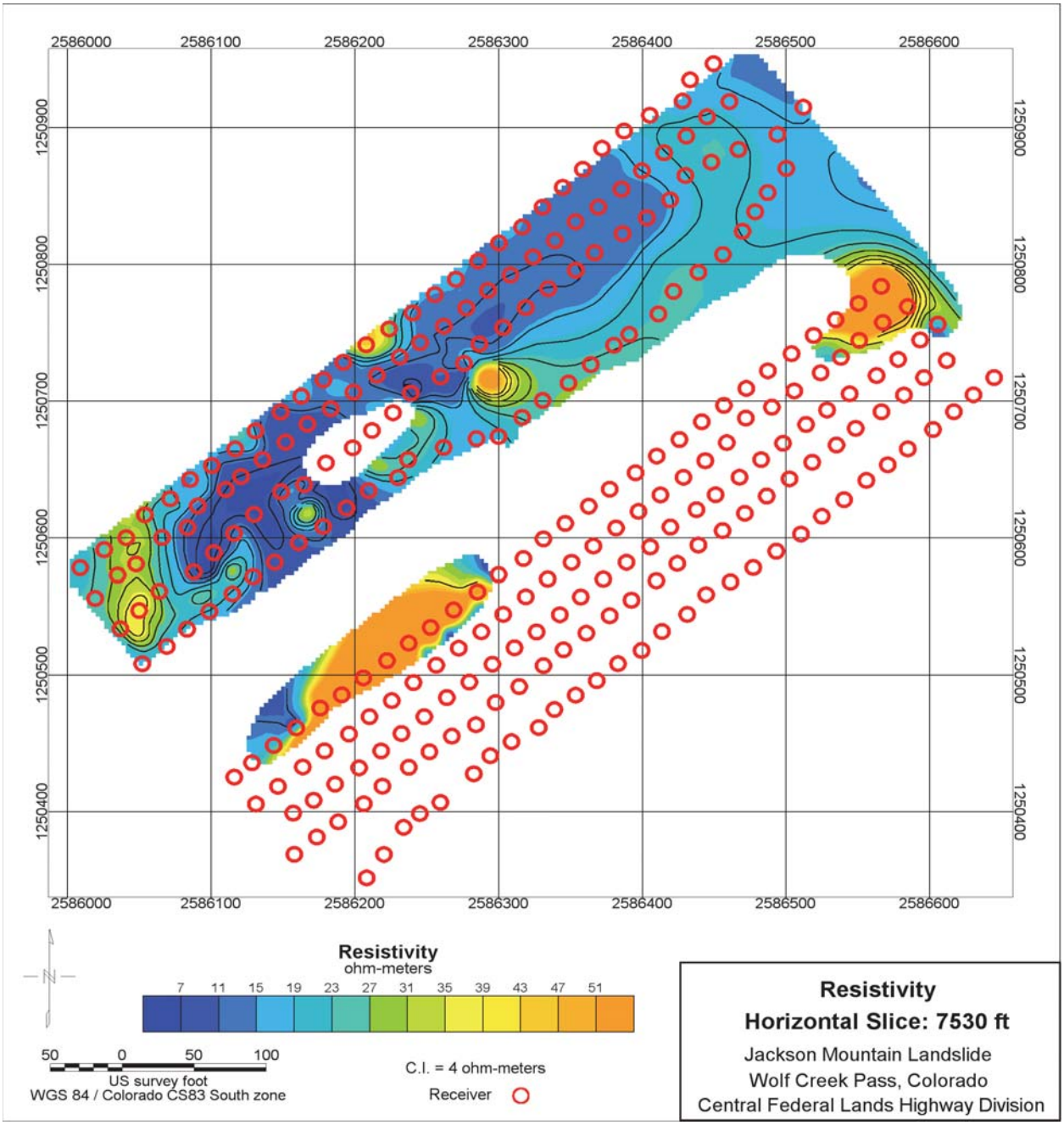

Figure 78. Map. Horizontal slice through the Jackson Mountain Landslide 3D resistivity volume.

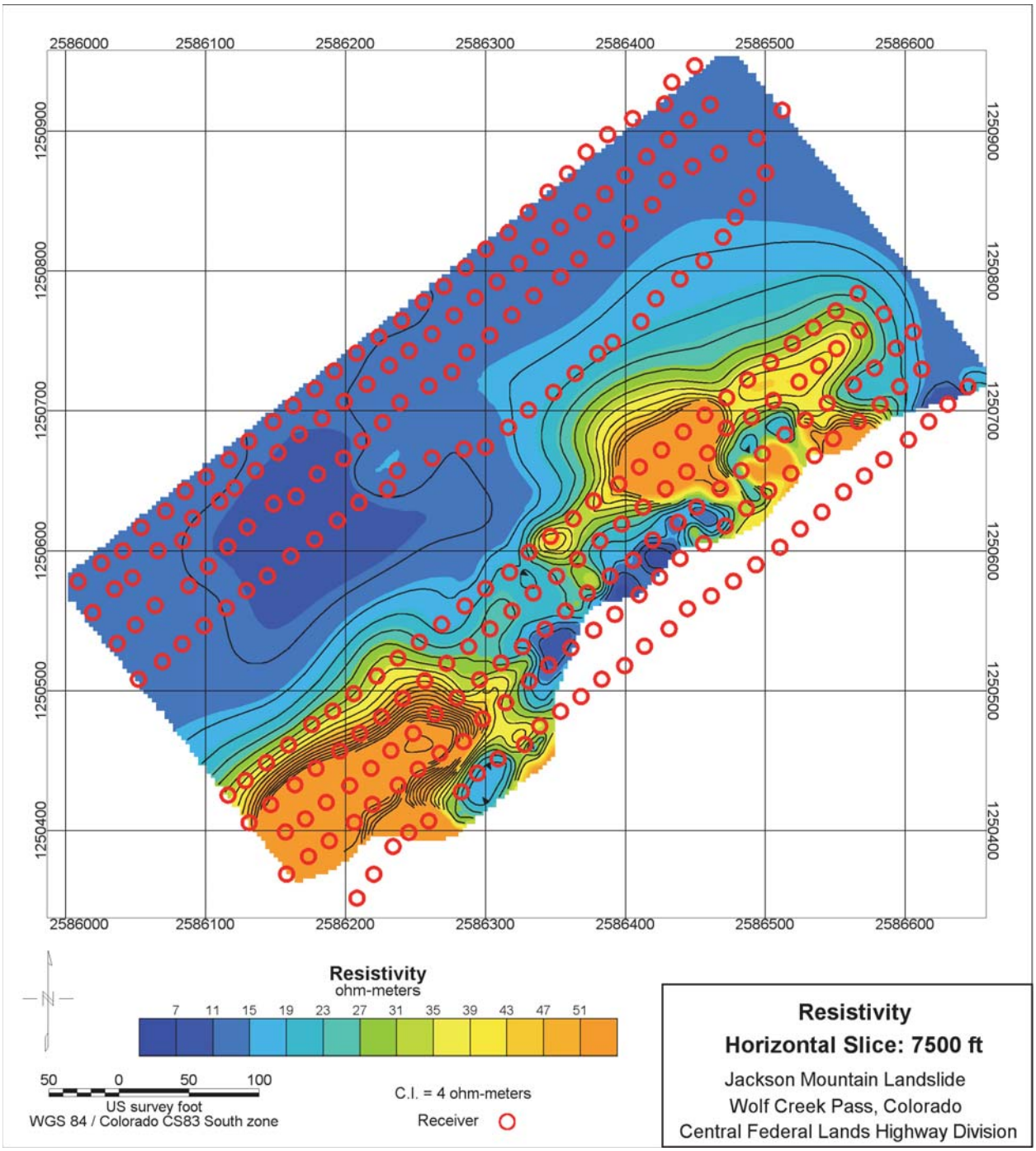

Figure 79. Map. Horizontal slice through the Jackson Mountain Landslide 3D resistivity volume.

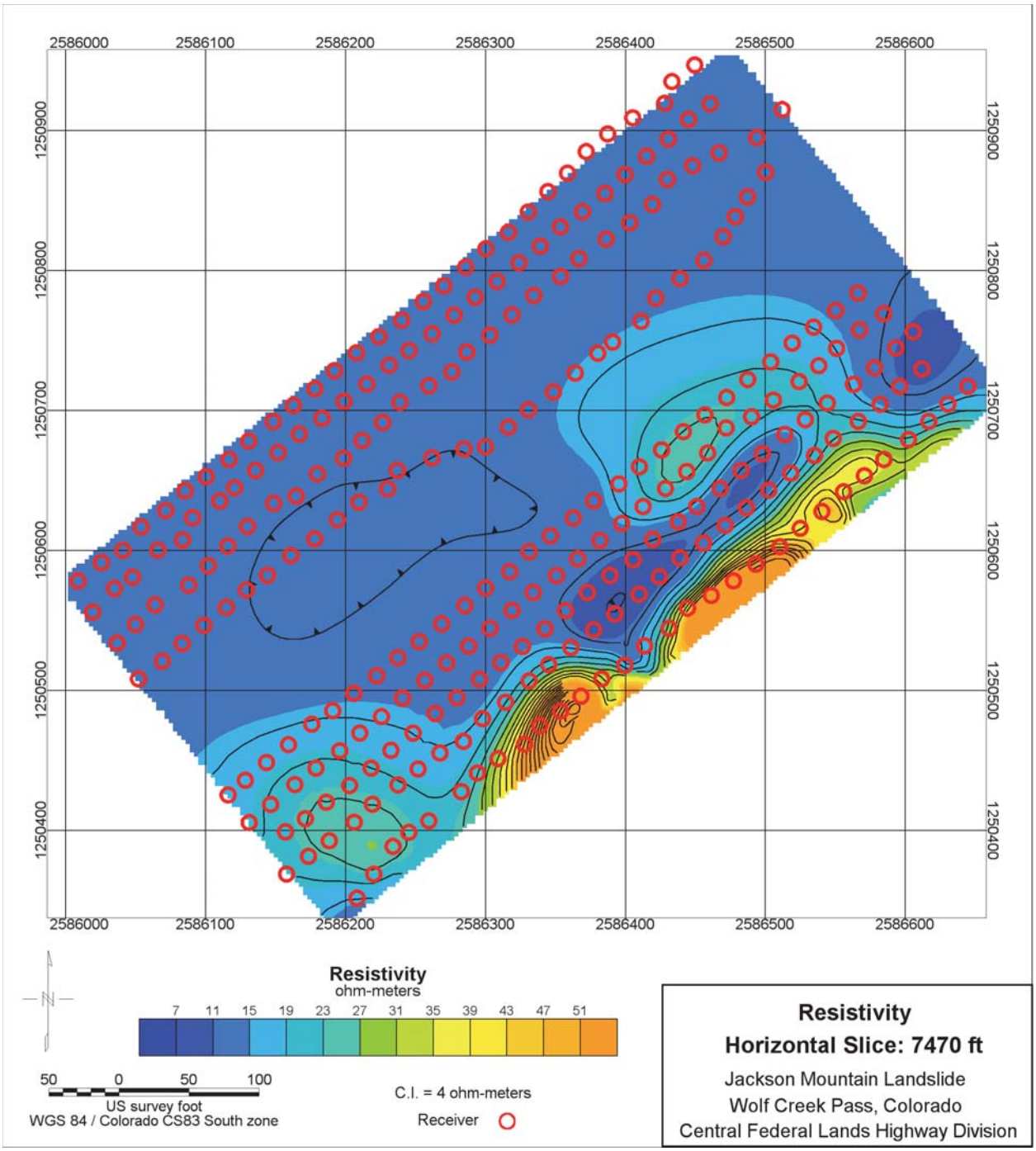

Figure 80. Map. Horizontal slice through the Jackson Mountain Landslide 3D resistivity volume.

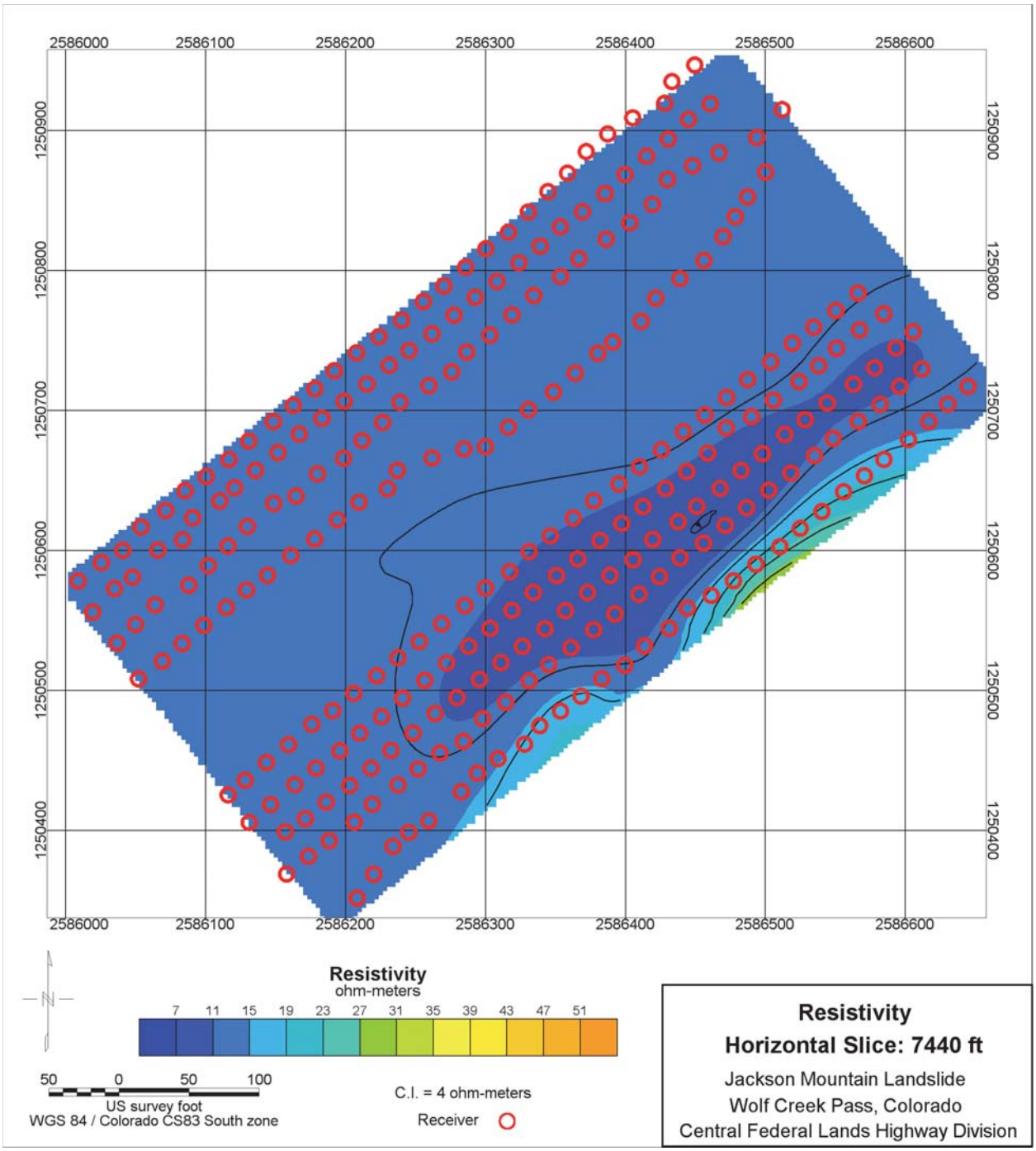

Figure 81. Map. Horizontal slice through the Jackson Mountain Landslide 3D resistivity volume.

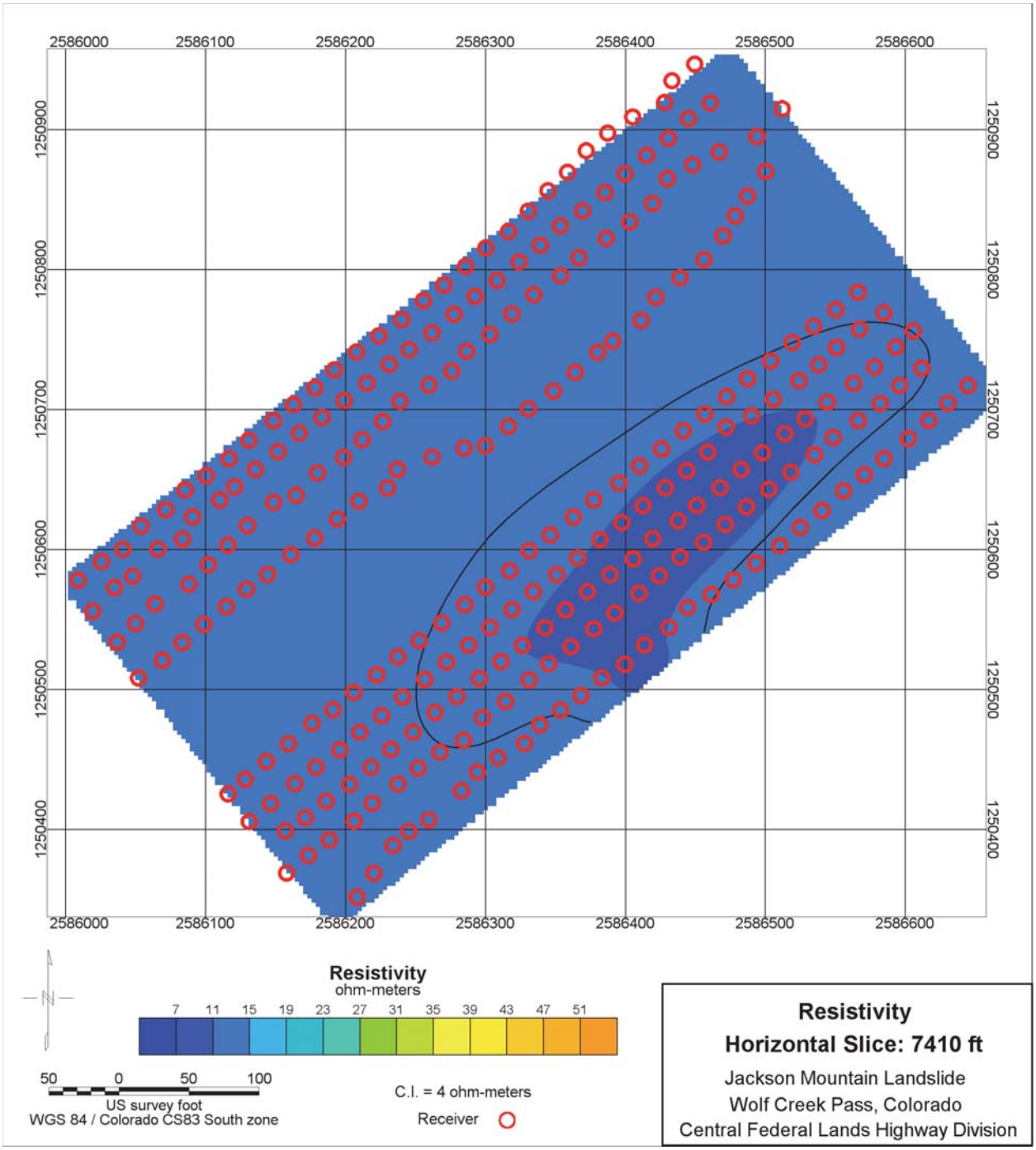

Figure 82. Map. Horizontal slice through the Jackson Mountain Landslide 3D resistivity volume.

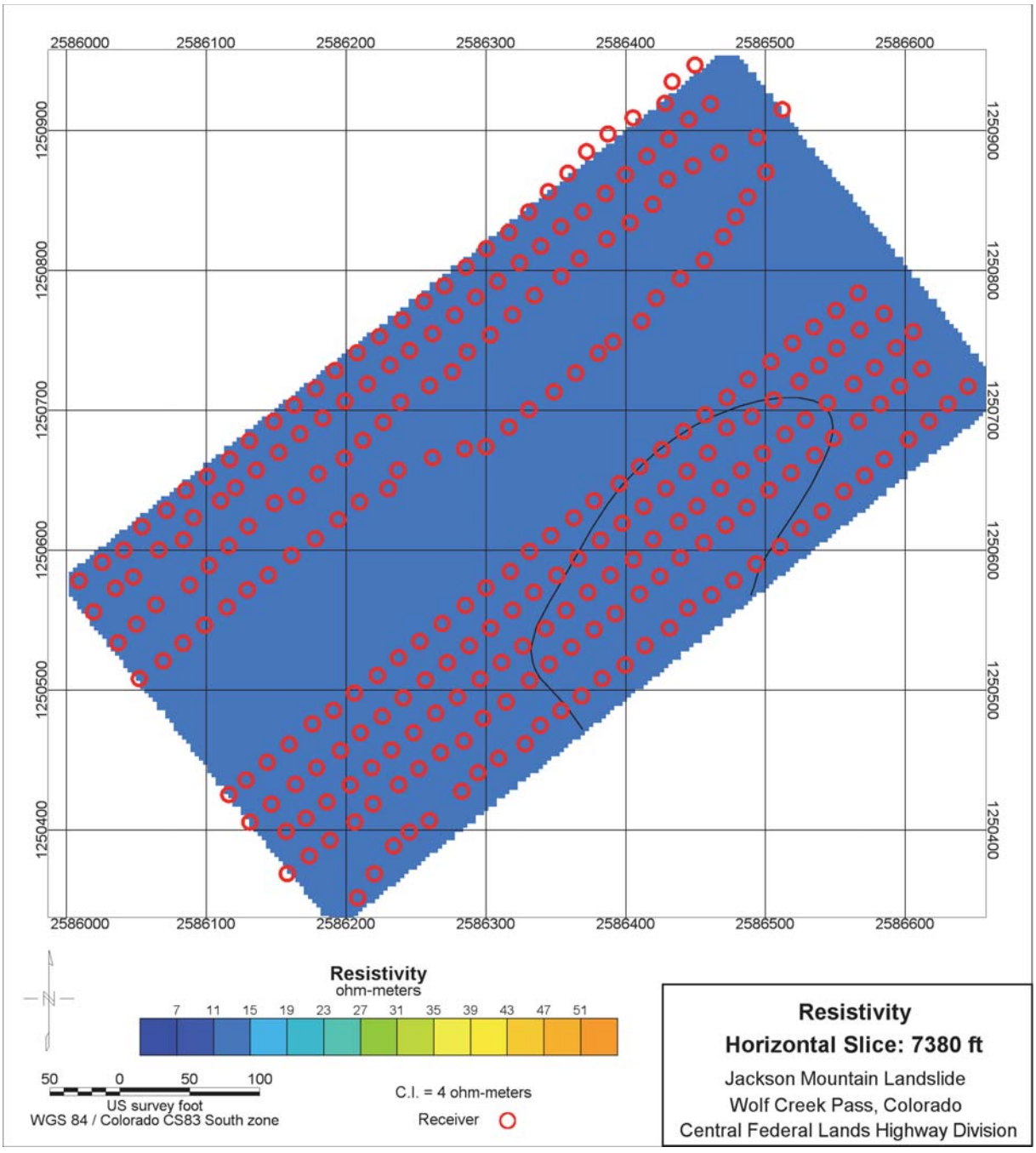

Figure 83. Map. Horizontal slice through the Jackson Mountain Landslide 3D resistivity volume.

The amplitude of the resistivity anomalies decreases rapidly with depth. The horizontal slices mix values from different subsurface depths producing asymmetric contour maps with the shallow portion displaying the bright yellows and oranges with high spatial frequency anomalies. To counter the varying depth below the ground surface of the horizontal slices a companion set of figures using surface following volumes is included in this section of the report. Figure 84 is the color scale for these slabs which are shown in Figures 85-89 for progressively deeper depths below the surface.

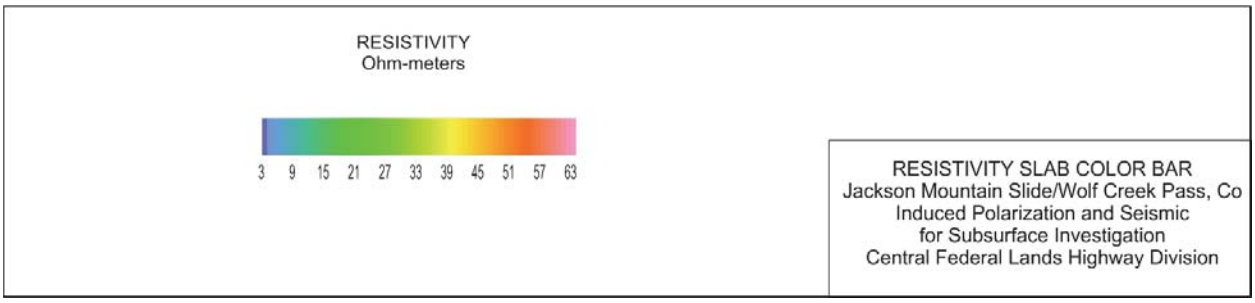

Figure 84. Graph. Color bar for resistivity slabs in ohm-meters.

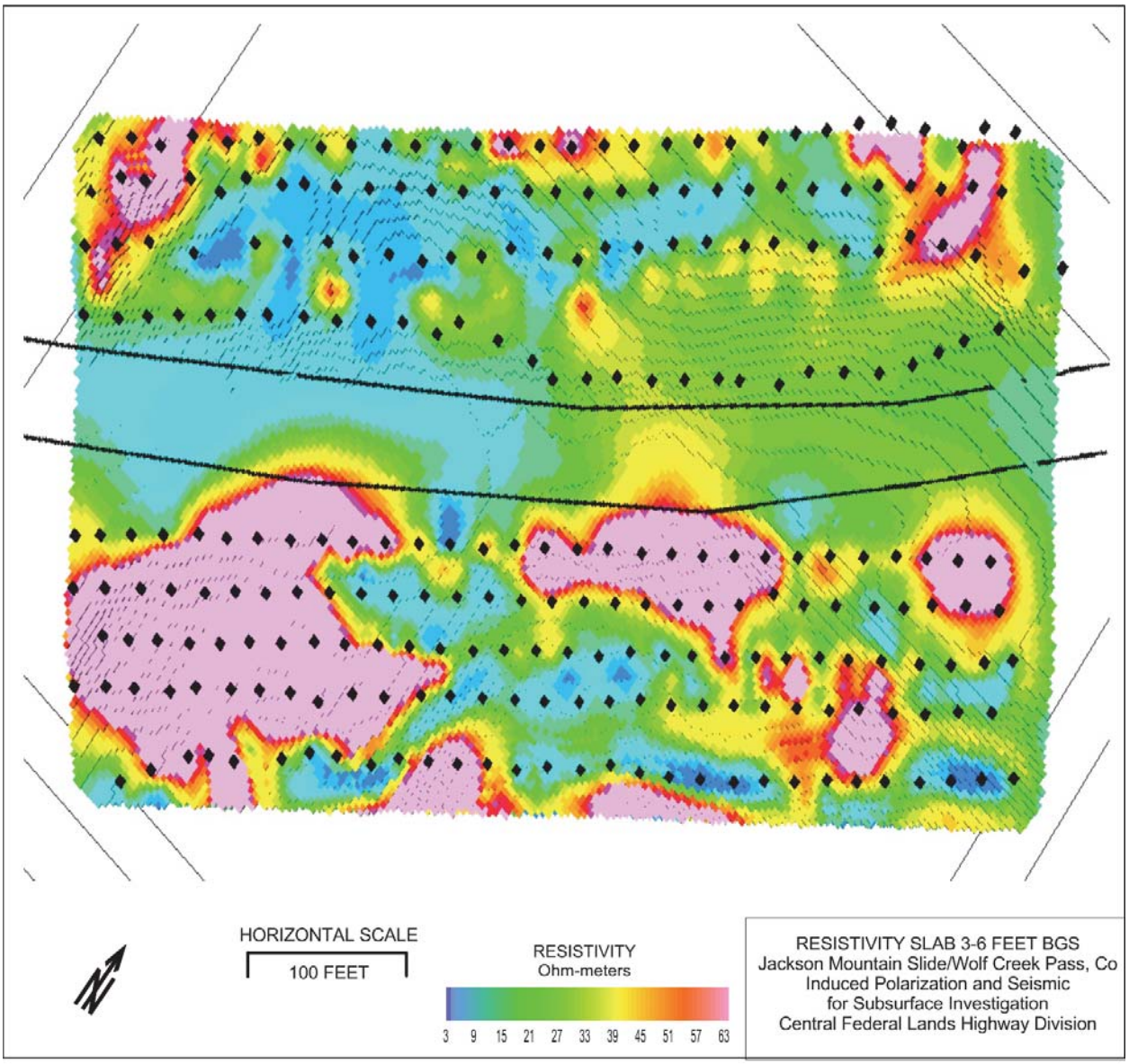

Figure 85. Map. Surface-following resistivity slab: 3-6 ft below ground surface with highway edge marked with black lines.

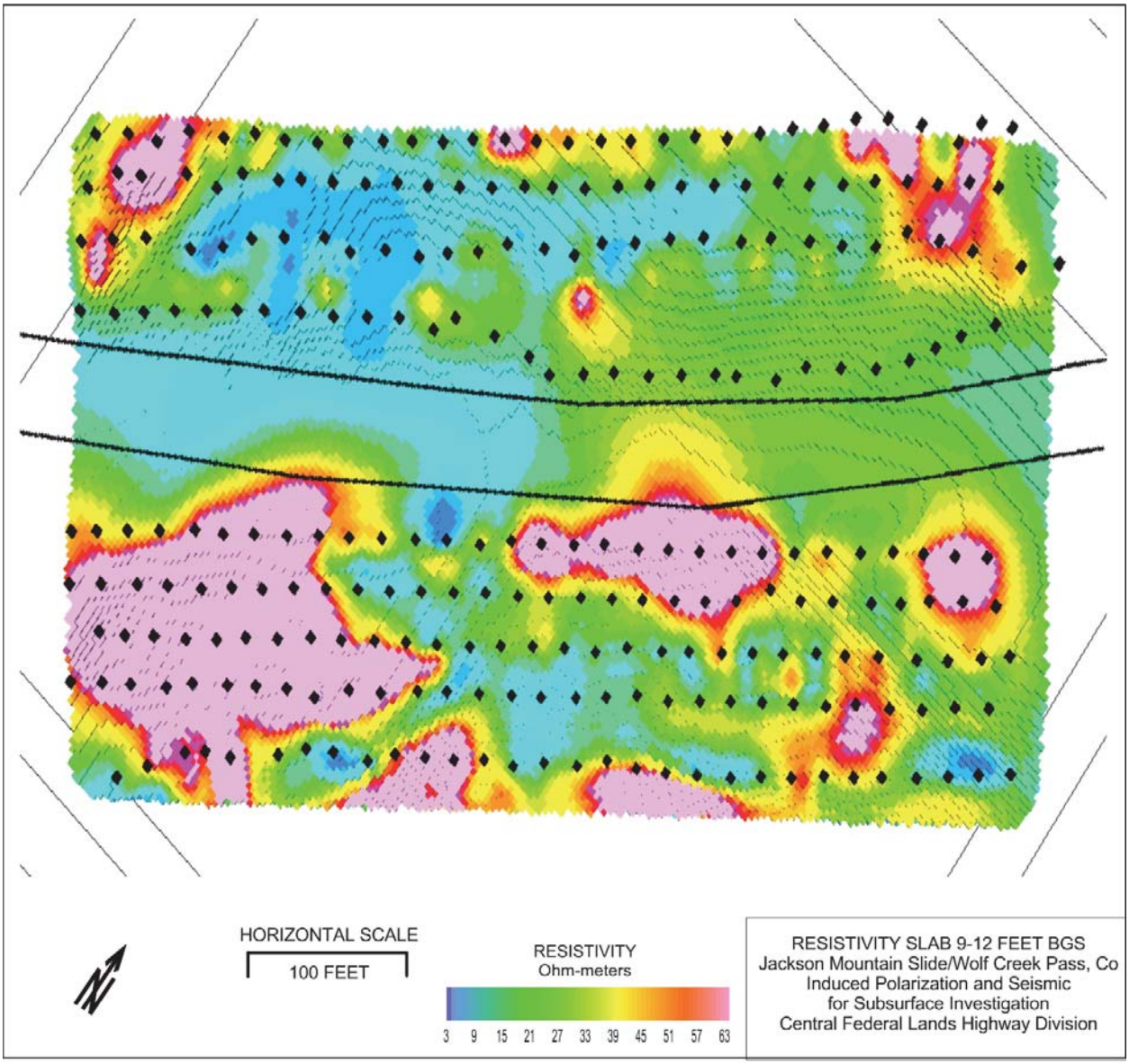

Figure 86. Map. Surface-following resistivity slab: 9-12 ft below ground surface.

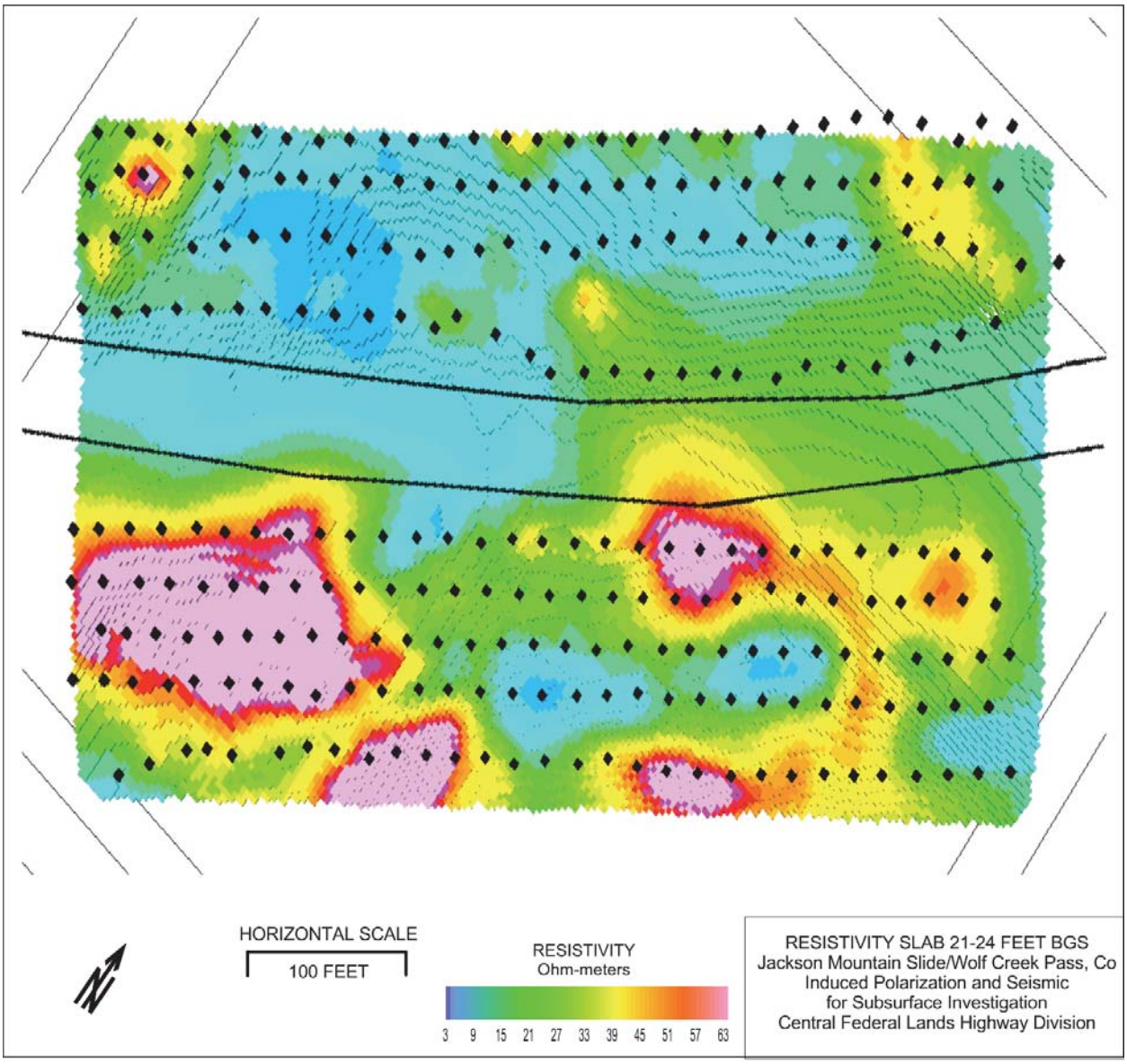

Figure 87. Map. Surface-following resistivity slab: 21-24 ft below ground surface.

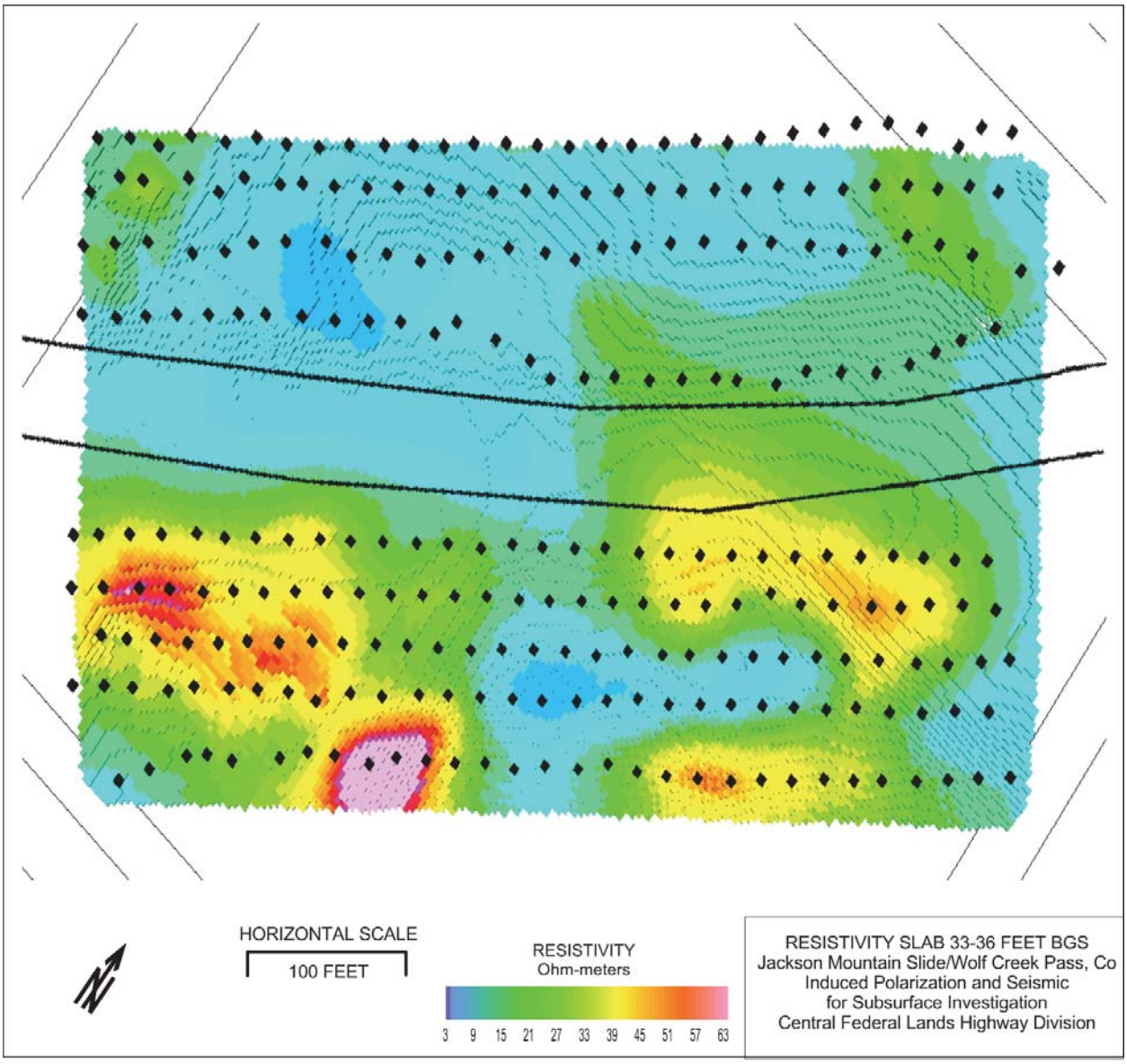

Figure 88. Map. Surface-following resistivity slab: 33-36 ft below ground surface.

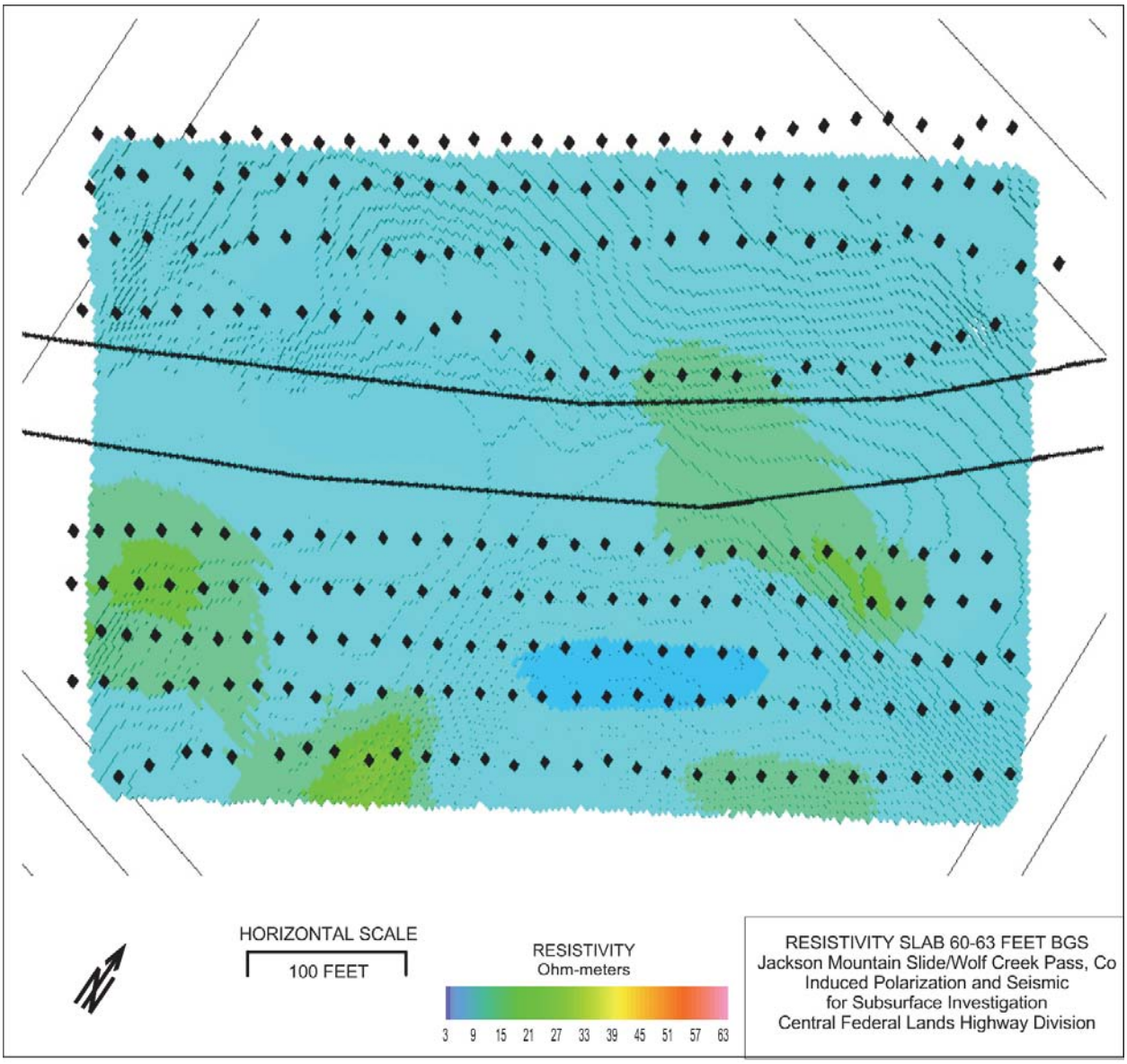

Figure 89. Map. Surface-following resistivity slab: 60-63 ft below ground surface.

Seismic Refraction

The 3D refraction seismic data for the Jackson Mountain Landslide were acquired with two separate 3D grids, one on each side of Highway 160. A gap exists in the geophone coverage as seen in Figures 65 and 90. The gap in the sensor array has a significant impact on the confidence level in the seismic results obtained at this site. This section presents a series of slices extracted from the 3D velocity volume, from the same position within the volume. The position of the slices is along the borings used for geologic correlation, cross-section B-B' (shown in Figures 90 and 102).

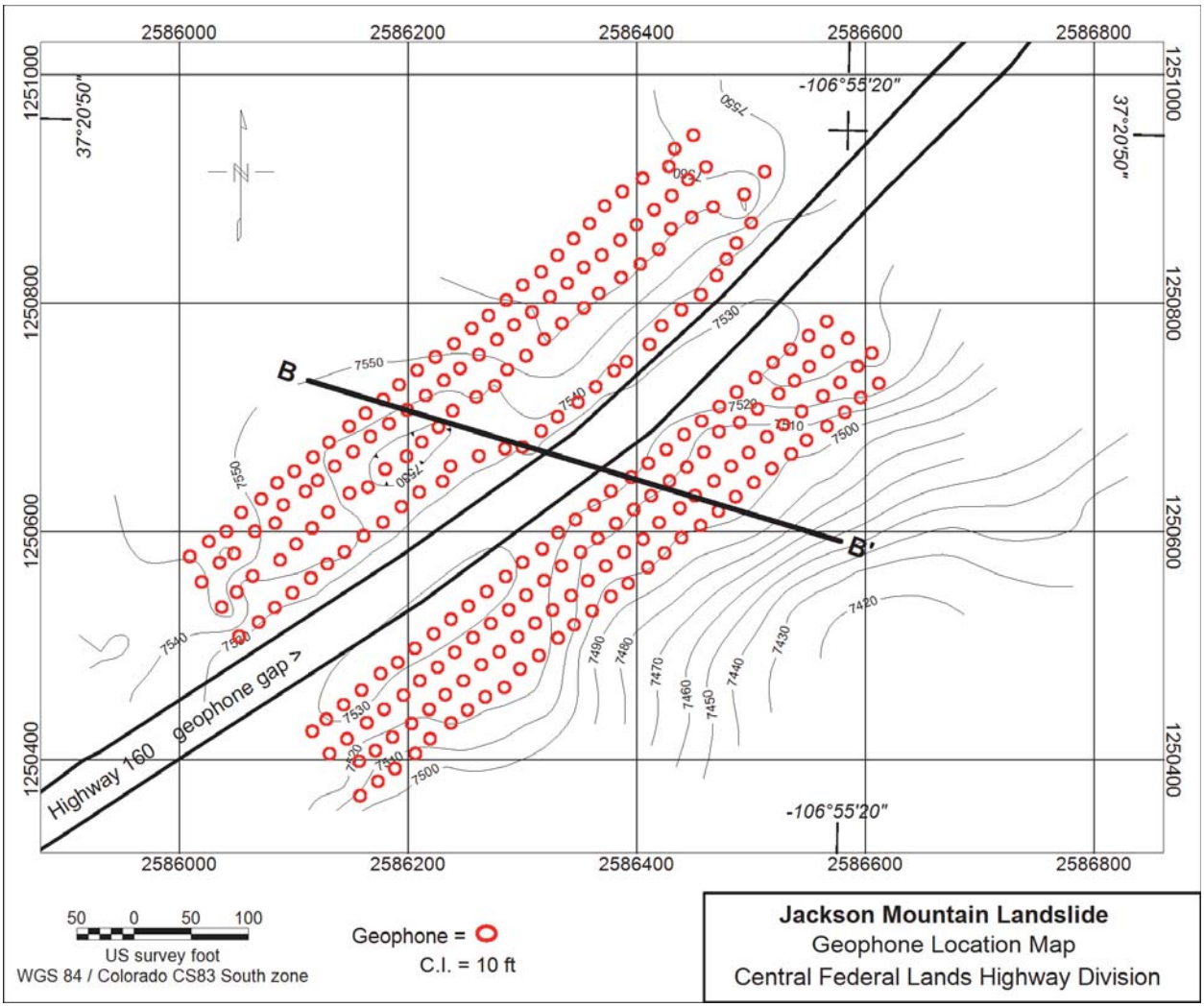

Figure 90. Map. Jackson Mountain Landslide geophone coverage on both sides of Highway 160 and cross-section B-B'

The entire 3D velocity volume, showing all the velocity data from the numerical modeling, is shown in Figure 91. The gridded area required velocities to be computed above the ground surface, which is not practical or effective. The following sequence of velocity slices along B-B', shown in Figures 92 through 95 are arranged in order of increasing confidence or usefulness of the results.

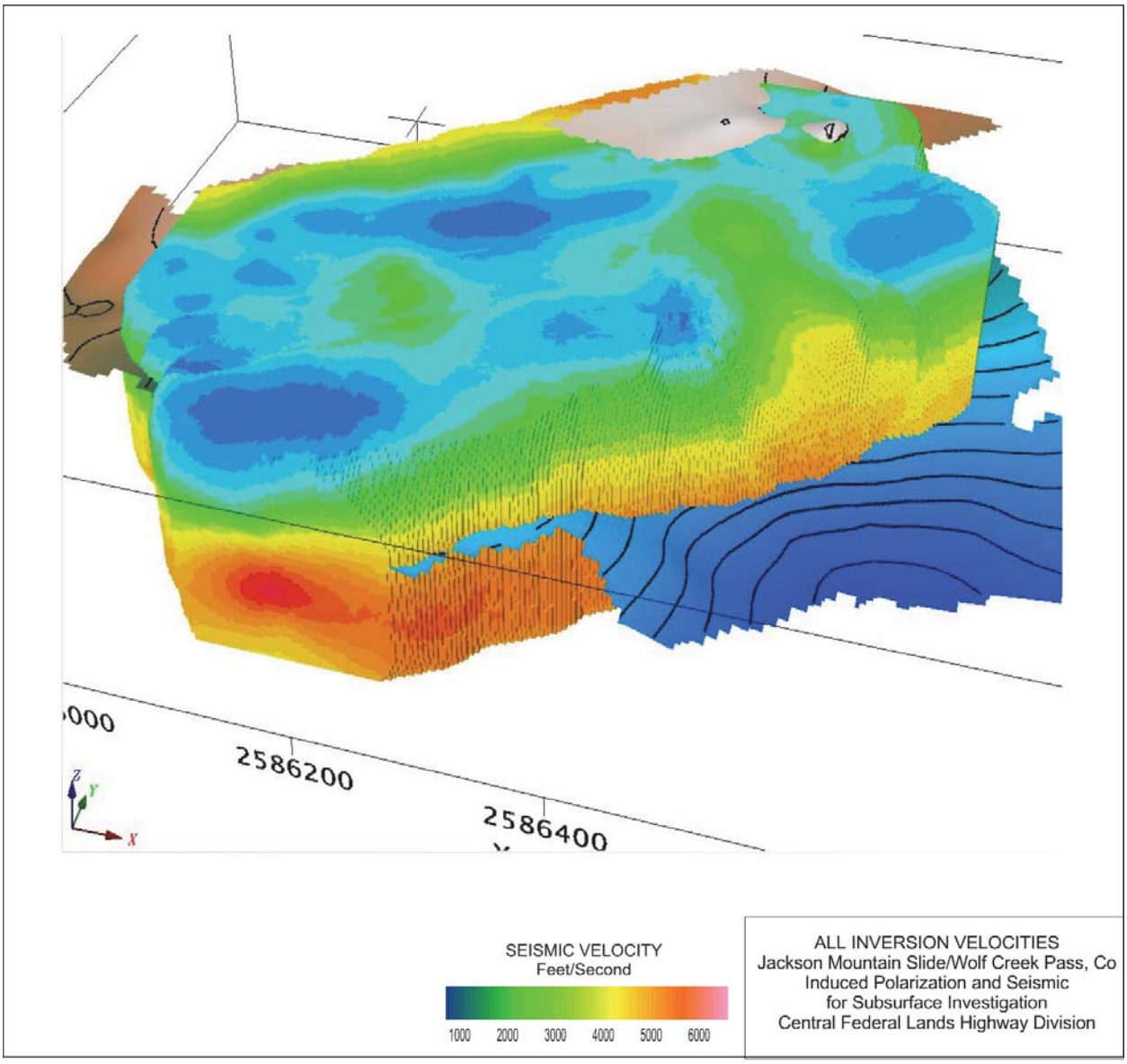

Figure 91. Model. All velocities calculated from 3D numerical modeling of Jackson Mountain Landslide refraction survey, with ground surface shown.

Figure 86 contains all the calculated velocity data for the entire 3D model. A reference boundary in the form of the ground surface as found from the surveyed GPS points is included. The data volume has velocity values where the mathematics indicates a ray path could exist which includes above the ground, to depths of low confidence, through the geophone gap due to the highway, and beyond the boundaries of the geophone array. The first velocity slice along B-B' on Figure 92 is a vertical slice through this entire cubic volume. In Figure 93 the velocity section has been cropped to use the ground surface as an upper boundary to remove phantom velocity values. The base of the section in Figure 93 was set at 90 feet bgs to allow for returning energy with longer travel paths.

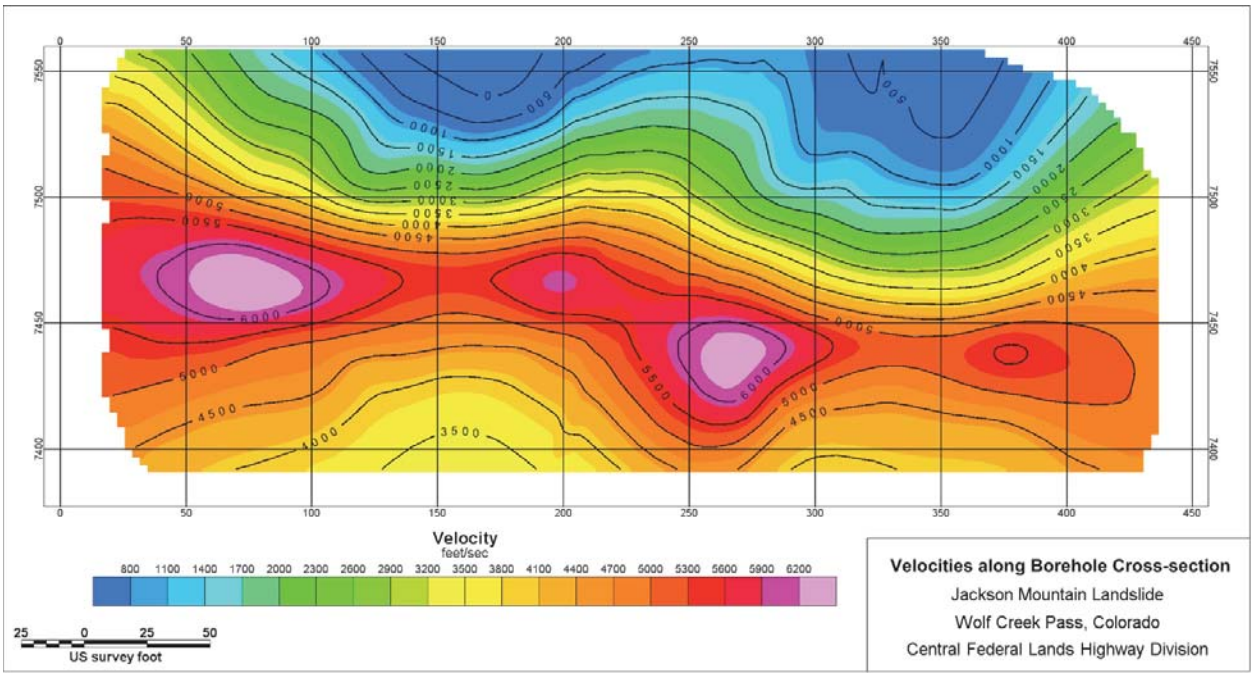

Figure 92. Model. Cross-section showing all velocities from 3D model inversion of Jackson Mountain Landslide survey. Data are present above the ground surface, below a high-velocity layer, and beyond the limits of the 3D geophone array.

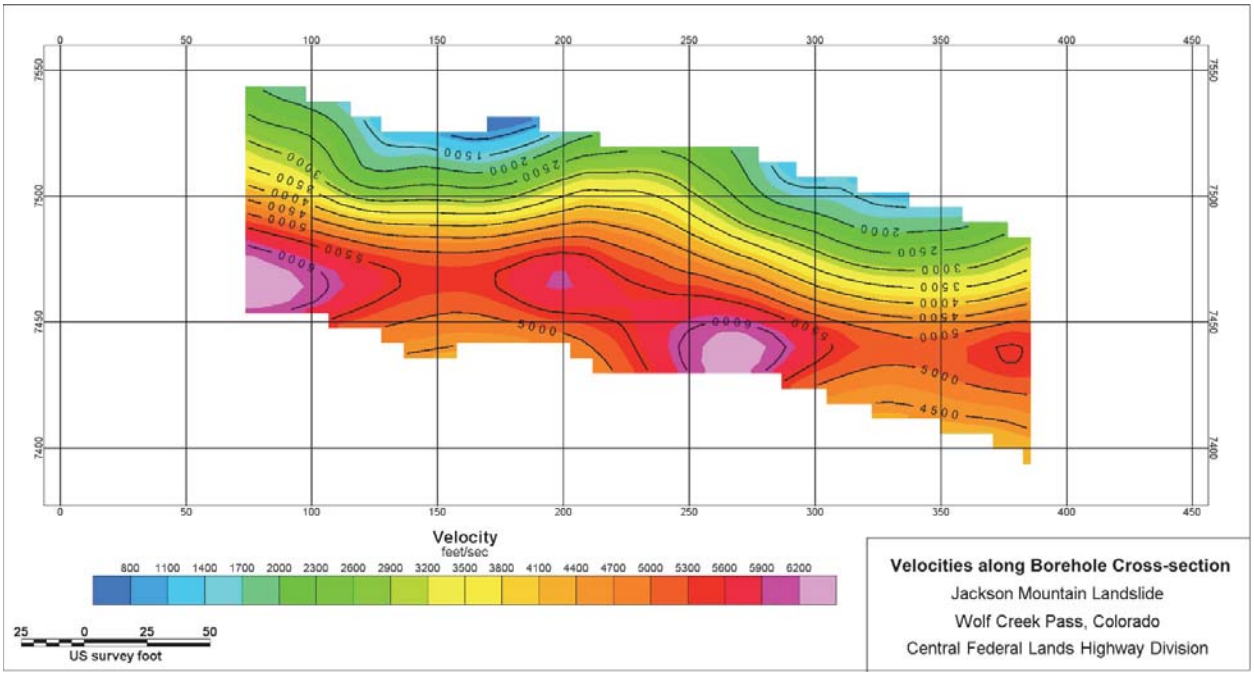

Figure 93. Model. Same cross-section as presented in Figure 92, showing only velocities below the ground surface and a ~90-foot depth of investigation.

Outside of the surface geophone coverage inversion artifacts in the form of higher velocities were also obtained. Velocity data obtained only beneath the actual 3D geophone arrays is judged to be better constrained and is presented in Figure 94.

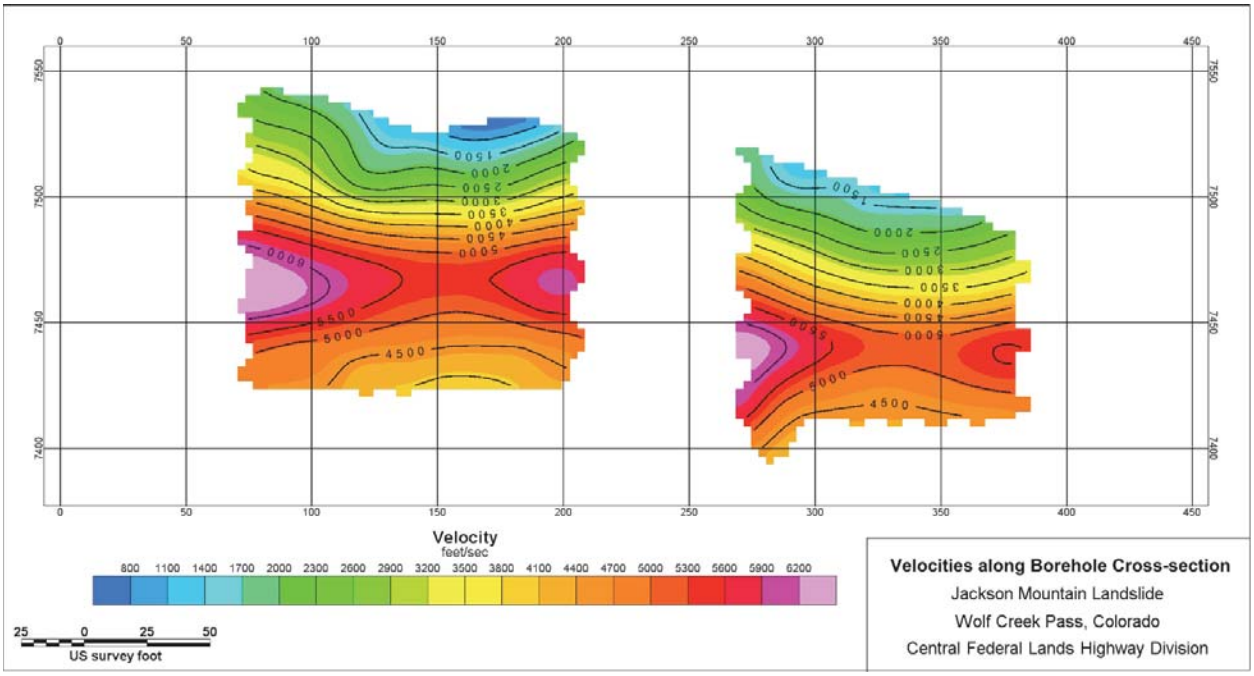

Figure 94. Model. Same cross-section as presented in Figure 92 showing only velocities below the surface where geophones were located.

Even below the 3D geophone arrays the calculations show velocity inversions. This decrease in velocity is thought to be an artifact of the particular 3D seismic refraction inversion algorithm used in this investigation. The low velocity layer at the bottom of the model does not makes sense physically or numerically, as refracted energy from this layer would not return to the surface without the presence of a deeper feature to cause refraction. The velocity section has been truncated at the level of the maximum velocity on Figure 95. The remaining velocity slice through the full 3D volume shown in Figure 91 that has the greatest confidence in the results is the values presented in Figure 95.

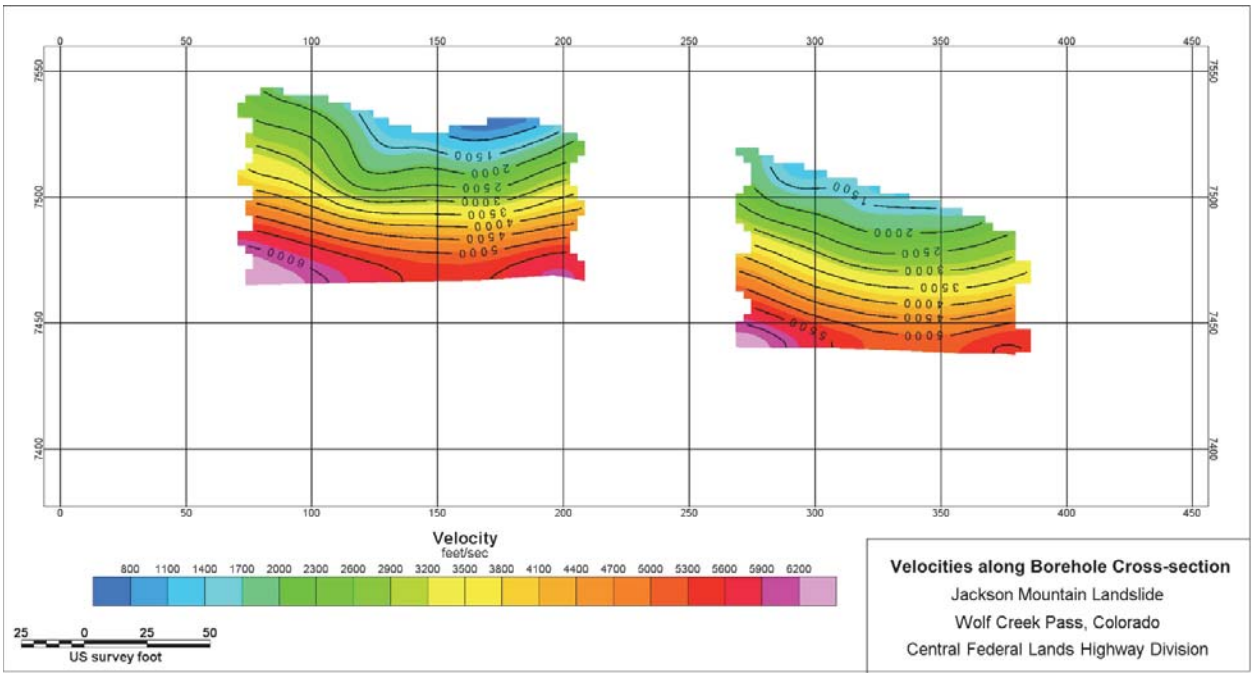

Figure 95. Model. Same cross-section as presented in Figure 92 showing only velocities with a positive vertical gradient.

2D Refraction Modeling

As the 3D refraction seismic grids were acquired with geophones along lines 2D processing and analysis tools can be applied to that 3D grid data. The location of an example of the 2D results is shown as Figure 96. A 2D slice through the velocity volume following the same geophones is also included for comparison on Figure 97.

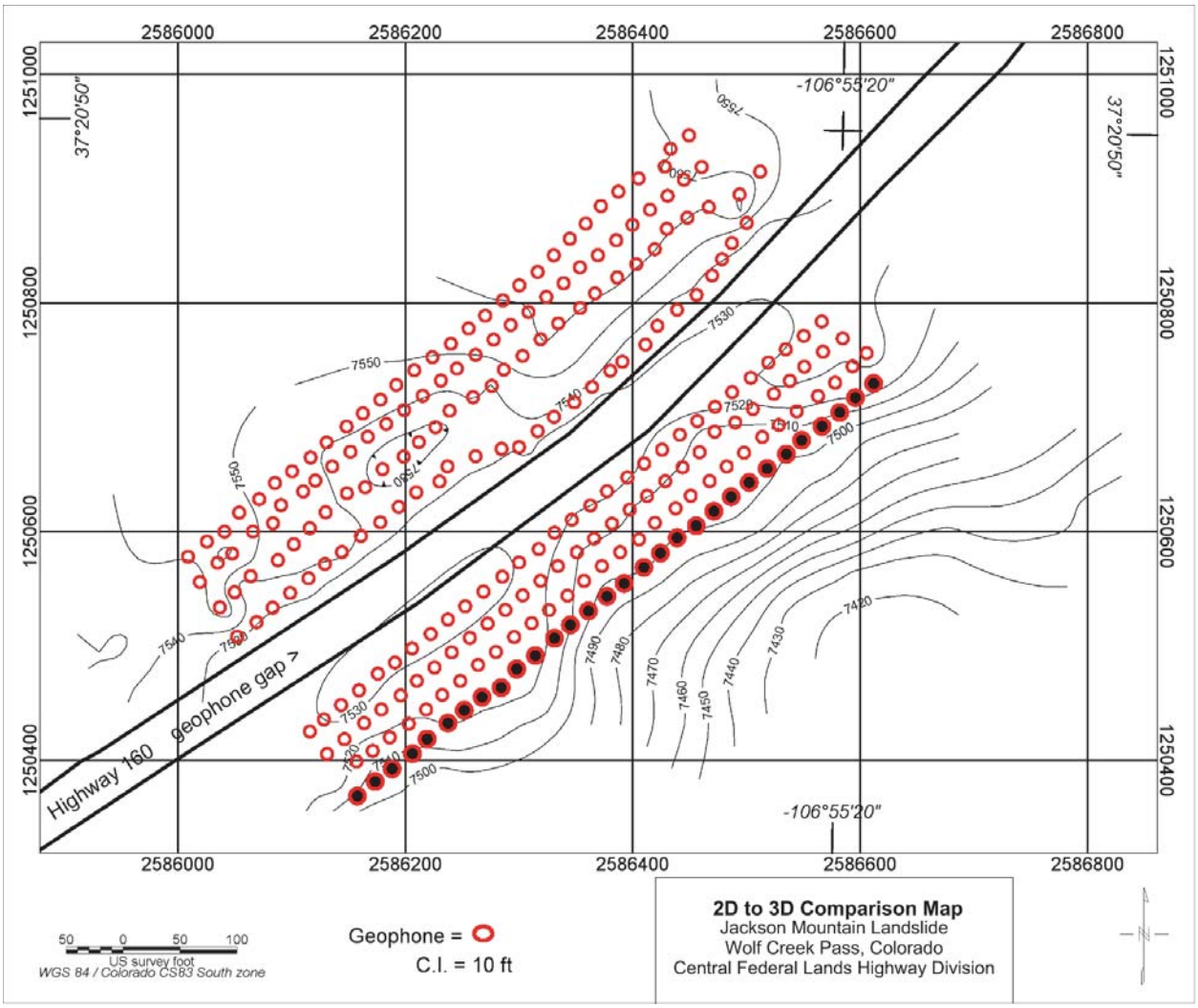

Figure 96. Map. Jackson Mountain Landslide geophone coverage with 2D & 3D refraction comparison along Line #2 (black centers).

Receiver Line #2 is marked in Figure 96 with the centers filled with black. The Rayfract (Version 3.11) program was used for 2D refraction modeling along Line #2. The 2D modeling shown in Figure 97 has a much greater depth of investigation and much higher maximum velocities. The color range for the 2D model is the same as that used for the 3D velocity slice figures illustrating confidence levels but the contour interval has been increased from 500 ft/sec to 1,000 ft/sec to display the high velocities below elevation 7,400 feet.

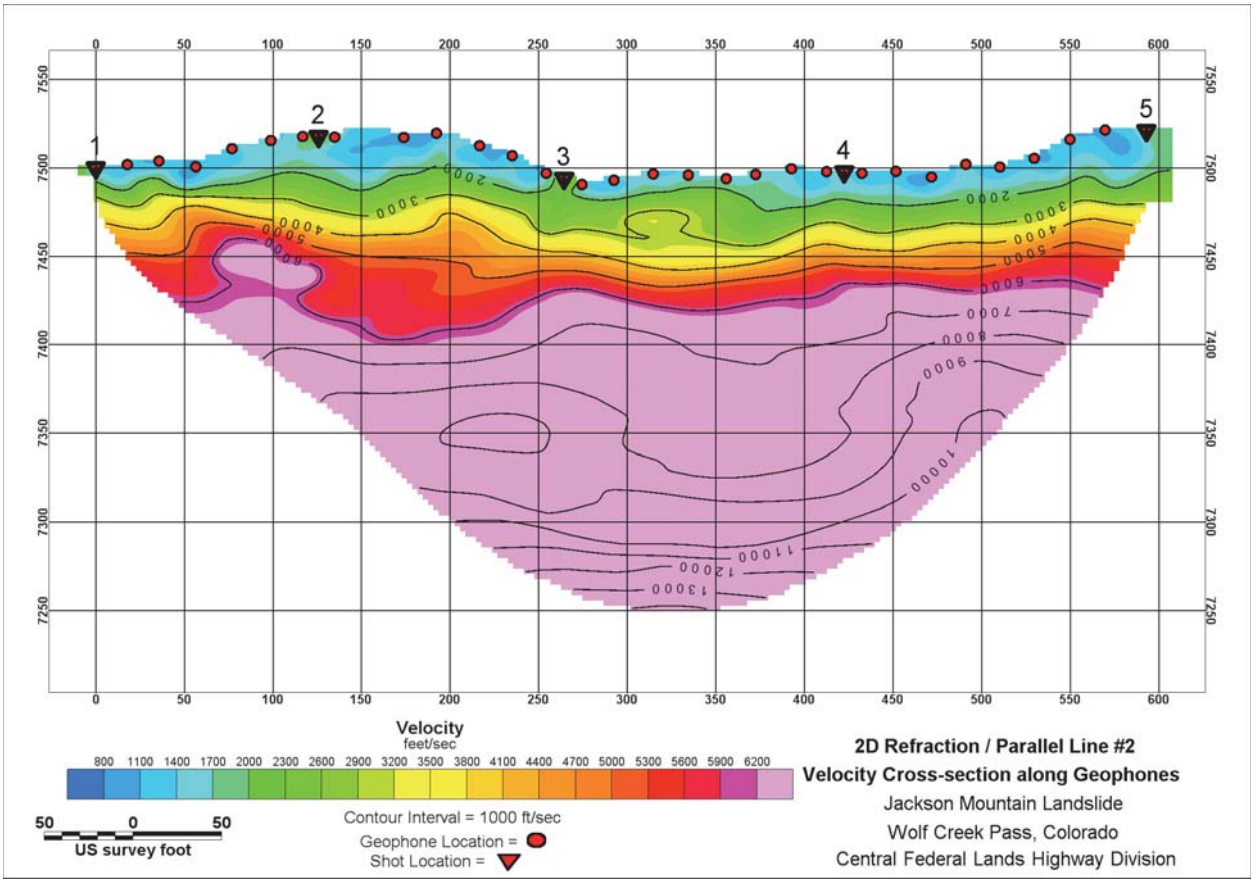

Figure 97. Model. 2D refraction velocity model along geophone Line #2.

The ray count for the bottom of the 2D model is low so the confidence in the exact velocity values below an elevation of 7,350 feet is low. Nevertheless, the high velocities (pink color) are indicative of bedrock. The gradient from the ground surface to 6,000 ft/sec is similar to that found in the edited vertical slice through the 3D velocity volume. The 2D velocity section has greater detail than the corresponding 3D slice shown in Figure 98.

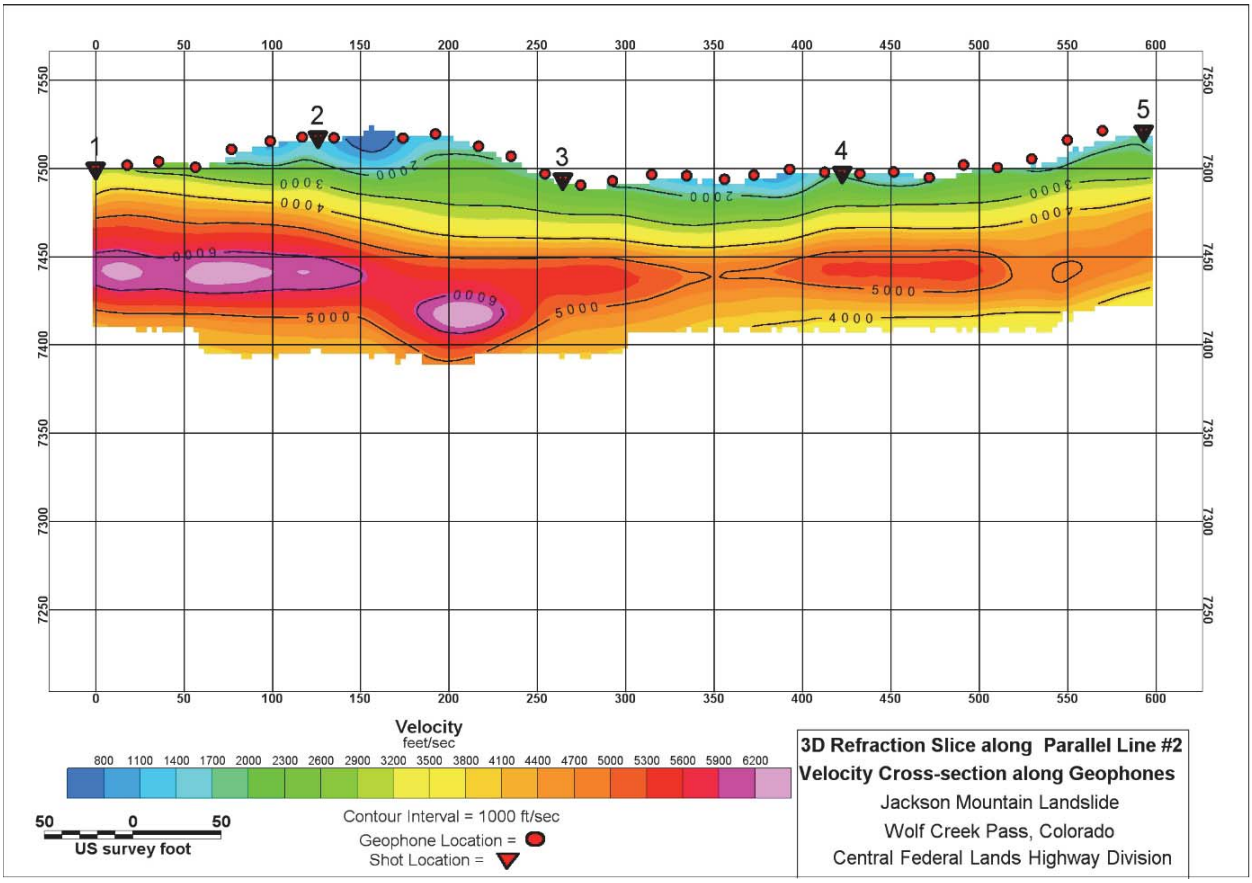

Figure 98. Model. Cross-section through 3D refraction model showing velocities along geophone Line #2.

Figure 99 is a 6-ft thick surface following slab of the velocity data volume viewed from directly above. Highway 160 is marked with black lines running across the velocity data. Receiver locations are noted with black cubes. Color range for all the velocity slabs runs from 500 ft/sec in dark blue to 6500 ft/sec in pink. A series of these surface-following slabs representing deeper sections below the ground surface are shown as Figure 100 and 101.

Note: the fast velocities along the highway are an artifact due to a gap in the geophone coverage. This high velocity "ridge" is seen in all the velocity slices.

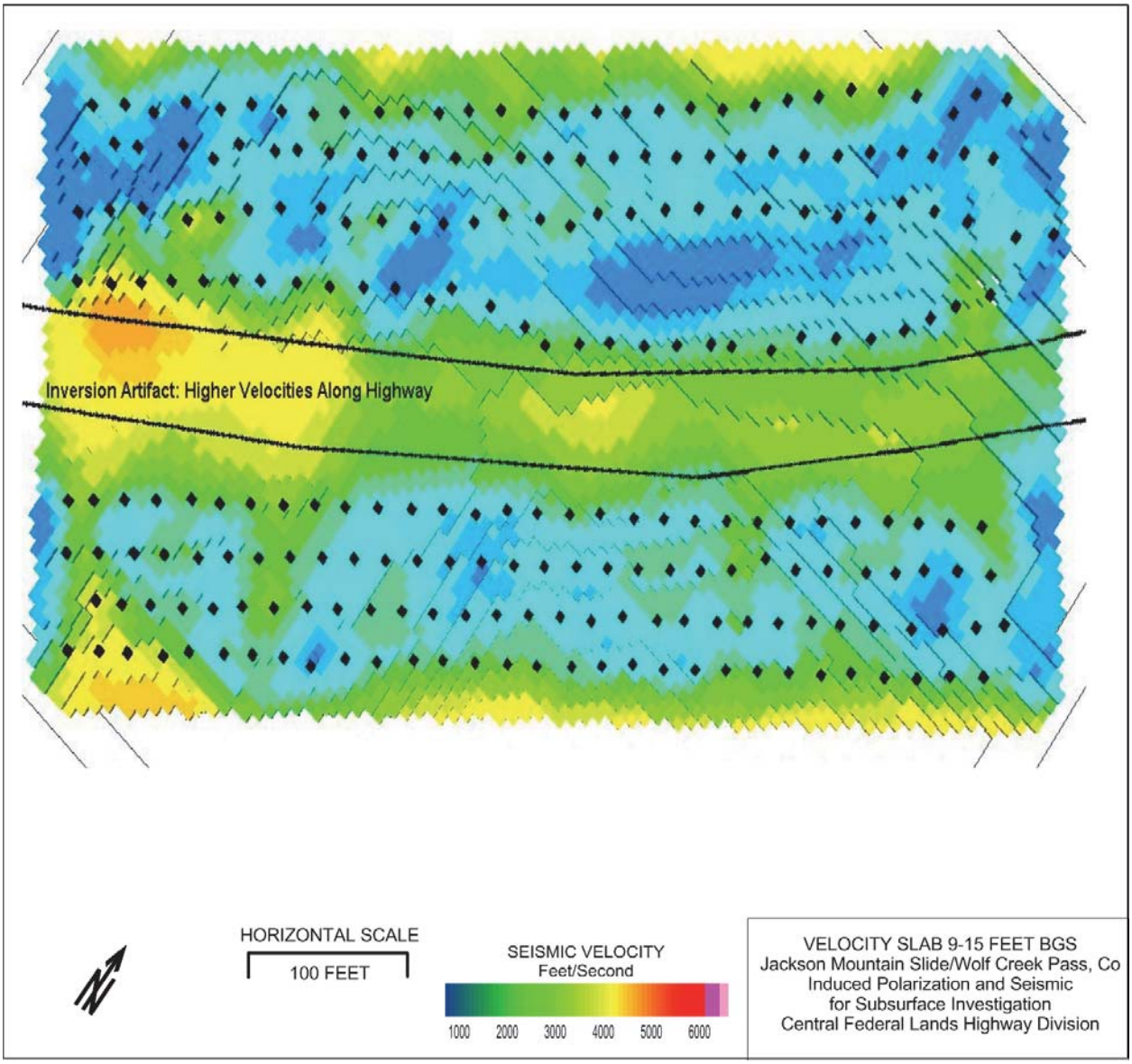

Figure 99. Map. Surface-following velocity slab: 9-15 ft below ground surface with highway edge marked with black lines.

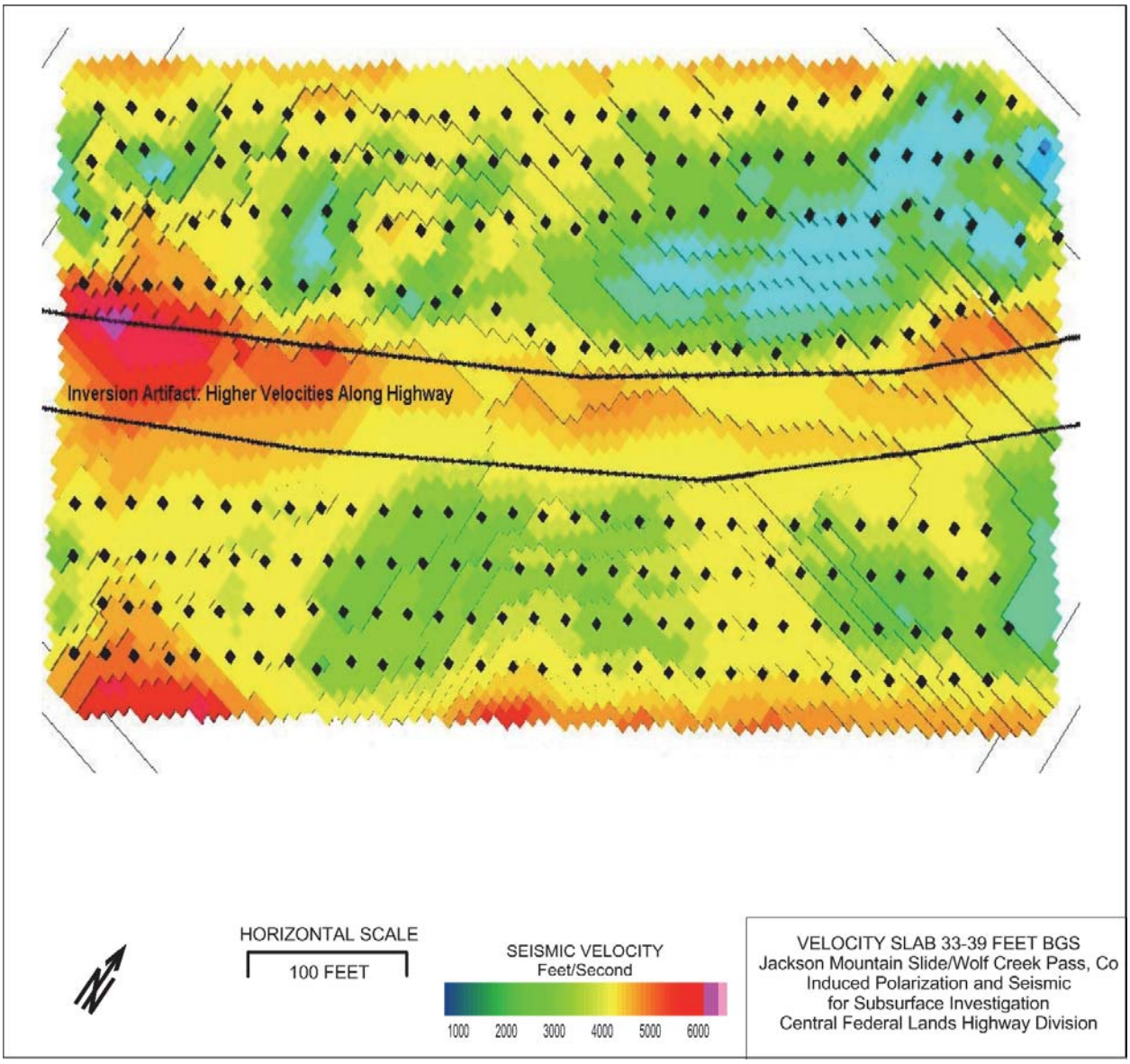

Figure 100. Map. Surface-following velocity slab: 33-39 ft below ground surface

The velocities inside the 3D sub grids (on either side of the highway) appear reasonable. The perimeters of the sub grids all have high acoustic speeds along the grid edges. The high values seem to be inversion artifacts.

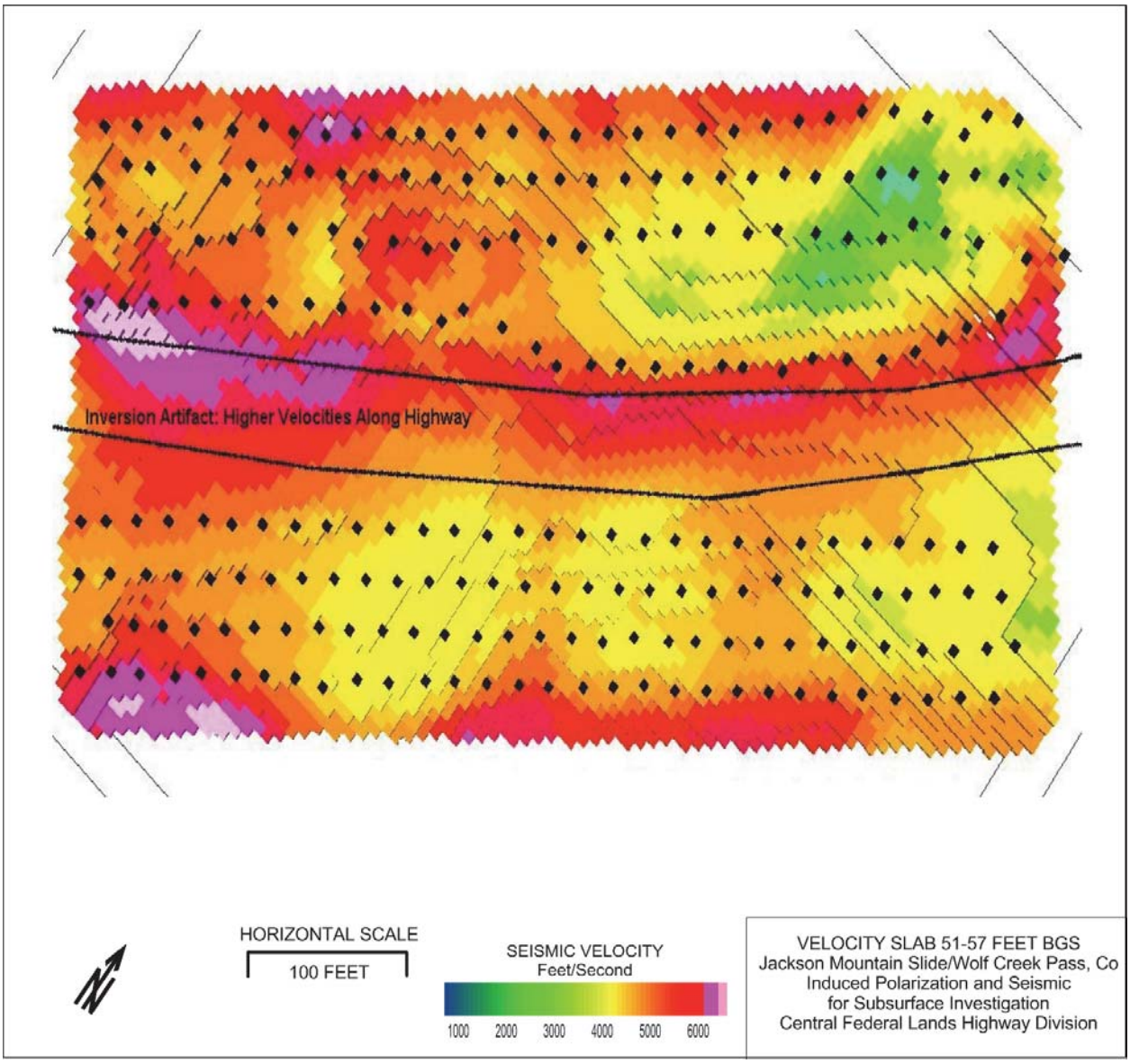

Figure 101. Map. Surface-following velocity slab: 51-57 ft below ground surface

The velocity range and average velocities both increase as the depth of the slab increases.

Borehole Correlation

The following lithologic log information for the Jackson Mountain Landslide comes from the geotechnical report prepared by Yeh and Associates (2007). The complete log information can be found in Appendix E. Figure 102 is a map showing the location of the three boreholes used for the cross-section comparison with the geophysical data in cross-section form. Figure 103 graphically displays the lithologic log information. Figures 104-106 display the geophysical data along the cross-section.

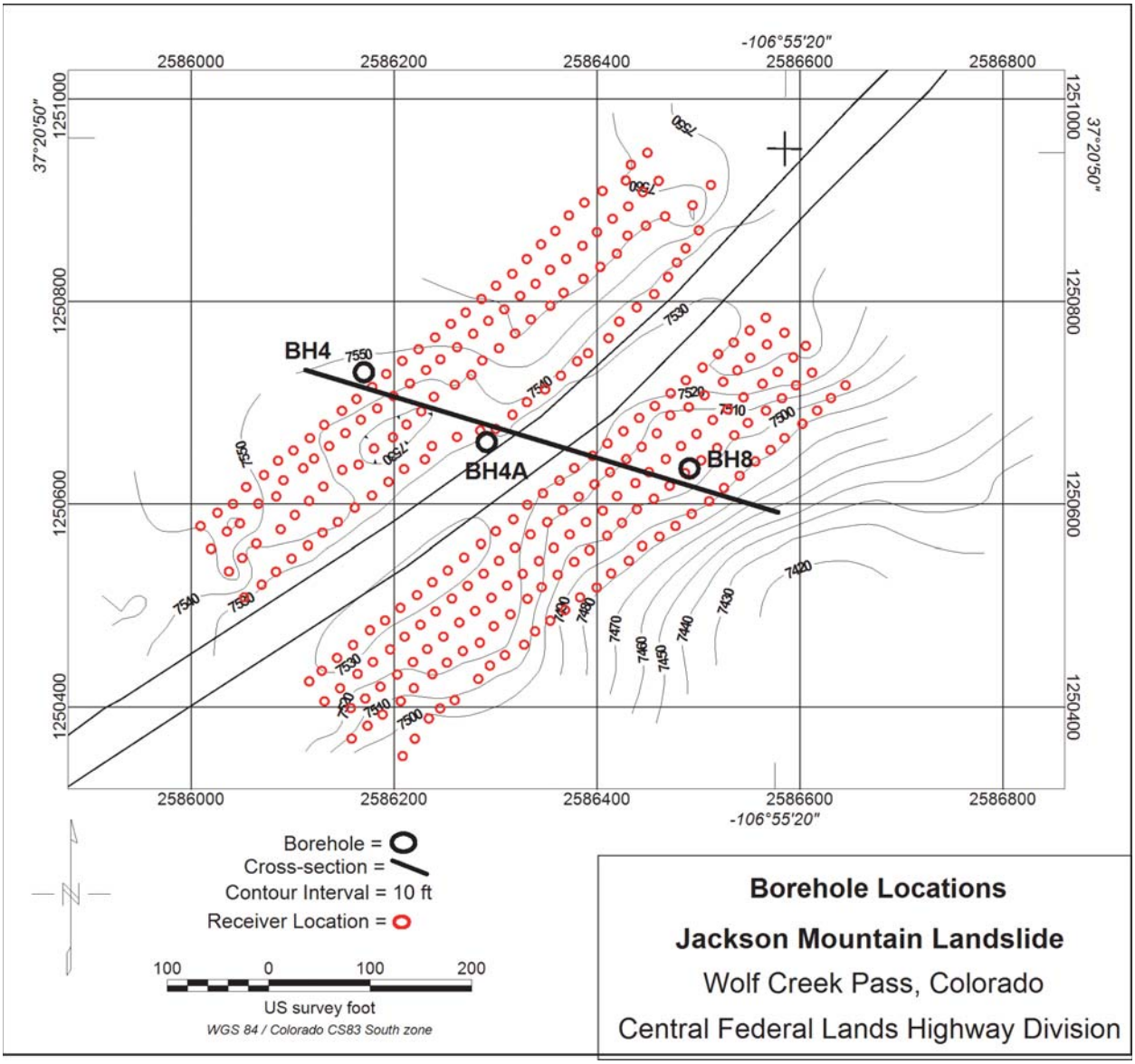

Figure 102. Map. Jackson Mountain Landslide Borehole and Cross-section Locations

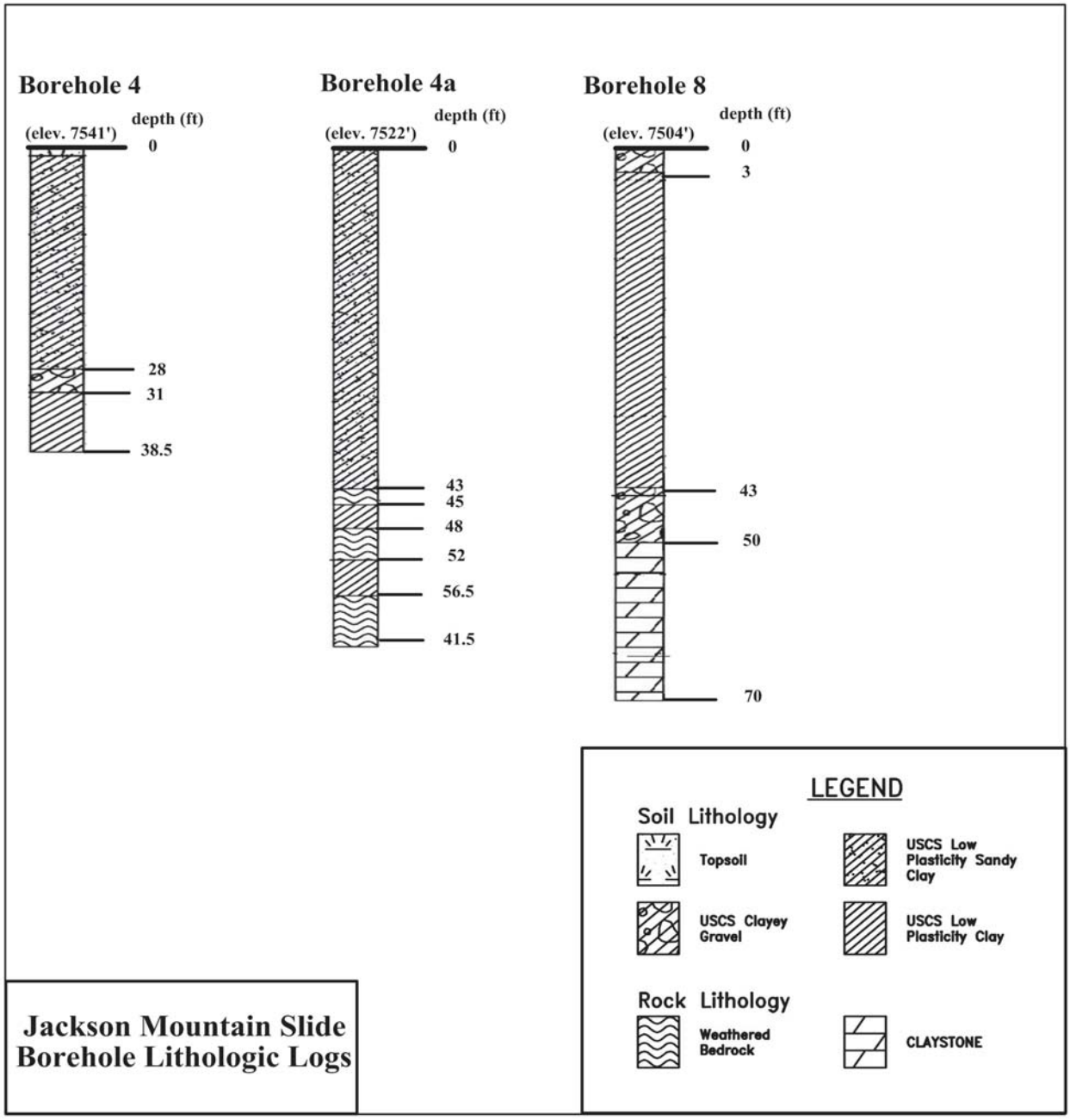

Figure 103. Diagram. Jackson Mountain Landslide Borehole Lithologic Logs.

The lithologic log for Borehole-4 shows sandy clay to a depth of 28 feet above a three foot thick layer of clayey gravel. For the remaining 7.5 feet to total depth the borehole encountered clay with varying amounts of weathered bedrock.

Borehole-4A logs shows sandy clay with bedrock fragments from the ground surface to 43 feet of depth. The bottom 20 feet of the borehole was weathered claystone and clay layers. From 48 to 52 feet and again from 56.5 feet to the bottom of the hole at 63 feet fine grained intrusive volcanics were interbedded with the claystone.

Below three feet of clayey gravel, the log for Borehole-8 has clay from three to 43 feet. Below the clay is a seven foot layer of clayey gravel. Claystone with interbedded fine grained intrusive volcanics was found in the bottom 20 feet of the borehole.

Groundwater was detected at 31.6 feet bgs in Borehole-4 when sampled on 12/20/05 and 1/13/06. The average groundwater depth for Borehole-4A when sampled on those same date was 23.3 feet bgs. Groundwater was not found in Borehole-8 on either date.

The largest IP anomaly on the cross-section through the well locations as shown in Figure 104 is near the BH-8 location. The IP value rises with increasing depth reaching 8 milliseconds (above background for the section) at 53 ft bgs. At BH-8 the IP anomaly begins at roughly the depth of the volcanic interbeds. BH-4A also has the intrusive interbeds with no comparable IP anomaly.

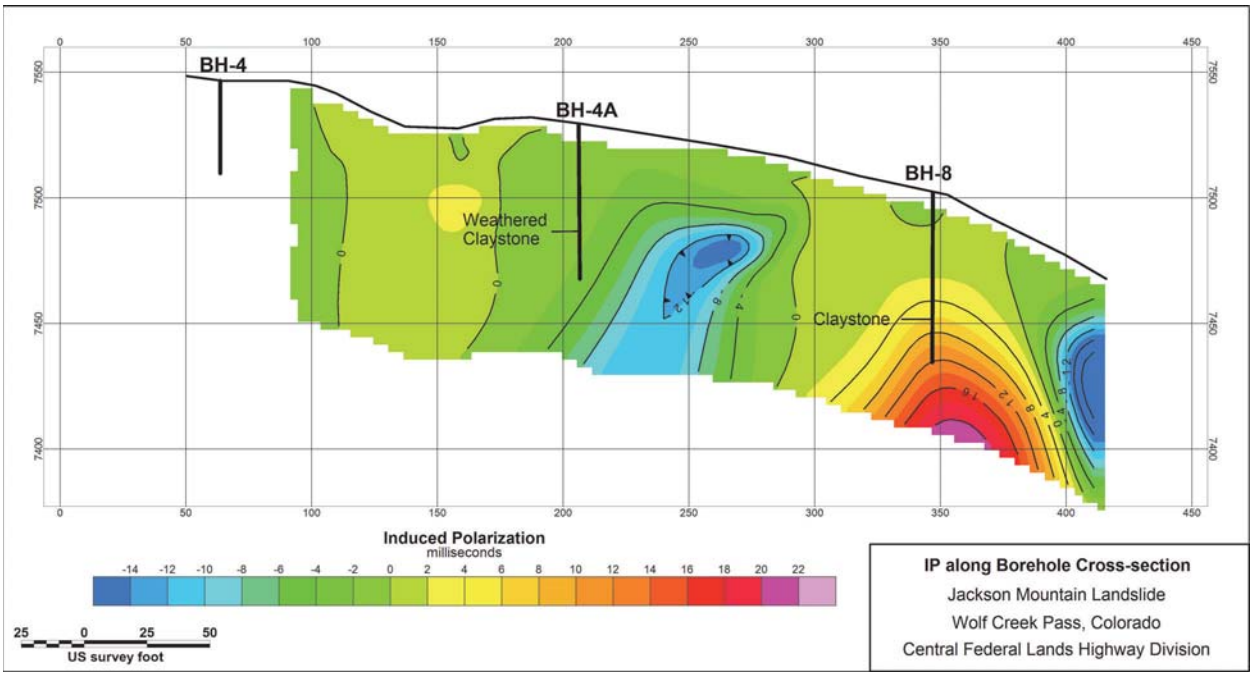

Figure 104. Diagram. IP Cross-section through Borehole Locations on Jackson Mountain Landslide.

There are several near-surface resistive features on the resistivity cross-section through the boreholes in Figure 105. The boreholes do not penetrate any of them, although BH-8 is on the edge of the most resistive area of the section. The highest resistivity found on the cross-section is over 100 ohm-meters (center of bright pink zone) at the ground surface. Below 40 feet the resistivity values are low, only a few ohm-meters, with low spatial variation across the entire section.

At BH-8 the 5000 ft/sec contour is 54 feet bgs. The claystone is first encountered at a depth of 50 feet. The claystone is found at 43 feet in Borehole-4A where the 5000 ft/sec contour is 45 feet bgs. Claystone was not encountered in BH-4. The 5000 ft/sec contour is projected to 51 feet for the location of BH-4, below the bottom of the hole. Given the lithologic control interpreting the 5000 ft/sec horizon as the claystone bedrock is reasonable.

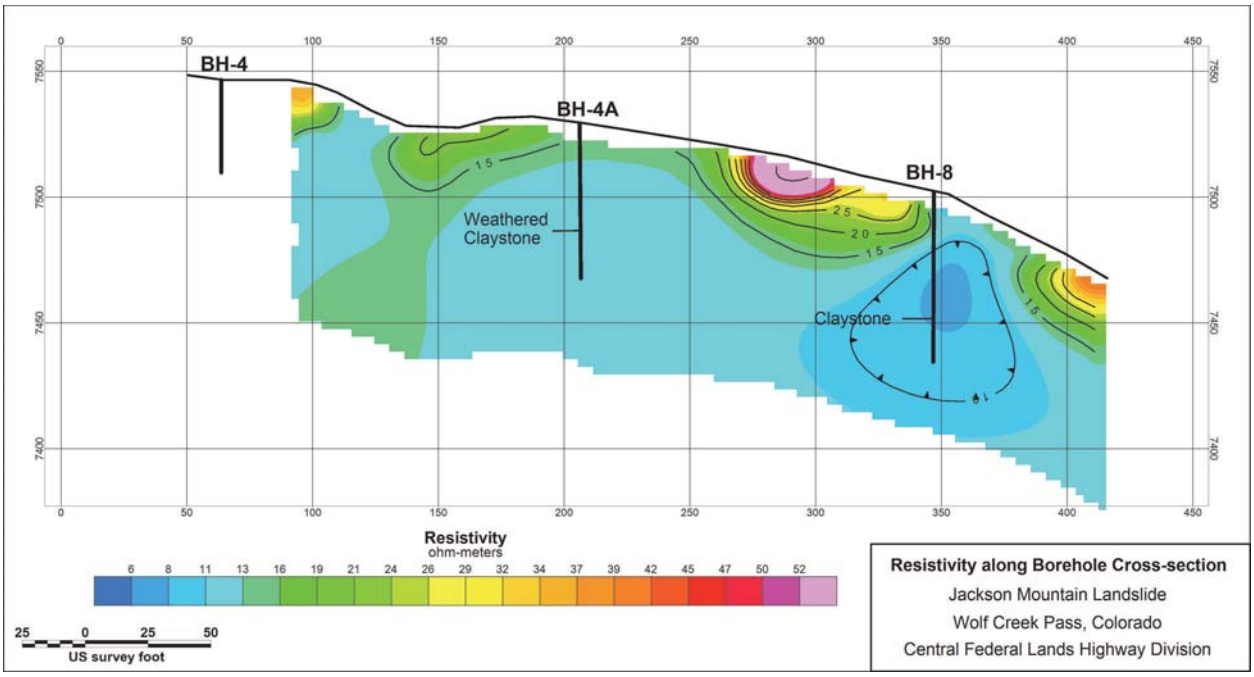

Figure 105. Diagram. Resistivity Cross-section through Borehole Locations on Jackson Mountain Landslide.

The velocity cross-section has higher values below BH-4A than below BH-8. The claystone in BH-8 is described as soft to very soft with a possible slip planes at 55 and 60 feet bgs. The claystone at BH-4A is much firmer and there is reference to a hard lens encountered at a depth of 43 to 45 feet. The higher velocities at BH-4A may reflect the greater stiffness materials encountered in the borehole at this location.

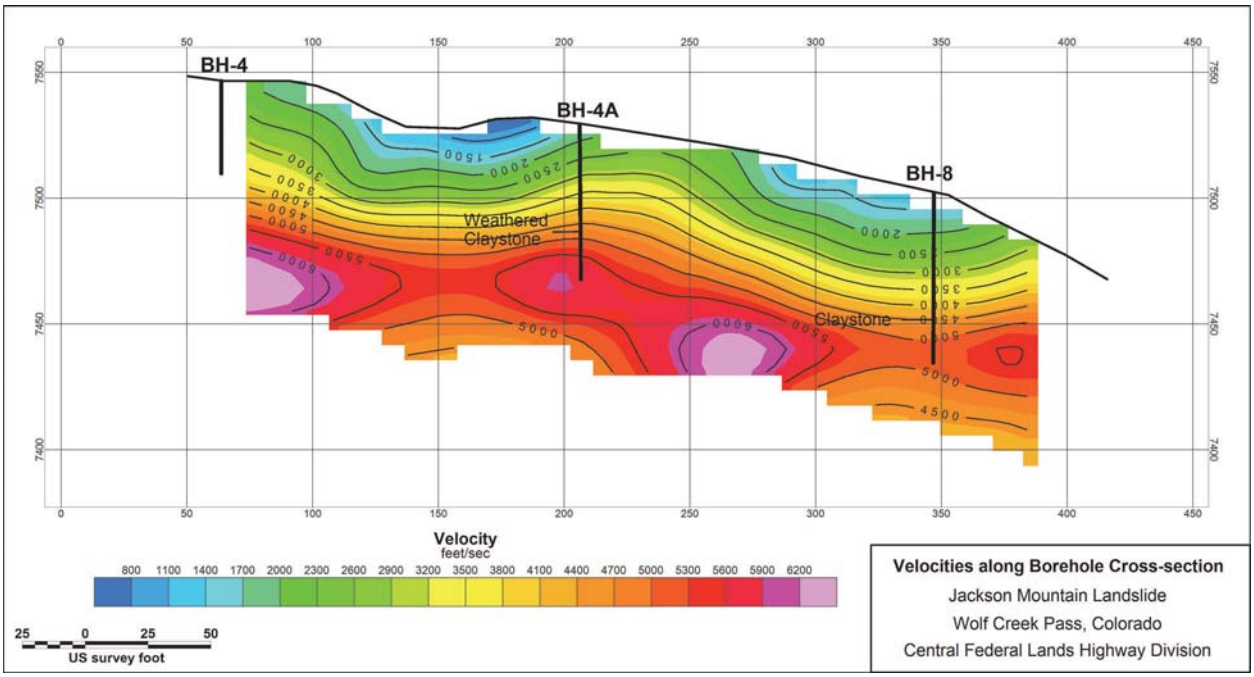

Figure 106. Diagram. Velocity Cross-section through Borehole Locations on Jackson Mountain Landslide.

CHAPTER 6 – SUMMARY

Based on analysis of the 3D data sets acquired on the East Fork and Jackson Mountain Landslides, the following sections present observations and conclusions regarding the application of induced polarization (IP), resistivity, and seismic refraction for imaging landslides. These concluding remarks are divided into geophysical observations, geophysical findings (per slide), summary, and overall conclusions with respect to the project objectives. In many cases the combination of the IP *and* the resistivity surveys, used for this investigation, are defined as the electrical method. The observations, findings and results (per slide) are not presented in any particular order of importance.

GEOPHYSICAL OBSERVATIONS

1) For both the electrical and the seismic refraction methods equipment and field procedures exist that are sufficient to acquire high-quality 3D data even in the difficult topography and surface conditions that will inevitably be encountered on landslides. Future applications of the wireless technologies (www.wirelessseismic.com) for 3D seismic imaging may be advantageous in the steep and vegetated terrain. Due to the difficult access and large lateral extent of big landslides, the seismic method will likely require the use of explosive charges for the source; this can be expensive and time-consuming compared to conventional impulsive sources used for engineering seismic investigations.

2) Geophysical forward modeling is a very important task that, if time permits, should be conducted for electrical and/or seismic surveys. The forward modeling should test the proposed acquisition geometry (i.e., field deployment of 3D arrays), as well as the instrumentation parameters anticipated for the geologic/site conditions. Currently, not all commercially available 3D software can accommodate significant topography, wide coverage, gaps in the array or non-rectangular arrays. In most cases, this limitation of the software can be overcome with practical forward modeling in order to anticipate the effects these issues will have on the resultant data (e.g., a highway bisecting the grid, or a metal gas pipeline lying on the ground surface, etc.). A forward modeling task would be particularly useful when potentially going to the field to investigate more than one landslide. Each slide has its own failure mechanism, geology and set of cultural or site conditions that can dictate the use of different 3D arrays, equipment, or acquisition parameters.

3) 3D tomographic inversion of electrical (IP & resistivity) and seismic refraction data can be accomplished successfully with available software. As previously stated, the current versions of software are not fully suited to handle the potential issues which may be encountered on highway landslide sites. A significant portion of the problem is not the inversion or numerical modeling itself, but rather the visualization and presentation of the 3D data in more useful formats for engineering design or remediation. A series of simple horizontal and vertical slices of the 3D volume data are presented herein, but more complex slices of the 3D volume are required.

4) It became apparent during the investigation of two landslide sites that sufficient resources for the processing must be allocated for the project (e.g., man-hours *and* high-speed computers). Resources will be essential when these type geophysical surveys become utilized as first-order

field surveys to aid in drilling operations, and data turn-around must be rapid. The data processing, interpretation, and presentation of large, complex 3D data volumes remain labor intensive.

5) The volume of data carrying the highest confidence is defined by the ground surface, the horizontal limits of the 3D array / grid, and the maximum depth of investigation for the particular method. Software algorithms will create 'artifacts' along the edges of the survey grid, and possibly in areas of array gaps, which are invalid results. Additionally, they will also produce results beyond the extent, limit, or depth of the real geophysical data. Volume editing and checking of data quality along the array edges and within the 3D volume is required in order to present high-quality results that are supported with seismic or electrical data, not artifacts of either the inversion algorithms or plotting methods used.

6) When comparing slices extracted from a set of results from the 3D volumes with cross-sections generated using conventional 2D analysis techniques, the results compare very well; that is, similar values, character and shape of anomalies are imaged. However, the 3D results were, in general, much shallower than the 2D results. This discrepancy could be a product of the 3D algorithm used for this investigation.

7) The magnitude of the observed 3D IP anomalies fit into the range of responses known or expected for clayey soils. The IP results indicate numerous, small, low-amplitude positive and negative IP anomalies. These small anomalies, generally located in the shallow subsurface, were scattered through the 3D volume, but no discernible pattern could be identified. Therefore, the scattered anomalies are likely the signature of formerly layered soil or geologic setting now jumbled by mass movement down slope. Larger IP anomalies were observed in the materials below the suspected slide plane (i.e., in the bedrock materials) which could not be explained.

8) 3D resistivity data indicate discrete zones of low-resistivity (high-conductivity) materials that are interpreted to be saturated or near-saturated conditions, and also high-resistivity zones which are most likely drained landslide deposits. Landslide deposits are susceptible to rapidly changing moisture content due to either topography or the presence of course-grained (permeable) soils.

9) Independent 2D and 3D refraction analyses confirm that the velocities obtained in the upper (approximately) 60 feet correlate well with one another. However, 2D refraction results did not confirm higher velocity gradients obtained near the edges of the 3D grids, nor the presence of a low-velocity layer beneath the high(est) velocities obtained in the 3D results. These two *apparent* anomalies in the 3D velocity data are artifacts from the GAP software used for the modeling. The GAP software used for the 3D analyses produced reliable velocities within the boundaries of the geophone array, vertically and laterally. However, the approach of an initial starting velocity model can cause the appearance of low-velocity zones beneath high-velocity layers. This artifact is simply the result of the numerical modeling method, not the geologic layering.

10) Working on an active landslide, immediately after mass movement, can be a dangerous proposition. 3D geophysical data were acquired at these two landslide sites about 15 months after mass movement in the Spring of 2008. Changing conditions in the subsurface almost

certainly occurred, but the methods used and the challenges faced to acquire the data show that geophysical methods can be deployed rapidly and image large volumes of the subsurface otherwise inaccessible to drilling or other standard geotechnical methods of characterizing the subsurface. The geophysical findings presented below are confined to the areas surveyed beneath the area investigated by the 3D grid(s), and are not generalizations of the entire landslide(s).

GEOPHYSICAL FINDINGS

East Fork Landslide

- Geophysical results obtained from 3D imaging at the East Fork Landslide are evaluated to be coherent, reliable and representative of subsurface conditions beneath the 3D grid.

- A chaotic set of IP anomalies characterize the shallow subsurface to about 50-60 feet. Numerous small, low-amplitude IP anomalies are present within the materials interpreted to be the slidemass, and below the slideplane (approximately 58 feet near the borings) the IP response is characterized as smooth and very small. It appears that IP can be used to identify the slidemass materials based on the chaotic IP response in the 3D volume for this translational landslide with high clay content soils and claystone bedrock.

- A wide coherent zone of low resistivities was identified 10 to 50 feet below the ground surface. Within the three borings the water table was encountered from 8 to 12 feet bgs; therefore, the low resistivities are interpreted to indicate high water content, possibly saturated conditions. This low-resistivity zone was observed in both the 2D and 3D data sets. However, the zone does not match the surface expression of the most recent (2008) landslide movement. Relative to the mapped edges of the 2008 landslide the low resistivity zone is narrower than existing slidemass. This fact is interpreted to mean the water in the materials along the edges is draining toward the middle of the slidemass, and as such they have lower moisture content.

- Several areas are characterized by near-surface P-wave velocities that are less than 1500 ft/sec. These very low-velocity materials, generally confined to the upper 10-25 feet, are interpreted as low density and significantly disturbed material. From the ground surface to approximately 50 feet bgs 3D velocity images reveal that most of the volume sampled is composed of material with P-wave velocities less than 2500 ft/sec.

- Claystone was encountered in all three borings, two of which are within the 3D grid. Depths to the claystone are different in each borehole but the soil/claystone contact correlates with a 4000 to 4,500 ft/sec velocity contour. Geotechnical indications are that the soil/claystone interface may be the slideplane at the East Fork Landslide. If the 4000 foot/second velocity is correlative with the slideplane, a velocity iso-surface could be used to visualize the slideplane away from the narrow area investigated by the three borings.

- P-wave velocities generally increased with depth from under 1,000 ft/sec to over 7,500 ft/sec reaching a maximum roughly 100 feet below the ground surface. One borehole encountered volcanic breccia at a depth of 82 feet, where the 3D velocities are about 6,000 ft/sec.

- Within the 3D grid there are a few small, localized features where velocities of ~4,000 ft/sec occur within about 15 feet of the ground surface. The localized velocity anomalies do not correlate with topographic highs or lows. These small velocity anomalies are interpreted to be more coherent blocks of dense/stiff soil, or possibly solid rock masses, embedded in the slidemass that moved with the translational mass movement, but were not disturbed as they slide downslope. A few of these block-like features can be observed on the surface.

Jackson Mountain Landslide

- Geophysical results obtained from 3D imaging at the Jackson Mountain Landslide are evaluated to be inconsistent, mostly unreliable and not very representative of subsurface conditions beneath the 3D grid. This inconsistency is the direct result of having a highway bisect the area of investigation, and the attempt to analyze the entire area in 3D. In retrospect, independent ***analysis*** of each smaller grid (on either side of Highway 160) may have yielded more reliable results, and the 3D geophysical data which potentially could have been more useful and correlative with the borehole geologic data would have been presented. Albeit the two 3D data sets would have been much smaller, but they would not have been plagued by data gaps and artifacts generated in the 3D analysis and presentation of the results. The following results are generalized from the data obtained across the entire 3D grid (i.e., both sides of the highway).

- The largest IP anomalies are imaged at depths at or below the weathered bedrock horizon found in the boreholes. The larger IP anomalies appear to correlate to the undisturbed (deeper) materials. The small, generally chaotic nature of the 3D IP anomalies observed at the East Fork Landslide are not observed at the Jackson Mountain Landslide, suggesting the soils or geologic conditions are considerably different.

- Resistivity imaging revealed a series of high- and low-resistivity zones which could not be directly correlated with groundwater or soil moisture conditions. A substantial wet, Fall snowstorm occurred just prior to obtaining the electrical data at the Jackson Mountain Landslide, which almost certainly affected the quality of resistivity data due to the influx of moisture at the surface. Although the moisture at the surface would not have effected results from deeper in the slidemass, the 3D resistivity results are difficult to interpret.

- The P-wave velocity range from the 3D model results obtained at the Jackson Mountain Landslide is lower than that modeled at the East Fork Landslide. The lowest velocities are similar (i.e., <1000 ft/sec) but the highest velocity material imaged is roughly 6,500 ft/sec, which is at least 1,000 ft/sec less than the highest velocity obtained in the breccia

at the East Fork Landslide. The bedrock at the Jackson Mountain Landslide is different and the lower velocities obtained are considered representative.

- Each of the 3D data sets were strongly affected by the field set-up of the two independent grids, separated by Highway 160, and as such edge effects, artifacts, and large gradients (i.e., rapid changing values) were consistently calculated beneath the road, where no data exists, as well as at the edges of the electrical and seismic grids.

- Based on the previous bullet item, correlation of the groundwater table and lithologic control with the electrical and seismic 3D geophysical results at the Jackson Mountain Landslide site is not very good. The only observation is a velocity of about 5,000 ft/sec appears to correlate with the soil/weathered claystone interface in the boreholes; this contact has been postulated as the slide plane.

GEOPHYSICAL SUMMARY

1. 3D IP anomalies in the upper 50 feet within the landslides were small in volume and unorganized. At the translational East Fork Landslide the IP anomalies were small amplitude, numerous and chaotic; and, at the Jackson Mountain Landslide the IP response is larger, more extensive and appear to be present at depth under and outside the 2008 mass movement on the East Fork Landslide. The translation failure mechanism and clayey soils at East Fork are conducive to imaging the slidemass from the underlying undisturbed materials with IP. Due to poor data quality, as well as the rotational-type of failure mechanism at the Jackson Mountain Landslide, the IP method does not appear to have imaged the difference between slidemass and underlying undisturbed materials.

2. 3D low resistivity anomalies correlate with higher water content at the East Fork Landslide based on water table measurements in the three borings at this site. This finding supports the idea that the low-resistivity (conductive) zone is related to the water table. Also, higher resistivity anomalies correlate with near surface topographic highs and/or with areas adjacent to steep(er) topography, each of which likely aided in drainage of the slidemass materials; particularly the coarse-grained soils. There is no large volume of lower resistivity material within the Jackson Mountain Landslide 3D grid, comparable to the zone seen at the East Fork Landslide, but the resistivity data quality is suspect as it was likely affected by snow and field set-up. However, the water table at the Jackson Mountain Landslide is significantly deeper than at the East Fork Landslide ranging from 23 feet bgs to more than the total depth of 70 feet, which may explain why resistivity imaging did not define the water table or high-moisture materials.

3. At the East Fork Landslide the velocities ranged from just under 1000 ft/sec to >7500 ft/sec while at the Jackson Mountain Landslide the velocities ranged from about 500 ft/sec to 6500 ft/sec. In the 3D velocity volumes the P-wave velocities generally increased with depth and had only minor lateral variations; however, there was not a clear correlation with the observed / mapped boundaries of the landslide. Within the East Fork and Jackson Mountain Landslides there were a few small/localized near-surface high-velocity materials, which are interpreted to be undisturbed blocks of soil and/or rock.

4. Data quality at the East Fork Landslide was good. The field set-up (single 3D array) and instrument parameters were appropriate for good 3D imaging using IP, resistivity and seismic. Data quality at Jackson Mountain Landslide was poor. The necessary field set-up (two 3D arrays) because of the busy highway, the field conditions during the electrical surveys (snowy), and the instrument parameters used affected the 3D volume results of the IP, electrical and seismic surveys.

CONCLUSIONS

The objectives of this project were to determine if the use of 3D imaging methods on landslides, for technology transfer, using electrical and seismic geophysical methods would be an appropriate use of the technology on future landslide characterization projects. The geophysical data could then be used to aid in engineering design and remediation of the landslide. The following over-arching conclusions can be made about this project:

1) The field deployment of existing equipment and use of existing software for data analysis used for electrical and seismic imaging were successfully applied under rugged and vegetated conditions at two landslide sites;

2) 3D subsurface characterization to image physical property contrasts associated with measuring IP (clay), resistivity (moisture), and seismic velocity (density/stiffness) were revealed;

3) the need to fully understand site conditions, possibly perform forward modeling prior to mobilization to the site, and how the conditions and geologic setting will affect data quality is imperative; and,

4) Each of the three 3D geophysical methods used show promise toward defining soil and/or rock properties over a large volume of material rather than single-point measurements (e.g., borings) which could then be used to optimize drilling or other site exploratory methods. It is beyond the scope of this project to translate these findings into geotechnical parameters which might forecast landslide behavior.

With respect to the applicability of these methods to other landslide problems:

1. Other than the chaotic and jumbled nature of the IP response within the slidemass, the use of induced polarization does not reveal coherent structures within the slidemass which might be of geotechnical importance. Additional IP studies and material properties correlations would be necessary for direct use in geotechnical evaluation/engineering.

2. The results of the resistivity measurements do correlate with high water content, a finding that was anticipated, but this result will be of great value when assessing a large 3D volume of material in order to design drainage systems, for example.

3. The results of the 3D velocity measurements do correlate with soft disturbed near-surface materials, and outline their presence and thickness. Also, the 3D velocity data indicate areas within the slidemass which may be coherent, or undisturbed blocks of soil or rock.

Correlation with the limited geologic/geotechnical data at each site yields promise that if well constrained, a velocity contour could be assigned to the slideplane and various forms of data visualization will permit the volume of material above the slideplane to be visualized and analyzed (i.e., volume calculations, amount of very soft materials, etc.).

4. Care must be taken for all three 3D imaging methods to avoid analyzing and including artifacts generated by the 3D software algorithms and/or the software used to produce volume images. 3D visualization of the data is not yet robust. For example, slices parallel to the topography (e.g., slabs as used at the Jackson Mountain Landslide) or at planes not horizontal may reveal much more about the slide geometry than tools currently available.

5. Using 2D conventional software and visualization methods to calibrate and confirm the 3D results is very important and useful to verify quality and usefulness of the results.

(blank page)

REFERENCES

Allen, N. F., F. E. Richart, Jr. and R. D. Woods, 1980, Fluid Wave Propagation in Saturated and Nearly Saturated Sands, Journal of Geotechnical Engineering Division, ASCE, GT3, p.235.

Bogoslovsky, V. A. and Ogilvy, A. A., 1977, Geophysical Methods for the Investigation of Landslides, Geophysics 42, 562-571.

Calvert, H. T. and Hyde, C. S. B., 2002, Assessing Landslide Hazards in the Ottawa Valley Using Electrical and Electromagnetic Methods, SAGEEP 15, 1-1.

Coggon, J. H., 1973, A comparison of IP electrode arrays, Geophysics, 38, 737-761.

Davis, T. L. and Lawton, D. C., 1985, Field testing of explosive surface seismic sources in the Canadian thrust belt, Geophysics 50, 56-62.

Haramy, K. Y., 2009, San Juan National Forest Landslide Elevation, East Fork Road, Geotechnical Report CO-FE-0667-09-01.

Lapenna, V., Lorenzo, P., Perrone, A., Piscitelli, S., Rizzo, E., and Sdao, F., 2005, 2D electrical resistivity imaging of some complex landslides in Lucanian Apennine chain, southern Italy, Geophysics 70, 11-18.

Nawawi, M., Saad, R. and Ghazali, S., 2006, Seismic Refraction and 2D Resistivity Surveys for Slope Remedial Works at Hulu Selangor, Malaysia, SAGEEP 19, 193-201.

Poulter, T., 1950, The Poulter Seismic Method of Exploration, Geophysics 15, 181-207.

Rainone, M. L., and Torrese, P., 2007, HR Reflection Surveys for Seismic Imaging of Unstable Slopes, SAGEEP 20, 528-536.

Roy, A. and Apparao, A., 1971, Depth of investigation in direct current methods, Geophysics, 36, 943-959.

Sumner, J. S., 1976, Principles of induced polarization for geophysical prospecting, El Sevier.

Suzuki, K. and Higashi, S., 2001, Groundwater flow after heavy rain in landslide-slope area from 2-D inversion of resistivity monitoring data, Geophysics 66, 733-743.

Tripp, A. C., Hohmann, G. W., and Swift, C. M., 1984, Two-dimensional resistivity inversion, Geophysics, 49, 1708-1717.

Yeh and Associates, Inc., 2007, Geotechnical Investigation Report: US 160 Jackson Mountain Landslide, Archuleta County, Colorado, Project Number 25-146.

Zonge, K. L, Wynn, J., Urquhart, S., 2005, Resistivity, Induced Polarization, and Complex Resistivity, in Butler, D. K., ed. Investigation in geophysics, Vol. 13, Society of Exploration Geophysicists, p 265-300.

(blank page)